Modelling Dynamic Thermal Responses of Pipelines in Thermal Energy Networks

Saleh Salavati Meibodi

School of Civil Engineering

University of Leeds

A thesis submitted for the degree of

Doctor of Philosophy

September 2020

Abstract

Thermal energy networks with the ability to integrate diverse energy sources including renewable energy sources are becoming increasingly popular for delivering thermal energy in dense urban environments. This raises new challenges for the networks to effectively deal with the large share of the fluctuating and intermittent renewable energy inputs while meeting the dynamic heat requirements of the end-users. The overall aim of this work has been to develop a computationally efficient dynamic model of heat losses and thermal responses of buried pipelines at a wide range of timescales.

Experimental facilities that represent a scaled-down district heating (DH) system have been developed to provide temperature and heat flux data for a wide range of operating conditions representative of DH systems. This has allowed study of both the short and long timescale dynamic behaviour and collection of data to validate the novel numerical models proposed in this research. Furthermore, a three-dimensional model of a buried pipeline with turbulent fluid flow conjugate forced convection and conduction heat transfer through the surrounding soil has been developed using the Finite Volume Method. This model has been used as a reference model for the other numerical models proposed in this work.

A novel one-dimensional model has been developed that represents the dynamic thermal behaviour of pipelines. The model combines the features of plug-flow and discrete stirred tank representations that take into account the thermal capacitance of the pipe material as well as radial heat transfer. This combination enables the proposed model to simultaneously handle the simulation of momentum and energy balance as well as simulation of the longitudinal dispersion in pipelines. The proposed model has been compared to short timescale experimental measurements. The results elucidated that the proposed model is not only able to capture the outlet temperature changes due to a step change with good agreement with experimental data but also offers advantages in reduced computational expense.

The long timescale transient behaviour of buried pipe systems has been modelled based on a response factor approach using a Dynamic Thermal Network (DTN) representation. A novel experimental procedure is presented to derive the weighting

functions required in the DTN approach using the measurement data obtained from step response experiments. This has validated the modelling approach and verified the applicability of some of its assumptions.

Finally, a novel approach is proposed combining the DTN model with one-dimensional discretised heat transfer fluid flow model. This combination enables the model to represent the temperature propagation through the pipeline along with transient conduction heat transfer over a wide range of timescales. The results have shown that the model is not only able to accurately simulate the dynamic behaviour of the buried pipe system with very good agreement with the experimental data, but also noticeably more computationally efficient than the finite volume method: more than five orders of magnitudes. This makes the model widely applicable for efficient thermal network design and analysis tasks.

Acknowledgements

First and foremost, I would like to thank my first supervisor, Prof. Simon Rees, for his inspiring guidance, encouragement and continuous support during the journey towards the PhD thesis. Without his expertise and enthusiasm, this endeavour would not have been possible. I am also deeply grateful to my second supervisor, Dr Fleur Loveridge, for her insightful comments and suggestions.

I would like to thank Mr. Roy Trembath for his help and technical support throughout my time working in the Building Physics Laboratory. I also wish to thank Dr Ida Shafagh who was always there to support me with precious advice during all the PhD.

Moreover, I would like to extend my sincere thanks to my friends who gave me the necessary distractions from my research and made my stay in Leeds memorable. Special thanks go to Hamid Arouni, Masoud Ghalaii, Shahab Dehghan, Marjan Samipour, Mahmood Parsi, Arash Valipour, Aida Payan and Kowsar Shahbazi.

Finally, I wish to thank the University of Leeds for the financial support to the project for four years that made this all possible.

Dedicated to my parents,

Sima

and

Hossein

Contents

List of Figures

List of Tables

Nomenclature

Symbol	Meaning	Unit
A	Area	m^2
C_p	Heat capacity	$W.K^{-1}.m^{-1}$
D	Depth	m
d	Pipe diameter	m^2
f	Friction factor	-
g	Gravitational acceleration	-
h	Heat transfer coefficient	$W.K^{-1}.m^{-2}$
K	Thermal conductance	$W.K^{-1}$
k	Turbulent kinetic energy	$m^2.s^{-2}$
L	Length	m
l	Length of pipeline	m
$\dot{m}$	Mass flow rate	$Kg.s^{-1}$
Nu	Nusselt number	-
P	Pressure	-
Pe	Péclet Number	-
Pr	Prandtl Number	-
Q	Heat transfer rate	W^3
q	Heat transfer rate	$W.m^2$
r	Radius	m
R	Thermal resistance	$K.W^{-1}$
Ra	Rayleigh number	-
Re	Reynolds number	-
T	Temperature	K
t	Time	s
u	Velocity	$m.s^{-1}$
V	Volume	m^3
$\dot{V}$	Volume flow rate	$m^3.s^{-1}$
W	Width	m
x, y, z	Cartesian coordinate positions	$-$

Greek Symbol	**Meaning**	**Unit**
α	Thermal diffusivity	$m^2.s^{-1}$
β	Expansion coefficient	-
ε	Emissivity	-
ϵ	Effectiveness	-
κ	Weighting factor	-
λ	Thermal Conductivity	$W.K^{-1}.m^{-1}$
μ	Viscosity	$Kg.m^{-1}.s^{-1}$
ρ	Density	$kg.m^3$
σ	Stefan-Boltzmann constant	$W.m^{-2}.K^{-4}$
τ	Dimensionless residence time	-
ϕ	Transported scalar	-
ω	Specific turbulence dissipation rate	s^{-1}

subscript	**Meaning**
a	Ambient air
$cond$	Conduction
$conv$	Convective
E	East
f	Fluid
g	Ground
in	Inlet
max	Maximum
min	Minimum
out	Outlet
p	Pipe wall
rad	Radiation
W	West

Abbreviations

ADPF	**A**xial **D**ispersed **P**lug **F**low
ATES	**A**quifer **T**hermal **E**nergy **S**torage
BHE	**B**orehole **H**eat **E**xchanger
BTES	**B**orehole **T**hermal **E**nergy **S**torage
CHP	**C**ombine **H**eat **P**ower
DHS	**D**istrict **H**eating **S**ystem
DTN	**D**ynamic **T**hermal **N**etwork
DTN-PFST	**D**ynamic **T**hermal **N**etwork combined with **P**lug
4GDH	**F**ourth **G**eneration **D**istrict **H**eating
GDHS	**G**eothermal **D**istrict **H**eating **S**ystem
GHG	**G**green-**H**ouse **G**ases
GSHP	**G**round **S**ource **H**eat **P**ump
NCST	**N**-**C**ontinuously **S**tirred **T**anks
NTU	**N**umber of **T**transfer **U**nit
PFNCST	**P**lug **F**low combined with **N**-**C**ontinuously **S**tirred **T**anks
PID	**P**roportional-**I**ntegral-**D**erivative algorithm
RES	**R**enewable **E**nergy **S**ources
RMSE	**R**oot **M**ean **S**quire **E**rror
TES	**T**hermal **E**nergy **S**torage
UTES	**U**nderground **T**hermal **E**nergy **S**torage

Chapter 1

Introduction

1.1 Background

Climate change has become one of the most crucial concerns of human beings in this century. The main source of global climate change is the human-induced changes in atmospheric composition. These perturbations mainly result from greenhouse gasses (GHG) emissions associated with the energy use, and international actions need to be taken to address this greatest challenge of humanity [Karl & Trenberth (2003)]. Accordingly, the EU energy policy is to reduce the greenhouse gas by (GHG) emission of 80% below 1990 levels. In the European Union, 84% of heating and cooling is still generated from fossil fuels while only 16% is generated from renewable energies. It is reported that about 80% of the final energy consumption in the UK used for heating purposes was derived from fossil fuels in 2014 [Eames *et al.* (2014)]. Therefore, considering the utilization of renewable energy sources (RES) as an alternative to fossil fuels, specifically in heating and cooling sectors seems necessary.

District heating systems with the ability to integrate diverse energy sources including renewable energy sources (RES) are becoming increasingly popular for delivering thermal energy to meet requirements such as domestic water heating, space heating for a group of buildings or single properties in dense urban environments. However, the expansion of such systems requires considerable development in their major components such as: heat generation centres, distribution networks and end-user heating/hot-water system. There are a number of recent studies, including Heat Roadmap Europe [Connolly *et al.* (2014)] reporting the importance of the role of dis-

trict heating systems in the implementation of future sustainable energy systems. However, it is emphasised the transition from the current fossil fuel and nuclear-based energy systems into future sustainable energy systems cannot be done unless the systems undergo a radical change into the low-temperature district heating networks integrated with smart energy systems [Lund *et al.* (2014)]. Accordingly, the next generation district heating systems are proposed as systems that operate in relatively low temperature and interact with low-energy buildings. These systems not only enable the extensive use of various renewable energy sources such as geothermal and solar energies as well as the residual resources such as waste heat and biomass, but also reduce the heat losses in their distribution networks.

It is expected that next generation district heating system designs should address the challenges of the integration of decentralized renewable energy sources and storage, low-temperature systems and high fluctuation of the supply temperature. One of the technical challenges for fourth generation district heating (4GDH) systems is that such systems should integrate large shares of fluctuating renewable energy inputs while improving the overall system efficiency. This is expected to be accomplished by reducing the distribution network temperature as close as possible to the consumer end-use temperatures. Such decrease in the network temperatures makes the role of heat losses from the distribution network of 4GDH systems more significant than current ones. It is due to the fact that heat losses from the supply pipes with lower temperatures are more likely to cause temperature drop that is not adequate for the heating requirements of the buildings at the end of the supply pipes, and consequently results in failing to supply the heating requirements. Therefore, evaluation of the dynamic thermal performance of the distribution pipelines considering the dynamic behaviour of the heat supply centres and consumers in 4GDH should be carried out accurately to ensure optimal system operation.

1.2 Research gap

Due to important role of the distribution networks in linking the intermittent and fluctuating heat generation centres with the end-users as well as reducing the energy consumption of district heating systems, proper modelling the dynamic behaviour of the buried pipelines is vital. This is true of district systems in general but is particularly important in optimized next generation systems. A literature review establishes there are no studies that propose a practical method for short, medium

and long timescale calculation of dynamic heat losses and dynamic thermal responses of buried pipeline networks. Therefore, the main motivation of this work is to develop a dynamic model with the ability of prediction of heat losses and thermal responses of the network of buried pipelines both in short and long term, and for implementation in simulating such systems with both dynamic heat supply and end-user demands. Such model development may have the further benefits of application to other buried pipeline systems and horizontal ground heat exchangers.

1.3 Aims and Objectives

The main aim of this project is to propose and develop computationally efficient models of the dynamic thermal response of pipeline networks in district heating systems over both short and long timescales. The main objectives of this research can be stated as follows:

1. Design and building the experimental facilities that represent a scaled-down district heating system to obtain reliable temperature and heat flux data for operating conditions representative of DH systems;

2. Develop a three dimensional model of a buried pipeline with turbulent fluid flow conjugate forced convection and conduction heat transfer through the surrounding soil. This model is to be used as a reference model for the other models further proposed in this work.

3. Develop a computationally efficient and accurate simplified one dimensional model with the ability to capture the short timescale dynamic effects of pipelines, e.g. the effect of longitudinal dispersion of turbulent fluid flow with radial heat transfer to surroundings;

4. Develop a dynamic thermal model for simulation of heat losses and dynamic thermal responses of fluid flow through long buried pipelines considering transient conduction in the soil over a wide range of timescales.

   The expected outcome is a new model for evaluation of dynamic heat transfer from both pipeline networks and ground surfaces with the high degree of accuracy in various operating conditions on timescales ranging from minutes to seasonal.

1.4 Overview of methodologies

The methodologies implemented in this research can be expressed in four major parts according to the identified objectives, which are briefly described as follows:

1. Implementation of experimental facilities in the building physics lab at the University of Leeds with a focus on closely investigating the dynamic thermal behaviour of the pipeline and the ground by applying step changes to the pipeline inlet temperature. In this work, three boundary conditions are used for the pipeline surface including uninsulated pipeline exposed to the ambient air, completely insulated pipeline, and the pipeline buried into sand undergoing short and long duration testing. The comprehensive temperature, heat flux and flow rate data obtained from both sets of the experiments are further used for validation of the numerical models developed in this research.

2. To develop and model the three-dimensional buried pipeline with conjugate forced convection heat transfer, the Finite Volume Method (FVM) has been used. Initially, the required meshes have been generated based on the geometry of the test rig using OpenFOAM library, then the heat transfer calculation has been conducted using an adapted solver. Considering the numerical models proposed in this research, different 3D models with distinct boundary conditions have been developed and further validated against the experimental data.

3. The approach taken in this research to modelling the short timescale dynamic thermal effects through the pipeline is to use a one dimensional discretised model of heat transfer fluid flow to be capable of precisely accounting for the effects of longitudinal dispersion and the thermal capacity of fluid flow along with radial heat transfer to surroundings. To this end, a discretised model has been proposed, using the concepts of plug flow combined with N-continuously stirred tanks validated with the measurement data for a wide range of operating conditions;

4. To evaluate the dynamic thermal behaviour of long buried pipeline networks, a response factor approach, known as the Dynamic Thermal Network (DTN)

method has been used. In this approach, a complex three-dimensional problem can be represented with time-varying boundary conditions. In this research, the DTN model is developed and adapted for representing the buried pipeline network with particular boundary conditions. The DTN model is combined with the proposed one dimensional model denoted as the combined dynamic thermal network and plug flow with stirred tanks (DTN-PFST) model to take advantages of both dynamic models in predicting the dynamic thermal response of pipelines and heat transfer in the ground over a wide range of timescale simulation.

1.5 Thesis Outline

This thesis is structured into eight chapters. This chapter introduces the background information about district heating systems with a focus on their distribution networks as well as the aims and objectives of this work. Chapter two is concerned with the literature review associated with the district heating and approaches to modelling the dynamic behaviour of the distribution network in such systems. Chapter three presents the details of the development of the models in this work, including the 3D model, modelling of dynamic fluid response and the DTN method, and the proposed combined method. Chapters four and five are concerned with the experimental method and results from a different set of experiments, respectively. Additional details regarding the calibration of the measurement systems, tuning PID controller and measurement of the sand thermal properties are given in separate Appendixes. Chapter six and seven presented the numerical results obtained from the models developed in Chapter three along with comparisons with experimental data over the short and long timescales, respectively. The conclusions and recommendations for further work are presented in Chapter eight.

Chapter 2

Literature Review

This chapter is concerned with a review of the literature regarding district heating systems (DHS), and approaches to modelling the thermal behaviour of distribution pipeline systems. District heating systems is a distribution system of the pipeline delivers heat from energy centres to the domestic or non-domestic buildings. These systems have been identified as one of the most cost-effective ways of reducing carbon emissions from heating and improving the efficiency of energy use. This led to a rising number of new developments in such systems. In recent years, a large body of research has focused on targeting lower-carbon technologies, and integration of smart energy systems. To meet these challenges the new generation has been proposed with the ability to reach 100% renewable non-fossil heat supply integration utilizing a low-temperature distribution network. The first sections of this chapter are concerned with an overview of current technologies and benefits of such systems particularly for the UK, and the challenges for the transition to the next generation. This is followed by reviewing the technologies proposed for the future district heating systems.

Literature concerned with the fluid dynamics and heat transfer associated with buried pipelines in the distribution network of DHSs is presented in the second part of this chapter. The aim of the literature review of this part has been to focus on understanding the details of the dynamic thermal behaviour of the buried pipelines and the ground.

Due to the important role of the distribution network, as main components in the next generation of DHSs, this component has more recently seen a growth of research interest. Accordingly, there is a large body of literature concerned with the distribution networks of DHSs. The last part of this chapter is concerned with an

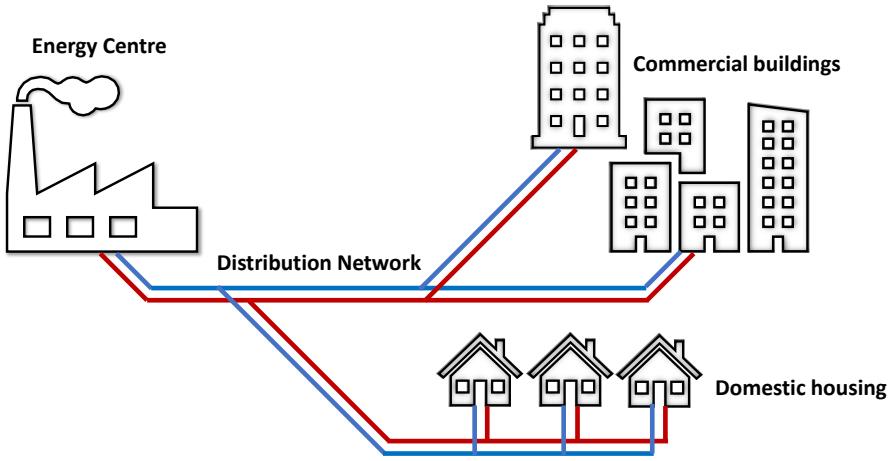

Figure 2.1: A schematics of a district heating system connecting the end-users to the heat production via the supply and return pipelines.

overview of the distribution network of such systems and approaches developed to modelling the network in the literature. More literature review concerning model validations and applications is discussed in relevant Chapters/Sections later in this thesis.

2.1 District Heating Systems

Climate change is now affecting every country around the world, and people are experiencing the remarkable impacts of climate change including changing weather patterns, rising sea level, and more extreme weather events. To address this problem, the United Nation (UN) have agreed to limit the average global temperature rise below 2°C, compared to pre-industrial levels. To achieve this target, greenhouse gases (GHG) will require to be reduced by 95% in 2050, compared to 2010 [Boesten *et al.* (2019)]. Recently, the UK government has committed to reaching net-zero emissions by 2050, which makes the UK the first major industrial economy to legislate this target. However, significant challenges are required to be addressed to meet the 2050 goals.

Heat, as the largest use of global energy, is recognized as a significant contributor to greenhouse gases (GHG) emissions as a consequence of accounting for over 50% of global energy consumption in 2015. Heating in buildings itself accounted for 40% of this heat consumed. In the UK, one third of the overall emissions come

from domestic, commercial and industrial heating. Therefore, to reach the net-zero emissions goal, a key transformation is required in providing heat supply for buildings [Revesz *et al.* (2020)].

Nowadays, heat supply for space heating or domestic hot water in buildings is mainly provided by individual heat sources or by district heating systems. The key advantages of DHSs over individual heat sources including delivering heat in a more efficient manner, more cheaply and with lower carbon emissions, attract the Governments' interest in deploying these systems. These systems are currently used noticeably in counties with a cold climate such as Scandinavia, Eastern European countries and Russia [Tunzi *et al.* (2016)]. For instance, 90% of the housing in Iceland is heated via district heating systems distributing the geothermal energy [Gida (2019)].

DHSs have a long and proven track record in the EU and the Nordic countries, but in the UK, it is only in recent years that the DHS has become part of the national strategy and new systems are bing developed in cities like Leeds, Leicester and Coventry. The plentiful supply of cheap natural gas and political climates are the main contributors that encouraged alternative heating in the UK [Millar *et al.* (2019)].

Currently, district heating systems provide only about 2% of the overall heat demand across the domestic, public, industrial and commercial sectors in the UK, but the higher share is expected to be achieved. It is suggested by the Government's research that 14-20% of the UK heat demand could be met by district heating systems by 2030 and 43% by 2050 [Chauvaud de Rochefort (2018)].

A district heating system (DHS) comprises an underground piping network which distributes the production of heat from a central plant to end-users, as shown in Fig. 2.1. These systems are used to meet different heating requirements such as domestic water heating, space heating and cooling as well as industrial process heat for a group of buildings or single properties. A district heating system may have more than one particular type of heat source. Heat sources which are utilized for a district heating system include cogenerating power plants, conventional boilers, municipal incinerators, solar collectors, industrial waste heat sources, heat pumps and geothermal energy [Lund & Lienau (2009)].

In general, a district heating system comprises three main subsystems: heat source(s), a network of end-users (consumers), and a distribution network. The complexity of the systems varies with the different parameters associated with these

subsystems and should be thoroughly considered in designing, analysing and optimizing of such systems. These parameters can be stated as: the type of heat source (e.g. geothermal energy, CHP, etc.), the number and variety of the users connected to the system, temporal and heat demand profile and spatial concerns (e.g. coordinates of all users) [Weber *et al.* (2007)].

District heating systems can also be categorized according to a number of different attributes. Rezaie & Rosen (2012) categorized DHSs based on two classifications: energy source (e.g. renewable energy, waste heat, etc.) and density (e.g. dense populated urban area, low-dense area, etc.). In another study, Talebi *et al.* (2016) classified the DHS based on five categories including geographical conditions, the scale of the DHS, density of the DHS, the level of end-user demands, and type of heat sources. Each type of DHSs requires a specific strategy for designing and optimising in a way of more energy-efficient and cost-effective of heating the buildings.

2.1.1 Advantages and Disadvantages of Current DHSs

District heating systems with the ability to use low-temperature energy forms for heating can offer a variety of advantages in terms of environment, efficiency and economics. In addition to the utilization of renewable energies, e.g. geothermal energy, these systems are able to use waste heat generated in different industrial processes which would otherwise be wasted. It is proven using waste heat in such systems not only reduces fuel consumption and increases efficiency but noticeably avoids GHG emissions and enhances the quality of the environment, since instead of being "wasted" by release into the ambient environment, they can be reused in such systems. [Patil *et al.* (2009)].

Moreover, DHSs have significant benefits for the communities including enhancing energy management and employment, increasing opportunities to use local heat sources, reducing fuel consumption and better ability to controlling the environmental emission, and air quality. The building owners and tenants can also take advantage of such a system by reducing heating costs, safer operation, reducing space requirements [Rezaie & Rosen (2012)].

Besides the aforementioned benefits, some drawbacks also exist in the implementation of the DHSs. The disadvantages include the difficulties in finding suitable sites for DHSs especially in populated areas, lower thermal comfort specifically in older DHSs where occupants have poor control over the water temperature, and the

limitation of knowledge and technical skills in DHSs. Additionally, the substantial front-end investment and the potential monopoly provided to the owner of DHSs are considered as economic disadvantages of implementation of DHSs, although appropriate governments regulations and supports can avoid some of these issues [Rezaie & Rosen (2012); Talebi *et al.* (2016)].

In spite of the variety of benefits of DHSs and its large potential, its market share around the world is still low. In the European Union, the average market share for district heating is only about 13% [Connolly *et al.* (2014)]. Besides social, economic, and technological issues related to the worldwide implementation of DHSs, the absence of suitable tools to design, analyse and optimize such systems is considered as the significant reason for neglecting DHSs [Talebi *et al.* (2016)].

The discussed benefits and limitations in DHSs have motivated the policymakers and researchers to move towards the implementation of novel ideas and strategies in energy sharing and management of DHSs [Talebi *et al.* (2016)]. Moreover, a number of studies concluded DHSs has a pivotal role to play in future sustainable energy systems [Gebremedhin (2014)]. Accordingly, the concept of next generation DHSs has been proposed to not only address the current challenges of implementation of DHSs and but also meet the future challenges of reaching 100 percent non-fossil heating supplement [Lund *et al.* (2014)].

2.2 Next Generation District Heating Systems

District heating systems can be observed over the centuries in various countries. In France, a district heating system has been used since the 14th century, and in the United State, the first commercial district system was constructed around the late 19th century [Rezaie & Rosen (2012)]. However, DHSs were not widely implemented until the last few decades when the DHS has become a significant technology in addressing the challenges of reducing carbon emissions and improving the efficiency of energy use [Lake *et al.* (2017)].

Concerning the importance of the development of district heating systems in meeting the challenges of more efficient energy use as well as being an integrated part of the smart electricity grid, the concepts of fourth [Lund *et al.* (2014)] and fifth [Wirtz *et al.* (2020)] generation of district heating have been proposed. According to the distribution and demand of district heating, these systems can be classified in five generations. The trend of development of district heating systems of each generation

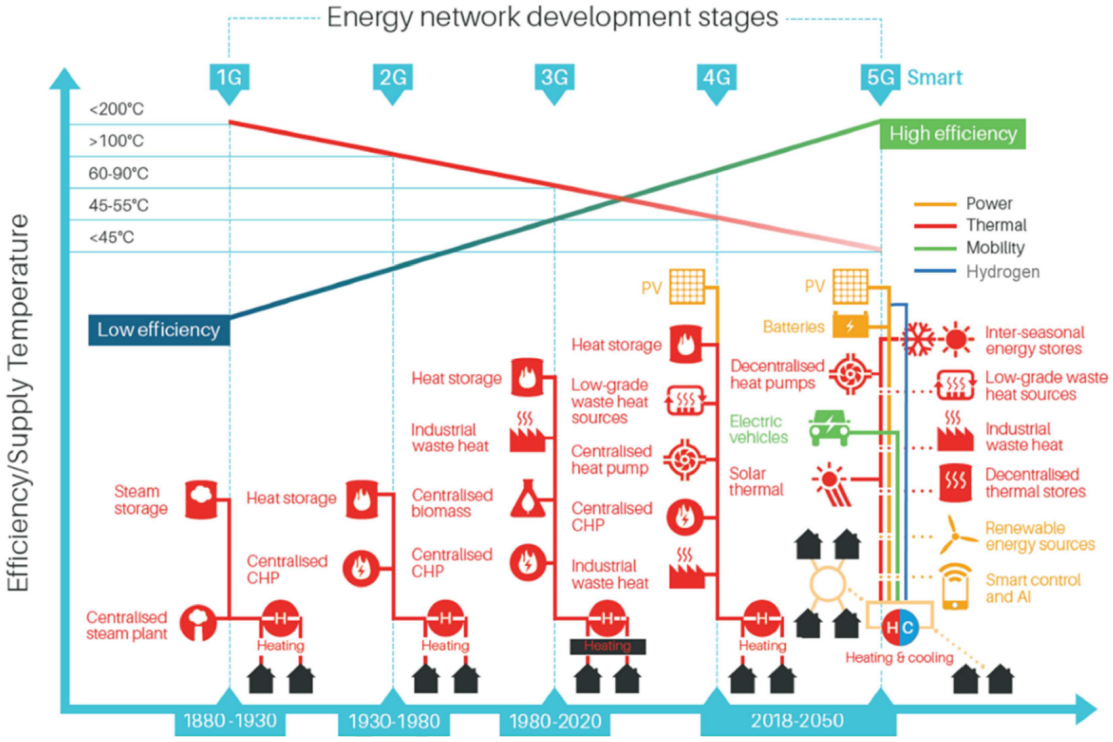

Figure 2.2: Comparison between the concept of 5th Generation District Heating and the previous generations [Revesz *et al.* (2020)]. (Reproduced with permission from Elsevier).

is illustrated in Fig. 2.2. It can be observed how the DHSs has been developing from high-temperature networks with low efficiency to lower temperature networks with higher efficiency and more diverse heat supply. Each generation of DHSs and their main specifications are defined briefly as follows.

The first generation of DHSs were introduced and utilized in the USA in the 1880s and were recognized as a state of the art system until the 1930s. This was the period of the development of electricity and tall buildings in places like New York and Chicago. These systems were operated with very high temperatures steam flowing through the concrete ducts, came from the power station fuelled by coal. Due to the noticeable heat losses and the hazard of steam explosions in such systems, this technology became outdated, although, in old New York and Paris heating systems, steam is still utilized as a heat carrier fluid.

The second generation of district heating systems utilized pressurized hot water with supply temperatures mostly over 100 °C instead of steam, as the heat carrier, until the 1970s. Unlike the first generation, these systems took advantage of the uti-

lization of large substations with tube-and-shell heat exchangers, that was found to result in better performance compared with the first generation. Most of the district heating systems that were established in the Former Soviet Union utilized this technology. However, due to the lack of any heat demand control, low efficiency, along with the large and inefficient components, e.g. large tube-and-shell heat exchangers, the 3rd generation of district heating were introduced to meet these challenges.

The third generation of the systems were introduced in the 1970s, and they are still utilized in some cities. Similar to the second generation, these systems use pressurized water as heat transfer fluid, but the supply temperature is typically between 60 °C and 90 °C. The typical components of these systems are prefabricated, pre-insulated pipes directly buried in the ground, compact substations using plate stainless steel heat exchangers, and material lean components. Currently, these systems are exploited in Europe, USA, Canada, China, and Korea. The 3rd generation technology allows district heating to replace the oil to various fuels such as coal, biomass, and waste energy and in some few cases, geothermal and solar energy [Lund & Mohammadi (2016)]. Moreover, the combined heat and power (CHP) systems are typically integrated to balance the electricity and heat demand of such a system, as well as increasing the overall efficiency of the system. CHP system is the simultaneous generation of usable heat and power (electricity) in a single process, that is able to reduce carbon emissions by up to 30% compared to the separate means of conventional generation via a boiler and power station. 46% of the Danish net heat demand in 2010 is met by DHS mainly based on Combined Heat and Power production (CHP) [Lund *et al.* (2010)]. In the UK, CHP capacity has increased 66MWe to 5,985MWe in production of electricity, and has risen 136 MWth to 20,722 MWth in 2019 compared to the last year, and accounted for 6.9% of all electricity supplied in the UK [Breeze (2019)]. Recent UK developments in district heating are mostly classified as third generation in terms of their operating temperatures and typically include natural gas CHP and solid waste heat sources.

As suggested by the trend of these three generations of district heating, fourth generation of district heating (4GDH) systems are expected to operate at lower temperatures, which is noticeably beneficial as not only does it enable the extensive use of waste energy and various renewable energy to be used, it also allows heat losses from the distribution pipes to be considerably reduced.

Lund *et al.* (2014) reviewed the different generation district heating and stated that 4GDH systems can be considered as coherent technological, and institutional

concept, which using smart thermal grids assists the appropriate development of sustainable energy systems. In fourth generation DHSs, the heat carrier water is expected to be less than 60 °C, flowing through the pre-insulated flexible (possible twin) pipes, rather than pre-insulated steel pipes using in the 3rd generation to take advantages of lowering the network heat losses. There are some studies which have proposed low-temperature district heating concerning the implementation of sustainable energy systems. Lund *et al.* (2018) have reviewed the status of the 4G network concept. In this study, the costs and benefits of 4GDH in future sustainable energy systems have been quantified. Costs involve an upgrade of heating systems and of the operation of the distribution grids, while benefits are lower grid heat losses, exploiting low-temperature heat sources and improvement in heat production compared to previous district heating systems. It has been shown how the benefits exceed costs by a safe margin using the integrated energy systems.

In the most recently published papers, it is highlighted that the future for district heating is likely to involve the use of lower temperature networks and the use of heat pumps [Wirtz *et al.* (2020)]. Fundamentally, fourth generation DHS has almost the same topology/structure as a 3G design with a single energy centre and pre-insulated pipework supplying heat outwards to the demands. However, they are significantly different in terms of having lower operating temperatures than the third generation, which allows them to be able to capture heat from low-temperature heat sources.

Lund & Mohammadi (2016) have investigated the role of smart energy systems in district heating systems for converting the present energy system into a 100% renewable energy system. It is concluded that the implementation of district heating systems must undergo a radical change into low-temperature district heating networks interacting with low-energy buildings as well as smart electricity grids, as far as fulfilling its role in future renewable energy systems is concerned.

The concept of fifth generation DH networks has not been identified extensively in literature until recently (Buffa *et al.* (2019)). As shown in Fig. 2.2, the trend of development in DHS displays gradual transition towards lower temperature heat networks. The fifth generation DHSs, also referred to as ambient thermal networks, have different topology including decentralised heat pumps rather than a single large energy centre. This gives rise to further opportunities for sharing (prosuming) heating and cooling in an ultra-low temperature loop. For instance, in a case study performed by Kauko *et al.* (2018), it is demonstrated that the heat production by the prosumers (data centre and supermarket cooling system) is sufficient to produce

the entire heating demand for the network. The ultra-low temperature also offers a more direct opportunity to capture low temperature heat sources that even a 4GDHS could not capture. For example, In urban areas, many opportunities are available to capture low-temperature heat sources that could be integrated into 5G networks, such as food retail stores [Revesz *et al.* (2020)].

In the 5GDH systems, heating and cooling consumers are connected to a thermal network which consists of a warm and a cold pipe. The temperature of the fluid in the warm pipe is around 10 °C higher than the temperature in the cold pipe, and the fluid temperatures in both pipes are close to the surrounding, between 5 to 30 °C. This keeps the network heat losses to a minimum [Wirtz *et al.* (2020)]. To raise the temperature level for space heating or domestic hot water, heat pumps are exploited in the buildings. Heat pumps use water from the warm pipe as a heat source. Cooled water from the evaporator is then discharged into the cold pipe. Likewise, chillers use the network as a heat sink. [Wirtz *et al.* (2020)].

One of the main characteristics of the next generations of DHSs is the operation of such systems at a lower temperature level. As much as the DHS operates at the lower temperature, in consideration of meeting heating demands of all the buildings involved across the network, more advantages can be taken from the systems including reducing heat losses and integrating more low-temperature heat sources. However, due to the large variations of the heating demand in energy supply systems both daily and seasonally, incorporation of the thermal energy storage (TES) into the system seems inevitable to keep the network temperature as low as possible. Thermal energy storage is the technology that transfers heat to storage media during the charging period, and releases it at a later stage during the discharging step. This allows the DHSs to balance both time and magnitude differences between heat generation and demand requirements that lead to reducing peak demand, energy consumption, costs and increasing overall efficiency of energy systems [Zhang *et al.* (2016)]. Additionally, the thermal energy storages are able to suitably deal with the intermittency and unreliability of the nature of low temperature heat sources, e.g. solar energy.

With reducing the peak flow rate in the distribution network, the pipe dimensions can be reduced resulting in a decrease of the initial investment cost. This can also make it possible to use twin pipes with two times lower heat loss coefficient than two single pipes. It is shown that by using a low temperature and small pipes, it is possible to reduce distribution heat losses by four times less than existing systems.

The use of small pipes increases the pressure requirement but this may be solved by the use of local pumps in the network or buildings [Lund *et al.* (2014)].

The fluctuations of low-temperature heat sources integrated with thermal energy storages and dynamic variations of thermal load of each end-user across the network should be suitably considered in the design and optimizing of the network system to provide the comfort temperature to consumers with as low network temperature as possible. This implies the necessity of developing efficient dynamic models to be able to effectively deal with the variations of supply and return temperatures of each component in the next generations DHSs to avoid over-design the thermal loads and pipe size. Prior to reviewing and describing the approaches and methods for modelling the distribution networks in the DHSs comprising a set of buried pipelines, it is necessary to recognize the basic principles of physical thermal phenomena influencing the distribution networks. In the following, the heat and mass transfer mechanisms of the buried pipeline systems are described.

2.3 Heat and Mass Transfer in the Buried Pipelines System

Principally, heat transfer can be defined as the science seeking to predict the energy transfer between material bodies as a result of a temperature difference. The science of heat transfer not only deals with how heat energy may be transferred, but also to anticipate the exchange rate occurring at the certain specified conditions [Holman (2010)]. The rate of heat transfer, i.e. heat energy, is the parameter of most interest in all thermal energy systems, e.g. district heating systems, and needs to be properly estimated and determined in design and optimization of different components of such systems.

Heat transfer may take place in three mechanisms: conduction, convection and radiation. In the buried pipeline systems, all three modes of heat transfer generally occur. Due to the fluid flow in the pipeline, convection heat transfer takes place between the internal fluid flow and pipeline wall, depending on the fluid flow conditions. Conduction heat transfer occurs between different materials constituting the pipeline and the layers of the ground. And heat transfer from the ground surface takes places as the combination of convection and radiation heat transfer.

In this Section, due to the importance of the flow conditions in the rate of heat transfer in the pipeline, the background to the hydrodynamics of pipe flow is firstly provided. Subsequently, the thermal aspects of fluid flow through the buried pipeline are discussed. Afterwards, the details of the heat transfer process in the ground relevant to the buried DH pipelines are presented. Since ground surface heat transfer strongly depends on the environmental conditions, the effects of different factors that play a role in determining the net ground surface heat flux are discussed for two cases: under lab conditions, and climatic conditions.

2.3.1 Fluid Flow Conditions

The rate of heat transfer from the fluid flow in the pipeline to its wall highly depends on the fluid flow regime, i.e. laminar or turbulent. Therefore, understanding the flow conditions in the pipeline is the first step to determine the heat transfer rate as characterised by the velocity and temperature profiles. In the laminar flow, the streamlines of the fluid flow tend to be linear and sheet-like, whereas, in turbulent fluid flow, the behaviour of the fluid flow is chaotic and randomly fluctuates in terms of the speed and direction. To characterize the fluid flow regime, Reynolds number (the ratio of inertial forces to viscous forces) is commonly used, as below:

$$Re = \frac{\overline{v} D_h}{\nu} \tag{2.1}$$

Where $\overline{v}$, D_h and ν are average fluid flow velocity, hydraulic diameter and the kinematic viscosity, respectively. For a circular pipe, the hydraulic diameter is equal to the inside pipe diameter. It is shown that for a circular pipe, laminar fluid flow takes place when $Re < 2300$. Above $Re = 2300$, the flow undergoes transitions to turbulence, until the full turbulence is reached at about $Re = 4000$.

The rate of heat transfer is higher in the turbulent compared to the laminar fluid flow. Therefore, turbulent fluid flow is more desirable and common in the thermal energy systems with pipes. In district heating systems, due to pipeline diameters and velocity of water flow, the Reynolds number is typically more than 10000, and the flow regime is considered turbulent [Gabrielaitiene *et al.* (2008)].

In the pipeline system, due to the contact of fluid flow with the pipe surface and the viscosity effects of the fluid flow, boundary layers develop in the length of

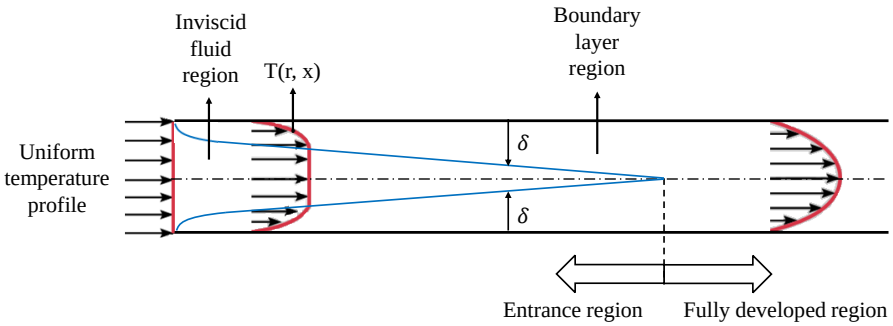

Figure 2.3: Thermal boundary layer development in a pipe (redrawn after Bergman *et al.* (2011))

pipelines. These developments continue until the boundary layers merge at the centreline. After this certain point, the velocity profiles become constant with respect to the length, and the fluid flow is fully developed, shown in Fig. 2.3.

Bergman *et al.* (2011) demonstrated that the distance from staring point of the pipe to the fully developed region depends on Reynolds number of turbulent flow and the diameter of pipe. This distance is called the entry length ($x_{h,turb}$) and for turbulent flow can be approximated to:

$$10 \leq (\frac{x_{h,turb}}{D_h}) \leq 60 \tag{2.2}$$

Bergman *et al.* (2011) also showed that there is an entry length for the pipe that similarly the temperature profiles become constant. This distance which is called thermal entry length is typically shorter than hydraulic entry length and equal to ($x_{t,turb} = 10D_h$). Therefore, when the hydraulic fully developed conditions are met, we can be sure that the shape of the temperature profile is constant.

It should be noted that the fully developed thermal conditions can be reached in a pipe for which there is either uniform surface heat flux or uniform surface temperature. These thermal surface conditions can be seen in many engineering applications, e.g. the surface was uniformly irradiated or heated. In the ground heat exchangers, for instance, the constant heat flux is often assumed as an appropriate boundary condition [Loveridge (2012)]. However, there is a mixed condition occurring in pipes in reality.

2.3.2 Radial Temperature Profile

In a real pipeline system, a simple temperature change at the pipe inlet propagated through the pipe is diffused according to the shape of the radial temperature pro-

file. This results in the outlet temperatures experience both damping and time lag. Accordingly, determining the temperature profile of thermal fluid flow can be useful to understand the dynamic thermal behaviour of the pipe.

The thermally fully developed temperature profile depends not only on whether there is laminar or turbulent flow, but also on which pipe wall boundary conditions is assumed. Moreover, The shape of the temperature profile for turbulent flow depends on Re number and Pr number (ratio of momentum diffusivity to thermal diffusivity). Accordingly, calculating the temperature profile for turbulent fluid flow is noticeably complex and difficult [Loveridge (2012)]. One way to deal with this issue is to treat the heat dispersion in the turbulent fluid flow, as the fluid scalar state variable e,g. chemical species. In this way, the shape of temperature profile can be obtained for the situations that there is no heat transfer to the pipe wall, where the shape of the temperature profile and velocity profile would be the same. This is a well-known problem in understanding the material flow profile in chemical engineering systems and commonly, the residence time distribution (RTD) theory is applied to deal with this issue [Gao *et al.* (2012)]. In the following, the residence time distribution is briefly described.

2.3.2.1 Residence Time Distribution (RTD)

The Residence Time Distribution (RTD) is defined as the distribution with time of transported scalar variables (chemical species) as they pass through a particular point (e.g. outlet) of a continuous flow system. RTDs are widely used to analyse chemical engineering problems and are approximated using a form of dispersion model or tanks in series models [Ham & Platzer (2004)]. The RTD of a system is commonly expressed as a function $F(t)$ representing the fraction of the fluid scalar state variable (chemical species or heat) at the pipe outlet for fluid flow at a given time: often plotted as a so-called F-diagram. In other words, when a step change in temperature is imposed at time $t = 0$, the variable $F(t)$ represents the proportional change of the temperature at the outlet at later time t, based on the shape of the velocity profile, as the elements near the centreline arrive faster than the average. The analysis is simplified by using the dimensionless time given by:

$$\tau = \frac{\bar{v}t}{l} \tag{2.3}$$

where l is the length of the pipeline. For laminar fluid flow, as the maximum velocity is double that of the mean fluid velocity, the temperature starts rising at τ

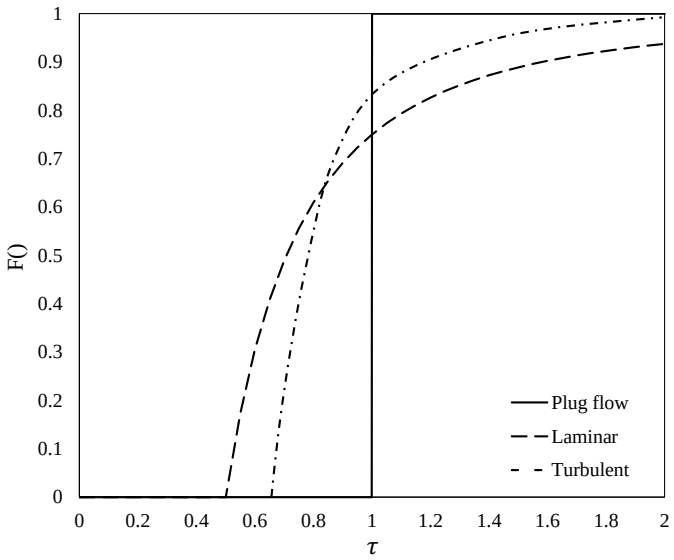

Figure 2.4: F-Diagrams for the Plug, Laminar and turbulant fluid flow (redrawn after Hanby *et al.* (2002))

$= 0.5$, and the $F(t)$ function can be calculated by integration of the velocity profile, as given below:

$$F(\tau) = 1 - \frac{1}{4\tau^2} \tag{2.4}$$

However, for the turbulent fluid flow, it is demonstrated that the shape of F-diagram depends on Reynolds number and the eddy diffusivity, and hence more complicated to be obtained, as illustrated in Fig. 2.4. Ham & Platzer (2004) proposed a semi-empirical formulation for calculating residence time distribution based on characteristic parameters that are determined from experimental results and this has been used as a reference in other work [Adeosun & Lawal (2010)]. In this model, the F-diagram can be calculated according to,

$$F(\tau) = \left[1 - \frac{\tau_k^N}{\tau^N}\left(1 - \frac{\tau}{\tau_{max}}\right)^N\right]^8 \tag{2.5}$$

where,

$$\tau_k = \frac{\tau_{min}\tau_{max}}{\tau_{max} - \tau_{min}} \tag{2.6}$$

The τ_{min} and τ_{max} parameters are the experimental minimum and the maximum dimensionless residence time of the tracer and τ is dimensionless residence time. N is also a model parameter that is obtainable based on the experimental minimum

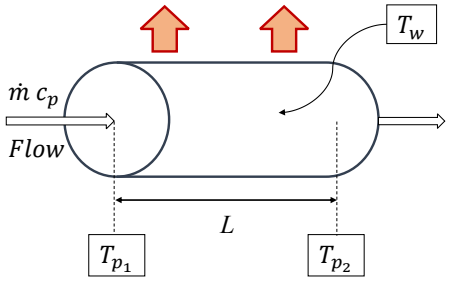

Figure 2.5: Total heat transfer in terms of fluid and pipe wall temperature difference.

and maximum dimensionless residence times. The shape of F-diagrams for both laminar and turbulent fluid flow are displayed in Fig. 2.4. We have used this model as a reference in validating models with perfectly insulated pipes in Section 6.2.

2.3.3 Heat Transfer Coefficients

The most important stage in calculation of heat transfer between the fluid flow and the pipe wall is to determine the heat transfer coefficient, h. Considering Newton's law of cooling and the energy balance on the fluid flow shown in Fig. 2.5 a convection relation can be expressed as :

$$\dot{m}c_p(T_{p1} - T_{p2}) = h(2\pi r)L(T_w - T_f) \tag{2.7}$$

where subscripts $p1$,$p2$,w and f denotes point 1, point 2, wall and fluid, respectively. Also, $\dot{m}$,c_p,r and L are the mass flow rate, thermal capacity of fluid, radius and length of the pipe, respectively. Based on Eq. 2.7, the rate of heat transfer can be related to the overall average temperature differences between the pipe wall and fluid flow and the surface area. It has been shown that for thermally fully developed conditions for turbulent fluid flow the heat transfer coefficient is constant over the pipe length depending on Re number and Pr number [Bergman *et al.* (2011)].

There are a number of empirical correlations for turbulent fluid flow in tubes that can be used to calculate the convective heat transfer coefficient. A classical expression for calculation of heat transfer in fully developed turbulent flow in smooth tubes is the Dittus–Boelter equation:

$$h_f = \frac{0.023\lambda_f Re^{0.8} Pr^n}{D} \tag{2.8}$$

where λ_f is the thermal conductivity of the fluid. In Eq. 2.8, $n = 0.4$ for heating, and $n = 0.3$ for cooling. This correlation is only valid for $Re > 10,000$ and tends to

overestimate the Nusselt number. Bergman *et al.* (2011) indicated that in some cases using this expression can result in up to 25% errors. To improve the calculation of heat transfer coefficient, Gnielinksi suggested a more complex correlation which can reduce the error to around 10%. Using Gnielinski's correlation, the pipe convection coefficient, h_f can be calculated as [Bergman *et al.* (2011)],

$$h_f = \frac{\lambda_f (f/8)(Re - 1000)Pr}{2r_p \left[1 + 12.7(f/8)^{1/2}\left(Pr^{2/3} - 1\right)\right]} \tag{2.9}$$

where f is the Darcy friction factor. Assuming the copper and steel pipeline as a smooth pipe, it can be estimated as,

$$f = (0.79\ln(Re) - 1.64)^{-2} \tag{2.10}$$

2.3.4 Heat Transfer in Soil

At the depth of a few metres from the ground surface, e.g. where the DH pipelines are buried, the ground can be thought of as a partially saturated medium where moisture content varies with time and depth. It has been demonstrated that water content in the soil can affect the thermal properties of the ground, and hence the heat transfer in soils [Rees (2016)]. Therefore, considering soil as a pure solid material is a significant assumption. In this section, the principles of heat transfer within soils are described first and then the effects of the water content in the soil heat transfer are briefly discussed.

Fundamentally, the three heat transfer mechanisms described in Section 2.3 take place within soils, but conduction is generally considered as the main and dominant heat transfer process unless significant groundwater flows are present [Rees *et al.* (2000)]. It has been illustrated for the large grain sizes where the pore spaces are sufficiently large, i.e. order of cm, the convection and radiation heat transfer may become important. Otherwise, these two heat transfer mechanisms in the soils are negligible, and can be ignored [Farouki (1986)].

Conduction heat transfer takes place through all the different soil constituents with various thermal conductivities. It can be shown that the rate of heat transfer is proportional to the temperature gradient in the direction of heat flow ($\frac{\partial T}{\partial x}$) depending on the thermal conductivity (λ) which is expressed as Fourier's law ($Q = -\lambda A \frac{\partial T}{\partial x}$).

The general three-dimensional heat conduction equation for the constant thermal conductivity can be written as below:

$$\frac{\partial^2 T}{\partial x^2} + \frac{\partial^2 T}{\partial y^2} + \frac{\partial^2 T}{\partial z^2} = \frac{1}{\alpha}\frac{\partial T}{\partial t} \tag{2.11}$$

where the quantity α is called the thermal diffusivity. This value shows how fast the heat diffuses through the solid material, i.e. soil. The larger the value of α, the faster the heat dissipates through the soil. The thermal diffusivity can be expressed as below:

$$\alpha = \frac{\lambda}{\rho c_p} \tag{2.12}$$

It should be noted that the heat flow through the soil is confined by surface contacts of the particles. Therefore, the water and air present in the pore space should be considered in the overall thermal conductivity of soils. Since water is more than thirty times more conductive than air, the soils with a higher level of saturation have higher thermal conductivity which affects the heat transfer process (discussed in the following section).

It is worth mentioning that the thermal conductivity of soils (even with a high level of saturation) is relatively low, e.g. typically between 0.1 to 4 $W/K.m$, compared with other solid materials, such as metals. Consequently, heat in soils is not transferred fast and –due to the low thermal diffusivity– far. Due to this fact, soils are potentially considered to be exploited as heat storage materials [Loveridge (2012)].

Due to importance of the role of thermal conductivity and thermal diffusivity of soil in the calculation of the conduction heat transfer, several tests have been performed to determine the thermal properties of the sand used in this work. The details of the measurements are described in Appendix C.

2.3.5 Influence of Soil Moisture on Ground Heat Transfer

One of the most significant factors in soil heat transfer is the effect of moisture, which can have an impact on the thermal properties of the soils depending on the water contents. Farouki (1986) experimentally studied the thermal properties of soils and showed that the thermal conductivity of dry and wet sands can vary up to a factor ten of dry and wet loams up to a factor five. He also reported that

the variation of thermal capacity is less sensitive to the water content than thermal conductivity, but still about doubles or triples from dry to wet state.

Moreover, in the unsaturated soils, increasing temperatures resulting in evaporation of the water in the soil pores, and absorbing the latent heat of vaporization. Due to the increase of the local vapour pressure, the water vapour is diffused through the soil to the region of lower vapour pressure depending on the temperature and then is condensed. This process is called the evaporation-condensation process and plays an important role in heat transfer mechanisms in unsaturated soil. This process also affects the thermal properties of the soil, as the degree of soil saturation is changed with moisture migration [Jassen (2004)].

In some situations, the soil moisture can be exposed to the freezing and thawing processes, specifically near the ground surface. In this process, a large amount of heat is transferred in latent heat effects, as during the freezing, heat is removed from the water to form ice, and during thawing, it takes place in the inverse direction. This process also affects the thermal properties of the soils, as the saturation degree varies with the presence of ice in the soil.

Considering the moisture fluxes and conduction of the soils, the ground heat transfer can be determined based on the variations of the ground surface temperature reflecting the weather conditions. In general, the thermal dynamic behaviour of the soils responding to the weather conditions varies diurnally and seasonally depending on the depth of soil. Since the DH pipelines are generally buried at a depth of around 1 m, the near-surface ground temperature characteristics should be taken into account in design and modelling. Due to the relatively high thermal capacity of the ground, the diurnal air temperature fluctuations are reduced at only a short distance below ground. It has been shown that at depths more than a few tens of centimetres, the temperature variations of soils are sufficiently damped that fluctuations occur seasonally rather than daily. Moreover, at depths of approximately 5 m, there is often no observable seasonal variation in temperature. In other words, the ground temperatures at these depths are isolated from monthly climatic variations [Rees (2016)].

2.3.6 Ground Surface Heat Transfer

Determining the ground surface heat transfer (boundary conditions) plays a key role in the proper modelling and simulation of buried pipelines in the ground. Heat

transfer from the ground surface occurs by convection and radiation driven by surface and atmospheric air temperature differences, and influenced by solar irradiation. In the following, the ground surface heat transfer processes are described for two cases: where there is no wind and solar irradiation (under lab conditions), and where the surface exposed to the combination of solar irradiation and wind (under natural climatic conditions).

2.3.6.1 Ground Surface Heat Transfer under the Lab Conditions

In principle, in the situations that there is no forced velocity (wind), but convection current exist resulting of the motion of the fluid due to density changes arising from the heating process, the heat process is referred to natural or free convection heat transfer. In this process, the variations in the density of the fluid are due to a temperature gradient, and the net effect is a buoyancy force, which induces free convection currents [Holman (2010)]. This situation can be seen at the ground surface where the wind speed is not noticeable. In this work, as the experimental setup is located at the lab with almost motionless air conditions, the correlations for the free convection heat transfer from the hot surface is used for calculation of total heat losses from the ground.

For the horizontal warm surface facing the cool ambient, the buoyancy force is exclusively normal to the surface. Conservation of mass dictates that warm fluid ascending from a surface must be replaced by descending cooler fluid from the ambient, as displayed in Fig. 2.6 It has been found that average free-convection heat transfer coefficients can be given in the following form for most engineering calculations:

$$\bar{h} = \frac{CRa^m\lambda}{L} \tag{2.13}$$

where C and m are constants and obtained according to the heat conditions, L is the characteristic length, i.e. the surface area over the perimeter of the surface ($L = A/P$), and Ra is Rayleigh number expressed as:

$$Ra = \frac{g\beta(T_w - T_a)L^3}{\vartheta\alpha} \tag{2.14}$$

where β, T_w, and T_a are the expansion coefficient, wall temperature and ambient temperature, respectively. The expansion coefficient can be determined based on the types of fluid. For an ideal gas, it can be calculated by:

$$\beta = \frac{1}{\rho}\frac{p}{RT_f^2} = \frac{1}{T_f} \tag{2.15}$$

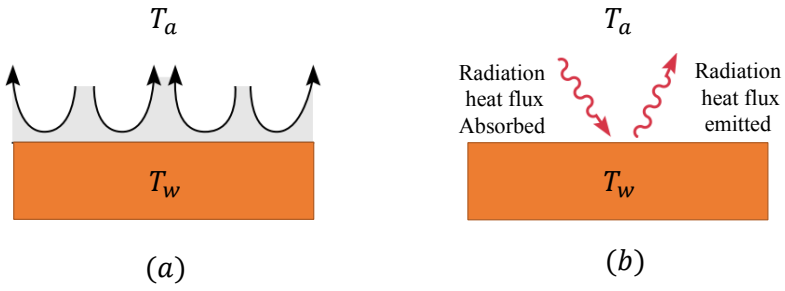

Figure 2.6: (a) Buoyancy-driven flows on the warm horizontal surface facing the cool ambient, (b) Radiation heat exchange at the surface (redrawn after Bergman *et al.* (2011))

Where T_f is the absolute film temperature ($T_f = (T_w + T_a)/2$). It should be noted that all properties in the calculation of Ra number must be evaluated at the film temperature. Considering the conditions of the experiments, the convection heat transfer coefficient from the ground can be obtained as [Bergman *et al.* (2011)]:

$$\bar{h} = \frac{0.54 Ra^{0.25} \lambda}{L} \tag{2.16}$$

In addition to the free convection heat transfer, radiation occurs on the ground surface due to the temperature difference between the surface and the ambient air. In general, thermal radiation is energy emitted by every solid surface that is at nonzero temperature and transported by electromagnetic waves. Unlike conduction and convection heat transfer, radiation does not need any material medium to be transferred, and occurs most efficiently in a vacuum. It is shown that the net rate of radiation heat transfer from the surface can be expressed based on the difference between thermal energy that is released due to radiation emission and that which is gained due to radiation absorption according to the *Stefan–Boltzmann law*, as below:

$$Q_{rad} = A\varepsilon\sigma(T_w^4 - T_a^4) \tag{2.17}$$

where σ and ε are the Stefan–Boltzmann constant ($5.67 \times 10^{-8}\ W/m^2K^4$) and the emissivity of the surface, respectively. There are many engineering applications where it is more convenient to represent the net radiation heat exchange in the similar manner to the convection heat transfer, as below:

$$Q_{rad} = h_r A(T_w - T_a) \tag{2.18}$$

where h_r is called the radiation heat transfer coefficient, and obtained by equalizing Eq. 2.17 and Eq. 2.18 as follows:

$$h_r = \varepsilon\sigma(T_w + T_a)(T_w^2 + T_a^2) \tag{2.19}$$

By modelling the radiation heat transfer in a manner similar to convection, the rate of radiation is linearised which makes the heat rate proportional to a temperature difference rather than to the difference between two temperatures to the fourth power. Considering the Eq. 2.16 and Eq. 2.19, the overall heat transfer from the ground surface can be calculated as below:

$$Q_{surface} = Q_{convection} + Q_{radiation} = (h_{conv} + h_r)A(T_w - T_a) \tag{2.20}$$

2.3.6.2 Ground Surface Heat Transfer under climatic Conditions

The heat balance at the earth surface can be defined in terms of short-wave radiation (R_{ns}), long-wave radiation (R_{nl}), convective heat transfer and the effect of evapotranspiration, as expressed below [Fan *et al.* (2013)]:

$$Q_{\text{Ground Surface}}/A = R_{ns} + R_{nl} + h_{conv}(T_a - T_s) + \rho_w L_w ET_0 \tag{2.21}$$

where h_{conv}, ρ_w, L_w, and ET_0 are the convection heat transfer coefficient of the ground surface, water density, the heat released when water vaporises, and the loss of water through evapotranspiration (m/s), respectively. The last term in the Eq. 2.21 represents the heat loss through "evapotranspiration" at the ground surface.

The short wave radiation absorbed by the earth surface (R_{ns}) is obtained from the balance between incoming and reflected solar radiation, as follows:

$$R_{ns} = R_s - \alpha R_s = (1 - \alpha)R_s \tag{2.22}$$

where R_s and α are incident short-wave radiation and albedo coefficient, respectively. The albedo coefficient is the measure of the diffuse reflection of solar radiation out of the total solar radiation. For instance, the albedo coefficients for bare soil and green grass are 0.17 and 0.25, respectively [Markvart & Castalzer (2012)]. The incident short-wave radiation or net solar radiation can be read from the local weather reports, e.g. TMY3 weather file, or measured by a proper radiometer.

The long-wave radiation R_{nl} can be calculated based on the procedure recommended by Walter (2005), which uses an effective sky emissivity, based on humidity

and cloudiness. In fact, the long-wave radiation is the difference between the long-wave radiation emitted from the ground surface to the sky and the long-wave radiation from the sky absorbed by the surface. Generally, the long wave radiation from the earth's surface and the sky can be calculated based on the Stefan-Boltzmann law ($q = \sigma\epsilon T^4$), which calculates the radiation from either sky or earth by multiplying the Stefan-Boltzmann constant, by the effective emissivity and its temperature to the power of four. However, in this approach, the sky temperature and the ground surface temperature are required, as well as the emissivity which is hardly known and needs to be calculated or estimated. Walter (2005) recommended the following equation for calculating long-wave radiation using the cloudiness and air humidity to calculate the effective emissivity, while only measured ambient air temperature is required for the calculation [Xing (2008)]. The relation can be expressed as follows:

$$R_{nl} = \sigma T_a^4 \ (1.35\frac{R_s}{R_{so}} - 0.35) \ (0.34 - 0.14\sqrt{e_a}) \tag{2.23}$$

where R_{so}, e_a are calculated clear sky solar radiation and actual air vapour pressure. In 2.23, the air humidity and cloudiness is basically used for calculation of the effective emissivity. The term $(1.35\frac{R_s}{R_{so}} - 0.35)$ represents the effects of the cloudiness in long-wave radiation. More clouds in the sky results in R_s decreasing, and hence the term decreases. The term is limited between 0.05 and 1 [Walter (2005)]. The clear sky solar radiation (R_{so}) can be calculated based on the solar radiation emitted at the sun surface, the longitude, latitude of the location and the solar angle at different times of the year. The term $(0.34 - 0.14\sqrt{e_a})$ expresses the effect of air humidity, and decreases when air humidity increases [Xing (2008)]. The air vapour pressure can be obtain based on the dew point temperature, as follows:

$$e_a = 0.6108 \ \exp(\frac{17.27 \ T_{\text{dew}}}{T_{\text{dew}} + 273.17}) \tag{2.24}$$

To calculate the overall ground surface heat transfer, the convection heat transfer from the surface requires to be estimated. There are a number of correlations proposed to estimate the convective heat transfer coefficient based on the wind speed (U_w) for different conditions. According to the ASHRAE handbook [Ashrae Standard (2001)], the convection heat transfer coefficient over a flat surface such as ground surface can be estimated as follows:

$$h_{conv} = C(\frac{1}{T_{ave}})^{0.181}(\Delta T)^{0.266}\sqrt{1 + 0.793U_w} \tag{2.25}$$

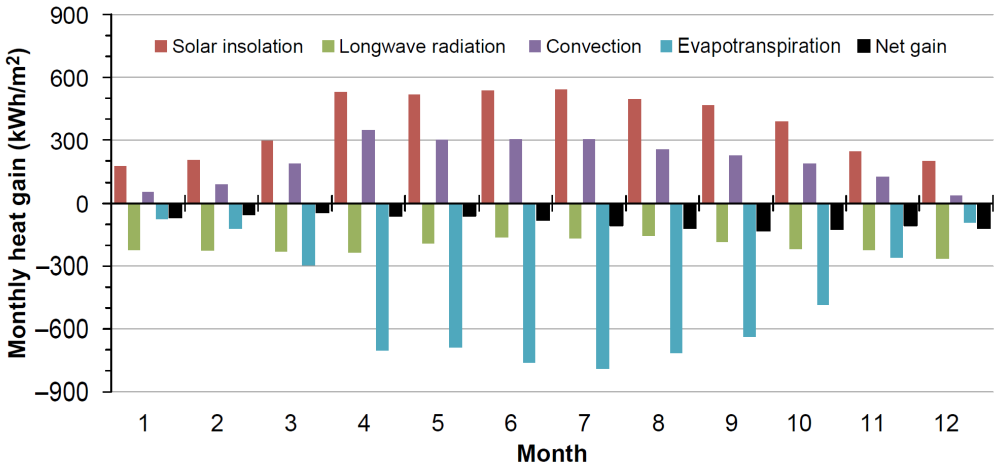

Figure 2.7: Monthly ground surface heat transfer budget, and the net value calculated for a site in Oak Ridge, Tennessee [Fan *et al.* (2013)]. (Reproduced with permission from Taylor & Francis).

where C is a constant taken to be 20.594 when the ground surface is warmer than air, and 11.241 when it is cooler than the air. As given in Eq.2.21, the heat losses from the ground surface also occur in the form of evapotranspiration. Evapotranspiration is a term that represents the loss of water from the earth's surface through evaporation and plant transpiration [Xing (2008)]. The moisture in the ground is drawn out by any plant growth and subsequently evaporated. Overall, the evapotranspiration is the loss of water through the evaporation of soil and plant surfaces. This phase change process causes temperature reduction at the ground surface since by evaporation at the soil and plans, a large amount of latent heat absorbed by the water during the process. The heat loss occurs through the evapotranspiration process can be obtained by multiplying the evapotranspiration rate by the water density (ρ_w) and the latent heat of water evaporation (L_w). The evapotranspiration rate, (ET_0), can be calculated using the well-known Penman-Monteith equation (Fan *et al.* (2013)), as follows:

$$ET_0 = \frac{0.408\Delta(R_{nl} + R_{ns} - G) + C_n\gamma U_w(e_s - e_a)/T_a}{\Delta + \gamma(1 + C_d U_w)} \tag{2.26}$$

where e_s, γ, Δ are the saturated air vapour pressure, psychometric constant, and the slope of the saturation vapour pressure-temperature curve, respectively. Also, C_d and C_n are empirical constants can be taken based on the type of ground surface cover, e.g. short-grass vegetation. In Eq. 2.26, the term G is the heat stored in the soil that has been shown well correlated with the net radiation ($R_{nl} - R_{ns}$). Further

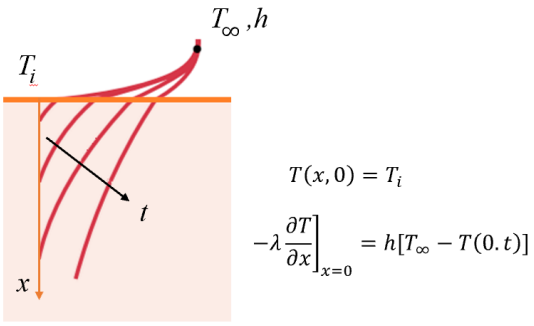

Figure 2.8: Transient temperature distributions in a semi-infinite solid with the convective boundary condition (redrawn after Bergman *et al.* (2011))

details and information about the evapotranspiration calculation can be found in Xing (2008) and Walter (2005).

The overall ground surface heat fluxes are balanced by the heat that is exchanged with the subsurface soil by conduction. These heat fluxes associated with the solar radiation, long-wave radiation, convection heat transfer and evapotranspiration have been calculated in one experiment by Fan *et al.* (2013) on a monthly basis and are illustrated in Fig 2.7. It can be observed the magnitude of the net ground surface heat flux is rather less than some of the heat flux components. This means that uncertainties in surface parameters or environmental conditions can have a significant effect on the predicted heat exchanger performance on DH pipeline modelling where they are buried in relatively shallow depth [Rees (2016)].

2.3.7 Convection boundary conditions

In most practical situations the transient heat conduction problem is connected with a convection boundary condition at the surface of the solid. For the semi-infinite-solid problem, in which the solid extends to infinity in all but one direction, the solid can be characterized by a single convective surface, as shown in Fig. 2.8. This can be used to determine transient conduction heat transfer near the ground surface. In these cases, the convective boundary condition for the differential equation must be modified to take into account this convection heat transfer at the surface. Since for the semi-infinite-solid, the heat losses from the surface is equal to heat conducted

Figure 2.9: District heating pipelines (Leeds city centre).

into the surface, the convection boundary condition can be expressed as below:

$$hA(T_\infty - T)_{x=0} = -\lambda A \frac{\partial T}{\partial x}]_{x=0} \tag{2.27}$$

The solution for this problem is rather involved; however, Holman (2010) presented the result of the equation as below:

$$\begin{aligned} \frac{T - T_i}{T_a - T_i} &= 1 - \text{erf}(\frac{x}{2\sqrt{\alpha \times \tau}}) \\ &- \left[\text{erf}\left(\frac{hx}{\lambda} + \frac{h^2\alpha\tau}{\lambda^2}\right)\right] \times \left[1 - \text{erf}\left(\frac{x}{2\sqrt{\alpha \times \tau}} + \frac{h\sqrt{\alpha \times \tau}}{\lambda}\right)\right] \end{aligned} \tag{2.28}$$

where T_i, h, x are the initial temperature of the ground, heat transfer coefficient and the distance from the surface in the ground, respectively. Considering the thermal properties of the ground as well as ambient and initial temperatures, the temperature of the ground at a different depth for the different time can be calculated from Eq. 2.28. The analytical solution for this problem is then used to compare with the numerical results obtained from the 3D model for the purpose of validation in Section 7.1.1.

2.4 Modelling Dynamic Thermal Response of Pipelines

Generally, because of the important role of the distribution network in linking the heat generation centres with the end-users, distribution networks are considered as

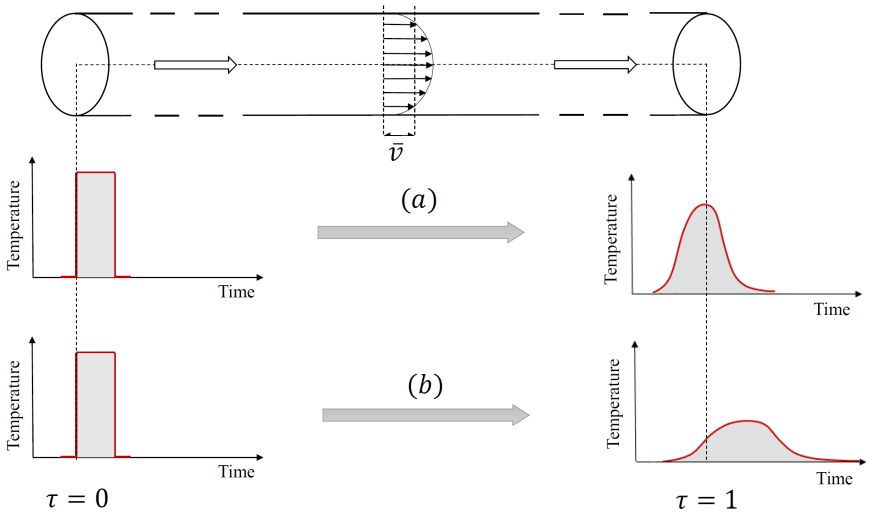

Figure 2.10: Longitudinal diffusion process for fluid flow through the pipeline, while a temperature pulse is entering the pipe. The diffusive pipe thermal response is shaped base on the velocity profile and turbulence, (a) assuming no heat loss , (b) compounding with radial heat losses.

one of the most significant components of DHSs [Lake *et al.* (2017)]. Therefore, understanding and representing the dynamic thermal behaviour of pipelines can be considered essential in simulating district heating system operation. Often, in the simulation of heating systems, the heat carrier fluid flow through pipes is treated as an ideal fluid with the uniform velocity profile i.e. plug flow. The dynamic transport of heat, as well as the thermal capacity of the fluid, are also often ignored. These assumptions can be deemed correct if the medium and long term simulations are of interest and the pipeline lengths are relatively short, but for short timescale simulations and the long DH pipeline, cannot be considered accurate. The long pipelines used in the DHS is illustrated in Fig.2.9.

In a real system, a simple temperature change at the inlet propagated through the pipe is diffused according to the shape of the velocity profile. This physical phenomenon needs to be considered particularly for systems with inlet temperature fluctuations in which case the thermal response at the outlet experiences both damping and time lag. This is shown in Fig. 2.10(a). This time delay can play a significant role in long pipes with the transit time of higher than a few minutes: possibly more than 30 minutes in district heating systems. These diffusive effects are further compounded when heat transfer occurs in the radial direction, e.g. heat loss from hot water supply pipes or into the ground in district heating, as illustrated in

Fig. 2.10(b). The well-known problem of predicting the temperature at a tap/faucet in drawing hot water from a tank, is a good example of a real system with these phenomena Comstock *et al.* (1974); Seliktar & Rorres (1994); Taylor (1954a). In the following, the modelling approaches to modelling the pipelines are briefly reviewed.

It is initially worth noting that a number of analytical solutions have been proposed to deal with this particular problem, i.e., modelling the fluid flow and heat transfer in a pipe [Arpaci (1966); Bosworth (1949)]. However, due to their mathematical complexity and limitations in the range of conditions where temperatures and flow rates fluctuate, they cannot be used for modelling a pipe in realistic situations.

For modelling the dynamic fluid flow and heat transfer in a pipeline, a number of numerical approaches have been proposed [Dénarié *et al.* (2019); van der Heijde *et al.* (2017); Wang & Meng (2018)]. The propagation of fluid flow through a pipe can be modelled by the so-called node method [Benonysson *et al.* (1995)]. In this approach, the heat propagation of the fluid flow is modelled by taking into account only two nodes, the inlet and outlet temperatures, and the time delay due to the transporting the fluid between these two nodes depending on the fluid velocity. Based on the temperature at the inlet node, the pipe wall temperature and mass flow rate, the temperature of the outlet node is calculated and updated from one node to the another by solving an energy equation for each node. In this method, the heat capacities of fluid and pipe wall are taken into account, and the model can be implemented to deal with dynamic heat losses to surroundings e.g. ground. The stability and accuracy of this method have been analysed in calculating temperature responses in district heating pipeline [Benonysson (1991)]. This method has also been implemented to modelling pipelines in such systems and shows a good agreement with measurement data [Gabrielaitiene *et al.* (2007, 2008)]. However, since in this model, the fluid flow is assumed as a "plug" flow, the model is not able to capture short timescale fluid dynamic effects.

The node method can also be implemented in a number of computational tools. Giraud *et al.* (2015) presented a Modelica library [Wetter *et al.* (2014)] for modelling the pipe in district heating systems called "NodeMethodPipe" and experimentally validated the model using long time series data. In another study, del Hoyo Arce *et al.* (2018) developed a Modelica library comprises models of distribution and their validation for dynamic modelling of district heating and cooling networks. Sartor and Dewalef proposed a node model taking into account the thermal inertia of the

pipes and heat losses and implemented this in the TRNSYS software library [Klein *et al.* (1997)]. They validated the model with experimental measurement. However, the basis of the TRNSYS software library is limited by also taking the plug-flow approach.

Another approach to modelling the fluid flow through a pipe is to use the Finite Element Method (FEM) or the Finite Volume Method (FVM). Gabrielaitiene *et al.* (2008) evaluated the FEM and node model for modelling the heat propagation in district heating pipelines and compared this method with a node model and the measurement data from an operating DHS. It was concluded that the models have limitations in the prediction of the peak values and temperature response time of the heatwave through the pipe in a short timescale. Dalla Rosa *et al.* (2011) used a FEM model (2D model) of the fluid flow in a pipe system with a focus on the heat losses in the steady-state conditions. Validation was studied using experimental measurements from a test rig and analytical formulas. In another study, Dalla Rosa *et al.* (2013) investigated the transient heat transfer in twin pipes in a short timescale. They proposed a modified node model and validated it against an FVM model (2D model) and measurement data from an experimental setup. It was shown that both the detailed FVM model and the proposed model can predict the pipe outlet temperatures when step changes or sinusoidal changes are imposed in the inlet temperature in comparison with the experimental data. Such numerical approaches are very computationally demanding, however.

A further approach to simulate the dynamic responses of pipes is to model the dispersion of the fluid flow, by applying a one-dimensional advection-dispersion equation, so-called the Axial Dispersion Plug Flow (ADPF) [Wen & Fan (1975)]. Skoglund & Dejmek (2007) demonstrated the ADPF model can be used to properly describe the dispersion (diffusion, turbulence and velocity profile) of the chemical concentration of fluid flows. In this method, the pipe is discretised into finite well-mixed cells (ideally stirred tanks), and an energy balance is applied to each cell to derive the time-varying temperatures.

Escudie & Laret (1994) briefly outlined this approach and demonstrated its advantages. This approach has been later applied to modelling the dynamic thermal response of conduits [Hanby *et al.* (2002)] and borehole heat exchangers [He (2012); Rees (2015)]. In the case of such one-dimensional approaches, the diffusive nature of the discrete formulation is an approximation to the physical diffusion processes that

are due to multi-dimensional variations in the flow velocity and temperature distribution. In this study, this approach has been used and modified for dealing with modelling the short timescale dynamic effect in pipelines, described in Chapter 3.

2.5 Conclusions

This chapter has provided an overview of the literature regarding the district heating systems, and approaches to modelling DH pipeline networks. DHS has been known as a critical player in addressing the challenges of reducing carbon emissions and improving the efficiency of energy use. However, due to some economic and technological issues, there has been little progress in its market share around the world and it is still low. Considering the benefits and limitations of the implementation of DHSs, implementing novel ideas and strategies seems necessary to improve the systems and overcome the challenges. A large number of researchers proposed new schemes and technologies to pave the way to meet the current challenges. Recently, a concept of next generation DHS has been proposed with the ability to reach a hundred percent renewable heat supply. This requires the network to operate at a lower temperature to reduce the heat losses from the distribution network, and allow more low-temperature energy sources to be integrated into the systems. Therefore, the role of the distribution networks in the next generation DHSs seems considerably more significant compared with the current systems as they should provide comfort temperature to the consumers, while operating at the lower temperature. Consequently, numerous authors have been dealt with developing efficient methods for modelling heat transfer of DHS pipelines.

The heat transfer and fluid dynamics characteristics of buried pipeline systems have been investigated theoretically and experimentally in the literature. The heat transfer process in the soil and ground surface have been evaluated for decades. In these research works, a large number of empirical relations have been suggested to deal with modelling heat transfer at the ground surfaces, and conduction in the soils. These empirical relations can be used in modelling the DH pipelines heat losses.

There are a large number of studies concerning the fluid flow and heat transfer through the pipeline. The flow through the pipeline is well understood, although the role of radial heat losses from the pipeline in the thermal response of pipes has been analytically evaluated only in a small number of studies. However, due to the limitations in the range of conditions of the proposed analytical models, they

cannot be implemented in a realistic situation where pipeline temperature fluctuates. Therefore, a number of numerical approaches have been proposed for modelling the fluid flow and heat transfer through the pipeline.

There are a variety of numerical approaches discussed in the literature, that have been applied to modelling the temperature propagation of fluid flow through the DH pipeline. However, in most of these works, the fluid flow is assumed as a plug flow with a uniform velocity profile. The literature review establishes there is no research that investigates the effects of the longitudinal diffusion process of fluid flow when compounding with radial heat losses in a short timescale. Moreover, the dynamic thermal response of pipelines considering the dynamic short timescale effects has not been experimentally investigated. Therefore, one objective of this research has been chosen to experimentally evaluate the dynamic thermal response of pipelines in a short timescale, and proposed a practical model to accurately predict the dynamic behaviour of pipelines.

Another numerical approach to modelling the fluid flow through DH pipelines is the Finite Element Method (FEM) or the Finite Volume Method (FVM). These methods have been used in a number of studies and have shown good validity against measurement data for both lab-scale and full-size DHSs. However, such numerical approaches are very computationally demanding. Besides these methods, the dynamic behaviour of pipelines has been modelled using the axial Dispersion Plug Flow (ADPF) model which models the dispersion of the fluid flow by discretization of the pipe into finite well-mixed cells. In such one-dimensional approaches, the diffusive nature of the pipeline is discretised as an approximation to the physical diffusion processes that are because of multi-dimensional variations in the temperature distribution. This approach has been used in a number of heat transfer applications, e.g. borehole heat exchangers. However, for using the approach for modelling the long pipeline with heat losses to the surroundings, the method requires some necessary modifications to make.

Although there has been much research on modelling the DH pipelines, there is no study proposing a model which is able to accurately model the dynamic thermal effects of buried pipeline systems by taking into account the ground transient conduction in a computationally efficient manner. Accordingly, the main aim of this study has been chosen to develop a model to accurately predict the dynamic thermal response of buried pipelines over a wide range of timescales by considering the transient heat transfer in the ground. The model is aimed to be able to simply

implement in modelling the operation of the buried pipeline in DHSs over annual periods, especially the next generation DHS where dynamic thermal behaviour of the pipelines is more important.

Chapter 3

Model Development

In this Chapter, the dynamic thermal modelling approaches developed in this work to simulate the dynamic thermal performance of district heating pipelines are described. Based on the objectives of this work to develop dynamic thermal models to represent the thermal performance of the buried pipelines in different operating conditions, a number of numerical models are developed. There are three cases that are of interest:

1. Short timescale thermal response in insulated pipes
2. Short timescale thermal response in uninsulated pipes
3. Long timescale thermal response in buried pipes.

The overall aim of this work is to arrive at one model with the ability to effectively deal with all these conditions, and to practically be implemented in modelling the dynamic thermal behaviour of buried pipelines. The main idea to achieve this is to combine a one-dimensional discretised model with the ability to effectively handle the simulation of momentum and energy balance as well as the longitudinal dispersion in pipelines, with the two-dimensional model able to represent the transient conduction heat transfer with complex and time-varying boundary conditions.

The terms of the short and long timescales are defined based on the period of time that the fluid flow in pipelines approaches steady-state conditions. In the cases where the pipeline is not buried (without the ground conduction heat transfer), this occurs in the order of the nominal transient time of the fluid flow (τ), and hence the term of short timescales used for these cases. On the other hand, in the

cases where the pipelines are buried in the ground, the length of time in which the pipeline approaches steady-state conditions is relatively long, depending on the thermal properties of the ground and the buried pipe geometry. This process may take days, months or even years. Thus, the term of the long timescales is applied for such cases.

In order to generate reference data for comparison with model and experimental data, a three-dimensional buried pipeline with the turbulent fluid flow with conjugate forced convection heat transfer and conduction heat transfer through the surrounding soil has been implemented using the Finite Volume Method (FVM). This is carried out for four cases based on the pipeline boundary conditions, i.e. insulated, uninsulated, buried in sand, and two timescales: short and long timescales. The objective of developing the 3D models is to represent the pipelines with the least possible assumptions with the ability to simulate the three-dimensional effects on the model predictions. The finite volume models developed are then validated against experimental data and analytical solutions presented in the literature. Having validated the 3D models, the generated outputs are used to compare with the results of other numerical models proposed in this work and the experimental data. This allows quantifying the accuracy and calculation time of the proposed models in the prediction of dynamic thermal responses of pipelines.

Due to the importance of the short timescale dynamic thermal behaviour of pipe systems in many heating, cooling and process systems, a numerical model has been proposed to predict the dynamic thermal response of pipelines considering the short timescale dynamic effects. In this model, a one dimensional discretised approach is used to modelling short timescale dynamic response of heat transfer fluid flow in pipelines which takes into account the thermal capacity and longitudinal dispersion of the fluid flow. The proposed model is then compared with the detailed 3D model and the experimental data.

The Dynamic Thermal Network (DTN) approach has been used for the long-timescale modelling dynamic thermal response of buried pipelines. The DTN method is able to deal with transient conduction in the pipe, insulation and ground materials with time-varying boundary temperatures. The DTN method has recently been applied in the modelling of a number thermal systems, e.g. energy piles [Rees & Van Lysebetten (2020)] and diaphragm wall ground heat exchanger [Shafagh *et al.* (2020)]. The details of the theoretical basis of the DTN method along with the boundary conditions of the surfaces are described in Section 3.3.

In this research, a novel combination of the Dynamic Thermal Network (DTN) method with a discretised heat transfer fluid flow approach is proposed. This novel numerical model, the so-called combined dynamic thermal network and plug flow stirred tanks (DTN-PFST) model, is developed to represent dynamic thermal behaviour of pipelines, while dealing with transient conduction with varying-time boundary conditions. The details and the advantages of implementation of the proposed model in modelling the long buried pipelines are explained in Section 3.4.

In this Chapter, a summary of the governing equations, finite Volume Method (FVM) and mesh generation are firstly presented. Secondly, the details of the discretised models used to modelling the dynamic response of pipelines with no heat transfer are presented, prior to the discussion on the details of the proposed model with the ability of predicting the dynamic thermal response of pipelines considering the longitudinal dispersion and radial heat transfer. Thirdly, details of the dynamic thermal network (DTN) approach and the theoretical basis of the method are outlined, along with the procedure of calculation of the weighting factor data required in this method. Finally, the combined DTN-PFST model is proposed, and the details of the implementation of the model in modelling the DHS pipelines are discussed.

3.1 Three-dimensional Model

In general, there are three numerical methods dealing with the partial differential equations involved in fluid flow and heat transfer problems: the Finite Difference Method (FDM), the Finite Element Method (FEM) and the Finite Volume Method (FVM). Among these approaches, the finite volume method (FVM) is one of the most frequently used methods for numerical solution of the partial differential equations in dynamic heat transfer analysis, because of its stability along with computational efficiency [Chung *et al.* (2009)]. The use of such a numerical method to solve the governing continuum mechanics equations enables high-fidelity CFD simulations of heat transfer applications. OpenFOAM as an open-source and open-access library is one of several software packages that exists to simplify this task. OpenFOAM implements the cell-centred finite volume method and has a variety of developed solver applications for different types of applications of continuum mechanics [Moukalled *et al.* (2016)]. In this section, an overview of the finite volume and solution methodology is given with the governing equations related to this work.

3.1.1 Governing Equations

Considering the flow as an incompressible, Newtonian, isotropic, Fourier conducting fluid, the governing equations for continuity, momentum (Navier-Stokes) and energy for fluid flow can be written as given below [Nguyen & Wereley (2006)]:

Continuity equation:

$$\nabla.\mathbf{u} = 0 \tag{3.1}$$

Momentum equation:

$$\rho_f \frac{\partial \mathbf{u}}{\partial t} + \rho_f \mathbf{u}.\nabla\mathbf{u} = -\nabla P + \mu\nabla^2\mathbf{u} \tag{3.2}$$

Energy equation for fluid flow:

$$\frac{\partial}{\partial t}(\rho_f h) + \mathbf{u}.\nabla.(\rho_f h) = \lambda_f \nabla^2 T \tag{3.3}$$

Where subscript f and s represent fluid and solid domain, respectively. $\mathbf{u}$ is velocity vector, T is temperature, ρ is the density, λ is the thermal conductivity, c_p is the specific heat capacity and h is enthalpy. The details of the derivation of the equations can be found in the reference fluid dynamics books such as [Moukalled *et al.* (2016); Nguyen & Wereley (2006)]. The energy equation for solid domains and the boundary condition at the interface between the fluid flow and the pipe wall can be expressed as follows:

Energy equation for solid domain:

$$(\rho c_p)_s \frac{\partial T}{\partial t} = \lambda_s \nabla^2 T \tag{3.4}$$

Energy equation at the boundaries between solid and fluid domains:

$$\lambda_s \frac{\partial T_s}{\partial n} = \lambda_f \frac{\partial T_f}{\partial n} \tag{3.5}$$

3.1.2 Turbulence Modelling

For Reynolds numbers above $\mathrm{Re}_{\mathrm{critical}}$, the behaviour of the fluid flow is chaotic and random. As shown in Fig. 3.1 in a certain point through a pipe, the velocity of the turbulent fluid flow oscillates around the mean value randomly over time. This behaviour is valid for the other quantities appearing in the governing equations, such as temperature, enthalpy and pressure [Holzmann (2017)]:

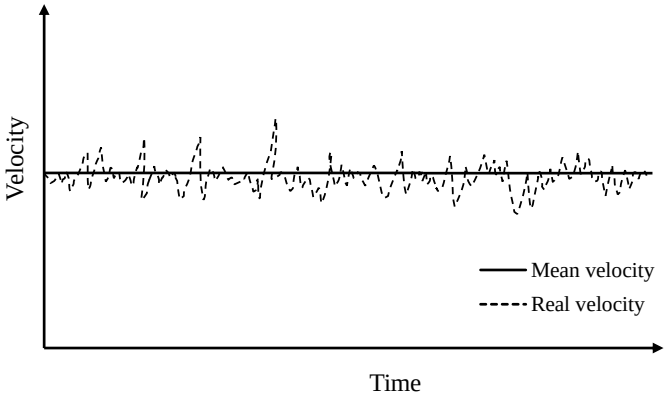

Figure 3.1: Fluctuation of the velocity at an arbitrary point located in a turbulent fluid flow (mean value, real value).

Considering this behaviour of the turbulent flow, the flow components, e.g. velocity vector, can be split into two parts: the mean part ($\bar{\phi}(x)$) and fluctuating part ($\phi'(x,t)$). Thus, the flow property can be written as:

$$\phi(x,t) = \bar{\phi}(x) + \phi'(x,t) \tag{3.6}$$

The mean value can be obtained by using the time-averaging method, which is also known as Reynolds averaging. In this method, the mean value is calculated by averaging the instantaneous flow variable ($\phi(x,t)$) in terms of time, as follows:

$$\bar{\phi}(x) = \lim_{T\to\infty} \frac{1}{T} \int_{t}^{t+T} \phi(x,t)dt \tag{3.7}$$

Please note that if T is long enough, the averaged value is no longer time dependent, thus that $\int \phi'(x,t) = 0$. By substituting all time averaged flow terms in the momentum (Navier-Stokes) equation (Eq. 3.2), the **Reynolds-averaged Navier-Stokes equations (RANS)** can be obtained as below [Versteeg & Malalasekera (2007)]:

Momentum equation:

$$\rho\frac{\partial \bar{u}_i}{\partial t} + \rho\frac{\partial}{\partial x_j}(\bar{u}_i\bar{u}_j + \overline{u_i{}'u_j{}'}) = -\frac{\partial \bar{P}}{\partial x_i} + \mu(\frac{\partial^2 \bar{u}_i}{\partial x_i \partial x_j}) + \rho g_i \tag{3.8}$$

and the continuity equation also can be expressed:

$$\nabla.\bar{\mathbf{u}} = 0 \tag{3.9}$$

In Eq. 3.8, the ($\rho\overline{u_i{}'u_j{}'}$) term is the turbulent stresses, known as **Reynolds stresses**. To solve the RANS equations, the Reynolds stresses need to be modelled.

Over the past years, several turbulence models have been developed to resolve the Reynolds stresses such as $k-\epsilon$, $k-\omega$, $k-\omega$ SST, etc. In this work, $k-\omega$ SST (Shear Stress Transport) model has been used for modelling turbulent fluid flow, as this model is proven to be more versatile than most of the other RANS models [Menter (1994)], and able to predict accurately the near-wall flow [Menter *et al.* (2003)]. Originally, this model has been proposed by Menter (1994), which is the combination of two models: $k-\epsilon$ model, and $k-\omega$ model.

The $k-\epsilon$ turbulence model was proposed by Launder & Spalding (1983) and is widely used in different industrial cases because of its stability and fast convergence, is not able to accurately predict the flow in certain applications, e.g. wall-bounded flows. On the other hand, the $k-\omega$ model proposed by Wilcox (1988), is able to accurately predict the near-wall flow, but is sensitive away from the domain boundary. Thus, it was proposed to combine the two models using blending functions. For further details of the models, the interested reader may refer to [Greiciunas (2019); Moukalled *et al.* (2016)].

3.1.3 Finite Volume Method

The finite volume method (FVM) is an approach to represent and evaluate the governing equations in the form of algebraic equations. Due to the stability and computational efficiency of the FVM, this approach is often being used in industrial applications. In this method, the domain is divided into a set of control volumes (CVs), and the governing partial differential equations are solved in the domain concerned [Wood (2015)]. The control volumes are created by discretisating the domain of interest into a computational mesh combining numerous cells, shown in 3.2. Then, the centroids of these cells are connected to form the CVs [Ferziger & Peric (2002)].

The finite volume method uses the integral form of the generic conservation equation as the starting point for a quantity (ϕ), as below:

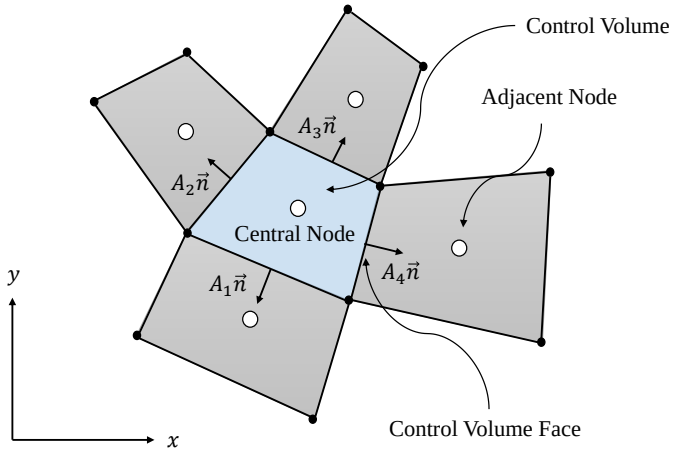

Figure 3.2: A representation of a two-dimensional structured-mesh for the finite-volume method.

$$\underbrace{\frac{\partial}{\partial t}\int_V \rho\phi dV}_{\text{Transient}} + \underbrace{\int_S \rho\phi v.nds}_{\text{Advection}} = \underbrace{\int_S \Gamma\nabla\phi.nds}_{\text{Diffusion}} + \underbrace{\int_V q_v dV}_{\text{Source term}} \tag{3.10}$$

where n, V, S and q_v are the outward surface vector, the control volume, the surface area and the source term, respectively. It is assumed that the cell volumes are time independent so that the time derivative comes out of the integral in the transient term.

3.1.4 Discretization Schemes

To solve the governing equations, the integral of Eq. 3.10 needs to be discretised so that the variables in the equations can be approximated. This is done by using different discretization schemes for each term in the Eq. 3.10. In the following, the discretization schemes used in this work are briefly presented. For better understanding the principles of the discretization schemes, a series of regular control volumes in one direction are used, as shown in Fig. 3.3.

3.1.4.1 Transient Term

In this work, the transient term is discretised using the *implicit Euler formulation of the first-order accuracy*. Due to very small timestep simulation required for the transient simulation in this study, this scheme has been chosen for saving the computational power, expressed as below [Ferziger & Peric (2002)]:

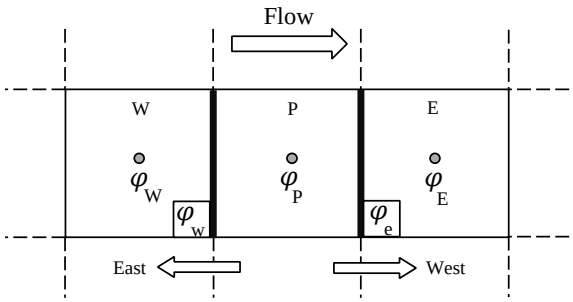

Figure 3.3: A series of regular control volumes with labels.

$$\frac{\partial}{\partial t}\int_V \rho\phi dV = \rho V \frac{\phi^{n+1} - \phi^n}{\Delta t} \tag{3.11}$$

3.1.4.2 Advection Term

Several numerical schemes have been proposed to use for the discretization of the advection (convection) term. In this work, the advection term is discretised using a *linear upwind scheme* with two accuracy levels. In the advection term, the variables are calculated in the surfaces between the CVs. This information is not available and is needed to be approximated and interpolated, since only the nodal values at the centre of CVs are calculated, and not CV surfaces. For simplicity, assuming the flow only from west to east, the term can be discretised to [Ferziger & Peric (2002)]:

$$\int_S \rho U_e \phi dn = \rho U_e \phi_e \Delta n_e \tag{3.12}$$

Where subscript e denotes values at the east face and Δn is the outward surface vector. With the assumption that the flow is only from west to east, ϕ_e can be simply approximated using wind interpolation as below:

$$\phi_e = \phi_E \tag{3.13}$$

Where subscript E denotes values at the centre of the east CV. The *upwind differencing scheme (UDS)* is stable and robust and never yields oscillatory solutions [Ferziger & Peric (2002)]. However, it is numerically diffusive, as this approximation has only first-order accuracy, and cannot deal with rapid variations. Accordingly,

second-order accurate discretisation, e.g. *linear interpolation*, is proposed and widely used for approximation of the advection term. In the linear scheme, the values of the faces of the CVs are interpolated between the two nearest nodes. For the east face, the ϕ_e can be approximated as follows:

$$\phi_e = \phi_E(\frac{x_e - x_p}{x_E - x_P}) + \phi_P(1 - \frac{x_e - x_p}{x_E - x_P}) \tag{3.14}$$

where subscript P denotes values at the centre of the CV. This scheme is less stable than the UDS but considerably more accurate. There are some more second-order accurate schemes proposed for the approximation, e.g. the *linear upwind scheme* and *Quadratic Upwind Interpolation (QUICK)*. In this work, the *linear upwind scheme* with two accuracy levels is used for discretising the advection term. This scheme is more stable with better solution convergence compared with the linear scheme, as it takes two upstream flow values into the account [Greiciunas (2019); Ferziger & Peric (2002)].

3.1.4.3 Diffusion Term

To discretise the diffusion term, the same linear interpolation of second-order accuracy can be used. Considering the east face of the CV, the diffusion term can be discretised as follows:

$$\int_S \Gamma(\frac{\partial \phi}{\partial x})_e dn = \Gamma(\frac{\phi_E - \phi_P}{x_E - x_P})\Delta n_e \tag{3.15}$$

The principles of Finite Volume Method discretization described in section 3.1.4 are not dependent on the type of grid and can be applied for any arbitrary unstructured or non-orthogonal grids. For further details of the aforementioned schemes and other numerical schemes, e.g. higher-order schemes using for approximating the integral of Eq. 3.10, the interested reader may refer to the two reference books [Chung *et al.* (2009); Ferziger & Peric (2002)].

3.1.5 Solution Procedure

Solving the governing equations needs numerical techniques to calculate the coupling of the pressure and momentum quantities, due to the difficulties of dealing with mass

conservation in the incompressible form of the Navier-Stokes equations. Considering the Eq.3.2, it can be seen that are four unknown quantities, the pressure and three velocity components, while there are three equations for momentum equations, i.e. in x, y and z directions. The mass conservation equation (Eq.3.1) can be added as a fourth equation in order to obtain the unknown quantities, but the problem is that the equation does not include the pressure involved in the Navier-Stokes equations. This problem is known as the pressure-momentum coupling problem, and this is why special techniques are required to calculate the pressure and momentum quantities [Holzmann (2017)].

The main idea of all techniques to resolve the problem is to implicitly rather than explicitly account for mass conservation in the calculation of the pressure and momentum quantities [Holzmann (2017)]. This is done by firstly discretising the momentum equations leading to a set of algebraic equations expressed in matrix form as [Greenshields (2019)]:

$$M\left[\mathbf{u}\right] = -\nabla P \tag{3.16}$$

where the matrix $M[\mathbf{u}]$ is the matrix of coefficients. This matrix can be separated into diagonal components ($\mathbf{A}$), and off-diagonal components ($\mathbf{H}$). By decomposing the $M[\mathbf{u}]$, the matrix can be stated as:

$$M\left[\mathbf{u}\right] = A\mathbf{u} - \mathbf{H} = -\nabla P \tag{3.17}$$

Rearranging Eq.3.17, the velocity correction equation can be expressed as:

$$\mathbf{u} = \frac{\mathbf{H}}{A} - \frac{1}{A}\nabla P \tag{3.18}$$

The mass flux equation can be then derived by interpolating $\mathbf{u}$ for the faces of each CV as follows :

$$\phi = \mathbf{u}_f.\mathbf{S}_f = \left(\frac{\mathbf{H}}{A}\right).\mathbf{S}_f - \left(\frac{1}{A}\right)\mathbf{S}_f.\nabla P \tag{3.19}$$

Considering the mass conservation law ($\nabla.\phi = 0$), the pressure equation can be obtained by substituting the calculated fluxes from Eq.3.19 in the mass conservation equation, as follows [Greenshields (2019)]:

$$\nabla.\left[\left(\frac{1}{A}\right)\nabla P\right] = \nabla.\left(\frac{\mathbf{H}}{A}\right) \tag{3.20}$$

Where (P) is only unknown in this equation. After calculating pressure, the mass fluxes are corrected at the cell faces, and in an iterative process, the new velocity field is updated until the residual is less than a specified value. It is worth noting that generally in these algorithms, rather than the pressure (P), the modified pressure ($P_{rgh} = P - \rho gh$) is used in the calculation to include the buoyancy term (ρg) in the pressure correction, although in this work the buoyancy effects are neglected.

There are three main pressure-momentum coupling algorithms proposed for the calculation of the pressure and momentum quantities: Semi-Implicit-Method-Of-Pressure-Linked-Equations (SIMPLE), Pressure-Implicit-Split-Operator (PISO) and Merged PISO–SIMPLE (PIMPLE). All these algorithms are implemented in OpenFOAM such that PISO and PIMPLE are both used for transient problems, whereas SIMPLE is used for steady-state problems. In this work, the PIMPLE algorithm is used to obtain the pressure and momentum quantities considering the transient behaviour of the fluid flow. The PIMPLE algorithm can be thought of as a SIMPLE algorithm for every time step, where outer correctors are set for more iterations in each time step, and once converged, it will move on to the next time step until the solution is complete. Consequently, better stability can be obtained from PIMPLE over PISO, and the maximum Courant number ($Co = u\Delta t/\Delta x$) can be consistently above one without divergence in the numerical solutions. More details about the pressure-momentum coupling algorithms can be found in [Chung *et al.* (2009); Ferziger & Peric (2002); Greenshields (2019)].

3.1.6 Geometry and Boundary Conditions

In this work, four sets of simulations have been carried out considering the different types of boundary conditions applied to the pipeline in the experimental studies. The vertical cross-section of the pipeline section and different fluid and solid regions are shown in Fig 3.4. The simulations performed in this work can be classified based on the types of boundary conditions applied to the pipeline and sand as follows:

A. Three-dimensional ideally insulated pipeline with turbulent fluid flow simulated over short timescales (using region 1).

B. Three-dimensional insulated and uninsulated pipeline with the turbulent fluid flow with conjugate forced convection heat transfer as (A) by using regions 1,2 and regions 1,2,3, respectively.

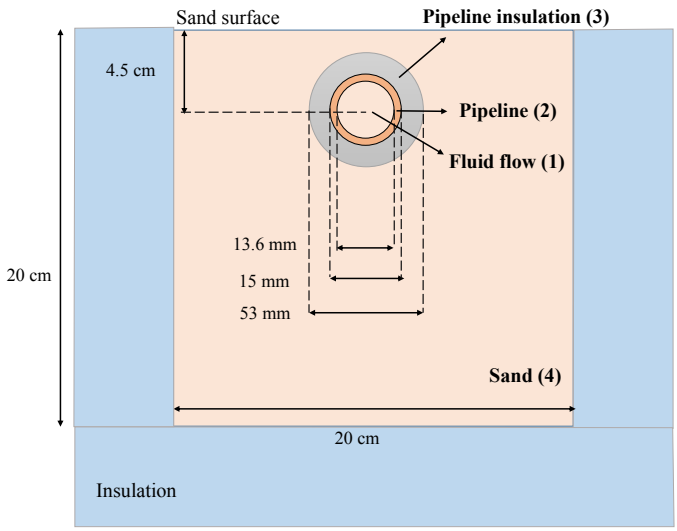

Figure 3.4: The vertical cross-section of the pipeline section in the experimental setup.

C. Three-dimensional buried pipeline with the turbulent fluid flow with conjugate forced convection heat transfer in the sand simulated over long timescales (using regions 1, 2, and 4).

D. Two-dimensional buried pipeline in the sand as (C) (using regions 2, and 4).

In all these cases, the initial temperatures are assigned for each domain based on the corresponding experimental values. In case one, a zero heat flux (adiabatic) boundary condition is applied to the inner surface of the pipeline. For case two and three, the conjugated heat transfer model is used for simulation of the heat interaction between the fluid flow and the pipeline. In case four, Robin boundary condition, or the mixed boundary condition, where the relationship between the temperature and the heat flux is specified ($\lambda \frac{\partial T}{\partial n}|_{Boundary} = h(T_f - T_{Boundary})$ are implemented in the models. The heat transfer coefficient of the pipeline is determined based on the measured flow rate and Re number of the fluid flow, the friction factor of the pipeline and Pr number of the fluid. This mixed boundary condition is also applied to the outer surface of the pipeline, pipeline insulation and sand surface in modelling the heat loss to the ambient air. The details of the calculation of the heat transfer coefficient are discussed in Section 2.3.3.

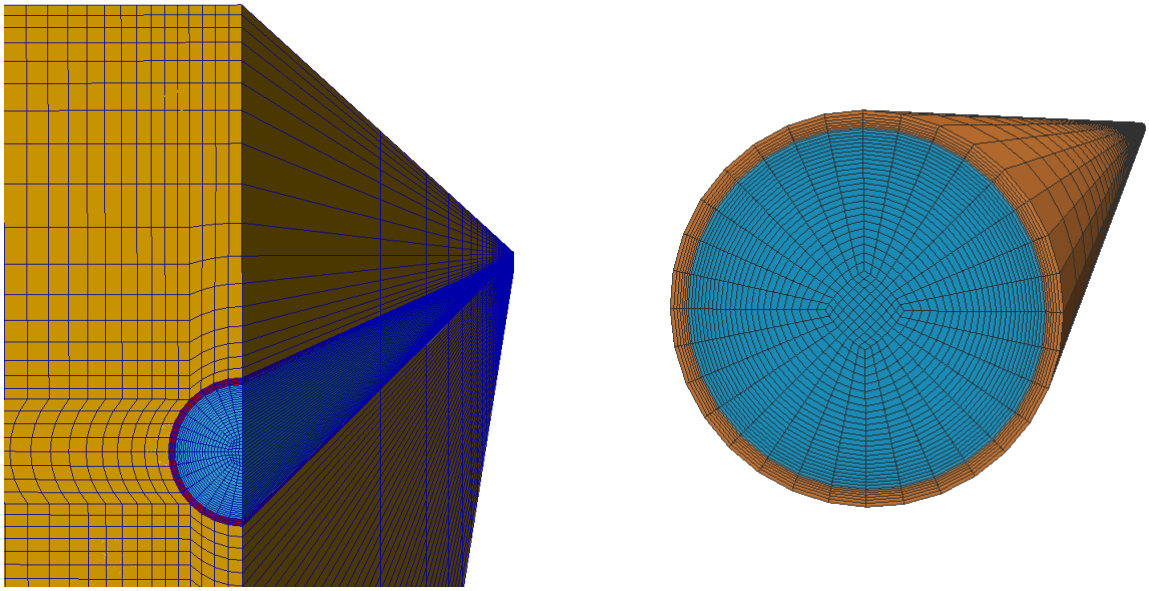

Figure 3.5: Multi-block structured meshes representing the half of the buried pipeline and the pipeline.

3.1.7 Mesh Generation

The pipeline system geometry has been discretised using a three-dimensional multi-block structured mesh generation approach. The structured mesh is generated using the meshing tool within OpenFOAM, blockMesh, such that all of the cells are hexahedral. Individual blocks define the pipeline, pipe and surrounding ground, i.e. sand, and the thermal and physical properties of the materials are set in the corresponding blocks. Using this meshing tool allows exponential reduction in the size of cells in the places where the temperature gradients are expected to be high, i.e. near the pipeline wall and ground surface exposed to air. Cell sizes are correspondingly increased where the gradients are not noticeable, i.e. far from the pipe and ground surface. In this way, the complex geometry of the buried pipelines can be modelled accurately with the moderate computational cost. Moreover, by using the blockMesh tool, the orthogonality of cells can be better controlled compared with unstructured approaches, e.g. the snappyHexMesh tool. Fig. 3.5 displays the discrete representation of the half of the buried pipeline and the pipeline. The mesh independence of the simulation results has been carried out for three cases with the

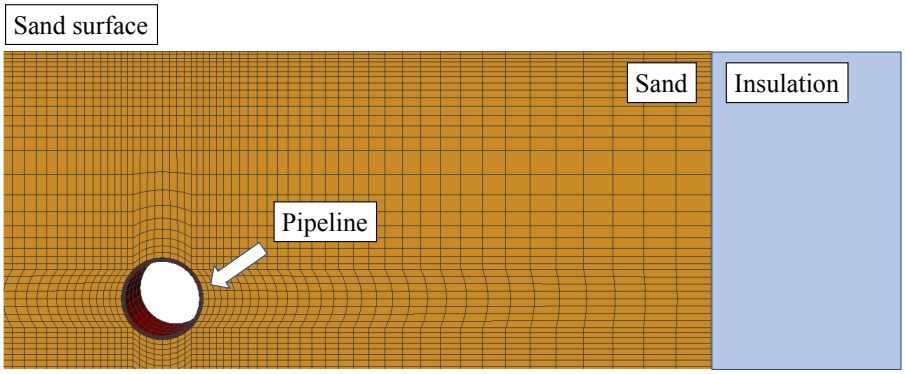

Figure 3.6: A multi-block structured mesh representing the conduction heat transfer from the pipeline in the ground.

different number of cells to make sure the numerical solution is reliable and independent of the geometrical mesh considering the reasonable computational cost. This is done by comparing the simulation results with the experimental data and analytical solutions reported in the literature. The results of mesh independence checking are given in Chapter 6.

In the three-dimensional pipeline model, the fluid flow domain (region 1) is represented by a cylindrical block with a dense mesh near the pipe wall. The pipe wall (region 2 and 3) is represented by a thin cylindrical block with the several layers close the fluid and ground blocks (region 4). The ground is represented by a rectangular block with the long length representing the soil surrounding the long-buried pipe. The top of the ground block is exposed to the ambient air, where the heat losses occur in the type of natural convection heat transfer between the ground surface and the adjacent air. To accurately capture the temperature gradients close to the ground surface as well as the pipeline, higher levels of refinement are needed near these surfaces, as shown in the left-hand side of Fig. 3.5.

According to the boundary conditions of the pipeline section described in the previous Section, a different set of meshes have been generated. For short timescale simulation, the pipeline has been modelled without conduction heat transfer to the ground. In this model, it is assumed that the outer pipeline surfaces are exposed to the air and convection heat losses occur from the pipe surface considering heat conduction occurring in the pipe wall, as shown in the right-hand side of Fig. 3.5.

For long-timescale simulations, the combination of the DTN approach and the plug flow N-continuously stirred tanks (PFNCST) model has been adapted and

Table 3.1: List of the finite volume models developed and their specific purposes.

Simulation case	Simulation timescale	Purpose
Case 1- 3D ideally insulated pipeline	Short timescale	Comparison with the one-dimensional model: axial dispersion plug flow (ADPF) model
Case 2- 3D uninsulated and Insulated pipeline	Short timescale	Comparison with measurement data as well as the one-dimensional models: the N-continuously stirred tanks (NCST), and modified plug flow N-continuously stirred tanks (PFNCST) models.
Case 3- 3D buried pipeline in the sand	Long timescale	Comparison with measurement data as well as combination of the dynamic thermal network (DTN) model and one-dimensional model i.e. the plug flow stirred tanks (PFST) model, so-called the combined DTN-PFST model.
Case 4- 2D buried pipeline in the sand	Long timescale	Calculating weighting functions

used in this work. In this method, the conduction heat transfer in the ground is firstly needed to be modelled to obtain weighting functions which are further used as inputs in the modelling. To this end, the buried pipeline is modelled using Robin boundary condition for the inner pipeline surface and sand surface, i.e. in case 4, without need to modelling the fluid flow directly, as illustrated in Fig. 3.6. The boundary conditions of the pipeline for each case and the purpose of developing the finite volume models are summarised in Table 3.1.

3.2 Short Timescale Modelling Dynamic Thermal Response of Pipelines

In this study, the approach to modelling short timescale dynamic response of heat transfer fluid in pipelines is to utilize a one-dimensional discretised model of the fluid flow through the pipe which takes into account the thermal capacity and longitudinal dispersion. Firstly, the ability of three forms of discretised one-dimensional models in prediction of the dynamic thermal response of pipelines considering the longitudinal dispersion of turbulent fluid flow with ideally insulated pipeline are discussed and examined. Furthermore, a model is proposed combining features of plug-flow and discrete stirred tank representations that take into account the thermal capacitance of the pipe material as well as radial heat transfer. This combination enables the proposed model to simultaneously handle the simulation of momentum and energy balance as well as simulation of the longitudinal dispersion in pipelines. The proposed model is further compared to experimental measurements in Chapter 4.

The assumptions made in this study to implement the approaches can be expressed as follows:

- Fluid flow is incompressible, homogenous and fully developed.
- There is axial symmetry in the temperature and velocity profiles in the pipeline.
- Conduction and convection heat transfer occurs in a radial direction.
- The thermal properties of the materials used in this study are considered constant and time-independent.
- Axial conduction in the fluid, pipeline and the insulation are negligible.
- Bends over the pipeline are treated as a straight pipe with equivalent length. The effect of fittings is not considered.

3.2.1 Modelling Dynamic Responses of Insulated Pipelines

There are a number of research regarding modelling the dispersion of fluid concentration in pipes [Levenspiel & Smith (1957); Taylor (1954b)]. Taylor (1954b) demonstrated that the dispersion of turbulent fluid flow in pipes for chemical species concentration can be successfully modelled by employing axial dispersion plug flow

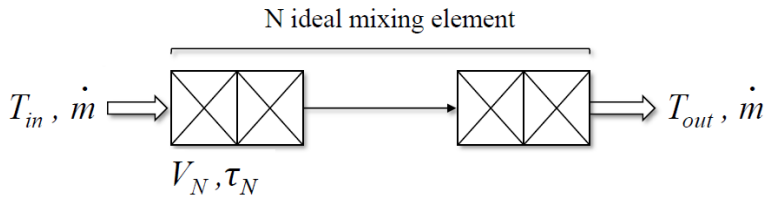

Figure 3.7: A diagram of modelling fluid flow through a pipe using the NCST model.

(ADPF) model. With no source term and no chemical reaction as well as no heat interaction, the one-dimensional of ADPF model can be written as,

$$\frac{\partial C(x,t)}{\partial t} + v\frac{\partial C(x,t)}{\partial x} - D\frac{\partial^2 C(x,t)}{\partial x^2} = 0 \tag{3.21}$$

where $C(x,t)$ is volume chemical concentration, v is the longitudinal velocity and D is the diffusion coefficient which depends on velocity profile and Reynolds number. For the calculation of diffusion coefficient an empirical relation [Wen & Fan (1975)] in terms of Peclet Number Pe (the ratio of advective transport rate to the diffusive transport rate) can be applied as follows,

$$\frac{1}{Pe} = \frac{D}{Lv} = \frac{2r_p}{L}\left(3 \times 10^7 Re^{-2.1} + 1.35 Re^{-0.125}\right) \tag{3.22}$$

where L and r_p are the length and radius of the pipe. Eq.3.21 can be converted to a one-dimensional thermal convection-diffusion form in terms of temperature, if $C(x,t)$ is replaced with $T(x,t)$ where there is no heat loss. The exact solution of Eq.3.21 can be found in the Laplace domain, as follows:

$$sT(x,s) + v\frac{\partial T(x,s)}{\partial x} - D\frac{\partial^2 T(x,s)}{\partial^2 x} = 0 \tag{3.23}$$

For the exit ($x = L$) variation to a step change, the transfer function can be defined by [Skoglund & Dejmek (2008)]:

$$G_{\mathrm{ADPF}}(s) = e^{vl/2D} e^{-(vl/2D)\sqrt{1+(4D/v^2)s}} = e^{-(Pe/2)\left(\sqrt{1+(4/Pe)\tau s}-1\right)} \tag{3.24}$$

Eq.3.24 can be solved only by mathematics software, e.g. Maple, for defined cases, but cannot deal with fluctuating fluid velocity and inlet temperatures. Due to

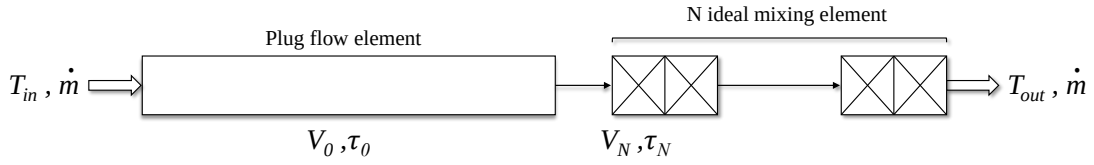

Figure 3.8: A diagram of modelling fluid flow through a pipe using the PFNCST model.

this fact, a number of discrete approximations have been proposed in the literature. The well-known approximation to the ADPF model is referred to as N-continuously stirred tank (N-CST) model. In this model, the pipe is represented by series of well-stirred tanks and is effectively a one-dimensional finite volume or finite difference representation, as shown in Fig. 3.7. However, it is shown by Hanby *et al.* (2002) that this model is sensitive to the number of tanks, and also tends to over predict the diffusivity of the dynamic responses. To deal with this issue, Wen & Fan (1975) derived an expression for the optimal number of tanks for the best approximation to the true ADPF model behaviour as follows,

$$N_{CST} = \frac{vL}{2D} = \frac{Pe}{2} \tag{3.25}$$

Skoglund & Dejmek (2007) proposed a novel model which is a combination of the plug flow with the N-continuously stirred tanks (denoted as the PFNCST model). In this model, a simple time delay is modelled as a plug flow and conceived as being in series with a series of continuously stirred tanks (Fig. 3.8). They showed this can achieve better accuracy to the analytical solution of the ADPF model compared with the N-CST model. Moreover, the number of tanks required in PFNCST model is considerably less than the former model.

In this model, the transit time for fluid flow through a pipe (τ) is divided into two types of elements associated with the transport time delay (τ_0), and remaining time through the N stirred tank elements ($N\tau_N = \tau - \tau_0$), as shown in Fig. 3.8. The heat balance equation on these two elements can be written as follows [Rees (2015)],

$$T_{i=0}(t) = T_{in}(t - \tau_0) \tag{3.26}$$

$$\rho C_p V_N \frac{\partial T_i}{\partial t} + \rho C_p \dot{V}(T_i - T_{i-1}) = 0 \tag{3.27}$$

Where T_i and T_{in} are the fluid temperature at the i-element ($i = 1, 2, ..., N$ denotes the number of ideal mixing tanks) and the fluid inlet temperature, respectively. Also, ρ, C_p, V_N, $\dot{V}$ are the density, thermal heat capacity, element volume and the volume flow rate of fluid flow, respectively. Skoglund & Dejmek (2007, 2008) demonstrated that τ_N can be calculated by Eq.3.28 with very good agreement with ADPF model.

$$\tau_N = \tau\sqrt{\frac{2}{NPe}} \tag{3.28}$$

Accordingly, the volume of each tank and plug flow element as well as τ_0 can be determined for a given number of tanks. It should be noted that this formulation does not consider radial heat exchange or the thermal capacity of the pipe material.

3.2.2 Modelling Dynamic Responses of Uninsulated Pipes

In the current work, we have sought to extend the PFNCST model for modelling dynamic thermal responses of pipes where there is heat exchange with the surroundings and to deal with the thermal capacity of the pipe material. To this end, the finite difference method is used for the calculation of the fluid temperatures and pipe wall temperatures by addition of a further node to take into account the thermal capacity pipe wall and to represent the radial temperature gradients as illustrated in Fig.3.9. This seems a reasonable approximation for relatively thin wall pipes. The model is formulated according to two heat balance differential equations for the fluid and pipe wall nodes as follows,

$$\rho_f C_{p,f} V_N \frac{\partial T_{f,i}}{\partial t} = \rho_f C_{p,f} \dot{V}(T_{f,i-1} - T_{f,i}) - h_f A_i (T_{f,i} - T_{p,i}) \tag{3.29}$$

$$\rho_p C_{p,p} V_N \frac{\partial T_{p,i}}{\partial t} = h_f A_i (T_{f,i} - T_{p,i}) - h_a A_i (T_{p,i} - T_a) \tag{3.30}$$

At each node and at each time step, the fluid temperature (T_f), and the pipe temperature (T_p) are updated by calculation of heat losses according to the fluid and pipe wall thermal capacities ($\rho_f C_{p,f}$ and $\rho_p C_{p,p}$), the heat transfer coefficient between fluid and the inner layer of the pipe wall (h_f), the heat transfer coefficient from the outer layer of the pipe wall to the surroundings (h_a), and the ambient temperature (T_a).

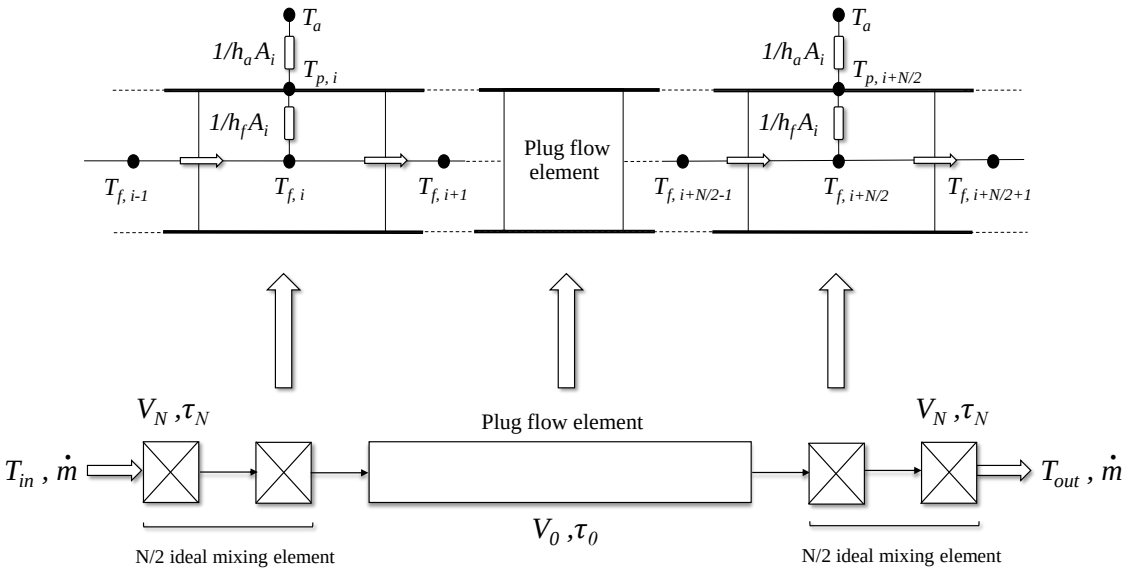

Figure 3.9: diagram of modelling fluid flow through a pipe using the proposed modification of the PFNCST model and the representation of heat transfer from each elements.

In the cases in which the pipe has an outer layer of insulation, the heat transfer coefficient from the pipe surface to the surroundings can be treated as effective overall values as follows [Bergman *et al.* (2011)],

$$h_a = 1/\left(\frac{r_{\text{ins}}\ln(r_{\text{ins}}/r_p)}{\lambda_{\text{ins}}} + \frac{r_{\text{ins}}}{h_{\text{conv}}r_p}\right) \tag{3.31}$$

While h_{conv}, λ_{ins} and r_{ins} are the convective heat transfer coefficient, the thermal conductivity of insulation, and the insulation radius, respectively. Due to the high conductivity of the pipe wall, i.e. generally steel, and the relatively low convection heat transfer coefficient from the pipe surface, the Biot number (the ratio of the heat transfer resistances inside of a body to the surface of a body) is expected to be very low in practical applications (much less than one). This indicates the assumption that temperature distribution through the pipe wall in the radial direction for each element is uniform.

In the PFNCST model, the length of pipe is divided into two main elements: plug flow element and a number of well-mixed tanks. For calculation of the pipe wall and the fluid temperature at the inlet and outlet of each tank element, two heat balance differential equations are solved for each time step. However, for calculation of the temperatures for the Plug Flow element which constitutes the portion length

of pipe, it is necessary to define a proper pipe inner surface boundary condition and a relationship between the wall temperature and the fluid temperature at the inlet and outlet of the element. A convenient way to formulate the relationship between these temperatures would be to use the arithmetic mean of the inlet and outlet temperatures and apply it in a convective boundary condition. However, due to the relatively long length of the Plug flow element in the model at typical flow rates, we found this approach performed poorly. Another approach is to make an analogy with an evaporating-condensing heat exchanger. In this approach, a pipe element is assumed to have the same wall temperature along its length and considered as a heat exchanger that is characterized by an effectiveness parameter ϵ, and the Number of Transfer Units NTU. This approach has been used by Strand (1995) in modelling pipes in underfloor heating systems and by Rees (2015) to model borehole heat exchanger. The relationship between effectiveness parameter which is the ratio of the actual fluid heat transferred to the maximum possible heat transfer is,

$$\epsilon = \frac{\dot{m}C_p(T_{\text{in}} - T_{\text{out}})}{\dot{m}C_p(T_{\text{in}} - T_{\text{p}})} \tag{3.32}$$

Using the evaporating-condensing isothermal wall assumption, the relationship between effectiveness and NTU can be expressed as,

$$\epsilon = 1 - e^{-NTU} \tag{3.33}$$

where,

$$NTU = \frac{2\pi r_p L h_f}{\dot{m}C_p} \tag{3.34}$$

For calculation of the pipe convection coefficient, h_f, the well-known Gnielinski's correlation (Eq. 2.9) has been used in this study, as explained in section 2.3.3. The heat balance at the pipe boundary can also then be formulated as:

$$\epsilon\dot{m}C_p(T_{\text{in}} - T_{\text{p}}) = h_a A(T_{\text{p}} - T_{\text{a}}) \tag{3.35}$$

Using Eq.3.32 and 3.35, the pipe wall and outlet fluid temperatures can be calculated explicitly for a given inlet temperature at each time step.

It was found that simply applying this approach to the PFNCST model proposed by Skoglund & Dejmek (2007) did not give realistic temperature responses where there was heat transfer to the environment. As the initial (and often longest) element

in the pipe represents plug flow but not heat transfer, the effects of heat transfer are also delayed. With a step change in inlet temperature, this is particularly unrealistic.

In this study, the arrangement of plug flow element and well-stirred elements in the PFNCST model has been modified to properly calculate the dynamic heat losses along the pipe. To this end, the number of ideal mixing elements was divided into two sections placed at the inlet and outlet of the pipe with the plug flow element between as shown in Fig.3.9. The new arrangement allows the model to modify the inlet temperature experienced by the plug flow element at each time step to reflect the dynamic heat losses occurring along the pipe. The volume of each tank element and the time required for passing the fluid flow through each tank are obtained in the same way as the PFNCST model. The ability of the proposed PFNCST model in the prediction of the outlet temperature of a pipe with heat losses is presented and discussed in the Chapter 6.

3.3 Long Timescale Modelling Dynamic Thermal Response of Buried Pipelines

For the simulation of the fluid flow and heat transfer in the buried pipeline system in the long timescale, e.g. on a monthly and annual basis, the transient conduction heat transfer through the ground needs to be properly modelled. This phenomenon can be neglected in short timescale simulation as temperature gradients relatively far from the pipeline can be assumed zero. This can be deemed correct due to the low thermal diffusivity of the ground and the insulations generally used around the pipelines resulting in a very small amount of thermal diffusion through the ground in the short timescale, e.g. on minutely basis. However, for the long term simulation, models are needed to be applied with the ability to include all details of the conduction heat transfer through the ground and the ground temperatures variations in the long term. In this work, The Dynamic Thermal Network (DTN) method has been used for the long-timescale modelling dynamic thermal response of pipelines and modelling the heat losses from the pipelines and ground. Then, the model is combined with a discretised heat transfer fluid flow model to equip the model to accurately represent the dynamic thermal behaviour of fluid flow through the pipeline. The details of the method and its theoretical basis are presented in the following sections.

The Dynamic Thermal Network (DTN) method is an approach representing transient conduction processes as a network describing the relationship between time-varying boundary heat fluxes and temperatures. This approach can deal with transient conduction heat transfer in any complex three-dimensional geometry with heterogeneous solid materials, and is specifically suitable for applying for the long-timescale simulations of thermally massive bodies [Fan *et al.* (2013)]. The concept of this approach has been firstly developed by Claesson (2002) for the simulation of heat transfer in building fabric components. The mathematical principles of this method have been extended from the network representation of the steady-state conduction process [Claesson (2003)].

The benefits of applying the DTN method for solving the conduction heat transfer problems compared to other numerical methods can be summarized as given below [Rees & Fan (2013)]:

- arbitrary three-dimensional shapes can be treated as well as simple walls;
- three or more surfaces with their own boundary conditions can be defined. This is useful where pipes are embedded in the structure;
- a response factor approach is likely to be more computationally efficient than a three-dimensional finite volume or finite element numerical method;
- exact discrete forms for piecewise linear boundary conditions can be derived;
- numerical models such as finite volume method can be used to pre-calculate the response factors for complex shapes;

These advantages along with computational robustness of the method motivate the author to use the approach to model dynamic thermal responses of pipelines and ground surfaces in the distribution network of district heating systems. It is worth noting that obtaining the step response and weighting factors in this method can involve some computational efforts for a three-dimensional problem. However, after the calculation of weighting factors for a three-dimensional case, they can be stored for later use in simulations for any operating conditions. In the following sections, the theoretical basis of the method and its discretized form is presented and subsequently the procedure of obtaining the necessary weighting factor data.

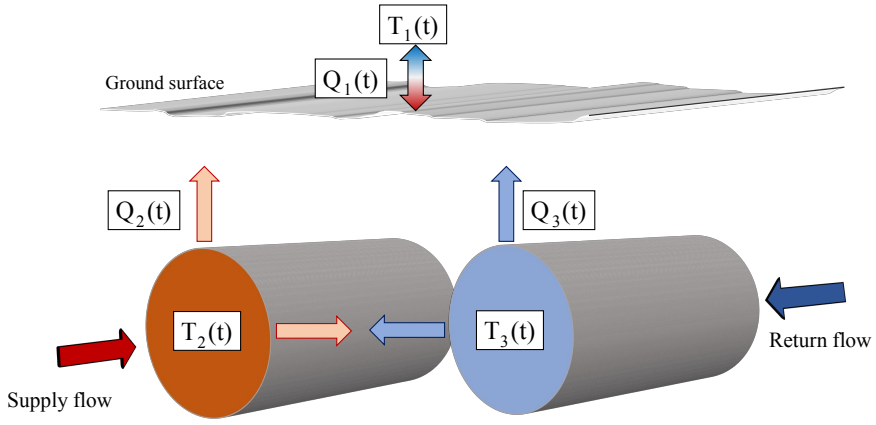

Figure 3.10: Heat transfer problem for two pipes and ground surface

3.3.1 Basic formula

The general formulation of a three-surface problem in the DTN approach can be explained as below (the two-surface formulation can be determined by simple reduction of this formulation). The surfaces can be arbitrary in form, and even can consist of a group of surfaces with the same boundary condition if convenient. In this method, a boundary temperature and flux are specified for each surface, as shown in Fig. 3.10 for buried pipelines in DHSs. In this application, two pipes as a supply pipe and a return pipe with time-dependent temperature ($T_2(t)$ and $T_3(t)$) respectively are situated under the ground, and heat flows from/to the pipes to/from the ground surface with the time-dependent temperature ($T_1(t)$). In this three boundary conduction problem, it can be shown that heat fluxes depend on the boundary temperatures, such that the heat fluxes can be calculated for a given boundary temperature for each surface at any time.

The dynamic thermal network for this three-surface application can be shown as Fig. 3.11. Each temperature of the surfaces is considered as a node which is connected with two other boundary temperatures. There are three surface thermal conductance K_1, K_2 and K_3, for the ground surface, supply and return pipes, respectively. The surface thermal conductances can be calculated by multiplying the surface area (A) in the heat transfer coefficient (h), e.g. $K_1 = A_1 h_1$. Moreover, there are other three thermal conductances K_{12}, K_{13} and K_{23} which are defined as the inverse of thermal resistances of between two surfaces in a steady-state condition, e.g. $K_{12} = 1/R_{12}$.

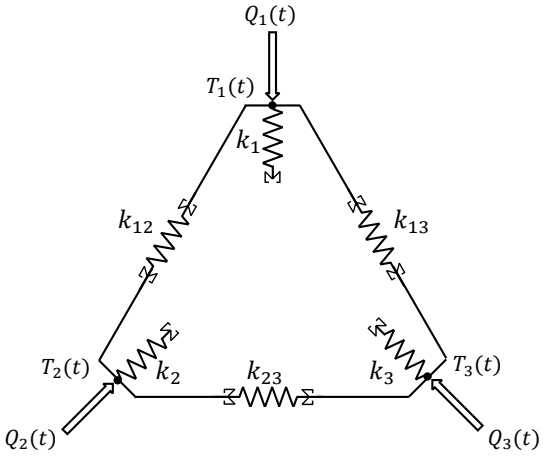

Figure 3.11: Dynamic thermal network representing buried pipelines in DHSs.

In the DTN method, the temperatures ($T_i(t)$) and fluxes ($Q_i(t)$) of the dynamic network are defined at the boundary temperature nodes i.e. environmental temperature nodes, rather than at the surfaces themselves. Accordingly, the terms "boundary" and "surface" are distinct in this method. Moreover, in the DTN approach, the boundary temperatures and fluxes are calculated based on the average current and previous temperatures at the boundaries. To indicate this, the reversed summation symbols (Σ) are used adjacent to the conductances as illustrated in Fig. 3.11.

In the DTN approach, the heat fluxes can be separated into the admittive (or absorptive) and transmittive components. Admittive fluxes are associated with the temperature changes at that boundary. For instance, at an ideally adiabatic surface, the fluxes are totally admittive, and there is no transmittive flux. Transmittive fluxes are associated with the heat transfer from one surface to another depending on the temperature differences between them. Generally, in the transient heat transfer process, both components are present at the surfaces, until the steady-state is approached in which the admittive components become zero. For the buried pipeline application as a three-surface problem, the heat flux at each surface consists of one admittive heat flux (Q_{1a}, Q_{2a}, Q_{3a}) and two transmittive heat fluxes (Q_{12}, Q_{13}, Q_{23}, Q_{21}, Q_{31}, Q_{32}), which are expressed as below:

$$\begin{aligned} Q_1(t) &= Q_{1a}(t) + Q_{12}(t) + Q_{13}(t) \\ Q_2(t) &= Q_{2a}(t) + Q_{21}(t) + Q_{23}(t) \\ Q_3(t) &= Q_{3a}(t) + Q_{31}(t) + Q_{32}(t) \end{aligned} \tag{3.36}$$

The dynamic relationship between boundary temperatures and heat fluxes for this three-surface application can be given in terms of current boundary and averaged temperatures as follows [Claesson (2002)]:

$$\begin{aligned} Q_1(t) &= K_1[T_1(t) - \bar{T}_{1a}(t)] + K_{12}[\bar{T}_{12}(t) - \bar{T}_{21}(t)] + K_{13}[\bar{T}_{13}(t) - \bar{T}_{31}(t)] \\ Q_2(t) &= K_2[T_2(t) - \bar{T}_{2a}(t)] + K_{12}[\bar{T}_{21}(t) - \bar{T}_{12}(t)] + K_{23}[\bar{T}_{23}(t) - \bar{T}_{32}(t)] \\ Q_3(t) &= K_3[T_3(t) - \bar{T}_{3a}(t)] + K_{12}[\bar{T}_{21}(t) - \bar{T}_{12}(t)] + K_{23}[\bar{T}_{23}(t) - \bar{T}_{23}(t)] \end{aligned} \tag{3.37}$$

While $T_1(t)$, $T_2(t)$, $T_3(t)$ are the temperatures of the surfaces, $\bar{T}_{1a}(t)$, $\bar{T}_{2a}(t)$, $\bar{T}_{3a}(t)$ are the admittive average temperatures, and $\bar{T}_{12}(t)$, $\bar{T}_{13}(t)$, $\bar{T}_{21}(t)$, $\bar{T}_{23}(t)$, $\bar{T}_{31}(t)$, $\bar{T}_{32}(t)$ are the transmittive average temperature (i,j= 1...N, and $i \neq j$). The general form of the temperature differences in Eq. 3.37 can be defined in terms of the current temperature and the average temperatures defining by weighted temperature histories for N surfaces as given below:

$$[\bar{T}_{ij}(t) - \bar{T}_{ji}(t)] = \int_0^\infty \kappa_{ij}(\tau).[T_i(t-\tau) - T_j(t-\tau)]d\tau \tag{3.38}$$

$$[T_i(t) - \bar{T}_{ia}(t)] = T_i(t) - \int_0^\infty \kappa_{ia}(\tau).T_i(t-\tau)d\tau, \qquad (i,j = 1...N,\ i \neq j) \tag{3.39}$$

where κ are the weighting functions that can be determined by applying step response function in the surfaces. The details of calculation of weighting factors are described in the following section. It can be shown that in the steady-state condition each average temperature is equal to the related boundary temperature ($\bar{T}_{ia}(t) = T_i$, $\bar{T}_{ij}(t) = T_i$), and the Eq. 3.37 can be converted to the general relationships between the overall conductances and boundary temperatures in the steady state ($Q_1 = K_{12}[T_1 - T_2] + K_{13}[T_1 - T_3]$, etc).

3.3.2 Basic Step Response Solution

In the DTN method, the weighting factors are considered as the main parameter in the model and need to be determined properly. The convenient way for deriving the weighting factors is to apply step changes in boundary temperatures and evaluate the heat fluxes from the surfaces due to each step change. For this purpose, at $\tau = 0$, while the temperatures of all surfaces are kept zero, the boundary temperature of one surface is changed from zero to one. This should be repeated for each surface to derive all the sets of weighting factor data. The transient heat fluxes including

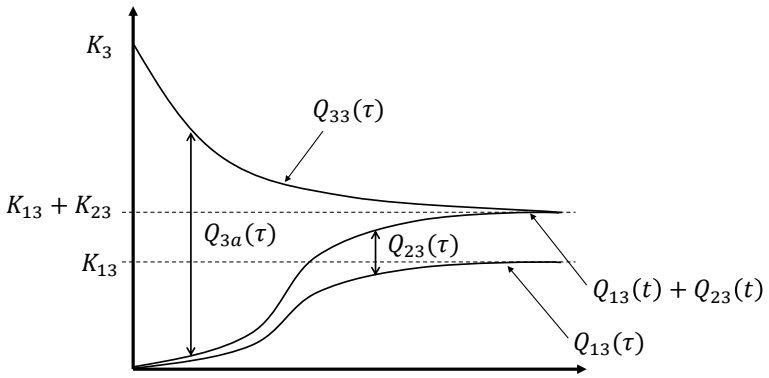

Figure 3.12: Character of the step response boundary fluxes for return pipe.

admittive and transmittive fluxes resulting from imposing a boundary step change for the return pipe is displayed in Fig. 3.12.

At the beginning of applying the step change, the heat flux from the surface is totally admittive, and its value is equal to K_3. As time proceeds, the admittive flux from the surface decreases, and the transmittive fluxes rise. The admittive flux becomes the differences between total heat fluxes from the surface and sum of two other transmitive fluxes of surfaces. As time is approaching the steady-state condition time, the admittive flux approaches zero, and heat flux values between surfaces reach steady-state thermal conductance. These step response fluxes can then be used to obtain the weighting functions, as given below [Claesson (2002)]:

$$\kappa_{ia}(\tau) = \frac{-1}{K_i}\frac{dQ_{ia}(\tau)}{d\tau} \tag{3.40}$$

$$\kappa_{ij}(\tau) = \frac{-1}{K_{ij}}\frac{dQ_{ij}(\tau)}{d\tau} \tag{3.41}$$

It is worth noting that the weighting functions are positive (or zero) and the integral of weighting functions is always equal to one:

$$\int_0^\infty \kappa_{ia}(\tau) = \int_0^\infty \kappa_{ij}(\tau) = 1 \tag{3.42}$$

Generally, the admittive weighting functions ($\kappa_{ia}(\tau)$) drops from high values at the beginning to zero at $\tau = \infty$. On the other hand, the transmittive weighting functions ($\kappa_{ij}(\tau)$) firstly increases from zero to a maximum value, then steadily decreases to zero at $\tau = \infty$. The form of the admittive and transmittive weighting functions are illustrated in Fig. 3.13.

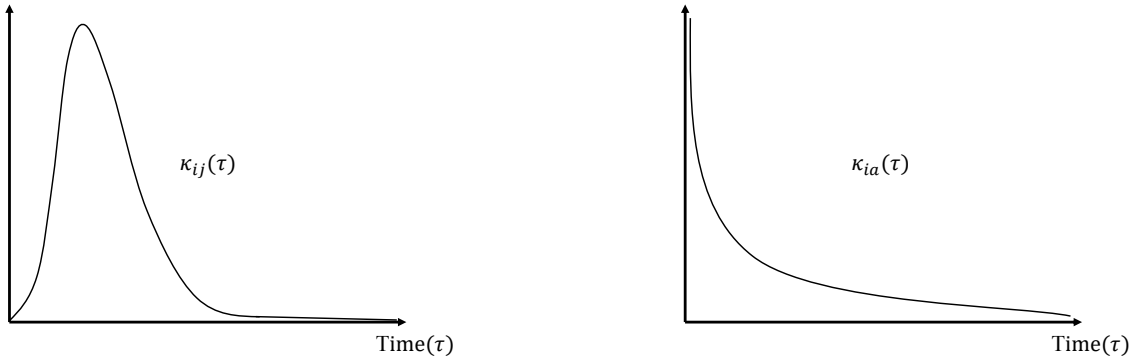

Figure 3.13: Character of transmitive (left-image) and admittive (right-image) weighting functions.

3.3.3 Discretization

In the DTN method, a discrete approximation is required for calculating the numerical solution. It is shown that the continuous functions in this approach can be represented in the discretized forms, in an exact way, when the boundary condition variations are piecewise linear [Claesson (2002), Claesson (2003)]. With discretizing the continuous equations (elaborated in section 3.3.1 and 3.3.2) in time series, the average temperatures can be calculated by the summation of boundary temperature sequences representing the state at previous time steps, multiplied by the weighting factor sequence. Accordingly, The continuous functions of Eq. 3.38, and 3.39 for the current time step (n) and sequence of previous time steps (v) can be expressed in discrete form as follows [Fan *et al.* (2013)]:

$$[T_{i,n}(t) - \bar{T}_{ia,n}(t)] = T_{i,n}(t) - \sum_{p=1}^{\infty} \kappa_{ia,p}.T_{i,n-p} \tag{3.43}$$

$$[T_{ij,n}(t) - \bar{T}_{ji,n}(t)] = \sum_{p=0}^{\infty} \kappa_{ij,p}.[T_{i,n-p} - T_{j,n-p}] \tag{3.44}$$

The admittive and transmittive response fluxes resulting from imposing step changes to the boundary conditions can be averaged over each time step as below:

$$\bar{Q}_{ia}(\tau) = \frac{1}{h}\int_{\tau-h}^{\tau} Q_{ia}(\acute{\tau})d\acute{\tau} \tag{3.45}$$

$$\bar{Q}_{ij}(\tau) = \frac{1}{h}\int_{\tau-h}^{\tau} Q_{ij}(\acute{\tau})d\acute{\tau} \tag{3.46}$$

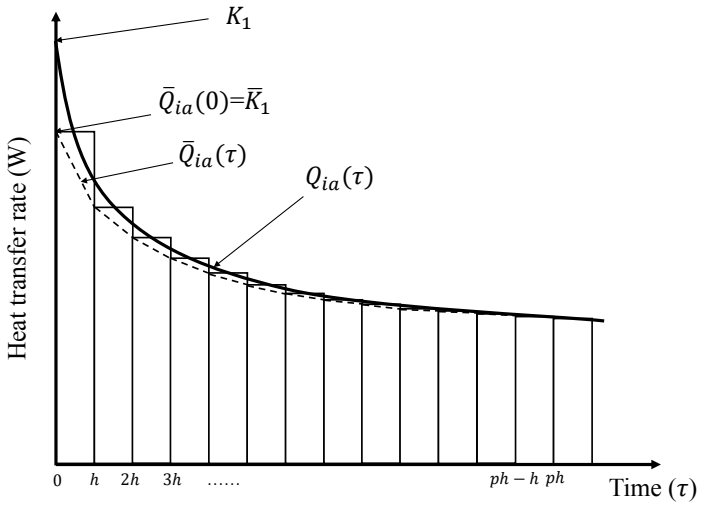

Figure 3.14: Character of the admittive fluxes (solid-line) resulting from an unit step change, with the average admittive fluxes (dot-line), and bars representing the average value over each time step.

In order to obtain the weighting factors, firstly the surface conductances are needed to be modified as follows:

$$\bar{K}_i = \bar{Q}_{ia}(0) \tag{3.47}$$

Considering piecewise linear boundary temperature variations, the weighting factors for the time step (h) can be calculated by dividing the average fluxes over each time step by the modified surface conductances, as given below:

$$\kappa_{ia,p} = \frac{\bar{Q}_{ia}(ph-h) - \bar{Q}_{ia}(ph)}{\bar{K}_i} \tag{3.48}$$

$$\kappa_{ij,p} = \frac{\bar{Q}_{ij}(ph-h) - \bar{Q}_{ij}(ph)}{K_{ij}} \tag{3.49}$$

The admittive step response fluxes (Q_{ia}), and the average admittive step response fluxes($\bar{Q}_{ia}$) over each time step (h) is illustrated in Fig. 3.14. Similarly, transmittive step response fluxes (Q_{ij}) and the average transmittive step response ($\bar{Q}_{ij}$) can be shown. According to the average step response fluxes and the modified surface conductances, the weighting factors can be calculated based on Eq. 3.48 and 3.49. The main advantage of the calculation of weighting factors based on the step response calculation can be stated as the independency of the calculations on the size of the time step. Principally, once the flux responses are calculated, the weighting factors can be derived for any desirable time step size.

3.3.4 Boundary conditions

In the DTN method, the step response heat flux data is calculated based on the assumption that surface heat transfer coefficients (h) are constant. However, in the complex cases with the variable boundary conditions, a more effective approach needs to be implemented. The approach taken in this research to deal with this is to define a boundary temperature, i.e. "effective temperature" (T_e), that when applied by using the predefined constant heat transfer coefficient, gives the expected surface heat flux as applying a more complex boundary condition model. In other words, the effective temperature, or environmental temperature, does not correspond directly to a physical boundary temperature but is applied in the DTN heat balance equations and when the weighted average temperature is updated. This concept has been successfully implemented in the DTN model developed for modelling diaphragm wall ground heat exchangers [Shafagh *et al.* (2020)], and energy pile [Rees & Van Lysebetten (2020)]. In this research, the approach is applied for two boundary conditions we have in the buried pipeline system: at the ground surface and at the pipeline surface.

At the surface exposed to the ambient air, the combination of short-wave radiation, long-wave radiation, convective heat transfer and the evapotranspiration effects takes place. The details of each of heat transfer mechanism occurring on the surface were described in Section 2.3.6.2. One of the considerable advantages of the DTN approach is that the model can effectively deal with the environmental conditions, e.g. solar radiation and wind speed, in both the short and long term simulations. This is done by calculating and updating the heat transfer coefficients for each time step using the well-known correlations and environmental data that are simply read from a file. In this research, the overall ground surface heat transfer coefficient is determined experimentally, using the heat flux data measured via the sensors placed at the ground surface as well as the surface and lab temperature data. This calculated overall heat transfer coefficient and measured lab temperatures are further used as input data to the DTN model.

Due to the significant role of the heat flux at the pipe surface in the driving of the network heat balance, the boundary condition of the pipe surface requires to be properly defined to relate the pipe boundary temperature with both the inlet and outlet temperature in the three dimensional DTN representation. As both the pipeline surface temperature and outlet temperature are initially unknown, it is

necessary to guess the outlet temperature, calculate the heat flux using the DTN model and update the outlet temperature from the fluid heat balance. This iterative procedure leads to both computational inefficiency and even divergence, particularly for very small time steps. [Rees (2015)]. The approach used in this study for defining the relationship between the fluid temperatures and pipeline surface is to make an analogy with an evaporating-condensing heat exchanger. The similar approach has been taken for calculation of the pipe wall and the fluid temperature in the simulation of short timescale dynamic response of the pipeline, described in Section 3.2.2. As mentioned, the assumption of this approach is that the pipeline surface does not vary along its length. This seems incorrect if the length of pipe is long, although by choosing very short timescales compared with the simulation time, e.g. tens of months, the model has shown acceptable results [Shafagh *et al.* (2020), Rees & Van Lysebetten (2020)]. The relationship between pipeline heat balance and the maximum possible temperature difference between the inlet and pipeline surface can be defined as follows:

$$Q_p(t) = \dot{m}C_p(T_{\text{in}}(t) - T_{\text{out}}(t)) = \epsilon\dot{m}C_p(T_{\text{in}}(t) - T_{\text{p}}(t)) \tag{3.50}$$

where the effectiveness (ϵ) can be calculated based on the the Number of Transfer Units ($NTU = (2\pi r_p L h_f)/(\dot{m}C_p)$), as follows:

$$\epsilon = 1 - e^{-NTU}. \tag{3.51}$$

The details of calculation of the pipeline surface heat transfer coefficient (h_f) using Gnielinski's correlation is explained in Section 2.3.3. As in the DTN model only effective boundary temperature (T_2) is required to be defined, the heat balance equations are rearrange to find a way to calculate T_2, without using a complex iteration process. Considering the convective heat transfer at the pipeline surface and Eq. 3.50, the instantaneous heat balance equation at the surface can be defined as:

$$\epsilon\dot{m}C_p(T_{\text{in}}(t) - T_{\text{p}}(t)) = h_p A(T_2(t) - T_{\text{p}}(t)) \tag{3.52}$$

On the other hand, the DTN heat balance equation for the pipeline surface (from Eq. 3.37) can be expressed as:

$$h_p A(T_2(t) - T_{\text{p}}(t)) = K_2[T_2(t) - \bar{T}_{2a}(t)] + Q_{12}(t) \tag{3.53}$$

The term with $\bar{T}_{2a}(t)$ is calculated based on the past temperature history and is known at the start of each time step. On the other hand, due to the very slow changes of the transmittive flux ($Q_{12}(t)$), i.e. because of large thermal mass of the ground, the most recently calculated flux can be taken in the DTN calculation. This approach with some differences is implemented in modelling energy piles [Rees & Van Lysebetten (2020)]. Therefore, the DTN heat balance equation can be rearranged with term ($\bar{Q}$) representing the group of historical fluxes, as follows:

$$h_p A(T_2(t) - T_{\mathrm{p}}(t)) - K_2(T_2(t)) - \bar{Q} = 0 \tag{3.54}$$

Accordingly, $T_{\mathrm{p}}(t)$ can be found by rearranging the Eq. 3.54 as follows:

$$T_{\mathrm{p}}(t) = T_2(t) - \frac{K_2(T_2(t)) + \bar{Q}}{h_p A} \tag{3.55}$$

By replacing $T_{\mathrm{p}}(t)$ into Eq. 3.52, the pipeline surface temperature is eliminated. Hence, the pipeline boundary temperature (T_2) can be calculated based on the inlet temperature and historical fluxes, as follows:

$$T_2(t) = (T_{in}(t) - \frac{\bar{Q}}{h_p A})/\left[1 - \frac{K_2}{h_p A} + \frac{K_2}{\epsilon \dot{m} C_p}\right] \tag{3.56}$$

Rearranging the fluid heat balance equation, the outlet temperature can be found as:

$$T_{out}(t) = T_{in}(t) - \frac{Q_p}{\dot{m} C_p} \tag{3.57}$$

In the DTN approach, the surface temperatures and fluxes are assumed constant in the stream-wise direction, i.e. the horizontal direction in this case, at each time step. Therefore, the pipeline is treated as one long element with the uniform surface temperature where the above calculation procedure is applied to calculate the pipeline outlet temperature, along with surface heat fluxes. In this research, a combined DTN-PFST model has been proposed that basically divides the length of the buried pipeline system into a number of sections according to the PFNCST model recommendation, i.e. based on Pe number. In this model, the initial undisturbed ground and fluid temperature can be assigned to each element of the simulation domain. Moreover, the thermal properties of the materials, e.g. soil properties, can be allocated to each element. This is especially useful for the long buried pipeline of DHSs. However, the main advantage of the proposed model is the ability of the

model to properly represent the dynamic thermal behaviour of fluid flow through the pipeline combining with the transient conduction of the ground. In the DTN-PFST model, the described calculation procedure is applied to each specific section while the outlet temperature of each pipeline element is treated as the inlet temperature of the subsequent pipeline element, by taking into account the time delay described in PFNCST model. More details and advantages of the proposed approach are discussed in Section 3.4.

3.3.5 Derivation of Weighting Factors

To derive the weighting factors, the transient heat fluxes resulting from applying a step boundary condition need to be modelled. The approaches used to calculate the factors can be either analytical or numerical methods. It was shown that for multi-layer walls, analytical methods can be used without much difficulty; however, for more complex geometries, a numerical method is recommended to be used [Fan *et al.* (2013)]. In this study, the weighting factors are extracted from two methods: a detailed numerical model and measurement data. To that end, an experimental setup that is a scaled-down DHS buried pipeline was designed and built. The heat flux sensors and different thermometers with high accuracy used to measure the required heat fluxes and temperatures. Based on the design parameters including: pipeline diameter and depth, insulation box dimensions and the total length of the buried pipeline, the geometry of the system has been generated and meshed using the OpenFOAM library [Weller *et al.* (1998)]. In the numerical model, the conduction heat transfer in the sand with convective boundary conditions is calculated over long timescales, since the time required for the system to reach steady-state condition is considerably long. The multi-block structured mesh used for calculating of conduction heat transfer with convection boundary conditions is illustrated in Fig. 3.6. Due to a large number of cells, i.e. order of hundred thousand, and the long duration of each test, the simulation time for each case is very high. Therefore, the solver used in this study was modified to use increasing time steps, to make the process more efficient. The details of the experiments designed for obtaining the transient heat fluxes resulting from imposing a step boundary condition are explained in Chapter 4.

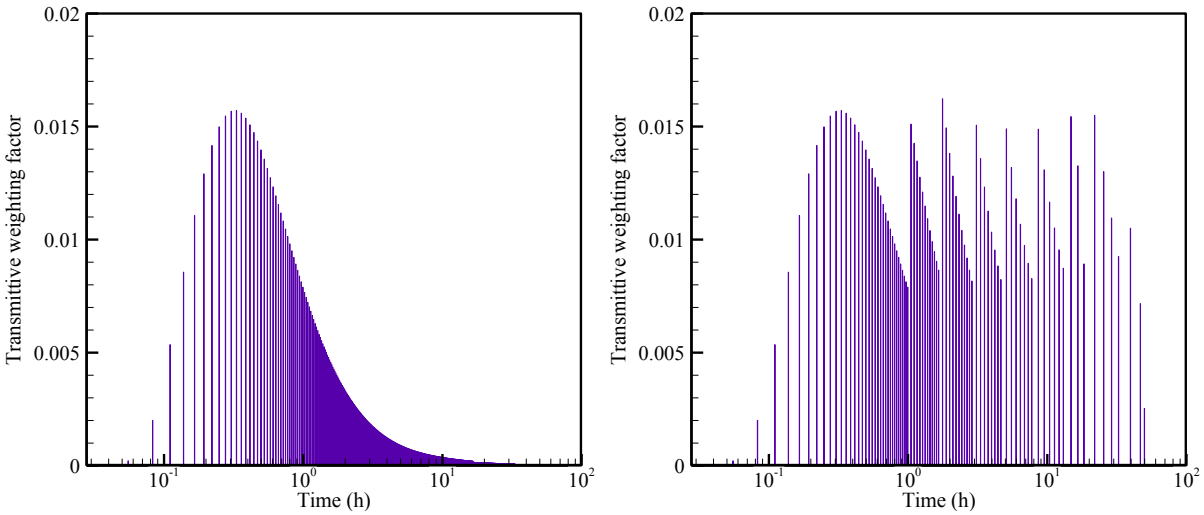

Figure 3.15: Admittive weighting factor series (left-image) and the corresponding reduced series (right-image) with the initial time step size of 100 seconds.

3.3.6 Weighting Factor Reduction

In the DTN method, the flux history can be calculated in varying time step, e.g. order of 1000 steps, to reduce the computational cost of the calculations. However, the weighting factors must be obtained in a fixed time step size (h) based on Eq. 3.48 and 3.49. Hence, the weighting factors can be calculated by interpolating the flux history. Using the fixed time step interval for weighting factor calculation, e.g. one hour, can result in more than a hundred thousand values for cases such as massive structures that the time of a hundred years or more is required to reach to steady-state. These weighting factor data series and the temperature histories are required to be stored and processed in the DTN method and can amount to a large data set in the case of thermally massive constructions. Updating the long temperature histories along with very large data storage requirements for such cases loses the advantage of this method over conventional numerical methods.

To resolve this issue and make this method more computationally efficient, a weighting factor reduction strategy has been developed and implemented by Wentzel (2005). In this approach, the admittive and transmittive weighting factors are aggregated by doubling the time step size in several steps. In this method, both the weighting factor series are divided into several levels (q) with increasing time step intervals. For the transmittive weighting factors (κ_{ij}), the initial time step value (h)

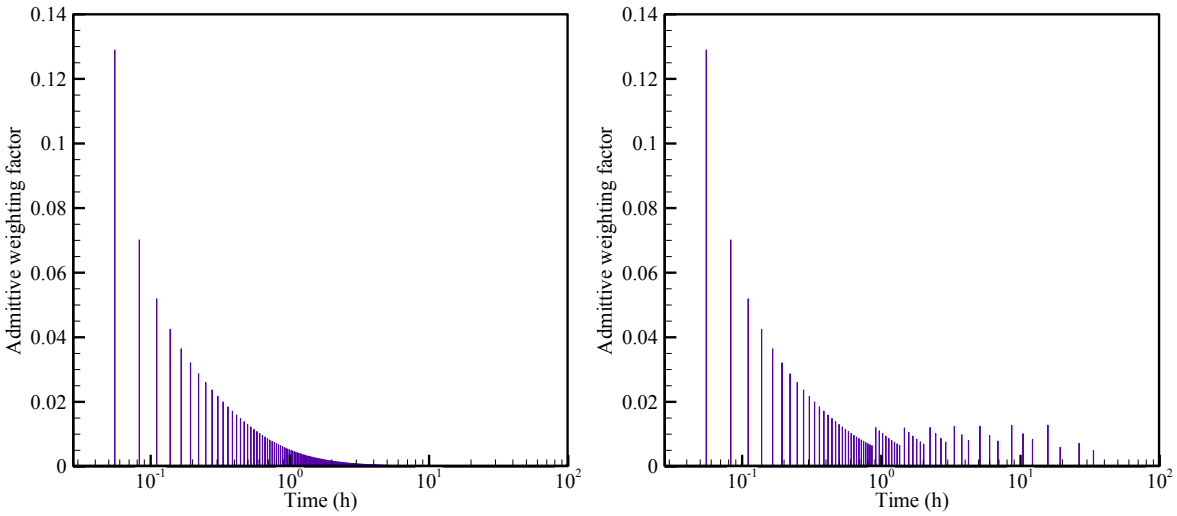

Figure 3.16: Transmittive weighting factor series (left figure) and the corresponding reduced series (right firgure) with the initial time step size of 100 seconds.

is used until the factors reaches to the maximum value, and decrease to the half of the maximum value. After it drops below the half of the maximum, the time step interval is doubled ($2h$) and accordingly the weighting factors aggregated. In the second level ($q = 2$), the series starts after being halved again, and the time step interval become ($3h$). This continues to the level of ($q = n$) where the weighting factors have halved to ($\kappa = \kappa_{max}/2^n$) with a time step size of ($(n-1)h$) that the summation of the weighting factor series approaches closely to 1.0. To ensure that the sum of the series is exactly 1.0, only the last value is slightly adjusted. This procedure is also performed to calculate the admittive aggregated weighting factors. The only difference is that in the calculation of admittive weighting factors the first level starts after the value falls to one-twentieth of the maximum value, due to the importance of properly taking into account the rapid changes of the admittive weighting factors at the beginning reflecting the high admittive heat flux rates. The transmittive and admittive weighting factor series for the heat fluxes in the buried pipeline are respectively illustrated in Fig. 3.15, and 3.16.

It is shown that by using the weighting factor reduction strategy proposed by Wentzel, the weighting factors required in the DTN method can be reduced by two orders of magnitude for structures with the modest number of factors [Wentzel (2005)]. However, for massive structures, even by using the reduction procedure, yet the number of weighting factors can be more than one hundred thousand [Fan

et al. (2013)]. This is due to the fact that the fluxes decay very slowly to reach the steady-state value, specifically for the transmittive heat fluxes. This large number of weighing factor data are then needed to be transferred to the simulation program, e.g. TRNSYS and would be unmanageable and very slow for the annual simulation purposes of massive structures.

Rees & Fan (2013) proposed a more aggressive reduction procedure to improve this situation. In this procedure, the number of weighting factors is limited to a fixed value (n) at each level (q). Therefore, after a given number of weighting factors are calculated at each level, the time step is compelled to double. This occurs independently of whether the weighting factors have not dropped under half of the previous values or not.

Fig. 3.17 illustrates the comparison between the aggressive reduction method and the original one over three levels of reduction calculated from a heat flux series between a buried pipe and ground. It can be seen that at the first level of reduction, 12 weighting factors can be replaced to 8 using the aggressive reduction method, which results in earlier level transitions and consequently lower number of factors compared with the original one. This approach has been used in modelling a number of structures such as foundation heat exchangers [Fan *et al.* (2013)] and the diaphragm wall ground [Shafagh *et al.* (2020)]. It is demonstrated that this procedure can reduce the computational cost by more than three orders of magnitude compared with the no reduction calculation and two orders of magnitude compared with Wentzel's approach [Rees & Fan (2013)]. In this study, the same approach of the weighting factors reduction has been applied in obtaining the weighting factors assigning in the DTN model to modelling the buried pipeline.

3.4 Combined DTN-PFST Model

The approach proposed in this research is to develop a model that represents the dynamic thermal behaviour of buried pipelines over a wide range of timescales. In this approach, the Dynamic Thermal Network (DTN) model constructed in the vertical direction is combined with a discretised model of fluid flow, i.e. PFNCST model. The advantages of applying Dynamic Thermal Network (DTN) approach to modelling the transient conduction heat transfer in any complex three-dimensional geometry with time-varying boundary conditions have been discussed in the previous Sections. However, since in the model the surface temperatures and fluxes are

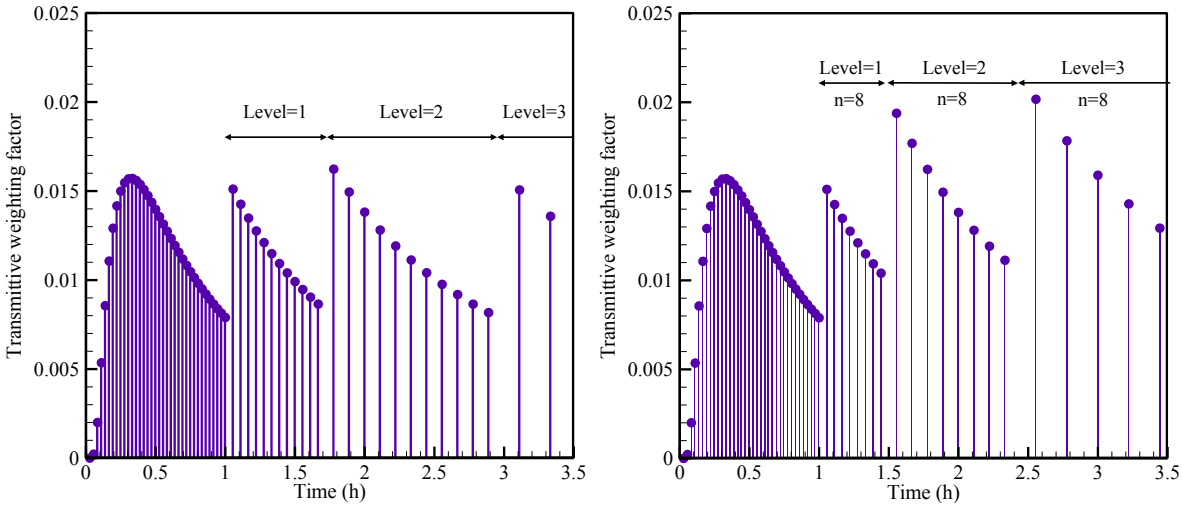

Figure 3.17: Transmittive weighting factor series calculated based on using the original method proposed by Wentzel (2005) (left-image), and the more aggressive reduction method proposed by [Rees & Fan (2013)] (right-image) over three level of reduction.

assumed constant in the stream-wise direction at each time step, the model cannot deal with the dynamic thermal effects of the long pipelines. Additionally, in the DTN mode, the initial temperature and thermal properties of the ground are defined for the entire system. This cannot be correct if the initial temperatures, soil thermal properties or surface properties vary with position along the buried pipeline. Therefore, the discretised model, i.e. the PFNCST model, is proposed to be combined with the DTN model to overcome these issues. The PFNCST model is shown to be able to accurately capture the dynamic short timescale effects of fluid flow in very good agreement with the experimental data [Meibodi & Rees (2020)], also it can be coupled with other numerical models, i.e. the FVM [Rees (2015)]. The combined DTN-PFST model not only allows accurate representation of the dynamic heat transfer through the pipeline but also precisely represents the dynamic transient conduction heat transfer through the ground over a wide range of simulation timescales. The diagram of the combined DTN-PFST model is illustrated in Fig. 3.18.

In the proposed combined model, the buried pipeline system is initially divided into the specific number of vertical sections calculated according to Pe number of fluid flow (the ratio of advective transport rate to the diffusive transport rate). Accordingly, the weighting factors are derived for each section based on the analysis

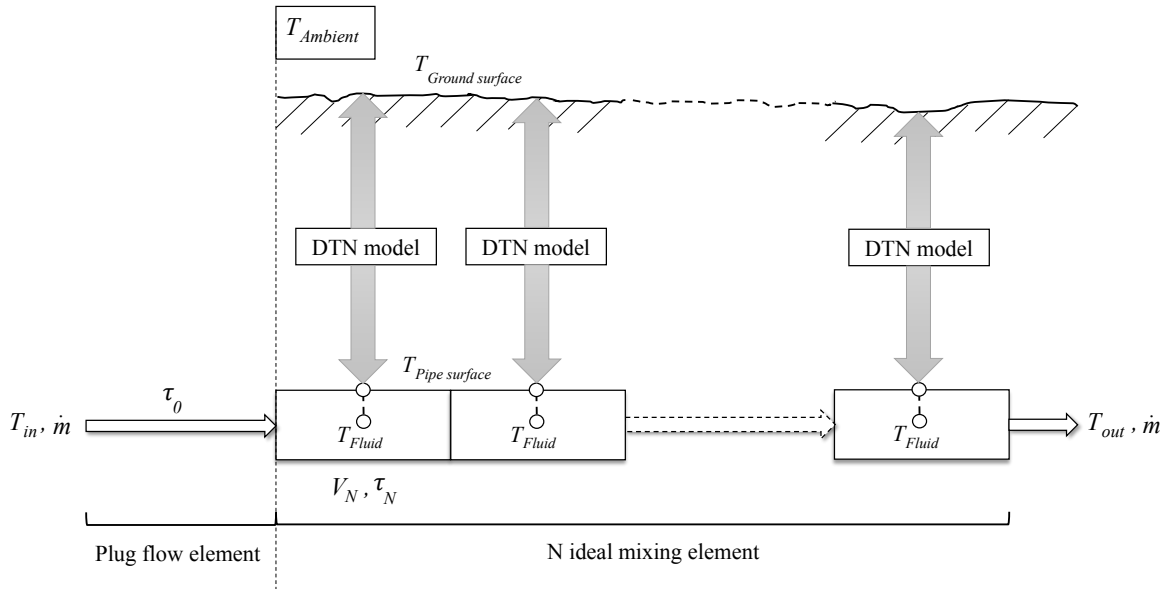

Figure 3.18: A diagram of the combined dynamic thermal network (DTN) method with the discretised heat transfer fluid flow model through a pipeline, i.e. the PFNCST model.

of the step response fluxes for each section. These weighting factors are used as inputs to the combined DTN-PFNCST model. This allows us to specify the certain weighting factors series for each section with different thermal proprieties of the materials and boundary surfaces. Having derived the weighting factors series, they are allocated to each well-stirred elements of pipeline. Then, the DTN approach is applied to each element, such that the outlet temperature of each element is treated as the inlet temperature of the subsequent element, and the boundary temperatures and heat fluxes are updated accordingly. It should be noted that it is shown the PFNCST model is not noticeably sensitive to the number of tanks. Therefore, the changes in the flow rate cannot produce a significant error in the calculation of the outlet temperature of pipelines [Meibodi & Rees (2020)].

It is worth noting that there is a fundamental difference between the modified PFNCST model and the PFNCST model used in the combined model. In the modified PFNCST model, the finite difference method is used to model the dynamic thermal response of pipelines without considering the transient conduction heat transfer to the surroundings, but only the thermal resistance of the pipeline and insulation. In the model, the actual length of the pipeline is divided into two main sections with heat transfer associated with the plug flow element and the number of

continuously stirred tanks. Considering the way that the heat balance equations are solved in the tanks at each time step, it is necessary to locate the plug flow element in the middle of the pipeline to modify the inlet temperature experienced by the plug flow element.

On the other hand, in the original PFNCST model (i.e. proposed by [Skoglund & Dejmek (2008)] and shown in Fig. 3.8) and adopted in the combined model, the buried pipeline system is divided only into the number of elements recommended for the PFNCST model considering the transient conduction heat transfer of the systems, and the simple time delay applied to the calculation based on the PFNCTS model calculation [$T_{i=0}(t) = T_{in}(t-\tau_0)$]. Accordingly, there is no need to replace the plug flow element, since the heat transfer of the entire pipeline systems is calculated according to the summation of heat transfer of each tank that reflects the dynamic heat transfer between the fluid and the ground material. This approach to combine the PFNCST model with other numerical models, e.g. finite volume model [Rees (2015)], has been implemented to modelling the borehole heat exchanger and has shown good ability in modelling the short timescale dynamic effects of the fluid flow.

The application of the combined DTN-PFST model proposed in this research consists of three main processes: step response flux calculations, weighting factors derivation, and model simulation process. In general, since the step response flux calculation is required to be analysed only once (unless the geometry or the thermal properties change), the heat flux series are stored to be used for calculation of weighting factors series. In this research, the step response flux data have been obtained both numerically and experimentally, used for derivation of weighting factors. The simulation steps of combined DTN-PFST model can be summarised as follows:

1. Determining the step response heat flux data for the entire thermal system either numerically or experimentally.

2. Calculating the optimal number of elements based on Pe number of fluid flow using the PFNCST model calculation, and dividing system in the axial direction into the calculated number of sections.

3. Analysis of the step response data for each element to calculate the weighting factor series.

4. Applying the weighting factor reduction procedure and storing the weighting factors.

5. Reading the weighting factor files and allocating them as well as the initial temperature for each section.

6. Calculating the surface heat fluxes using time-varying boundary conditions for each section.

7. Updating the mean temperature data series.

8. Calculating the model outlet temperature according to the PFNCST model and summation of the surface heat transfer rates of each section to calculate the entire heat transfer rates of the surfaces.

Steps 1-5 are pre-calculated prior to the simulation and stored as necessary. Steps 6-8 are needed to be repeated to the end of the boundary condition time series. It is worth noting that since in the model, only the simple heat balance equations are solved and the data is shifted in the temperature update process for each time step, the long time series data can be dealt very efficiently. The accuracy and computational cost of the proposed model are further compared with that of other numeral models in modelling the long buried pipelines in Chapter 6.

3.5 Implementation of the model for simulating DHS pipelines

The main aim in proposing the novel DTN model was to be able to model the thermal performance of current and future district heating pipelines with high computational efficiency. The novel DTN model with the ability to simulate conditions with time-varying inlet fluid temperatures, flow rates and climatic conditions that may fluctuate over sub-hourly timescales can be implemented for modelling the systems over a wide range of timescales up to several years. This makes the model well-suited for routine design and simulation of such systems.

In the proposed approach, a preliminary step is to obtain a weighting factor series. Once these series are determined using either numerical model or experimental data, the fluid temperatures and heat losses of district heating pipeline system

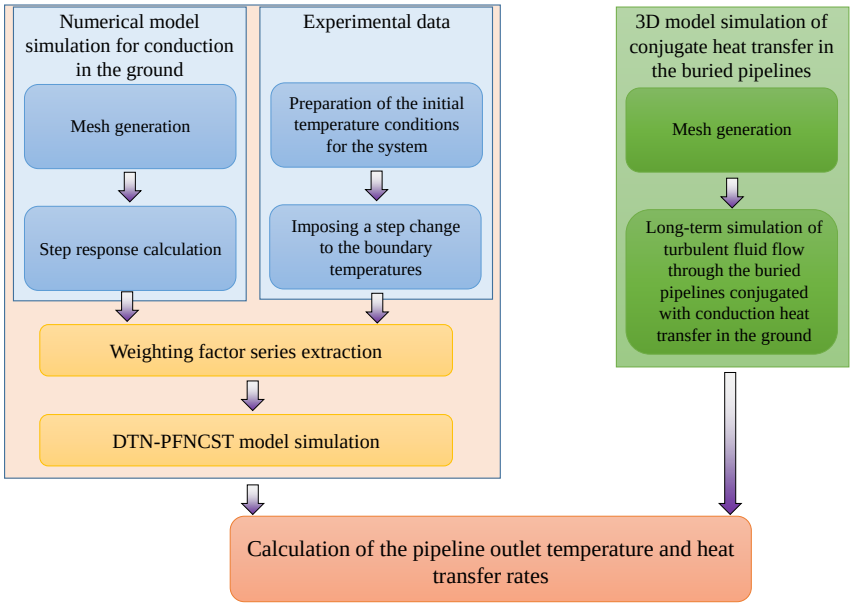

Figure 3.19: A flow diagram presenting the process of deriving the DTN weighting factors from two methods and the DTN simulation, along with the 3D model simulations.

can be obtained using the pipeline inlet temperature and fluid flow data along with climatic conditions (e.g. solar radiation, and wind speed).

To generate the weighting factor series, the step response heat fluxes from the surfaces of the DH pipeline system are required. Once the heat flux data are determined from a convenient way either numerically or experimentally, the weighting factor series can be obtained as explained in Section 3.3. The beneficial feature of the model is that the process of determination of weighting factors needs to be done only once. As a result, the model can use them as many times as the operating condition changes. This enables the model to simulate the dynamic thermal behaviour of the DH pipelines with a relatively very low computational cost for various pipeline configurations over different timescales from sub-hourly to monthly, through the steps described in Section 3.4.

Considering the advantages of implementation of the proposed model in modelling the buried DHS pipelines, it has been sought to validate the proposed model using the experimental data from the scale-down district heating pipeline under different operating conditions. The approach for validation of the model has been to use the measured inlet and ambient temperatures as well as flow rates as boundary conditions to the model and compare the predicted and measured outlet temperatures and heat losses.

In this work, the weighting factor series are calculated according to two methods: using the measurement data from the experimental setup and numerical results from the detailed numerical model developed in this work. Using the measured step response transient heat transfer from the pipeline and ground surfaces, the weighting factors can be calculated based on the approach explained in Section 3.3.6. To numerically calculate the weighting factors, the numerical model (case 4) is developed considering the geometry and thermal properties of the soil and pipeline. In a similar way, by applying the temperature step change to the boundaries of the buried pipeline, the transient heat transfer, and the weighting factor values can be determined.

Using these two sets of the weighting factors, i.e. obtained numerically and experimentally, the model simulation can be carried out to calculate the outlet temperatures and heat losses using the measured inlet and ambient temperatures as well as flow rates. The outputs of the proposed model are then compared with the results of the detailed 3D model (case 3) and measurement data in terms of the prediction of the outlet temperatures and heat transfer rates. Fig. 3.19 displays the DTN modelling process in a flow chart describing the process of calculating weighting factor series from two methods inputted in the model for calculating the heat fluxes and outlet temperature of the pipeline.

3.6 Conclusions

In this chapter, a three-dimensional buried pipeline with the turbulent fluid flow and conduction heat transfer through the surrounding soil using the Finite Volume Method (FVM) has been defined. The mesh approach has been used to generate the mesh such that all of the cells are hexahedral. In the process of mesh generation, the mesh sizes have been adjusted near the surfaces where the gradients are expected to be high, so that the complex geometry of the buried pipelines could be modelled accurately with the noticeably lower computational cost. Moreover, in this chapter, the details of the governing equations and finite Volume Method (FVM) have been discussed. In the following chapters, the detailed 3D numerical models developed are used for three main purposes, as follows:

- Comparison of the 3D model simulation results with the proposed modified PFNCST model in terms of prediction of outlet temperature of pipelines for

short timescale simulation. This allows us to evaluate the accuracy and computational time of the proposed model in comparison with the detailed 3D model.

- Calculation of the step response heat flux data to derive the weighting factor series as the main parameter of the DTN approach. The output of the DTN calculation using the weighting factor series obtained numerically and experientially are then compared with the measurement data to investigate the approaches of deriving weighting factor series.

- Comparison the 3D model simulation results with the dynamic thermal network model (DTN) and the combined DTN-PFST model in terms of prediction of heat transfer rates and the outlet temperature of the buried pipelines in order to evaluate the accuracy and computational time of the proposed model.

In this research, a numerical model has been proposed to modelling the dynamic thermal response of pipelines considering the short timescale effects affecting the pipe thermal responses. In this model, a discretised approach is used to modelling short timescale dynamic response of heat transfer fluid flow in pipelines which takes into account the thermal capacity and longitudinal dispersion of the fluid flow. The proposed model is able to simultaneously handle the simulation of momentum and energy balance and the simulation of the longitudinal dispersion in pipelines. The proposed one-dimensional model is then compared with the detailed 3D model and the experimental data to evaluate the proposed model in terms of the accuracy and computational expense in chapter 6.

Moreover, the Dynamic Thermal Network (DTN) approach has been adopted for the long-timescale modelling dynamic thermal response of pipelines. This method, as a novel approach is able to properly deal with transient conduction in the heat flow region with time-varying boundary temperatures. However, the dynamic behaviour cannot be considered in this approach, and furthermore, the thermal properties of the system including the surface condition and the initial temperature cannot be defined for different sections of the buried pipeline. To overcome these two main issues, a combination of the dynamic thermal network (DTN) approach with the plug flow with N-continuously stirred tank (PFST) model has been proposed.

The details of the combined DTN-PFST model and the theoretical basis of the method along with the boundary conditions of the surfaces have been described in

this chapter. Validation of the DTN model and the combined DTN-PFST model developed in this research are discussed in Chapter 7. Moreover, the advantages of the combined DTN-PFST model over other numerical models when applied to efficient routine dynamic thermal analysis of the district heating pipeline are also discussed in chapter 7.

Chapter 4

Experimental Method

This chapter describes the details of the design of the experimental setup and measurement systems, followed by the explanation of the methodology used to make the experimental measurements. The details of the calibration and uncertainty calculation of the measurement systems are elaborated in Appendix A. The primary purposes of building the experimental setup and conducting the experiments can be stated as below:

- to evaluate the dynamic thermal behaviour of the pipeline with different boundary conditions.
- to study the short timescale dynamic effects occurring in delivering the hot water in the pipelines for a range of operating conditions.
- to provide the reliable experimental data for validation of the proposed numerical models for both the short and long timescale thermal responses.

Data collected from the experimental setup is used both as input data for the numerical model, i.e. the DTN model, and as the reliable data for validation of the novel numerical models proposed in this research including the modified PFST model and the combined PFST-DTN model.

The literature review established that there are no experiments focusing on the short time scale dynamic effects of buried pipelines with heat transfer to the surroundings. Although, in a number of recent research studies [Dalla Rosa *et al.* (2013); del Hoyo Arce *et al.* (2018); van der Heijde *et al.* (2017)], the short timescale response of a range of pipelines have been experimentally investigated. However,

in these works, the short dynamic thermal response of pipelines is only evaluated without considering the effect of heat conduction in the ground and heat losses from the ground surface. Therefore, it seemed worthwhile to gather further experimental data focusing on the short timescales dynamic thermal responses of the pipelines, specifically used in the DHSs, for different operating conditions. To this end, a new experimental facility was designed and developed that represents a scaled-down pipeline in district systems, and two main types of the experiments have been conducted.

The objective of the first set of experiments is to experimentally evaluate the short timescale dynamic effects, such as longitudinal dispersion, on the dynamic thermal response of the pipeline over a typical range of operating conditions representative of DH pipelines. To this end, a step change is imposed on the inlet temperature of the pipeline, and the fluid temperature is measured at different distances from the pipeline inlet, along with the fluid flow rate in very short intervals (of the order of one second). In this way, the shape of the temperature profile due to the step change can be determined, and the effects of the dynamic transport of heat, the pipe wall and fluid flow thermal capacities as well as the longitudinal dispersion of fluid flow can be investigated. The test duration of this set of the experiments is around the nominal transient time of the fluid flow (τ), i.e. the time required for the fluid flow to reach the specific location from the inlet (Eq. 2.3). According to the fluid velocity and the distances of the temperature sensors from the pipe inlet, the duration of this set of the tests varies between a few seconds to less than a hundred seconds. Therefore, this set of experiments is termed as "short timescale experiments" in later discussions.

The main objective of the second set of experiments is to investigate the effects of dynamic conduction heat transfer of the ground on the thermal response of the pipeline. For these purposes, a temperature step change is applied to the pipeline and ground surface to evaluate the thermal response of the pipeline along with the dynamic heat losses from the surfaces. The ground material is represented by sand added to bury the pipe below a simulated ground upper surface exposed to the lab environment. This is carried out by measuring the heat fluxes in addition to fluid flow temperatures from the moment of applying the step change until the system reaches the steady-state conditions (of the order of ten hours in the scale buried pipe system). Therefore, this set of experiments is termed as "long timescale experiments". The experimental data from both experiments are further to use for

validation of the proposed numerical models. The details of measurement, control and procedure of both sets of the tests are elaborated in the following sections.

4.1 Experimental Design

The main experiments in this study comprised a series of step change thermal response tests conducted on the pipeline system with different boundary conditions over a range of operating conditions. In these experiments, the pipeline inlet temperature and fluid flow rate were varied in a way to allow the proper temperature step change to be applied over the typical range of water velocities found in the DH pipelines. Accordingly, one consideration in designing and building the experimental set up was to control the circulating water such that the range of the water flow rate and Reynolds numbers to be in a comparable range to the operating DHSs. The typical water velocity in DHSs is reported between 0.3 to 1.1 m/s [Sartor & Dewalef (2017)]. Therefore, the experimental setup was designed and built to provide the range of the variation of the water velocity in the pipeline section close to this range, i.e. 0.25 to 1.25 m/s. However, due to scaling down the pipeline and particularly the diameter of the pipeline, the Reynolds number becomes considerably lower those found at full scale. The range of the Reynolds numbers of flowing water in the down-scaled pipeline can be varied between almost 4000 and 20000. These Reynolds number values are lower than typical Reynolds numbers found in the main distribution pipes of full-scale systems, i.e. 7.5×10^4 and 8×10^6 [Gabrielaitiene *et al.* (2008)]. However, they frequently occur in oversized pipelines and in the networks that serve low heat density areas [Gabrielaitiene *et al.* (2008)].

The main experiments conducted in this research can be classified according to the timescale represented. In the short timescale experiments, the pipeline's dynamic thermal responses are evaluated for the pipeline with two boundary conditions: uninsulated copper pipeline surface exposed to the air (maximum possible heat transfer from the pipeline surface), and completely insulated pipeline (minimum heat transfer from the pipeline surface). The thermal response of the pipeline is investigated under these two boundary conditions by applying a step change in temperature at the pipeline inlet and by measuring the variations of fluid temperature at certain distances along the pipe at four different flow rates. These temperature data are later used to validate the short timescale modelling dynamic thermal response of pipelines, proposed and developed in this research.

In the long timescale experiments, the dynamic thermal behaviour of the buried pipeline in the sand is investigated under imposing the step change to the fluid temperature in the pipeline or by removing insulation at the ground surface. In one set of the long timescale experiment, the initial temperature of the buried pipeline system is equal to the lab temperature, and a step change is applied to the inlet temperature of the pipeline. In another long timescale experiment, the buried pipeline system is completely insulated by thoroughly covering the ground surface, and heated up to reach the desired temperature. Having reached the desired temperature, a step change is imposed to the ground by removing insulation at the ground surface. In both experiments, the transient condition of the sand and thermal response of the buried pipeline are assessed over the experiments from the moment of applying the step change until the system approaches steady-state conditions.

One objective of the long timescale experiments is to evaluate the effects of dynamic conduction heat transfer of the surrounding ground on the buried pipeline's thermal responses. This is carried out by measuring the inlet and outlet temperature of the pipeline once the step change has been applied to the pipeline or ground surfaces. Another objective of the long timescale experiments is to measure the dynamic heat transfer rates from the pipeline and ground surfaces. This step response heat transfer data is further used as the main input for obtaining the weighting factor series required in the DTN model and validation of the proposed models. Table 4.1 presents the summary of the sets of experiments conducted in this research in terms of the timescales, boundary conditions, and the type of temperature step change imposed at the boundaries.

In the long timescale experiments, the step response heat fluxes from both the pipeline and ground surfaces need to be measured appropriately. For the ground heat flux measurement, three precise heat flux sensors have been placed on the sand surface to detect even tiny surface heat flux variations and measure them accurately. The measured heat flux data along with measuring the surface and ambient temperatures are also used to determine the convective heat transfer coefficient of the ground surface. The details of the heat flux sensors and their placement, as well as the temperature sensors, are described in 4.3.4.

The calculation of the pipeline surface heat fluxes is made by solving the fluid heat balance equation at each time step, based on the measured temperature difference between the inlet and outlet of the pipeline, and the mass flow rate. Since the dynamic conduction process is mostly of interest in this set of experiments, the

Table 4.1: The thermal and boundary conditions of the main sets of experiments.

Test types	Timescales	Pipe boundary conditions	Boundary at which the step change is applied	Initial condition
Case 1	Short timescale	Uninsulated	Pipe inlet	Pipe inlet temperature
Case 2	Short timescale	Insulated	Pipe inlet	Pipe inlet temperature
Case 3	Long timescale	Buried in sand	Pipe inlet	Pipe inlet temperature
Case 4	Long timescale	Buried in sand	Ground	Lab temperature

fluid flow rates are required to be constant and similar for both long-timescale step change tests on the pipeline and the sand surfaces. Later, the convection coefficient can be adjusted for the final proposed model for different fluid flow rates. The details of controlling and measuring the fluid flow rate in the system are described in Section 4.3.

In addition to the measurement of fluid flow temperature, ground surface heat flux, and fluid flow rate, the lab temperature also needs to be measured and recorded during the tests. In the short timescale tests, the lab temperature is used to calculate the dynamic pipeline heat losses. In the long timescale tests, the lab temperature is used as an essential parameter in the model calculation. It should be noted that all the step response heat flux data measured in the long timescale experiments are then scaled to find values equivalent to a unit step change (0-1), as required in the DTN models. In this way, the step response heat flux data becomes independent of the initial temperature conditions of the experiments. The experimental results for both short and long timescale tests are explained and discussed in Chapter 5.

It is worth noting that many long timescale experiments have been conducted in almost six months before achieving two set of acceptable experimental data. The difficulties and challenges of performing the long timescale experiments took many efforts and time in this research. The main challenges of this set of the experiments can be stated as: (i) keeping the lab temperature constant in an acceptable range over almost two days, i.e. less than 0.9 K (ii) tuning the PID controller in a way to properly deal with nearly 22 K step change at the beginning of the experiments and

keep the inlet temperature constant with acceptable variations, i.e. almost less than 0.2 K. The tuning process particularly took considerable time and efforts, due to dynamic of the system and involvement of conduction heat transfer in the system, that makes it longer for the system to be stabilized with the lab temperature in order to repeat the required tests for PID tuning purposes. Failure in keeping the lab temperature constant, e.g. opening the lab door by someone during the tests, or the PID controller resulted in repeating these two-day tests for several times. Additionally, several preliminary long timescale experiments have been conducted to ensure the working temperatures and range of fluid flow rate are suitable for both tests.

4.2 Description of the Experimental Apparatus

The scaled-down district heating system pipeline is built in the building physics Lab (G02a) in the School of Civil Engineering at the University of Leeds. The depth, diameter, and length of the pipeline in the rig have been chosen in a way to be proportional to the typical characteristics of realistic pipeline networks in the DHSs within the space limitations of the lab and practically achievable pressure drops.

Due to the relationship between the length and diameter of the pipeline, pressure drop, and head of the pump, there is a limitation in designing and sizing the pipeline. This issue should be carefully considered in choosing the length and diameter of the pipeline and a suitable type of pump. To this end, considering the copper pipeline diameters available in the market (e.g. $12\,mm$, $15\,mm$, $22\,mm$, etc.) and the space constraints in the lab to bury the longest practically possible pipeline in the boxes (e.g. two boxes, three boxes and four boxes), the total pressure drop of the system was calculated for different scenarios. Based on the calculated pressure drop and the available adjustable speed pump in the market, three boxes were chosen to include the $15\,mm$ pipeline. Considering the typical DH pipeline sizes, e.g. DN250, and their typical depth, i.e. between 0.8 to 1.2 m, the depth of the copper pipeline is chosen 4.5 cm by scaling down the sizes to the typical DH pipe sizes and their depth. Due to the space constraints in the lab, the pipeline is buried into the three boxes $5\,m$ long to have the longest practical length of the pipeline. This allows having a long pipeline in relation to the pipe diameter, such that the distance between the pipeline inlet and outlet is $15.5\,m$. The sketch and dimensions of the test rig are illustrated in Fig. 4.1.

To build the boxes, the Styrofoam insulation board (*FLOORMATE™ 300-A*) with a thickness of 50 mm has been used. These insulation board with considerably low thermal conductivity, i.e. 0.033 W/Km, are used to construct the boxes with 200 mm width in order to insulate each box of sand from another and surroundings properly and to limit interaction between the pipes. All three boxes are placed into the external wood box to ensure the test rig is sturdy enough to stand the further insulation boards and weights required to put on the top of the sandboxes in one part of the experiments explained in detail in Section 4.5. The pipeline in the test rig is shown in the insulation and buried in the sand in Fig. 4.2.

The sand filling the boxes is the specific dry fine sand also used in a related research project in Sheffield (PLEXUS - Priming Laboratory Experiments on Infrastructure and Urban Systems). Due to the importance of the thermal properties of the sand in modeling the buried pipeline, these properties were measured by the precise TEMPOS Thermal Properties Analyser. The details of the thermal properties measurement and the uncertainty of the measurement are discussed in Appendix C. These thermal properties, including thermal conductivity and thermal diffusivity of the sand, are further used to be set into the numerical models developed in this work.

To provide the required circulating hot water with specific temperature and flow rate based on the objectives of the experiments, the hydraulic circuit has been divided into two parts, which are separated by solenoid valves. One sub-circuit represents the pipeline section shown in Fig. 4.2 to be tested, and the other represents a heat source to provide circulating hot water at a controlled temperature. The schematic diagram of these two pressurised circuits in the experimental system is

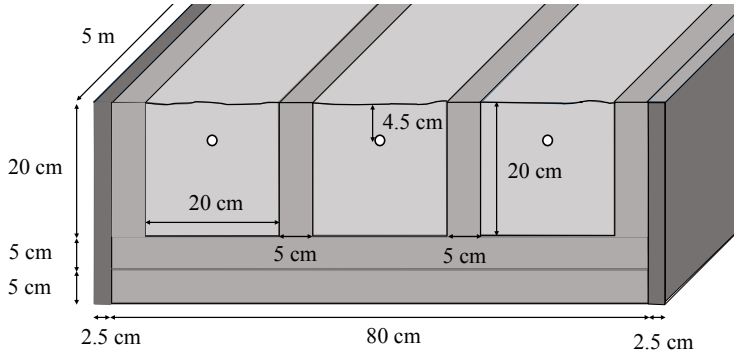

Figure 4.1: The sketch of the buried pipeline in the test rig.

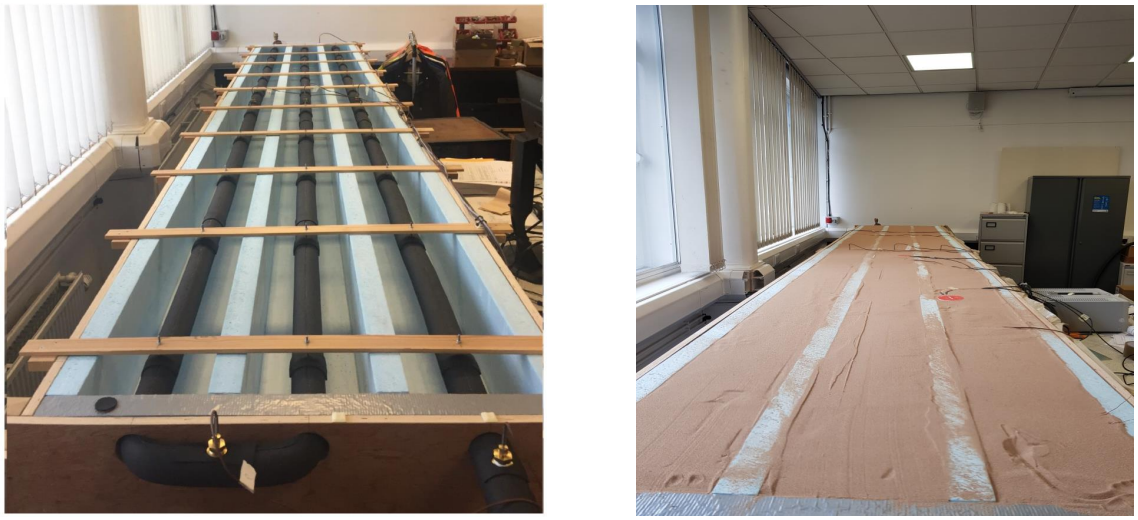

Figure 4.2: Photographs from the pipeline section in the experimental setup for the cases that pipeline were insulated (left-image), and buried into the sand (right-image).

illustrated in Fig. 4.3. The second sub-circuit providing circulating hot water consists of an adjustable-speed pump, a flow-meter, two electric heaters, two solenoid valves, an expansion vessel, a fast response pt100 sensor (accuracy 1/10 DIN) inserted into the pipeline and used to measure the inlet temperature for the test pipeline section. The second sub-circuit with the components is illustrated in Fig. 4.4.

In the all set of the experiments for both short and long term tests, applying a step change in the inlet temperature to the pipeline test section was required for the evaluation of the dynamic thermal response of pipeline. To this end, the heat source circuit is pre-heated by circulating fluid through the heaters whilst the main test section is at ambient temperature. When conditions are stabilised, the step change in inlet temperature is applied by opening the solenoid valve between the two circuits and the heat input is controlled by the PID controller to maintain a constant inlet temperature. Temperatures and the flow rate are measured and logged during the tests at the specific interval depending on the type of the experiments, i.e. short or long term tests. The details of the procedure of each type of experiments are discussed in Section 4.4 and 4.5.

The temperature sensors used in the pipeline section are thermocouples type T, with a sheath diameter of 1.5 mm, which are inserted into the pipe to measure the water flow temperature directly. The ambient temperature in the experiment

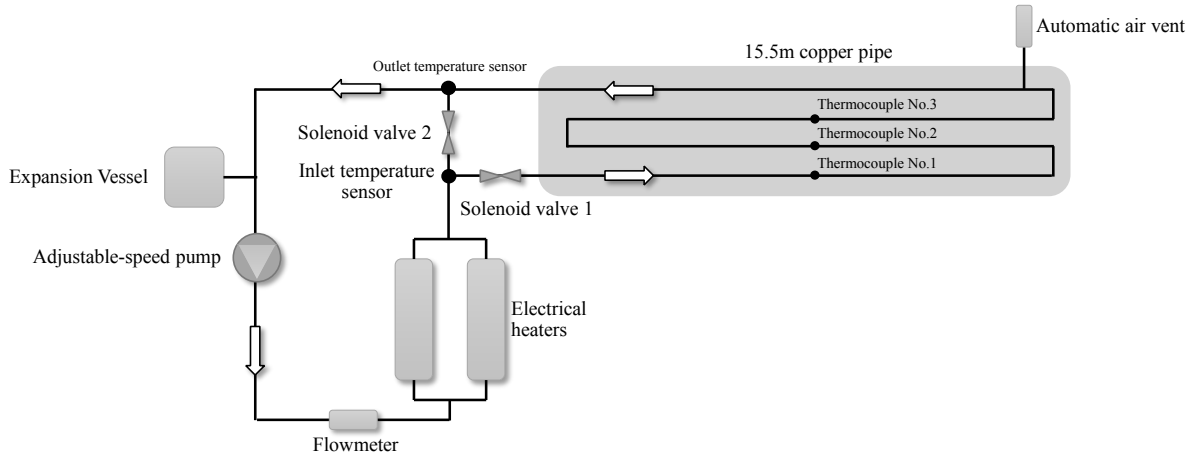

Figure 4.3: A Schematic of the experimental system.

is also measured with a thermocouples type T, near to the test rig. It is worth to note that all temperature sensors are calibrated using a calibration oil bath and a reference RTD (Resistance Temperature Detector) so that the uncertainty in the temperature measurements have been estimated to be 0.17 K. The details of the calibration and uncertainty calculation are discussed in Appendix A. The mass flow rate in the experiments is measured by a vortex flowmeter with less than 2 percent of measurement values uncertainty. The variable speed pump allows flow rate to be controlled and varied through a range to allow a range of Reynolds numbers to be studied. More details of each component and the measurements and control systems are described in Section 4.3.

4.3 Description of measurement and control systems

Based on the type of the experiments, i.e. short and long timescale experiments, several variables need to be carefully controlled, measured and logged. Since the main aim of all the experiments is to evaluate the dynamic thermal responses of the pipeline to a step change at various operating conditions, the main challenge is to impose a suitable step change at the pipeline inlet temperature and/or maintain the inlet temperature constant for a range of fluid flow rates. This requires precise control and measurement system to control the heater power to keep the pipeline

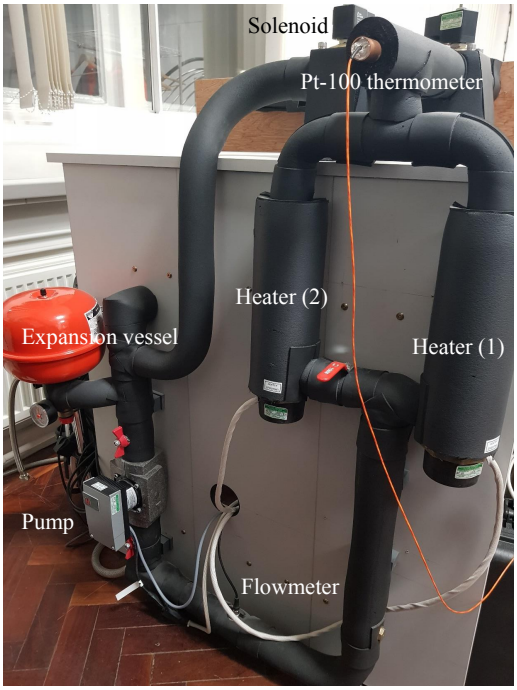

Figure 4.4: A photograph from the heat source circuit of the experimental setup providing circulating hot water through the pipeline.

inlet temperature constant as well as the pump power to provide suitable water flow rate through the pipelines. Besides these variables needed to be measured and used to control the system, other variables such as the lab temperature, ground surface heat transfer, fluid flow temperature at certain locations from the pipe inlet also need to measured and recorded. Table 4.2 presents the variables which are measured and used for control purposes during each type of the experiments as well as the main objectives of the measurements.

In this work, all the electronics components for measurement and controlling the experimental setup are placed at the control box located beside the pipeline test section, as shown in Fig. 4.5. The measurement and control systems of the test rig can be categorized into the four subsystems:

- Controller subsystem. The compact controller (NI CompactDAQ-9135) is used to collect, process and analyse the sensor data, and control the electrical equipment of the experimental setup.

- Flow rate control and measurement subsystem. This comprises the variable speed pump (Wilo-Yonos ECO BMS-30) and the flowmeter (Vortex Flow

Table 4.2: Main variables measured and recorded during the experiments conducted in this research along with their purposes of measurements.

Variables	Experiment type	Purpose of Measurement
Pipeline inlet temperature	All tests	Recording the variations of pipeline inlet temperature & feedback value to control the heaters. power
Pipeline outlet temperature	Long timescale tests	Recording the variations of pipeline outlet temperature & using for calculation of heat balance in the pipeline and pipeline heat losses.
Fluid temperature at certain pipeline locations	Short timescale tests	Measuring the variations of thermal response of pipeline due to a step change.
Lab temperature	All tests	Recording the variations of lab temperature to use as environmental parameters in the developed models.
Fluid flow rate	All tests	Recording the water velocity through the pipeline & Feedback value to control the pump power.
Ground surface heat flux	Long timescale tests	Measuring the dynamic variations of the ground surface heat losses.

Transmitter series 200) to control and measure the water flow rate through the pipeline.

- Heater control subsystem. This consists of the heaters (6 kW immersion heaters), PID controller and the fast response pt100 sensor inserted into the pipeline to control the input heat power to the system in order to keep the inlet temperature to the pipeline section constant.
- Temperature and heat flux measurement subsystem. This is the measurement system used to monitor, record and gather the temperatures and heat fluxes from the sensors placed at the specific locations of the systems.

In the following, the details of each measurement and controlling subsystem are discussed.

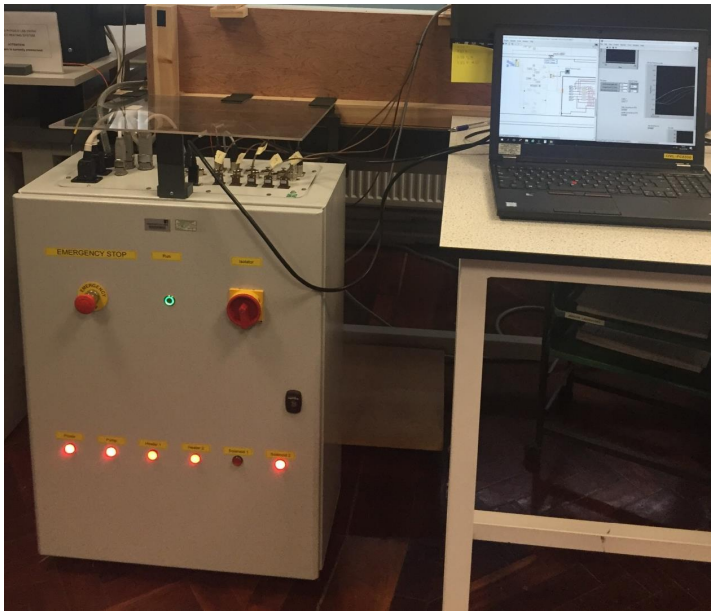

Figure 4.5: A photograph of the experimental system control unit.

4.3.1 The Controller System

In this work, the experimental system is controlled by a CompactDAQ system. The CompactDAQ is a data acquisition platform built by National Instruments that includes a broad set of compatible hardware and software [Wang (2014)]. The

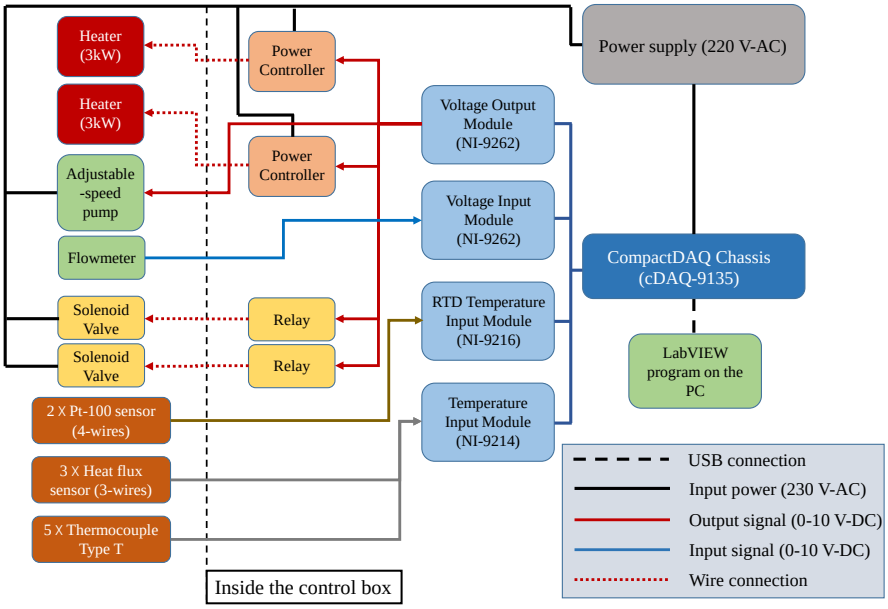

Figure 4.6: Schematic diagram of the elecrical componenets in the experimental rig.

CompactDAQ integrates hardware for input/output data with LabVIEW software that allows collecting, processing and analysing sensor data. The compactDAQ system used in this work is a NI CompactDAQ-9135 with eight input/output module slots managed by a chassis controller module. The cDAQ is connected to a PC via a USB connection that enables us to program the cDAQ via LabVIEW software to control the signal data sources and to log data accurately. In this work, four I/O modules plugged in the cDAQ, given as follows:

- Voltage Input Module (NI-9205): For collecting the voltage signal from the flowmeter
- Voltage Output Module (NI-9264): For generating a voltage signal to the adjustable speed pump, two relays controlling the solenoid valves, two power controllers controlling the heaters.
- Temperature Input Module (NI-9216) coupled with a front-mount terminal block (TB-9214): For measurement of heat fluxes and temperatures from the T-type thermocouples
- Temperature Input Module (NI-9214): for measurement of temperatures from RTDs, i.e. the Pt100 sensors.

Fig. 4.6 illustrates the outline of the electrical components and their connections used in the experimental setup. The details of the various rig components, as well as their roles in the experimental setup, are described in the following sections.

4.3.1.1 Software implementation

In this work, all the input/output signals to/from the cDAQ-9135 are controlled via the LabVIEW 2018 SP1 software. LabVIEW (Laboratory Virtual Instrument Engineering Workbench) is a system-design platform and development environment for a visual programming language from National Instruments. LabVIEW uses a graphic interface that enables the elements to be connected together in order to provide the required data flow. LabVIEW integrates the creation of user interfaces, i.e. virtual front panels into the development cycle [National Instrument (2003)].

LabVIEW software allows the user to program a so-called virtual instrument (VI) for each specific application. Each VI has three components: a block diagram, a front panel, and a connector pane. The last is used to represent the VI in the block diagrams of other, calling VIs. The virtual front panel is built using controls and indicators. Controls are inputs: they allow a user to supply information to the VI. Indicators are outputs: they indicate, or display, the results based on the inputs given to the VI. The back panel, which is a block diagram, contains the graphical source code. All of the objects placed on the virtual front panel will appear on the back panel as terminals. The block diagram also contains structures and functions which perform operations on controls and supply data to indicators. All the structures and functions are shown as nodes and connected to one another using wires [National Instrument (2003)].

Different parts of the main VIs programmed in this research are described in the following sub-sections for each specific application.

4.3.2 Flow Rate Control and Measurements

Controlling and measuring the fluid flow rate of the circulating hot water is carried out using an adjustable speed pump and flowmeter installed in the heat source sub-circuit. Having estimated the total pressure drop due to both major and minor pressure losses, and the required range of water flow rate, an adjustable speed pump (Wilo-Yonos ECO BMS - 30) was chosen based on the pump characteristics curve. The pump allows the circulating water to flow in the desired range of the Reynolds

number through the pipeline. The adjustable speed pump and the characteristic curve of the pump are displayed in Fig 4.7.

It is necessary to control the pump in a way to have a constant set flow rate, and measure and record the velocity of water flow through the pipeline. To this end, a vortex flow transmitters (DN10) from the Clark Sonic Ltd. is used to monitor the flow rate, as shown in Fig. 4.8. Vortex shedding flowmeters present the flow in a pipe with a bluff body in the flowmeter. As velocity increases, alternating vortices are formed on each side of the bluff body and travel downstream. The flowmeter uses sensors located downstream of the bluff body to detect the generated vortices. The frequency measured is proportional to the flow velocity. Based on the flow factor provided by the manufactured the measured frequency can be converted to the volume flow rate of water. It should be noted that the flowmeter requires 5 Vdc power input, and the output is a square pulse frequency 0 to 5 Vdc.

Based on the input signal from the flowmeter and its conversion to the water flow rate, the analogue output signal to the adjustable speed pump is adjusted to reach a desirable pump speed and hence the desirable water flow rate through the pipeline. Once the desirable pump speed is acquired based on the provision of the required water flow rate through the pipeline, the voltage signal is fixed for each experiment.

According to the manufacturer's data-sheet, there is a linear relationship between the analogue input signal and the pump speed, and hence, by changing the output signal from 3 to 10 Vdc (between 0 to 3 Vdc the pump is on but does not rotate), the desirable water flow rate can be obtained. To this end, the input/output signals

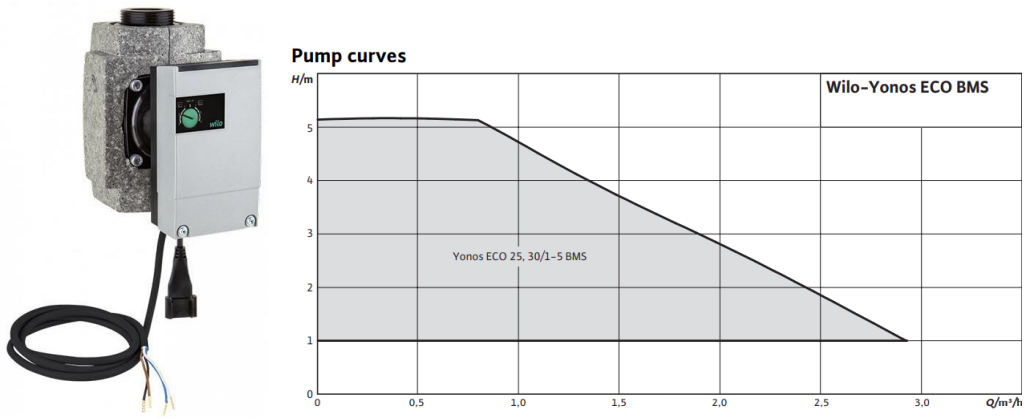

Figure 4.7: The adjustable speed pump and the characteristic curve of the pump.

Figure 4.8: The vortex flow transmitter.

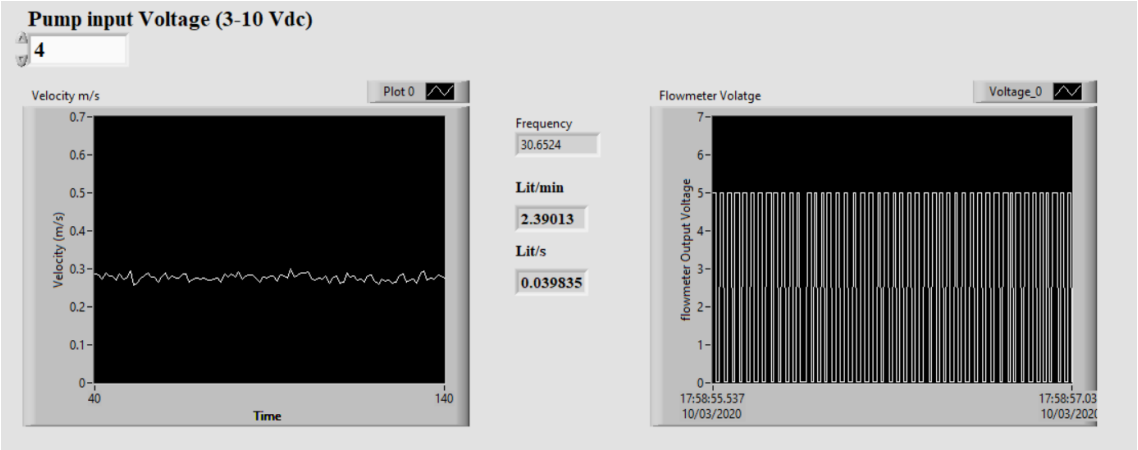

Figure 4.9: The view of the front panel showing the flowing water velociy in the pipeline and the input voltage from the flowmeter.

to/from the module in the cDAQ are processed via the main VI programmed in this research. The display of the input voltage from the flowmeter and the velocity of water circulating in the pump is illustrated in Fig. 4.9.

4.3.3 Heaters control

Controlling the heaters in such a way to keep the pipeline inlet temperature constant was necessary in all the experiments. Achieving control in order to approximate a step change in inlet temperature is a key objective and challenge. Accordingly, many preliminary experiments were designed and carried out to ensure this was achievable based on the installed equipment and control system.

The circuit contains two immersion electrical heaters (Willis External Immersion Heater 3kW Element and Copper Shell) controlled by a PID controller programmed in the cDAQ unit. The heater element and its shell are illustrated in Fig. 4.10.

Based on the measured temperatures from the fast response pt-100 sensor placed after the heaters, as shown in Fig. 4.3, the PID controller controls the heaters. The pt-100 sensor is inserted into the pipeline to measure the hot water outgoing from the heaters accurately. The sensor is also used to measure the pipeline inlet temperature when the hot water flows through the pipeline test section during the experiments.

To achieve the stabilized inlet temperature after imposing the step change and have better control over the heaters, the heat source circuit needed to be preheated before each experiment as the equipment has its own thermal mass. Having pre-heated the heat source circuit, a step change is applied to the inlet temperature to the pipeline test section, using two brass solenoid valves (with maximum 50 ms opening/closing time) to simultaneously close the heat source circuit and open the pipeline test section. This allows the hot water to flow through the pipeline test section from the heat source circuit as quickly as practically possible. The solenoid valves used in this experimental setup is shown in Fig. 4.11.

To control the solenoid valves, two relays were used and connected to the voltage output module in the cDAQ to turn on/off the valves. The solenoid valves are normally closed until receiving the required voltage to be open. The input signals to the relays connected to the valves are controlled by the main VI programmed for the experiments as displayed in Fig 4.12.

During both main experiments, i.e. short and long term tests, the pipeline inlet temperature is required to be kept constant by precisely controlling the heaters via the PID controller programmed in the cDAQ controller. In general, a PID controller operates to minimize the discrepancy between the actual value of a system, i.e. the

Figure 4.10: The immersion heater element and copper shell.

Figure 4.11: The brass solenoid valves arrangment in the test rig.

inlet temperature, and the desired amount of the system, i.e. the setpoint temperature. This is done by continuous calculation of an error value between the desired setpoint and a measured variable by the controller and applies a correction based on proportional, integral, and derivative terms. These PID controller parameters need to be determined according to the suitable tuning method and set in the controller for the desired control response.

In the control heating application during the experiments, at any given moment, the difference between the inlet temperature as the process variable and the setpoint temperature is used by the control system to drive the power of heaters. Based on the setpoint temperature and the PID parameters, the PID controller determines the desired output signal (between 0 and 10 V dc) to the heater controllers. The voltage signal is proportional to the input power of the heater which can be varied between 0 and 6 kW. The details of the PID controller used in this work are described in Appendix B. The view of the block diagram and front panel of the PID controller in the main VI is illustrated in Fig. 4.13.

4.3.4 Temperature and Heat Flux Measurements

The temperature measurements in this work have been made with two types of temperature sensors: thermocouple type T, and resistance temperature detector (RTD) type pt-100. Due to the better accuracy of the pt-100 sensors, they were used

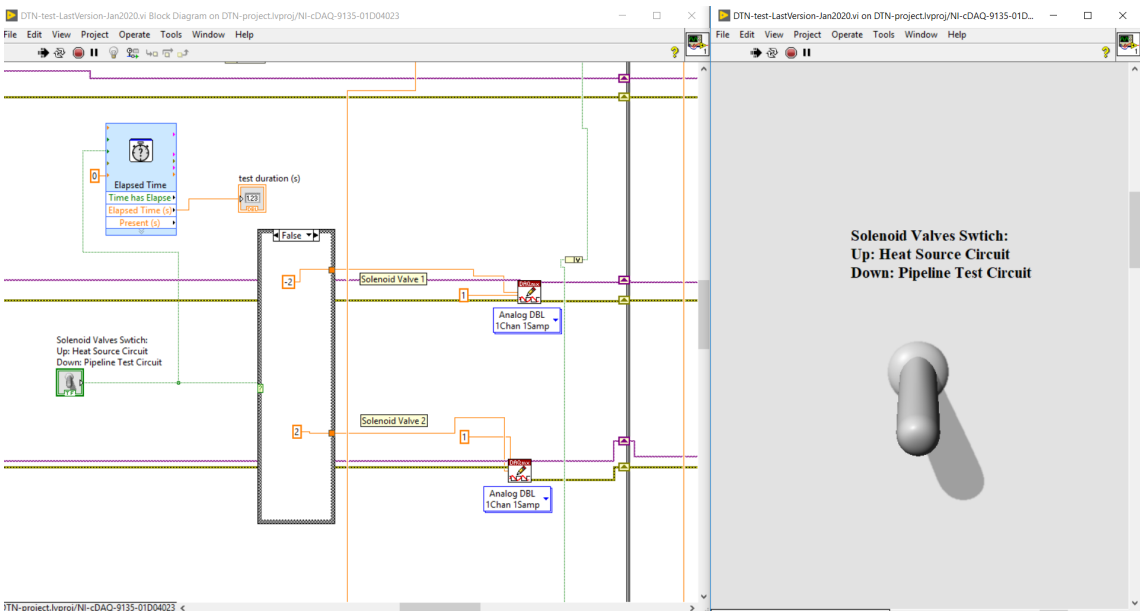

Figure 4.12: The view of the block diagram and front panel of the solenoid valves controlling in the main VI.

to measure the fluid temperature difference between inlet and outlet of the pipeline as the differences are relatively small. The water flow temperatures and dynamic responses at the different points of the pipeline and the ambient temperature near to the test rig are measured with the fast-response thermocouple type T. It is found that the thermocouple type T, i.e. copper constantan thermocouple, has the better accuracy for the low-temperature measurements, i.e. -40 C°to 120 C°, compared with the other types of the thermocouples. At the specific locations at the pipeline, the proper tee fittings were used allowing thermocouples with a sheath diameter of 1.5 mm and sheath length of 50 mm to be directly inserted into the pipeline. The distances from the pipeline inlet to the points of water temperature measurement are 5.35, 7.93 and 10.52 m. These thermocouples are needed to be calibrated before using in the experimental system. The details of the calibration of the thermocouples are described in Appendix A.

The temperature input module (NI-9216) mounted in the cDAQ is used for recording temperature measurements. This module is coupled with a front-mount terminal block (TB-9214), including several cold-junction compensation (CJC) sensors to increase the overall accuracy of measurements. The main VI programmed in LabVIEW is used to interpret the input signals from the thermocouples, and record

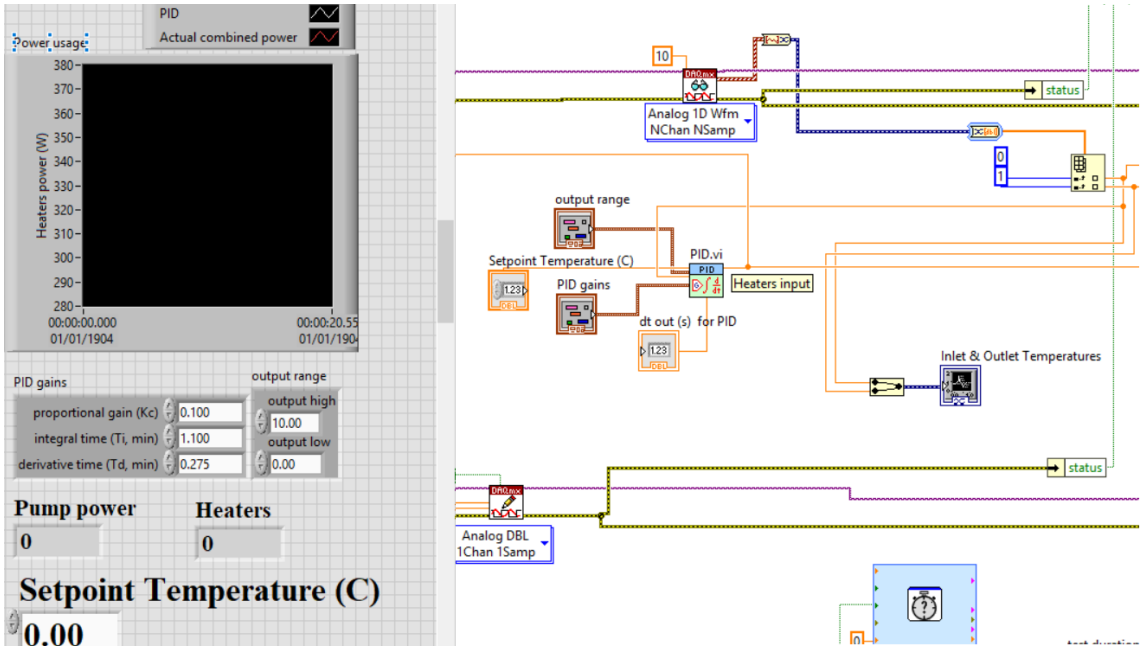

Figure 4.13: The view of the block diagram and front panel of the PID controller in the main VI.

them in a desirable time step, depending on the type of the experiments, i.e. short or long term tests.

For measuring the inlet and outlet temperature of the pipeline section in the test rig, two fast response pt-100 with high accuracy, i.e. accuracy class 1/10 DIN, has been used. Both pt-100 sensors with the sheath length of 150 mm inserted horizontally to the pipeline in such a way that almost entire sensors were immersed in the flowing water. The temperature input module (NI-9214) is used for temperature measurements of the Pt100 sensors with four wires. The 4-wire connection completely eliminates the influence of the connection lead on the measuring result since any possible asymmetries in the lead resistance of the connection lead are also compensated.

The heat fluxes from the sand surface are measured using three self-calibrating heat flux sensors (HFP01SC from Hukseflux Ltd.). The HFP01SC is a combination of a heat flux sensor and a film heater. The sensor output is a voltage signal which is proportional to the heat flux through the sensor. This high sensitive heat flux sensor incorporates the film heater to self-test and self-calibrate the sensor to compensate for the measurement errors caused by the thermal conductivity of the surrounding

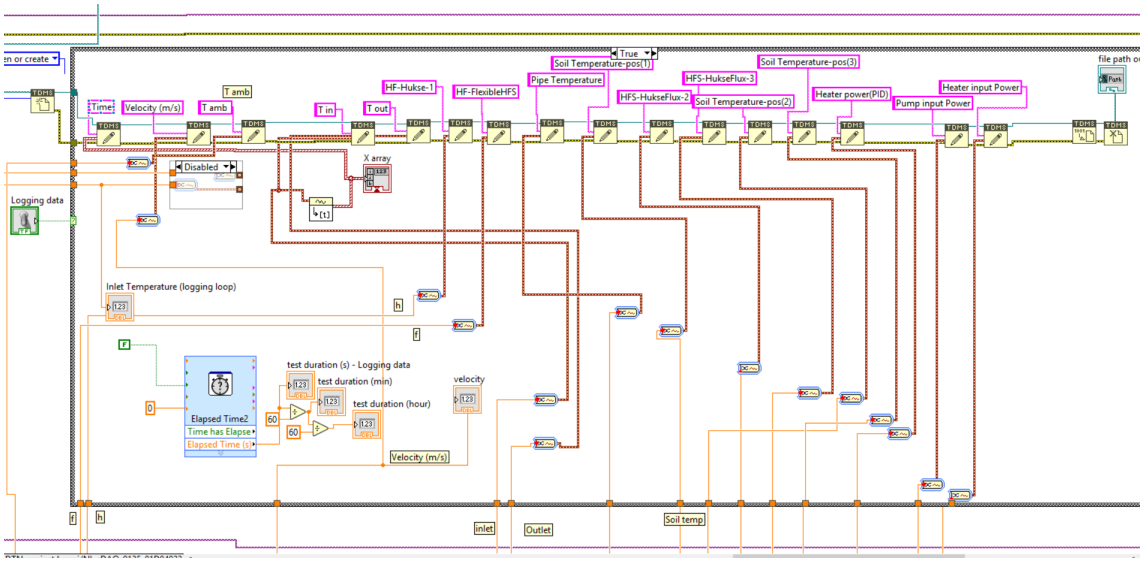

Figure 4.14: The view of the front panel of the PID controller in the main VI.

soil and sensor contact to the soil. These three self-calibrating heat flux sensors (HFP01SC) have been placed on the top of the sandboxes to measure the dynamic ground surface heat losses accurately. Since the diameter of the heat flux sensor is 8 cm, they are positioned in a way to cover all width of the sandbox, i.e. 20 cm. Therefore, by averaging the measured heat fluxes from the sensors, the average ground heat loss can be obtained. More details of the heat flux sensor and calibration method has been explained in Appendix A.

The module (NI-9216) is used for recording heat flux measurements. The main VI programmed in LabVIEW used to interpret the voltage input signals from the heat flux sensors in a similar way with the thermocouples, and record them in a desirable time step. The part of main VI used to record the data into the TDMS file, i.e. LabVIEW output file which can be converted to a portable format such as a CSV file, is illustrated in Fig 4.14.

4.4 The Short Timescale Experimental Procedure

The short timescale experiments aim to investigate dynamic thermal effects on the thermal response of pipelines by imposing a step change at the inlet temperature of the pipeline section, and measuring the temperature response of fluid flow at the

different points along the pipeline at timescales of the order of hundred milliseconds. To apply the step change to the pipeline inlet temperature, the solenoid valves have been used to switch the flowing hot water from the heat source section to the pipeline section as quickly as practically possible. In these set of the experiments, two pipeline boundary conditions have been applied. Firstly, the bare copper pipeline is tested to evaluate the dynamic thermal response of the pipeline at short timescales with the highest possible heat losses to the ambient. Secondly, the copper pipeline is thoroughly insulated with the 19 mm pipe insulation (Armaflex Insulation), and the effect of insulation is investigated on shaping the temperature response of pipeline at short timescales.

Having filled the system with running water and pressurized the system, the water flow rate is adjusted using the Labview interface to adjust the pump speed based on the feedback from the flowmeter. After reaching the desired water flow rate, the solenoid valves are set to circulate the water only in the heat source circuit. Using the immersion heater elements, pt-100 sensor and the PID controller programmed for this application, the temperature of the circulating water rises to reach and stabilise to the setpoint temperature, e.g. 40 ℃. After stabilization of the temperature of the circulating water in heat source circuit, the solenoids valves switch the direction of the water to the pipeline test section. Once the valves are switched, the temperatures of the fluid flow at the three points of the pipeline starts to be logged into the cDAQ. The circulating water and ambient temperatures, as well as the flow rate, is recorded every 0.25 s during the tests which take between 40 s to 90 s, depending on the water flow velocity varied between 0.3 to 1.2 m/s. In this set of the experiments, the inlet temperature is maintained constant during each test. The experimental results from the set of the short timescale experiments are given and explained in the following chapter.

4.5 The Long Timescale Experimental Procedure

The long timescale experiments aim to investigate the dynamic thermal response of the buried pipeline considering the dynamic thermal effects of the fluid flow combined with the transient conduction heat transfer process in the ground. In the long timescale experiments, two types of step change experiments are required to carry out on the boundary conditions of the buried pipeline, i.e. the pipeline and ground boundaries. During the tests, the heat transfer rates from the pipeline and

ground surfaces, the pipeline inlet and outlet temperatures as well as the water flow rate are simultaneously measured and recorded. One of the main aims of the long timescale experiments is to obtain the step response heat flux data due to the step change to the surfaces and use it to calculate the weighting function series required in the DTN method. To this end, the heat flux data needs to be post processed and rescaled to correspond in equivalent to a unit temperature step change (0-1).

Having filled the system with cold water and pressurized the system similar to the short time scale experiment, the temperature of the entire system needs to be stabilized around the temperature of the lab. To make sure that the temperature of the system is stabilized, the system is left for approximately two days. During this time the temperatures of the sand and water at different location in the pipeline are monitored to see if the system is stabilized. After the stabilization of the system, a step change is imposed to the inlet temperature of the pipeline, by providing circulating hot water with the desired temperature and flow rate at the heat source circuit inlet. During the experiment, the inlet and outlet temperatures of the pipeline are accurately measured with pt-100 sensors inserted to the pipeline. These measured temperatures, along with the measured flow rate, are used to calculate the heat balance in the pipeline to determine the heat losses through the pipeline. To measure the ground heat flux, three self-calibrating heat flux sensors (HFP01SC) have been used and placed on the top of the sandboxes, in a way that by averaging the measured heat fluxes from the sensors, the average ground heat loss can be obtained.

Both long-timescale experiments last until the system closely approaches a steady-state condition, and this takes approximately 42 hours from applying the step change. Due to the adverse effects of lab temperature variations on the experiments, the experiments were performed during the weekends. To perform the experiments, the lab heaters were turned off from Friday morning, and the door kept close during the test to prevent the entry of fresh air to the lab. By doing so, the lab temperature variations could be kept below almost 0.9 °C during the tests.

To impose a step change to the ground surface, one approach would be for the lab temperature to undergo a step change, while the sand and water flow are stabilized. Since applying the step change to the lab temperature is too difficult and practically impossible, considering the lab conditions, another approach is implemented for this purpose. In this approach, the sand is heated up, and the step change applied to the ground surface in the reverse direction, i.e. from the sand to the lab air instead of

Figure 4.15: The pipeline test section coverved with Armeflux insulaton sheet (right-image), and sticked to the insulation board compressed by the sands bags weights during preprating of the test rig for imposing a step change to the ground surface (left-image).

from the lab air to the sand. In this way, the ground step response heat fluxes can be obtained simply by changing the sign of the values. The details of this process are described below.

Firstly, the sheet insulations (with the thickness of 19 mm) were thoroughly stuck to the insulation boards using double-sided glue tape. Then, the insulation board covered with the Armaflux sheet insulations were placed on the top of the pipeline test section to insulate the test section completely. To make sure that the test rig thoroughly insulated without any air leakage from the top, several sandbags were put on the top of the insulation boards to weigh up the boards so that the sand surface and the insulation were perfectly in contact without any trapped air, as shown in Fig 4.15.

Having insulated the upper surface of pipeline test section, the hot water is circulated through the pipeline to heat up the sand to the desired temperature. Due to the low thermal conductivity of the sand, the sand heat up process takes a long time, i.e. a few days, to reach the steady-state condition. The temperature

variations of in different points of the sand were monitored during the heat up process, prior to applying the step change. After heat up the section to desirable temperature, e.g. 40 °C, the insulation boards are taken off in the shortest possible time. This results in a step change in the ground surface temperature between the sand and lab temperature. The heat fluxes and the temperatures are measured and recorded similar to the previous experiment.

The water velocity in both the long timescale experiments needs to be turbulent and constant flow, as the main interest of this set of the tests is to investigate the effects of dynamic conduction process in the buried pipeline. In the final model proposed in this work, i.e. the combined DTN-PF model, the flow rate and in turn, the convection coefficient can be adjusted for each timestep. Considering the pump and pressure drop in the pipeline, low water velocity is chosen to have a higher possible difference between the pipeline inlet and outlet temperatures, i.e. Reynolds number is around 5500. It is worth mentioning that although increasing step change temperature allows having a higher inlet and outlet temperature difference, it causes heat losses from the test rig box to the ambient air to increase and introduce larger uncertainty in the results. Therefore, some preliminary experiments have been conducted to make sure that the temperature difference is high but not enough that heat losses occur from the test rig box that adversely affects the experimental results.

4.6 Conclusions

This chapter describes the details of the experimental facilities designed and developed in this research for the purpose of investigation of the dynamic thermal behaviour of the pipeline with different boundary conditions both over short and long timescales. The details of the main components used in both the electrical section and the test section are explained, along with the systems used in controlling and measuring the required data. The main experiments performed in this research have been carried out in two main sets of tests: short timescale experiments, and long timescale experiments. In the short timescale tests, the impacts of the short timescale dynamic effects, e.g. longitudinal dispersion, on the thermal response of pipeline have been experimentally investigated for a range of operating conditions. To this end, the thermal responses of the pipeline due to temperature step change at the pipeline inlet has been evaluated by measuring the fluid flow temperature at different distances from the pipeline inlet. The procedure of performing this set

of the experiment was described in detail, including the temperature and flow rate measurement and control the system. In these experiments, the shape of temperature responses were determined for the specific locations of pipeline and flow rates. This data will be used to validate the short timescale dynamic models proposed in this research, e.g. the modified PFNCST model. In the short timescale models developed in this work, the temperature step change is applied to the inlet of pipeline similar to the conditions of the experiments, and the predicted responses are later compared with measurement data obtained from the corresponding experiments. This allows assessing the ability of the models in dynamic prediction of thermal response of pipeline in terms of the accuracy and computational costs.

In the long timescale experiments, the main focus was on the evaluation of the effects of the dynamic conduction heat transfer of the ground on the thermal response of the pipeline, along with the heat losses from the pipeline and ground surfaces. For this purpose, two sets of temperature step change are applied to the pipeline and ground boundaries, and the step response heat flux and temperature data were measured in both experiments for constant turbulent fluid flow from the moment of applying the step change until the system approached the steady-state conditions. The procedures of performing these two experiments were described in detail, illustrating how to properly conduct the tests and control the system in order to collect the desirable required set of the temperature and heat flux data. The step response heat flux data obtained from both experiments, i.e. applying temperature step change to the pipeline and ground surfaces, is then normalized by the initial temperature conditions to be expressed in equivalent to a unit temperature step change (0-1). In this way, the admittive and transmittive heat flux data required for obtaining the weighting function series and the DTN calculation can be determined without using any analytical or numerical solutions. The simulation results from the numerical models developed in this research are later compared with the measured heat flux and temperature data in terms of accuracy and computational expense in the prediction of surface heat losses. These comparisons are presented in Chapter 7.

Chapter 5

Experimental Results

The experimental results from the experiments described in Chapter 4 are presented and discussed in this chapter. The experiments were performed with two main aims. Firstly, evaluate the short timescale dynamic effects occurring in delivering the hot water in the pipelines. To this end, a step change at the inlet temperature of the pipeline section is applied with two boundary conditions: the bare copper pipeline exposed to the lab air, and the completely insulated pipeline. These two boundary conditions were chosen to investigate the dynamic thermal response of the pipeline with the minimum and maximum possible heat losses to the ambient. The temperature of fluid flow through the pipeline for these two boundary conditions were measured and gathered for different fluid flow rates over timescales of the order of magnitude of the nominal transit time of the fluid. The results of the experiments are discussed in Section 5.1.

The second primary aim of conducting the experiments was to investigate the dynamic thermal response of the buried pipeline considering the transient conduction heat transfer in the ground. For this purpose, a temperature step change is imposed on the buried pipeline and ground (sand) surfaces while the system is stable with constant initial conditions. The step response heat flux and temperature data, as well as the fluid flow rate, were measured and recorded during these experiments from the moment of applying the temperature step change until the system reaches the steady-state conditions and this took approximately 42 hours. Through analysing the step response measurement data obtained from the experiments, the effects of dynamic conduction heat transfer can be investigated on the thermal responses of buried pipeline and heat losses. The experimental results of these long

Table 5.1: Experimental conditions of short timescale tests for both the copper and insulated pipeline.

Test case	Water velocity (m/s)	Reynolds Number	Step change temperature difference	Initial temperature
Copper Pipeline- test1	0.307	4520	10.75	19.25
Copper Pipeline- test2	0.609	8970	11.15	26.85
Copper Pipeline- test3	0.933	13750	10.3	23.7
Copper Pipeline- test4	1.14	16800	11.3	22.7
Insulated Pipeline- test1	0.321	4600	9.9	22.1
Insulated Pipeline- test2	0.589	8680	10.3	31.7
Insulated Pipeline- test3	0.902	13290	9.8	26.2
Insulated Pipeline- test4	1.244	18330	9.1	22.9

timescale experiments are presented in Section 5.2. The experimental data collected for both the short and long timescale experiments have been further used to validate the numerical models developed in this work and are discussed in Chapter 6.

5.1 Dynamic Thermal Responses of Insulated and Uninsulated Pipelines

To evaluate the dynamic thermal responses of the pipeline, a range of experiments have been conducted for various operating conditions. The initial and boundary thermal conditions of the tests along with the water velocity are presented in Table 5.1. In this set of the experiments, four water velocities thought to be typical in the DHS pipelines have been applied: 0.3, 0.6, 0.9 and 1.2 m/s. The thermal responses of the pipeline were evaluated at the distances of 5.35, 7.93 and 10.52 m from the inlet of the pipeline by measuring the fluid flow temperature variations at these locations. Firstly, the experiments were conducted for the bare copper pipeline (with maximum possible heat losses), and then with 19 mm pipe insulation to approximate well-insulated conditions (with minimum heat losses). The thermal properties of the pipe insulation, copper pipe and water used in the experiments are presented in Table 5.2.

The main focus of this set of the experiments was to evaluate the short timescale

effects including the longitudinal dispersion, thermal capacity of the fluid flow, and dynamic transport of heat on the dynamic thermal response of the pipeline. To that end, a step change is applied to the inlet temperature of the pipeline, and the variations of the fluid flow temperature at the locations noted above were measured and recorded. This allows determination of the shape of the temperature profile due to the temperature step change at the pipeline inlet. The nature of the thermal step response of pipeline provides useful data to study the effects of the time delay due to the transit time of the fluid travelling through the pipeline, and the longitudinal dispersion of the fluid flow combined with the effect of radial heat losses through the pipeline.

The pipeline heat loss is expected to be influenced by the temperature differences between the fluid flow and the lab temperatures as well as the heat transfer coefficient between the pipe surface and the ambient air. Hence, the lab temperature was measured and recorded, in addition to the pipeline fluid flow temperatures during the experiments. Since the duration of each test is relatively short, the lab temperature is assumed constant during each test. In this set of experiments, the collecting data during each test comprises the water flow temperatures at the specific locations of the pipeline, lab temperature and the flow rate of flowing water through the pipeline which is all recorded in every 0.25 sec. The velocity and Reynolds number of the flowing water through the pipeline is then calculated according to the measured flow rate.

In this set of the tests, after the system temperature is stabilized, a step change of approximately 10 K is applied at the inlet of pipeline section using the solenoid valves in less than 50 ms. Once a step change is applied to the inlet temperature of the pipeline, the measurement data is collected to evaluate the levels of diffusion and delay to thermal response of the pipeline.

Table 5.2: Thermal properties of the pipe materials and fluid

Material	Thermal capacity $(J/kg.K)$	Thermal conductivity $(J/m.K)$	Density (kg/m^3)
Copper pipe	385	401	8960
Water	4181	0.61	998
Insulation	1300	0.034	40

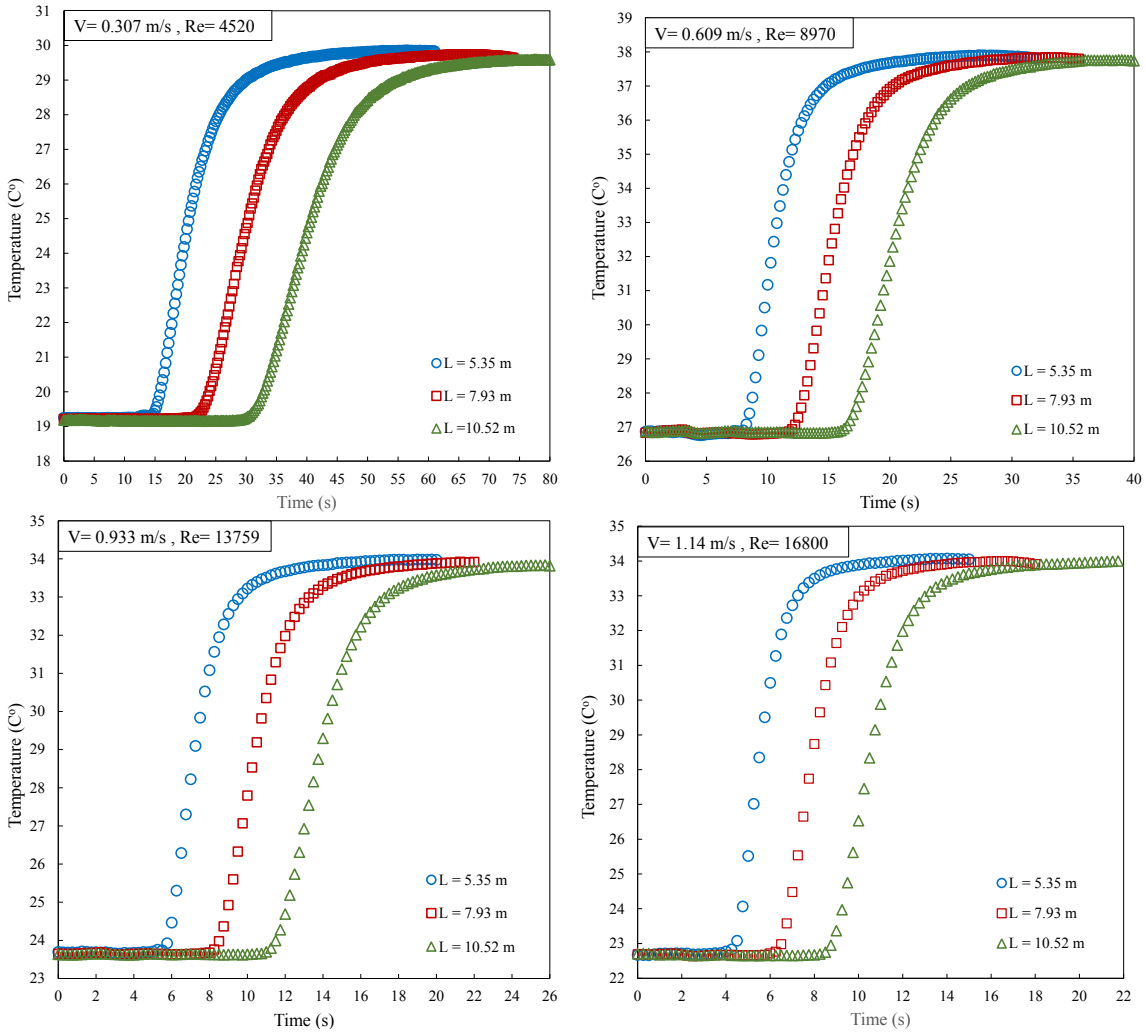

Figure 5.1: The uninsulated pipeline outlet temperature profiles at three distances and four different flow rates.

In this set of the experiments, particularly, the pipeline distance, fluid flow rates and the pipeline boundary conditions are varied to investigate the effects of these significant factors on shaping the thermal responses of the pipeline. Fig. 5.1 and Fig. 5.2 show the measured temperatures at three distances from the inlet of the pipeline for four water velocities and the corresponding Reynolds number for the uninsulated and insulated pipeline, respectively. Once the hot water is pushed into the pipeline section, heat losses occur through the pipeline due to the temperature differences between flowing hot water and the copper pipeline. This results in a diffusive shape for the pipeline temperature responses. It can be observed from the figures that by an increment of distances from the pipeline inlet, the thermal

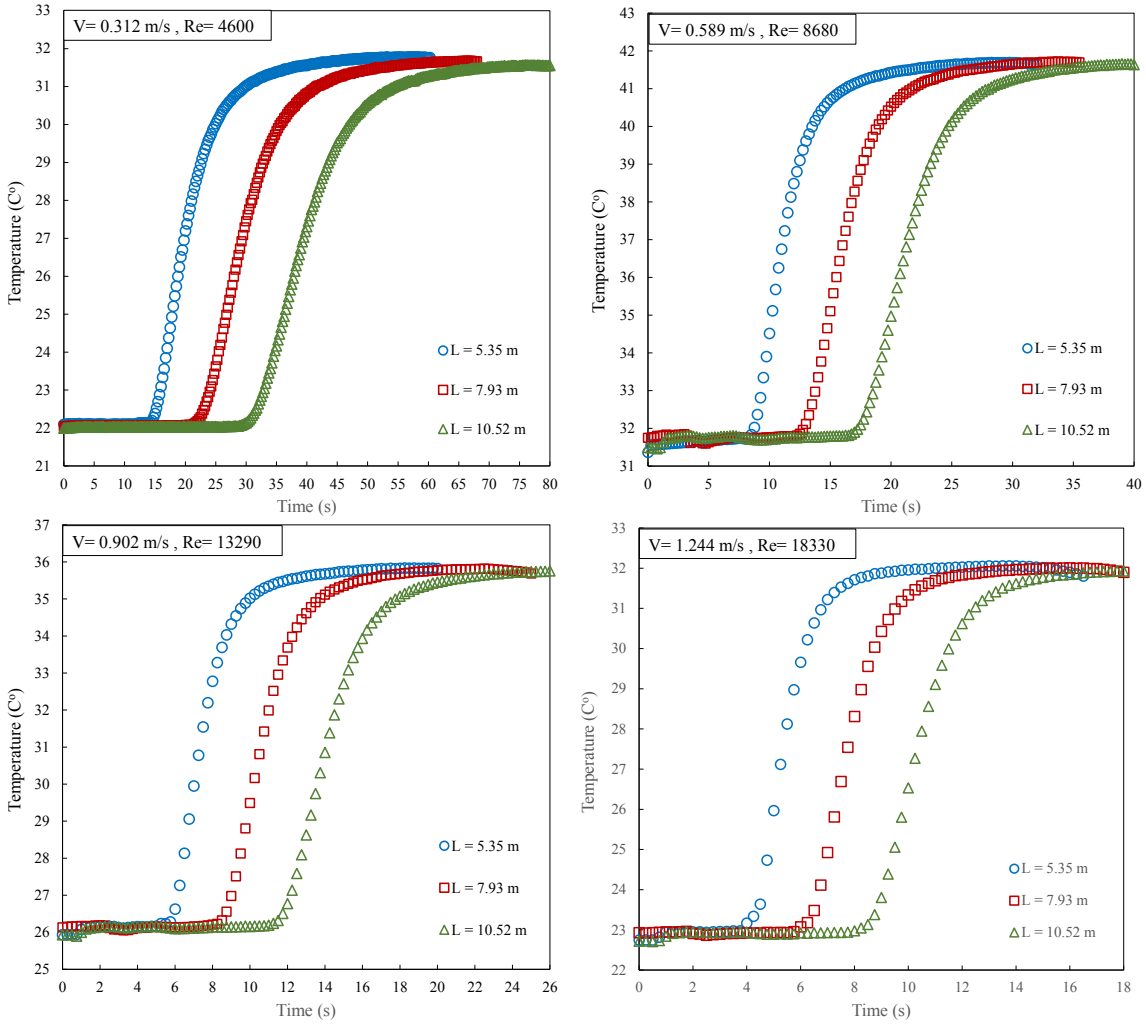

Figure 5.2: The insulated pipeline outlet temperature profiles at three distances and four different flow rates.

responses tend to be more diffusive. This is due to the fact that longer distances at the same flow rates cause longer transit time required for the flowing hot water to reach the location, and hence more heat transfer occurring in the pipeline leading to more diffusive responses.

In order to be able to compare the measurement data obtained from the uninsulated and insulated pipeline, it was necessary to express the temperature profile at the pipe outlet with the dimensionless form of the outlet temperature with respect to the dimensionless time (vt/L). Dimensionless form of the outlet temperature can be defined by:

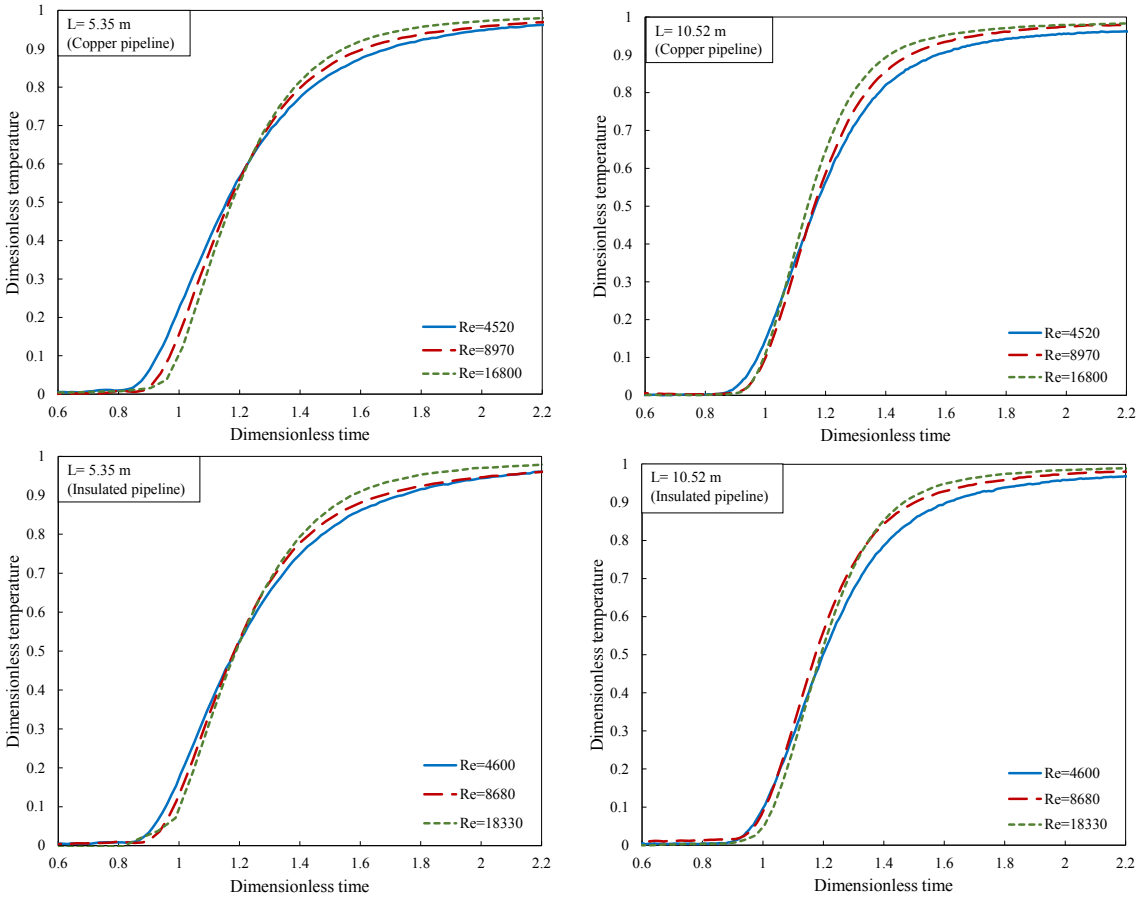

Figure 5.3: The diffusive forms of the step response temperature profiles at the shortest and longest distances for three Reynolds number.

$$T_{\text{dimensionless}} = \frac{T_{\text{outlet}} - T_{\text{initial}}}{T_{\text{inlet}} - T_{\text{initial}}} \tag{5.1}$$

Fig. 5.3 displays the shapes of the temperature response due to the step change at the shortest and longest distances for three flow rates. In these figures, the temperature response is shown in dimensionless values with respect to dimensionless time to be able to make better comparisons between the pipeline thermal responses for different flow rates. It can be observed increasing the Reynolds number results in sharper thermal responses of the pipeline. This can be due to the fact that at higher fluid flow rates the temperature differences between the fluid at the centre of the pipeline and near pipe wall is lower, i.e. the velocity profile is flattened.

The sharper thermal response of the pipeline also results in increasing the rising time of the thermal response of the pipeline. The rising time can be defined as

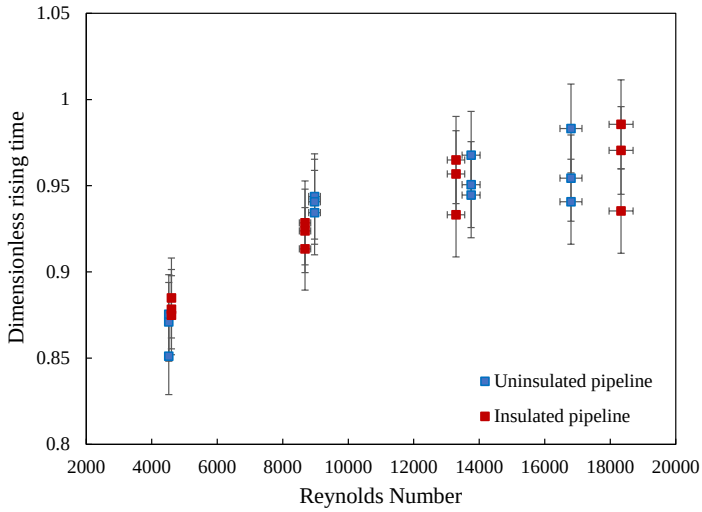

Figure 5.4: Variation of dimensionless rising time over a range of Reynolds numbers.

the time that the temperature of the pipeline at the outlet starts to rise due to the step change at the inlet of the pipeline. To better investigate this issue, the dimensionless rising times in relation to the transit time are plotted with respect to Reynolds numbers with the error bars in Fig. 5.4. The criterion for defining the start time of the rise is the time that the pipeline outlet temperature rises more than 5 percent of the step change value. The error bars shown in the figure are calculated based on the uncertainty of the water velocity measurement (2%) and temperature measurement ($0.17\,K$). It can be observed that with the increase of Reynolds number in these tests, the dimensionless rising time increases. This implies at higher Reynolds numbers, the thermal response tends to be flattened.

To investigate the effects of the outer insulation cover on shaping the short timescale temperature response of the pipeline, the dimensionless temperature response of the lowest and highest water velocity are compared in respect to dimensionless time at the furthest distance from the inlet (10.52m). Fig 5.5 illustrates the comparisons between the dimensionless temperature responses of the pipeline to a step change in these cases. It can be seen that despite using different boundary conditions for the outer surface of the pipeline, the dimensionless temperature responses are very close for both the lowest and highest fluid flow rates. This implies the dynamic thermal response of the pipeline in these experiments was shaped based on the thermal mass of the pipeline and the Reynolds number. Therefore, it is concluded that the thermal inertia of the pipeline plays a dominant role in shaping the

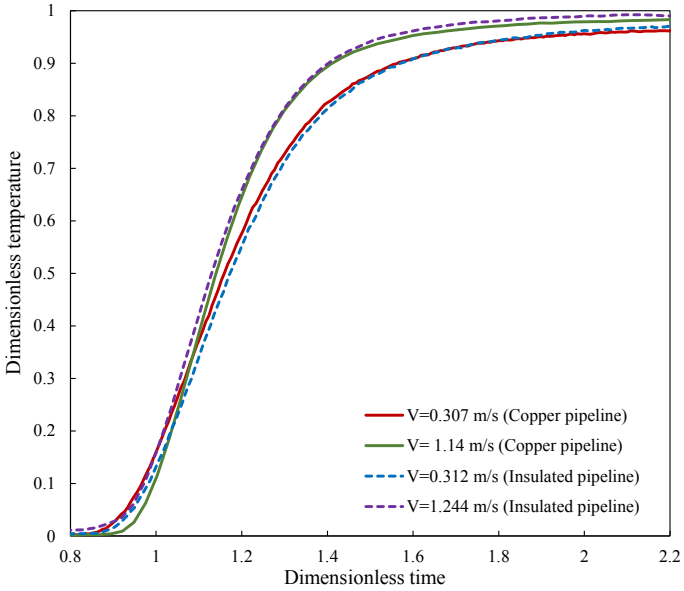

Figure 5.5: The dimensionless outlet temperature profiles for the copper and insulated pipeline for the lowest and highest water velocity at 10.52 m.

temperature profiles in the short timescale experiments.

Comparing the pipeline thermal response of the pipeline in all tests conducted over short timescales shows that each thermal response of the pipe has different rising time and profile shape depending on the distance from the measurement point to the inlet of pipeline and the flow rate of the flowing hot water. The rising time, in turn, the time delay along with the shape of the temperature profile in the pipeline are considered as significant characteristics of the dynamic thermal response, which are determined in this set of the experiments. The experimental data obtained from this set of the experiments are further used for validating the proposed numerical model developed in this work, i.e. the modified PFNCST model.

5.2 Dynamic Thermal Responses of Buried Pipelines

The evaluation of dynamic thermal responses of buried pipelines has been conducted by performing a series of experiments to arrive at two complete sets of experimental data on the buried pipeline described in Section 4.2. In this set of the experiments, besides the temperature response measurements of fluid flow through the pipeline, the dynamic heat flow through the sand was also monitored. Over these longer

Table 5.3: Experimental conditions of long timescale tests for the buried pipeline.

Test case	Water velocity (m/s)	Reynolds Number	Step change temperature difference	Average lab temperature	Initial temperature
Ground surface step change- case1	0.273	5450	22.7	15.3	38.0
Pipeline surface step change- case2	0.246	4900	21.8	16.2	16.0

timescales (approximately 42 hours), the heat transfer between the pipeline, surrounding ground, and the ambient air and the corresponding dynamic storage of heat in the ground material is expected to have significant effects on shaping the temperature responses and temperatures at each boundary surface and the corresponding fluxes.

To evaluate the dynamic thermal response of the buried pipeline and the ground, a step change has been applied to the boundary temperatures of the buried pipeline system, i.e. pipeline and ground surfaces. In these experiments, it was aimed to keep the surface temperatures isothermal to most closely correspond to the conditions assumed in the DTN modelling method. The step response heat flux data from the surfaces along with temperature data and water flow rate are obtained from this set of experiments and used to analyse the effects of the dynamic conduction heat transfer of the ground on the thermal response of the buried pipeline.

To obtain the transient pipeline heat loss over the experiments, the pipeline heat balance equation is solved based on the temperature differences between the pipeline inlet and outlet, and the water flow rate. This calculation is made for the data collected at each collecting time interval, i.e. 4 sec. Table 5.3 presents the experimental conditions for both long timescale experiments for the buried pipeline. The experimental results obtained from both tests are presented and discussed in the following sub-sections. The uncertainty of temperature and ground surface heat flux measurement are estimated to be 0.062 K and 0.63 percent, respectively, while the uncertainty of calculated fluid heat balance is estimated at 2.18 percent (see Appendix A).

5.2.1 Step Change applied at the Ground Surface Boundary

In this set of experiments, it was aimed to determine the step response heat flux data from the pipeline and ground surfaces by imposing a step change to the ground surface. This set of the data along with the step response heat flux data obtained from applying a step change to the pipeline surface can be used for determining the admittive and transmittive heat fluxes over the experiments. These data can then be used in derivation of weighting factors for the DTN modelling approach and comparison with 3D modelling results. Analysing these measured step response heat fluxes provides useful information for evaluating the dynamic thermal behaviour of the ground.

Prior to conducting each test, the buried pipeline section was required to be prepared as described in Section 4.5. For this purpose, the upper surface of the pipeline test section was thoroughly insulated, and hot water is circulated through the pipeline for a couple of days to heat up the sand to the desired temperature. The sand temperature was maintained high enough to ensure the temperature difference between the inlet and outlet of the pipeline were sufficiently large to limit the magnitude of the uncertainty in the fluid heat balance calculation. On the other hand, increasing the sand temperature results in undesirable heat losses from the insulated sandboxes and test rig to the ambient, which leads to producing errors in the experiment. Considering these issues, several preliminary experiments were conducted to find a suitable temperature for the sand. Accordingly, the temperature of 38 °C has been chosen for the sand to be applied as a temperature step change to the buried pipeline system. Moreover, the water velocity is adjusted as low as possible with the consideration that the flow regime should be turbulent in order to increase the pipeline temperature difference. Accordingly, the hot water was circulated with velocity of approximately $0.273\,m/s$ (Re=5450).

Due to the low thermal conductivity of the sand, the initial stabilization process took a long time, approximately three days, depending on the desired sand temperature. In this experiment, the sand temperature is monitored at different locations and depths during the preparation process to ensure the buried pipeline system reached the desired initialization temperature throughout its volume.

Having prepared the buried pipeline system, the upper surface insulation sheets were taken off as quickly as possible and collecting required data was started. In this way, a required step change is applied to the ground surface boundary temperature

equal to the difference between sand and lab temperature, and step response heat flux data from the surface can be determined. It should be noted that the direction of the heat in this experiment is the reverse of the heat fluxes required in the DTN approach. Therefore, the sign of the ground surface heat flux data obtained from the experiment needs to be changed and rescaled to represent a unit change in temperature when applied in the DTN model.

Fig. 5.6 shows the variations of the inlet and outlet temperatures of the pipeline, as well as water velocity over the test. It can be seen at the beginning of the experiment, the outlet temperature drops faster. This reflects the effects of the applied step change to the ground surface and the fact that the difference between the exposed ground surface and the lab air are at their greatest at the start of the experiment. As time proceeds, the heat losses to the air slowly decrease, resulting in the rate of change of outlet temperature reducing until the system closely approaches a steady-state where the heat losses and consequently, the outlet temperature becomes constant.

Due to the highly dynamic behaviour of the system at the beginning, the variation of the inlet and outlet temperatures of the pipeline along with the temperature difference is illustrated for first four hours in Fig. 5.7. As the pipeline is buried at a depth of $4.5\,cm$ (the distance from the centre of the pipeline to the surface), the inlet and outlet temperatures are almost constant during the initial 30 minutes until the heat losses from the ground surface affect fluxes at the pipe surface and hence pipe outlet temperature.

Since the outlet temperature changes in the initial hour are very small (and also the temperature differences), the 3 KW heater should deal to compensate the very small amount of the losses, and maintain a smooth constant inlet temperature. However, this was found difficult to achieve in practice since the small heat output is difficult to modulate in the 3kW heater element and so some spikes in inlet temperature can be seen in the data. Tuning the performance of the control system allowed these effects to be limited to a 0.5K band in the final data, as shown in Fig. 5.7.

Fig 5.8 displays the variations of the heat fluxes from the pipeline and ground surfaces, due to applying the step change to the ground surface boundary temperature. The ground surface heat fluxes are obtained by averaging the heat fluxes measured by the three heat flux sensors placed on the sand surface at specific locations. The pipeline heat fluxes are calculated based on the pipeline heat balance

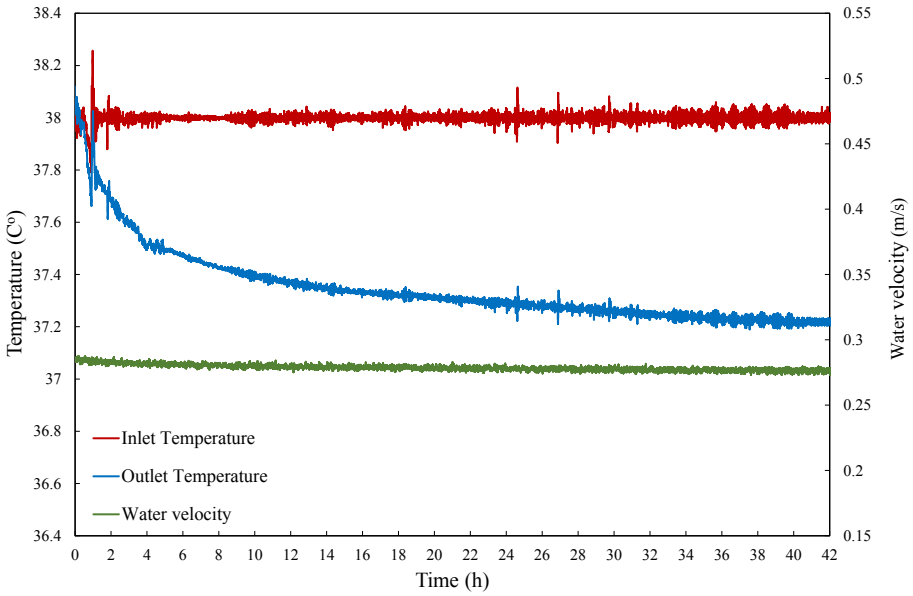

Figure 5.6: Variations of the pipeline inlet and outlet temperatures as well as water flow velocity for test case (1).

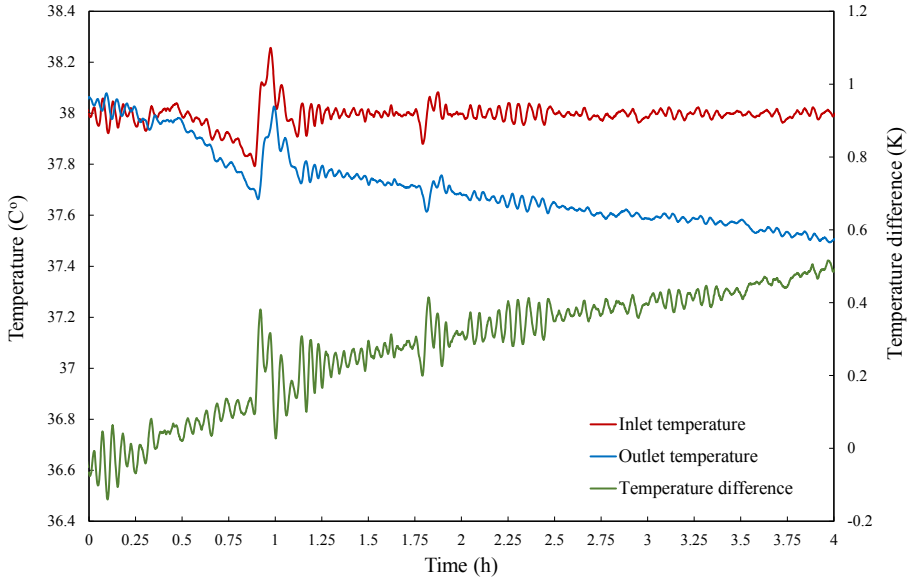

Figure 5.7: Variations of the pipeline inlet and outlet temperatures as well as temperature differences for the test case (1) at the first 4 hours.

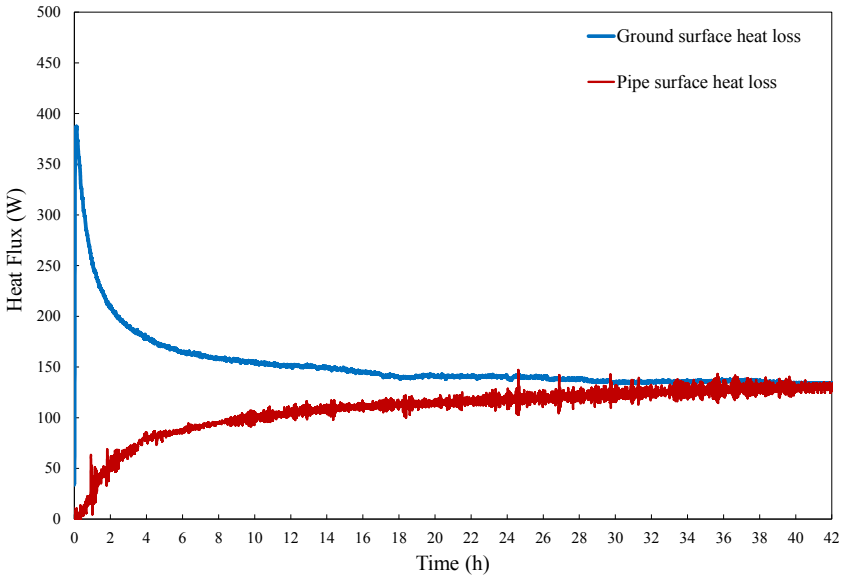

Figure 5.8: Variations of the pipeline and ground surface heat losses for the test case (1).

equation according to the temperature differences between the inlet and outlet of pipeline and the water flow rate. Small fluctuations can be observed in the pipeline heat fluxes over the experiment. This is because of the small fluctuations in the temperature differences between the inlet and outlet of pipeline used in the calculation. In other words, the fluctuations in pipe heat flux are relatively larger as the temperature differences between the pipeline inlet and outlet become smaller.

In the numerical models developed in this work, the ground surface heat transfer coefficient is required to be set into these models. The ground surface heat transfer consists of two main heat transfer mechanisms: convection and radiation heat transfer, as discussed in Chapter 2. The combined heat transfer coefficient can be determined both experimentally and theoretically. Since the heat fluxes from the ground surface, as well as the surface and ambient air temperatures, are measured in the specified time step, the heat transfer coefficient can be calculated based on Newton's cooling law. The heat transfer coefficient can also be estimated theoretically based on the well-known empirical relations discussed in Chapter 2. Fig 5.9 illustrates the variations of the sand surface heat flux and temperature, ambient air temperature, and the heat transfer coefficient calculated based on this measurement data. It can be seen that the ground surface heat transfer coefficient is almost constant during the test. This indicates that the surface heat transfer coefficient is independent of the surface temperature changes since it mainly depends on the flow

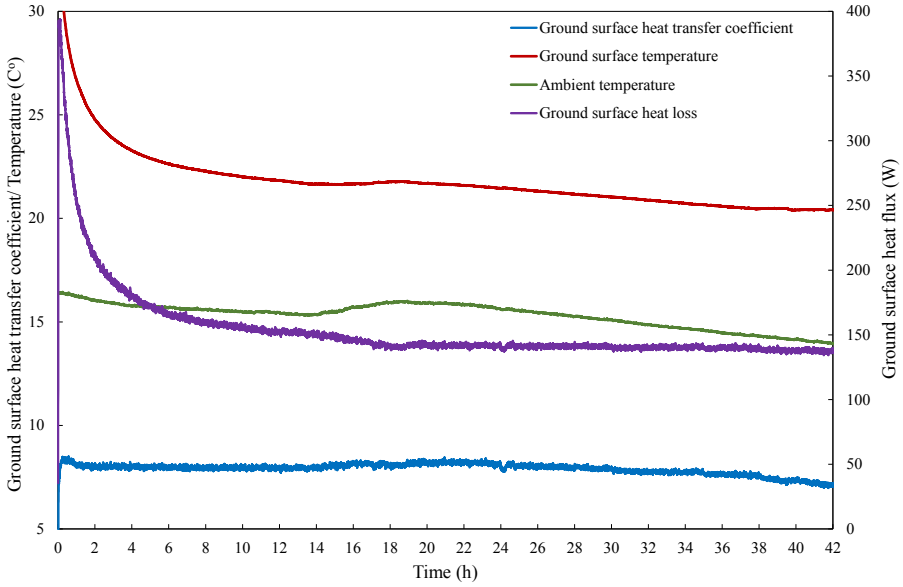

Figure 5.9: Variations of the ground surface heat flux, temperature, and heat transfer coefficient as well as lab temperature over the experiment.

condition of the air near the surface, and the emissivity of the surface, which are both unchanged over the tests. The sand surface heat transfer coefficient calculated here has been used in the numerical models developed in this work, namely the three-dimensional model, and all implementations of the DTN model.

5.2.2 Step Change applied at the Pipeline Surface Boundary

To apply a step change to the pipeline boundary temperature, firstly it was necessary to leave the system at the lab temperature for approximately two days to make sure that system temperature including the water and sand temperatures are stable. Having prepared the system, the circulated water is heated up in the heat source circuit via the immersed heater controlled by the PID controller to reach the desired inlet temperature to achieve a step change of approximately 21.8 °C. The step response heat fluxes obtained from both long timescale experiments are later scaled equivalent to a unit step change (0-1) and expressed independently of the initial temperature conditions of the experiments.

The PID controller is relied upon to tuning process to keep the pipeline inlet temperature constant by accurately controlling the heater. The details of the tuning

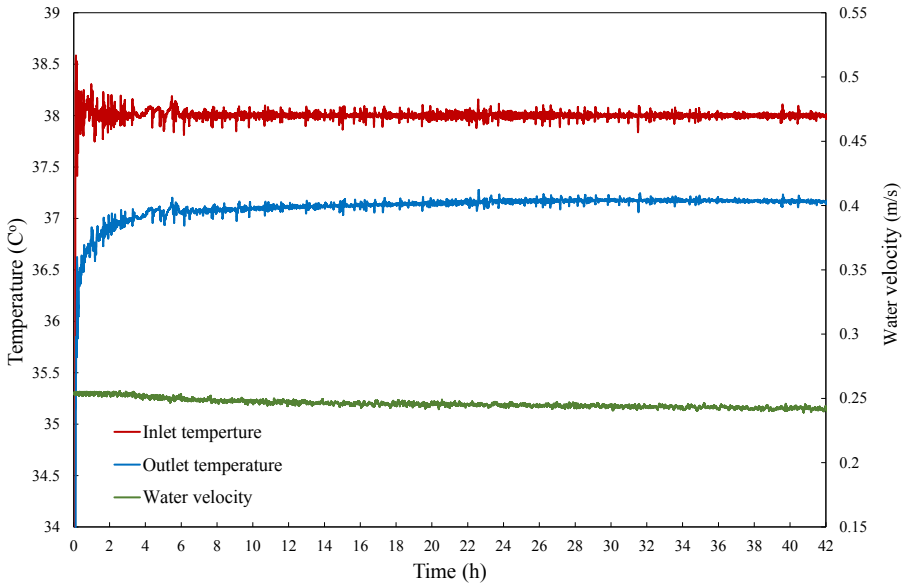

Figure 5.10: Variations of the pipeline inlet and outlet temperatures as well as water flow velocity for test case (2).

process are described in Appendix B.

One of the objectives of this set of experiments was to obtain the weighting function series required in the DTN model calculation from the measurement data. For the calculation of the weighting factor series, the surface heat transfer coefficients need to be the same in all the step response tests. Since the velocity of water through the pipeline and in turn Reynolds number affects the value of the heat transfer coefficient in the pipeline, the water velocity was chosen close to the first experiment, i.e. $0.246\,m/s$ (Re=4900). The velocity and Reynolds number differences between these two experiments are less than 0.027 m/s and 550, respectively. However, it is found that the model is not sensitive to the small differences between the heat transfer coefficients in extracting weighting factors, also in the final calculation of outlet temperature in the DTN model, the heat transfer coefficient is updated based on the current velocity and in turn Reynolds number. Hence, it was not necessary to repeat the test with a range of Reynolds Numbers.

Fig. 5.10 displays the variations of the inlet and outlet temperatures of the pipeline, as well as water velocity over the experiment. It can be observed that during the initial hours of the test, the outlet temperature rises relatively quickly, following the applied step change. The pipeline heat fluxes calculated in this initial phase of the experiment is representative of admittive heat flux of the pipeline. As

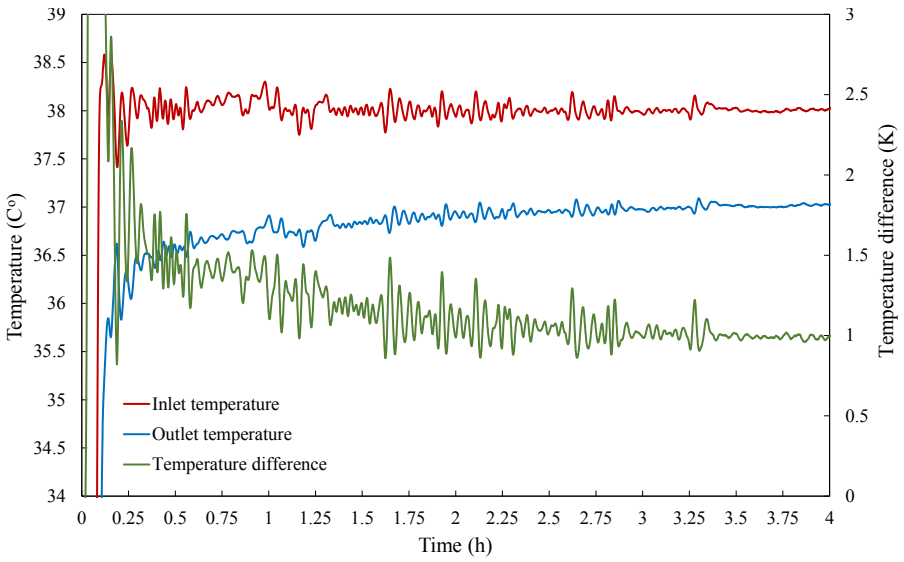

Figure 5.11: Variations of the pipeline inlet and outlet temperatures as well as the temperature differences for test case (2) at the first 4 hours.

time proceeds, the surrounding sand adjacent to the pipeline warms up, and thus the amount of heat loss from the pipeline to the sand decreases resulting in slowing down the outlet temperature rises until approaching a constant temperature near the steady-state condition. Due to the highly dynamic behaviour of the system at the beginning, the variations of the inlet and outlet temperatures of the pipeline along with the temperature differences are shown in the first four hours of the test in Fig. 5.11. It can be seen during the initial minutes after applying the step change, some small fluid temperature spikes occurred. Again, this was due to the limitations in the dynamic control of the heater output as noted above rather than a physical heat transfer phenomena. These short term fluctuations are not significant given the overall timescale of the test.

Fig 5.12 shows the variations of the heat fluxes from the pipeline and ground surfaces, due to applying the step change to the pipeline boundary temperature. The ground surface heat fluxes are obtained by averaging the heat fluxes measured by the three heat flux sensors on the sand surface, and the pipeline heat fluxes are calculated based on the pipeline heat balance equation. The small fluctuations in the pipeline heat fluxes over the test is because of the small fluctuations in the temperature differences between the inlet and outlet of the pipeline used in the calculation (Shown in Fig. 5.11). These fluctuation are fall mostly within the accuracy of the pipeline heat balance calculation, i.e. 2.18 percent. Therefore, it can be concluded that this

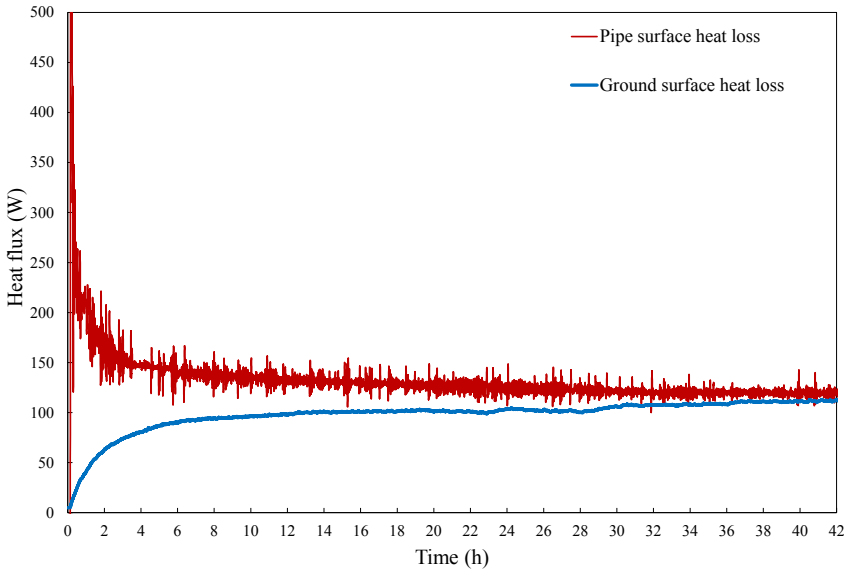

Figure 5.12: Variations of the pipeline and ground surface heat losses for the test case (2).

is an acceptable level of the noise given the overall time and heat flux scales.

Having determined the pipeline and ground surface step response heat flux data from both experiments, the admittive and transmittive heat fluxes can be obtained. To that end, the step response data needs to be expressed equivalent to a unit temperature step change (0-1). Hence, all heat flux data obtained in the experiments is divided by the temperature differences between the step change temperature and initial temperature of the system ($Q_{Normalized} = Q/(T_{Step\,Change} - T_{Initial})$). In this way, the obtained heat fluxes are normalized to the applied temperature step change. This allows comparing the step response heat flux data independent of initial temperature conditions of the system and the amount of step change. Fig 5.13 illustrates the normalized step change heat fluxes obtained from two experiments from the moment of applying the boundary step change until the system approaches steady-state conditions. It can be seen that both normalized heat fluxes from the ground surface to the pipeline surface and vice versa obtained from each test are very close. These values should be theoretically the same since they represent the conductive heat transfer process from the one surface to another depending only on the thermal properties of the materials and the geometric arrangement. Moreover, it can be seen as time proceeds all heat fluxes approach to the same value, i.e. the steady-state conductance. This shows consistency of the experiments, as the steady-state values of both long timescale experiments closely approach the same the steady-state

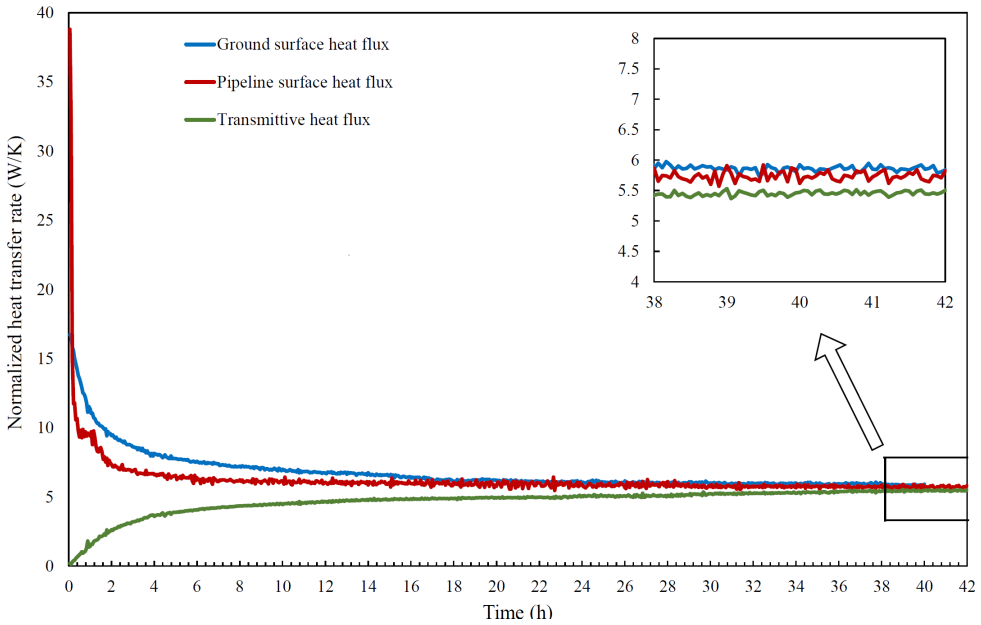

Figure 5.13: Variations of the normalized heat flux step responses of the pipeline and ground surface.

conductance.

Fig 5.14 shows the normalized admittive and trasmittive heat fluxes calculated based on the normalized step response heat flux data determined from both experiments. At the beginning of applying the step change to the boundary temperatures, the admittive heat fluxes are maximum, i.e. equal to the surface conductances, while the transmittive heat flux is zero. As the buried pipeline system approaches the steady-state conditions, the admittive heat fluxes approach zero, whereas the transmittive is getting close to the steady-state conductance. Fig 5.14 illustrates the normalized admittive and transmitve heat flux by the corresponding conductances over the experiment time. It can be observed the ground surface admittive heat flux drops more gradually than the sharp fall of the pipeline surface admittive heat flux, particularly at the first few hours of the test. This is because the pipeline surface losses considerably more heat once the step change applied compared with the ground surface. This issue is reflected in the value of heat transfer coefficient of the surfaces, as this value for the pipeline surface is almost a hundred times higher than that of the ground surface.

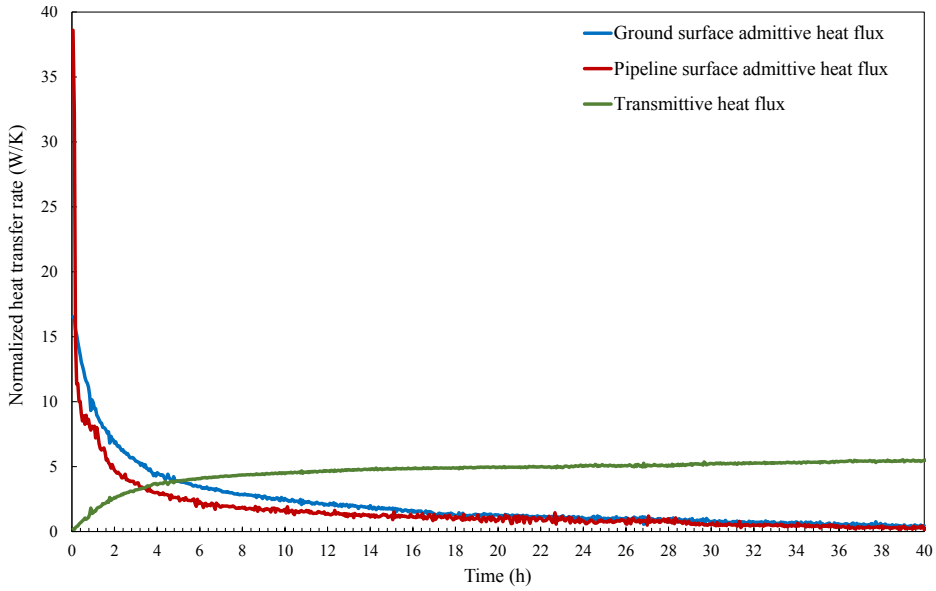

Figure 5.14: The admittive and transmittive step response heat fluxes for the buried pipeline system.

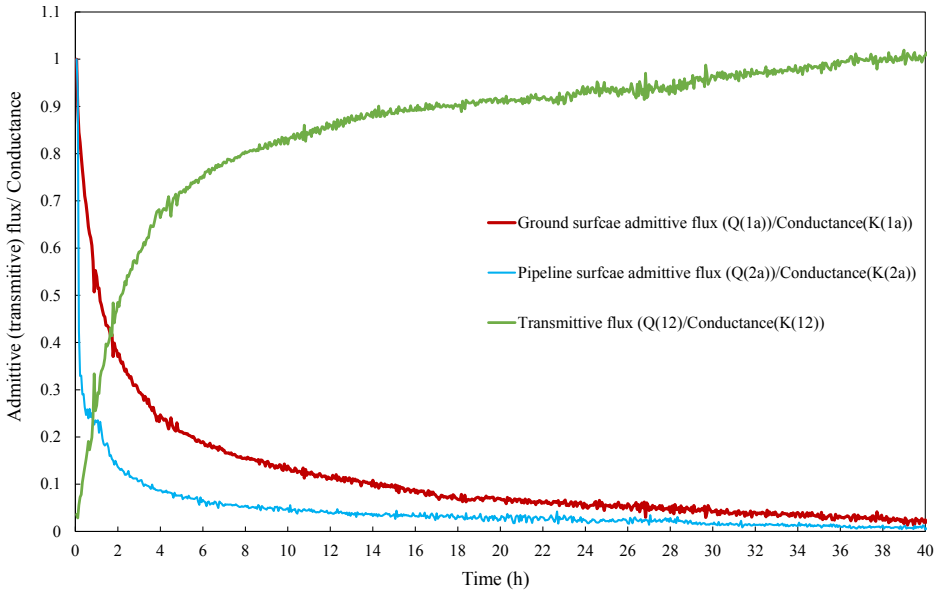

Figure 5.15: The admittive and transmittive step responses normalized by the corresponding conductances.

5.3 Conclusions

In this chapter, the experimental results of the dynamic thermal response experiments both in the short and long timescale are presented and discussed. The experimental results provided important information about the effects of the short timescale dynamic effects on the thermal response of pipelines, as well as the impacts of the dynamic conduction heat transfer of the ground on the thermal behaviour of the buried pipeline. These experimental data are further used for validation of the proposed numerical models for both the short and long timescale thermal responses.

Firstly, the dynamic thermal responses of the pipeline over short timescales have been evaluated considering the imposition of a step change in inlet temperature. Two pipeline external surface boundary conditions including the uninsulated and insulated pipeline were used, while a step change was imposed on the inlet pipeline temperature. The rising time and shape of the temperature profile at three locations were assessed for both boundary conditions and four water flow rates. These data reveal the effects of heat transfer and fluid dynamics on shaping the temperature profile in pipelines at shorter timescales of the order of magnitude of the nominal transit time of the fluid. Moreover, comparing the experimental results obtained from both sets of the tests revealed that despite using different boundary conditions for the outer surface of the pipeline, the dimensionless temperature responses are approximately close to each other. This implies that the thermal inertia of the pipeline plays a dominant role in shaping the temperature profiles in the pipeline at short timescales. The data obtained from this set have subsequently been used for validation of the proposed numerical model developed in this research, presented in Chapter 6.

The dynamic thermal response of the buried pipeline considering the transient conduction heat transfer in the ground has been experimentally investigated over longer timescales approaching steady-state heat transfer conditions. To evaluate the dynamic thermal response the pipeline and ground, a step change was imposed to the pipeline and ground surfaces, and the heat fluxes and temperatures of the surfaces were measured and recorded over the tests. The experimental results elucidate the effects of the transient conduction heat transfer through the ground on the dynamic thermal response of pipeline over these longer timescales. Furthermore, the data elucidates the role of dynamic heat losses from the ground surface on the thermal behaviour of the buried pipeline. It was found that the heat losses from the sand

surface to the ambient can affect the pipeline heat losses, as in the steady-state conditions, almost 0.35 W/K is lost in per meter of the pipeline to the ambient (almost 6 percent of the total heat delivering by the fluid flow through the pipeline). However, this data is for a single uninsulated pipe buried in the dry sand with the low turbulent fluid flow. The long timescale experimental data is further used to extract weighting factors to set into the conventional and modified DTN model, and to validate the 3D model, DTN model and the combined DTN-PFST models, and this is discussed in Chapter 6.

Chapter 6

Short Timescale Model Results

The results of the numerical calculations of the dynamic thermal response of pipelines at short timescales are presented in this chapter. The short timescale models developed in this research, including the three-dimensional model, and four forms of discretised one-dimensional models are used to modelling dynamic thermal behaviour of the pipeline at various operating conditions. The three-dimensional numerical calculations have been made to make comparisons with the experimental and analytical results to examine the suitability of one-dimensional numerical models proposed in this research.

Firstly, the three-dimensional finite volume model described in Section 3.1 was evaluated in terms of predicting turbulent velocity profile and residence time distributions. The 3D numeral results are compared with the experimental data and analytical results in the literature. This data has been used to carry out a preliminary mesh independency study. Given successful validation of the numerical model, it is regarded as a reference model for tests of other models in this research.

The numerical results obtained from the short timescale dynamic thermal response models (described in Section 3.2) are presented and discussed in the second part of this chapter (Section 6.2). Firstly, the numerical results from the NCST and PFNCST models are compared with the analytical solution of ADPF model in terms of prediction of the dynamic thermal response of a pipeline without radial heat losses (ideally insulated). Moreover, the ability of the proposed model, i.e. the modified PFNCST model, is investigated in simulating the heat propagation through the pipeline by comparing the calculated results with the 3D reference model and experimental data. The details of the short timescale dynamic thermal

effects impacting the dynamic thermal responses of pipelines are also discussed.

6.1 The Three-dimensional Reference Model Validation

The validation of the three-dimensional model has been carried out by comparing the simulation results with the experimental data and analytical results in terms of the pipeline velocity profile and residence time distributions. Firstly, a straight pipeline is modelled using the FVM to examine the simulated turbulent velocity profile by comparing the simulated results with published experimental data. Further comparisons are also made for different mesh sizes to study pipeline mesh independence. Moreover, the 3D pipeline model is evaluated in terms of predicting the RTD using the semi-empirical model and the experimental conditions reported by [Ham & Platzer (2004)].

6.1.1 Turbulent Velocity Profile

To validate the pipeline 3D model developed in this work experimental data from the literature have firstly been used. Due to the importance of velocity profile in the turbulent pipe fluid flow [Reynolds number is higher than 4000] on the RTD and dynamic response of pipes, the first objective in the validation exercise to verify the models' predictions of the pipe velocity profile. Many researchers have conducted different types of experiments to study fully developed turbulent pipe flow. In the current work, experimental data from particle image velocimetry (PIV) experiments [Eggels *et al.* (2006); Peng *et al.* (2018)] have been chosen as these are thought to represent the lowest levels of uncertainty: reported to be less than 2 percent.

Fig. 6.1 shows a comparison of predicted and measured mean velocity profile normalised by the bulk flow velocity with respect to the pipe radius for a 10m straight pipe at a Reynolds number of 5300. The numerical simulation results show very good agreement with the experimental data over most of the radius. In order to check the mesh size independence, five mesh sizes were generated to compare the Root Mean Squire Error between the velocity profiles obtained from the numerical model and experimental data, as illustrated in Fig. 6.2. The RMSE between the predicted values and observed values has been calculated according to Eq. 6.1. This calculation

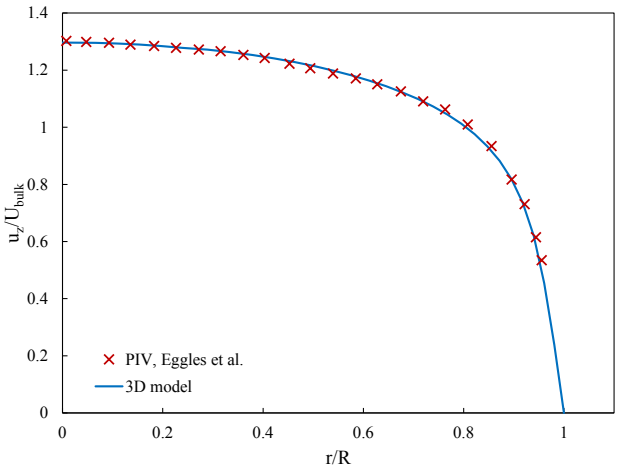

Figure 6.1: Axial mean velocity profile normalized by the bulk flow velocity.

is used for a couple of times in this research for making different comparisons between the results.

$$RMSE = \sqrt{\frac{1}{n}\sum_{i=1}^{n}((Y_{\text{simulation,i}} - Y_{\text{experimental data},i})^2} \tag{6.1}$$

In Eq. 6.1, Y is the longitudinal velocity at radial measurement point (i) shown as X for published data in Fig. 6.1. It was observed by increasing cell number from 47,000 to 208,000, the RMSE decreased from nearly 4.3 to 1.35 percent. Considering the computational cost, a mesh with intermediate density (159,000 cells) was chosen to model the pipe flow and heat transfer in later calculations.

6.1.2 Residence Time Distributions

To validate the pipeline 3D model in terms of predicting the Residence Time Distribution (RTD), the semi-empirical model with the experimental data presented by Ham & Platzer (2004) for a straight pipe has been used as a reference. Based on the experimental conditions in their work, a 9.6 m straight pipe with 15 mm diameter was modelled where the mean velocity, Reynolds Number and kinematic viscosity were 0.21 m/s, 4500 and 7×10^{-7} m^2/s, respectively. The measured mean residence time is reported as 45.7 s. The minimum and maximum residence times were measured as 38.89 s and 77.01 s, respectively. These two parameters indicate

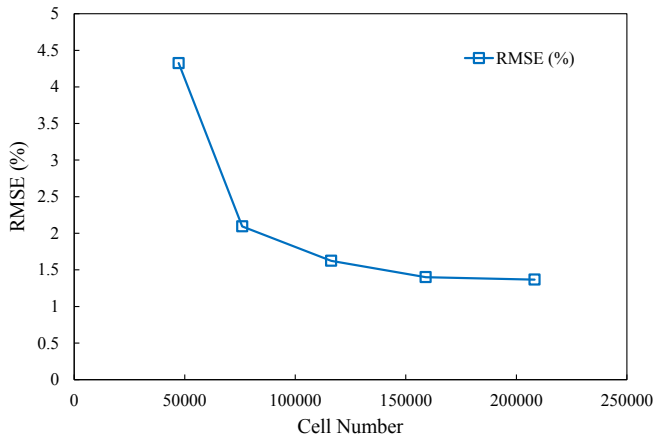

Figure 6.2: RMSE between the normalized velocity profile measured by Eggels *et al.* (2006) and calculated by the 3D model for five mesh sizes.

the time required for any transported variable to start reaching the specific point (minimum residence time) and completely exit the point (maximum residence time).

Applying these experimental conditions and using the semi-empirical model from Ham & Platzer (2004), the F-diagram can be plotted based on Eq. 2.5. Fig. 6.3 displays this F-diagram generated using the 3D model and the semi-empirical model according to the experimental data. A very good level of agreement between the semi-empirical model and the 3D model developed in this work has been demonstrated.

6.2 Short Timescale Dynamic Thermal Response Models

In this section, the numerical results obtained from the short timescale dynamic thermal response models including the one-dimensional models, and the three-dimensional model described in Section 3.2 are presented and compared with the measurement data collected in this research. Initially, the one-dimensional NCST and PFNCST models are assessed in terms of prediction of the dynamic thermal response of a pipeline without radial heat losses (ideally insulated) in Section 6.2.1. The assessment is conducted by comparing the calculated results with the analytical solution of the ADPF model for a long pipeline.

The one-dimensional models are also evaluated in the prediction of the dynamic thermal response of a pipeline with heat losses to the surroundings. The main focus

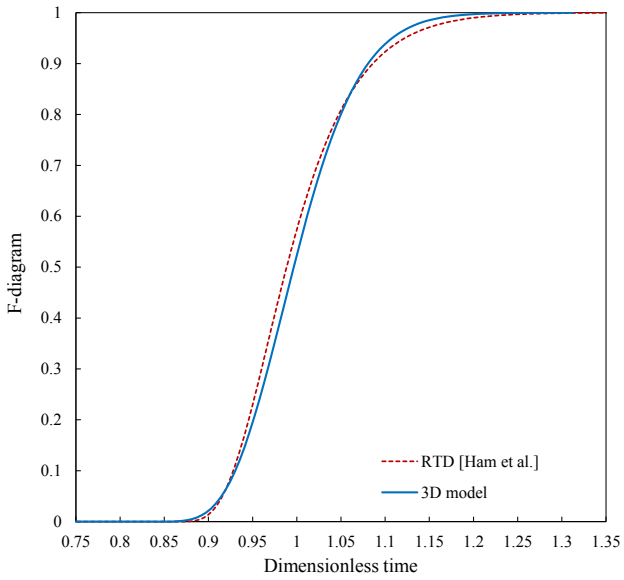

Figure 6.3: Comparison of F-diagram calculated by using the 3D model and the semi-empirical model.

of Section 6.2.2 is to assess the novel numerical model proposed in this research [the modified PFNCST model] by comparing the numerical results of modelling the dynamic thermal response of the pipeline with heat losses with the experimental data. To this end, the experimental results obtained by applying a step change to the inlet temperature of uninsulated and insulated pipeline are used to assess the modified PFNCST model results in terms of prediction of the shape of the temperature profile at the particular distances for a wide range of fluid flow rates. The comparisons between the temperature step response of pipes predicted by the proposed models and the analytical solutions as well as experimental data for various operating conditions are presented in the following sections.

6.2.1 Dynamic Response of an Ideally Insulated Pipe

To investigate the models developed for the simulation of the dynamic responses of the ideally insulated pipe, the results of the two discretised models, the NCST and PFNCST, have been compared to the exact solution of the ADPF model. The sensitivity of the predictions to the number of tanks in the model is evaluated. To this end, responses in a 10 m straight pipe of 15 mm diameter have been studied. In this comparison with the available analytical solution, the water flow velocity and Reynolds number were 0.5 m/s and 9700 respectively. In this case, the inlet

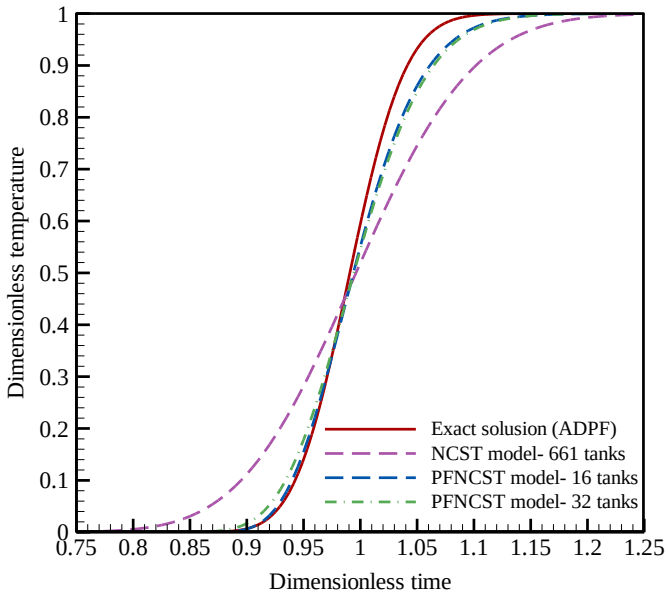

Figure 6.4: Comparison between the outlet temperature responses to a step change calculated by the NCST, PFNCST models and the exact solution of the ADPF model for an insulated pipe.

temperature of the pipe is imposed with a step change of 60 K, from 20 °C to 80 °C, while the initial temperatures of the water and pipe wall are 20 °C. It is considered that heat transfer at the pipe wall is zero, so an adiabatic boundary condition is applied for the inner surface of the pipe. In this situation, the physical phenomena are limited to transport delay and longitudinal dispersion according to the velocity profile.

Fig. 6.4 displays the variations of the dimensionless outlet temperature responses to a step change calculated by three models, including the NCST, PFNCST and the exact solution of the ADPF models. Based on Eq. 3.25, the optimal number of tanks in the NCST model was calculated to be 661, and two tank numbers suggested in the literature for this model [16 and 32] were selected for the PFNCST model.

The data in Fig. 6.4 illustrates good agreement between the PFNCST model and the exact solution of ADPF in the prediction of the outlet temperature. The NCST model tends to overpredict the diffusion in responses to a step change: as reported elsewhere [Hanby *et al.* (2002); Rees (2015)]. This is indicated by the early initial rise in temperature and slower approach to the steady solution. It has also been found that the number of tanks required for the PFNCST model is much lower than that recommended for the NCST model and furthermore, that the variation

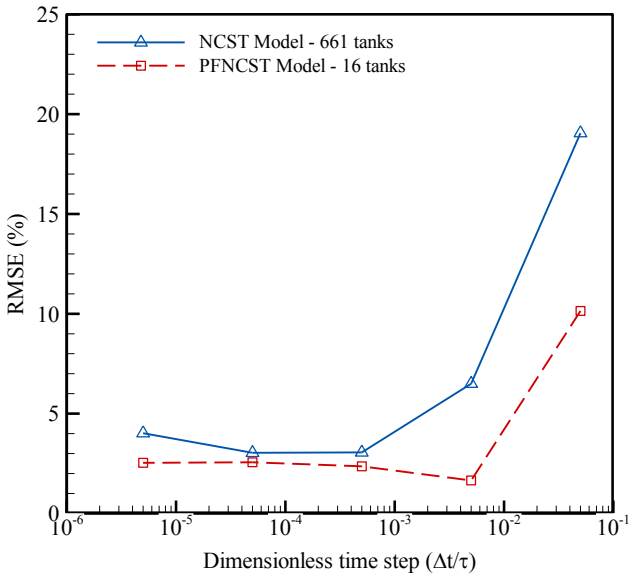

Figure 6.5: RMSE between temperature responses to a step change calculated by the NCST, PFNCST models and the exact solution of the ADPF model for an insulated pipe.

of the number of tanks in the PFNCST model does not have noticeable effects on the accuracy of the prediction of dynamic responses, i.e. the model is robust in this respect.

To investigate the effect of the time step size on the results, the dimensionless time step over a duration of 20 s is varied between 5×10^{-6} and 0.05 in the NCST and PFNCST models. The comparison between the results is made by RMSE calculation between the predicted outlet temperature at a particular time of the exact solution of the ADPF model and the numerical models, as shown in Fig. 6.5. It is observed by setting the dimensionless time step less than 0.01 in the models, the RMSE between the exact solution of the ADPF model and the temperatures predicted by the models does not noticeably vary with the time steps. Therefore, the accuracy of the outlet temperatures predicted by the models can be considered independent of time, that by choosing the dimensionless time steps short enough, i.e. 0.01 for the PFNCST model or 0.001 for the NCST model to have RMSE of less than 5 percent.

6.2.2 Dynamic Responses of Uninsulated Pipeline

To evaluate the prediction of the dynamic thermal responses of uninsulated pipe to a step change in inlet temperature, a range of experimental data has been examined, summarised in Table 5.1. The details of the experimental conditions of short

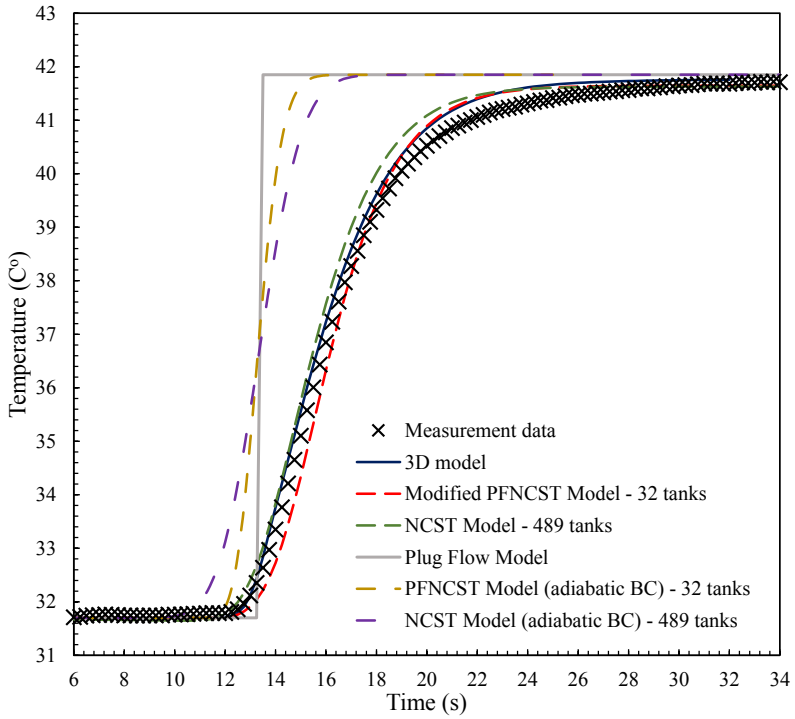

Figure 6.6: Comparison between outlet temperature calculated by the NCST, PFNCTS models for the ideally insulated pipe and the NCST, modified PFNCST models and measurement data ($L = 7.93\,\mathrm{m}$, $v = 0.589\,\mathrm{m/s}$)

timescale tests for both the uninsulated and insulated pipeline and the measurement data are described in Section 5.1.

Fig. 6.6 illustrates the comparison between different models in calculating outlet temperature to a step change and measured data. In this case, the water velocity and Reynolds number are 0.589 m/s and 8680, respectively. The water flow temperature in the insulated copper pipe was measured at 7.93 m from the pipe inlet once the step change of almost 10 K is applied at the pipe inlet temperature. According to these experimental conditions, the outlet temperature has been calculated using the proposed model (modified PFNST model) with other existing models developed in this research to assess the accuracy of the model predictions. It is observed there is a good agreement between the measurement data and both the NCST model and modified PFNCST model. However, the number of tanks in the modified PFNCST is less than one-tenth that of the NCST model and this feature can be considered an important advantage in terms of computational resources.

Other data in Fig. 6.6 show an idealised plug-flow response (i.e. without any

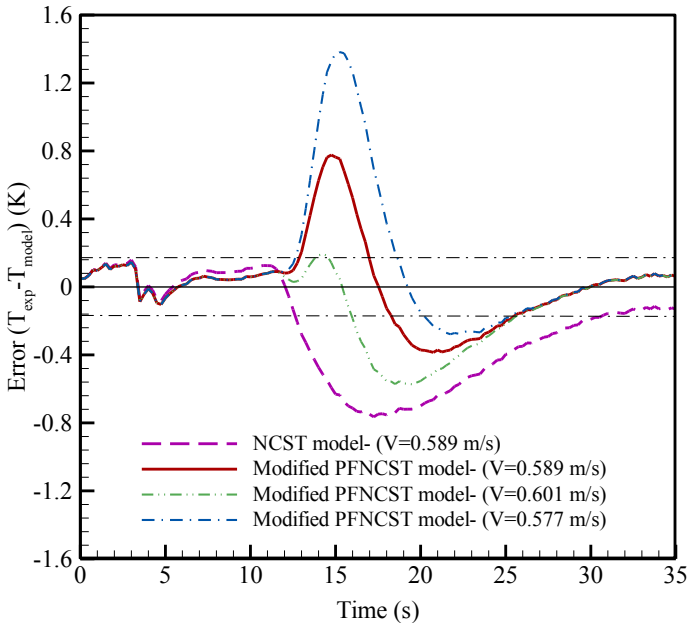

Figure 6.7: The error between measured temperature and the temperature calculated by the models for the measured velocity and ±2 percent of the measured velocity ($L = 7.93\,\mathrm{m}$, $v = 0.589\,\mathrm{m/s}$)

diffusion) and the NCST, PFNCST model responses assuming no heat loss. These responses demonstrate that, although the shape of the velocity for turbulent fluid flow has a diffusing effect on the shape of the outlet temperature, the thermal inertia of the pipe is dominant in determining the overall level of diffusion in such cases over short timescales. The fact that the NCST model over-predicts diffusive effects means that the prediction of outlet temperature is better in this case than without heat transfer. This seems largely coincidental. As the modified PFNCST works well both with and without heat transfer, further studies have focused on this model.

Fig. 6.7 is plotted to display the range of errors between the measured temperatures and the temperatures calculated using the proposed modified PFNCST model as a function of time and for different flow rates. The dashed lines show the accuracy of the thermocouple used for measuring the temperature. It can be seen that the differences fall mostly within the range of thermocouple accuracy but with larger differences during the time of rapid temperature change. Due to the importance of the flow velocity on the outlet temperature response, the differences at the upper and lower limits of the flow meter error (two percent of the measured value) were also calculated. This has an effect on both the magnitude and means difference.

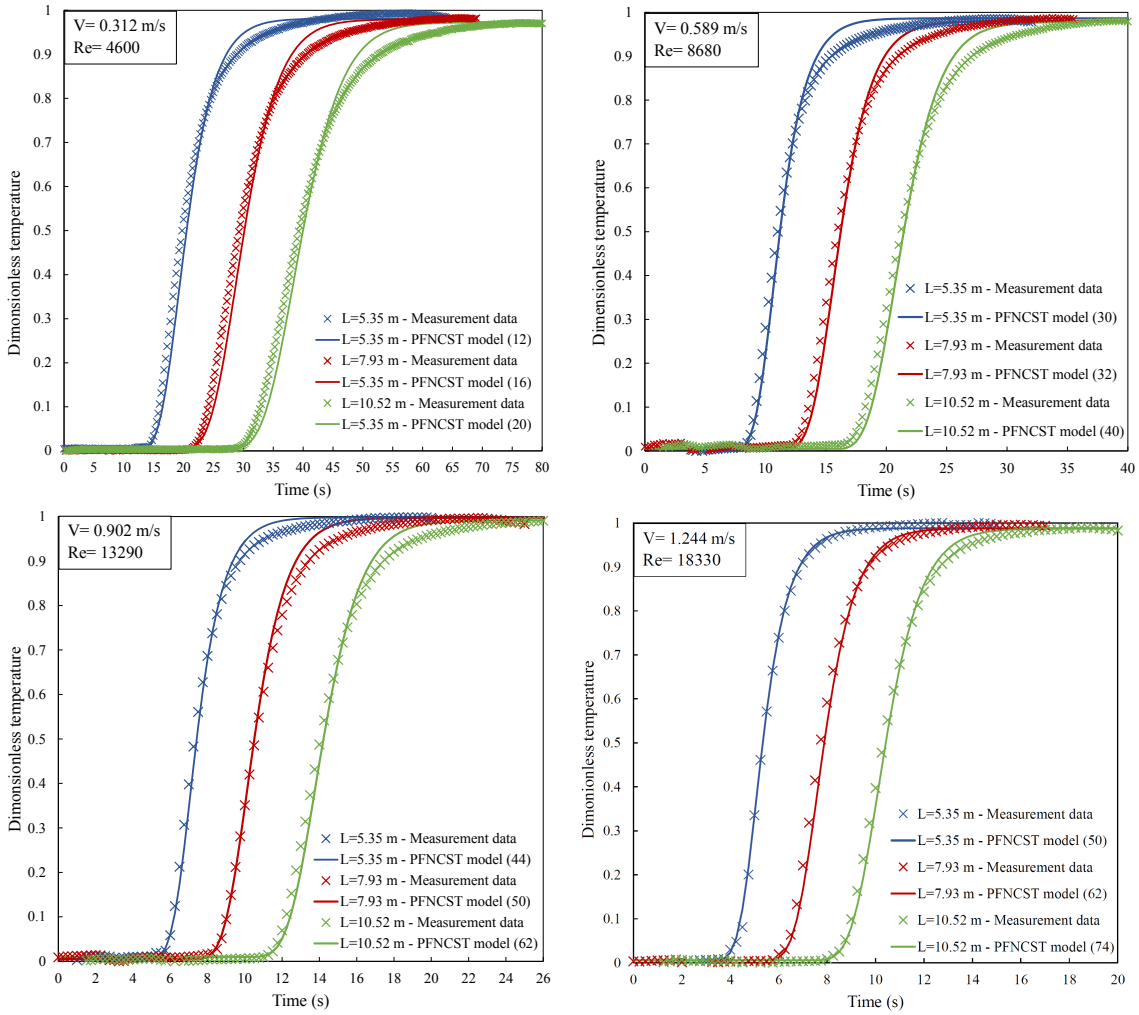

Figure 6.8: The insulated pipeline outlet temperature profiles at three distances ($5.35\ m, 7.93\ m, 10.52\ m$).

Results for the full range of flow conditions studied are presented in Fig. 6.8 and Fig. 6.9 and show comparisons between dimensionless measured temperatures at three distances, and the proposed modified PFNCST predictions of outlet temperature response. The figures unveil the modified PFNCST model results are in good agreement with experimental data for all cases. For the cases with higher Re numbers, the agreement between the model predictions and measurement data is even closer. The ability of the modified PFNCST model to predict both the time of initial temperature rise and the following temperature rise profile is consistent across the range of conditions studied.

It has been found that in cases where heat transfer is present, there is some

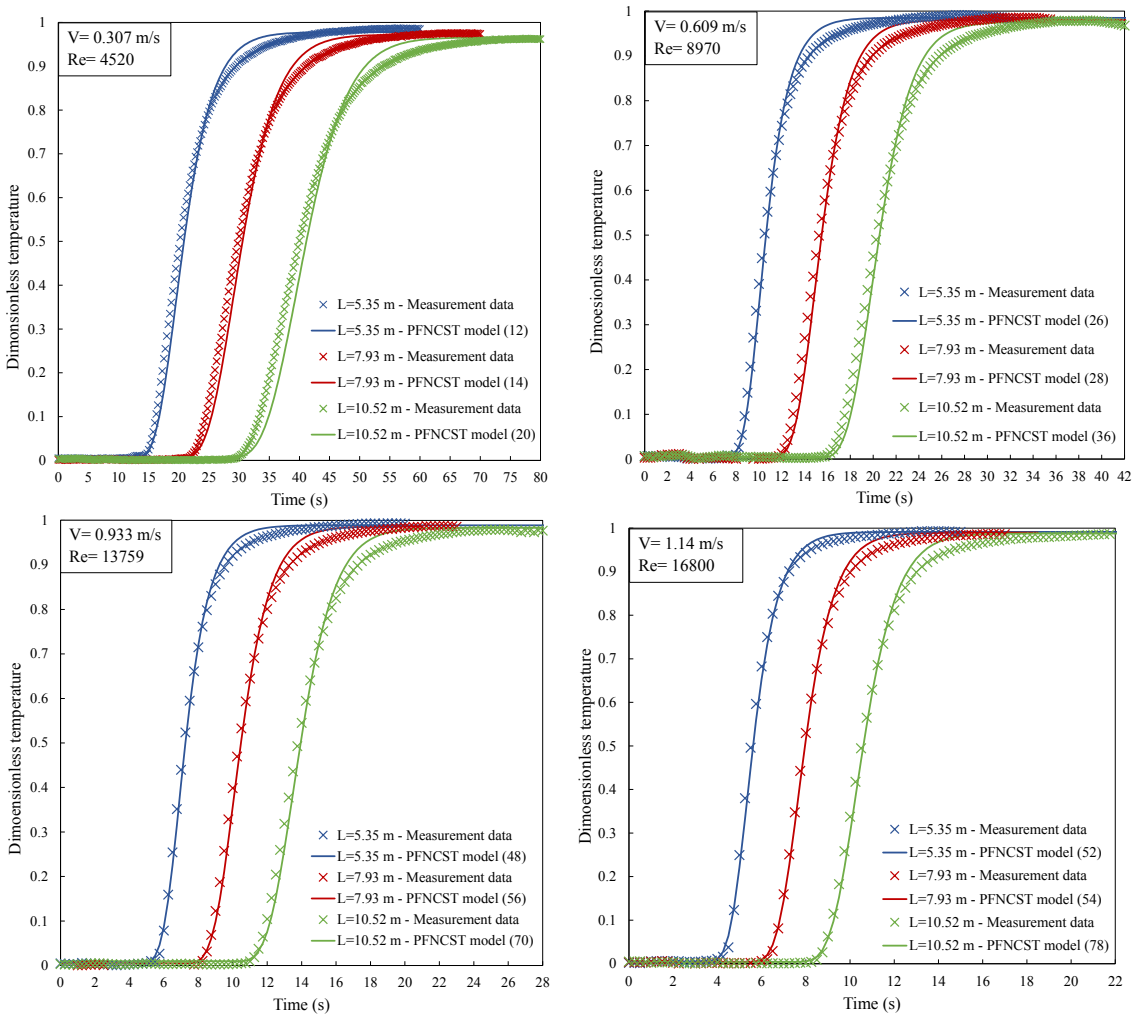

Figure 6.9: The uninsulated pipeline outlet temperature profiles at three distances ($5.35\ m, 7.93\ m, 10.52\ m$).

sensitivity to the choice of the number of tanks such that an optimum number of tanks can be found that minimises the differences between model and measurement.

Fig. 6.10 shows the variation of outlet temperature RMSE using the modified PFNCST model and measured temperatures for the different number of tanks for the case of insulated pipe with a water velocity of 0.589 m/s and at three distances from the pipe inlet. The RMSE is calculated based on the difference between the predicted temperature of the fluid by the model and measurement data integrated over the time of tests. Although optimising the number of tanks can improve the accuracy of the model, it can be seen that for a wide range of tank numbers, the RMSE value is still acceptable, i.e. about 0.4 K (less than 5 percent of the step

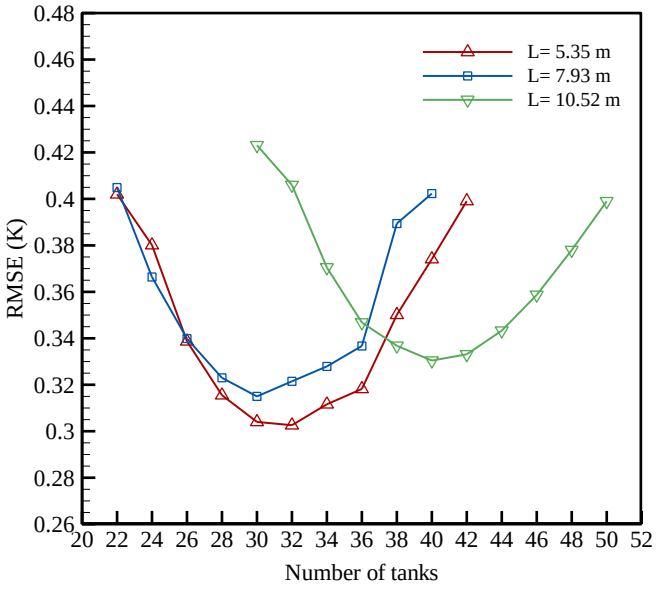

Figure 6.10: RMSE between measured temperature and that calculated by the modified PFNCST model where the flow velocity is 0.589 m/s

change temperature), showing minor sensitivity of the model to the tank numbers. As the same way for these three cases, the RMSE for other cases can be calculated, and the optimum number of tanks can be found. The optimum number of tanks for the proposed model have been used in each case shown in Fig. 6.9 and Fig. 6.8.

For the case shown in Fig. 6.6, the outlet temperatures calculated by the modified PFNCST model for the different number of tanks are illustrated in Fig .6.11. It can be seen that a lower number of tanks causes a slightly sharp thermal response to a step change (less diffusive) and vice versa. This is a result of the diffusion processes being more complex in cases with heat transfer through the pipe wall: heat is diffused both axially and radially. In these calculations, it is sought to investigate whether a rule or correlation can be identified to guide the appropriate choice of the number of tank elements in cases with pipe wall heat transfer.

In a similar way to the NCST model, it has been found that the optimal number of tanks is well correlated with the Peclet Number. The preferred values of the number of tanks for a range of flow conditions have been obtained by carrying out parametric calculations and evaluating the RMSE to find the optimal value. This has resulted in the data shown in Fig. 6.12 where Pe is calculated based on Eq. 3.22. A well-defined trend is evident, and this can be approximated by a linear correlation

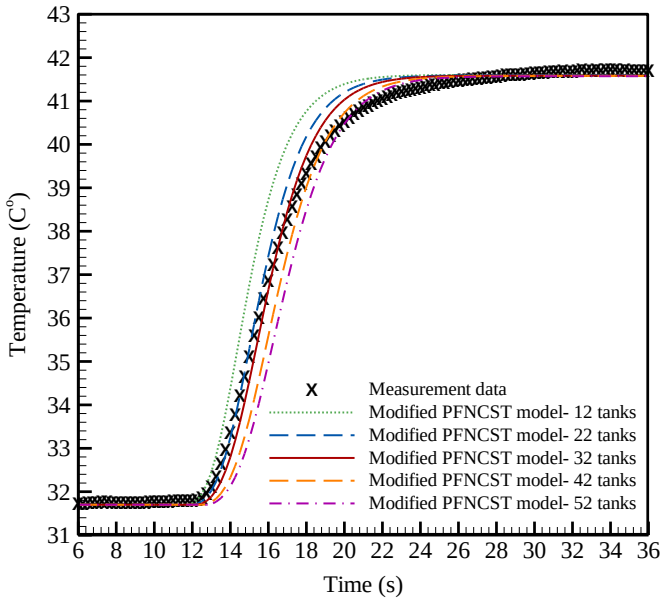

Figure 6.11: Comparison between the outlet temperature response calculated by the modified PFNCST model for different tanks number and measured data ($L = 7.93\,\mathrm{m}$, $v = 0.589\,\mathrm{m/s}$).

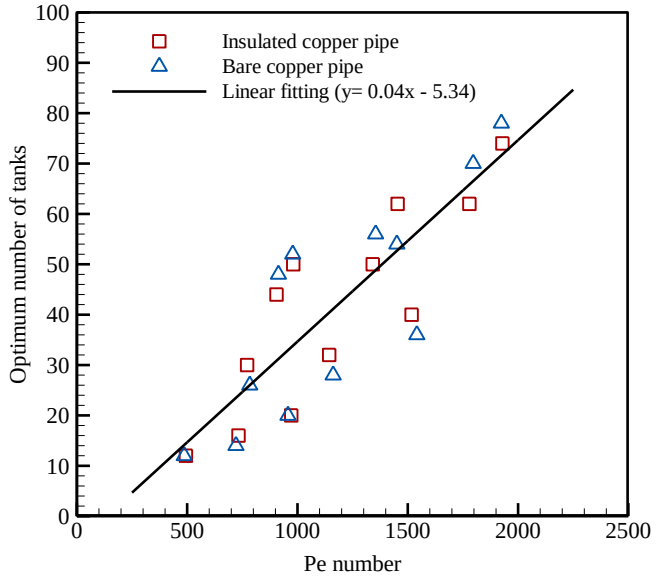

Figure 6.12: Variation of the optimal number of tanks for the modified PFNCST model and Pe number

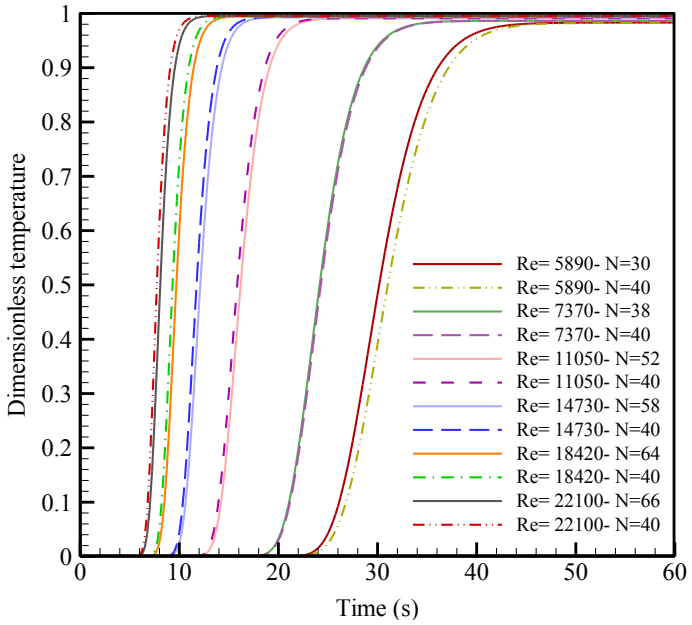

Figure 6.13: Comparison between the sensitivity of the PFNCST model to the number of tanks on the outlet temperature response for different flow rates (L=10.0 m).

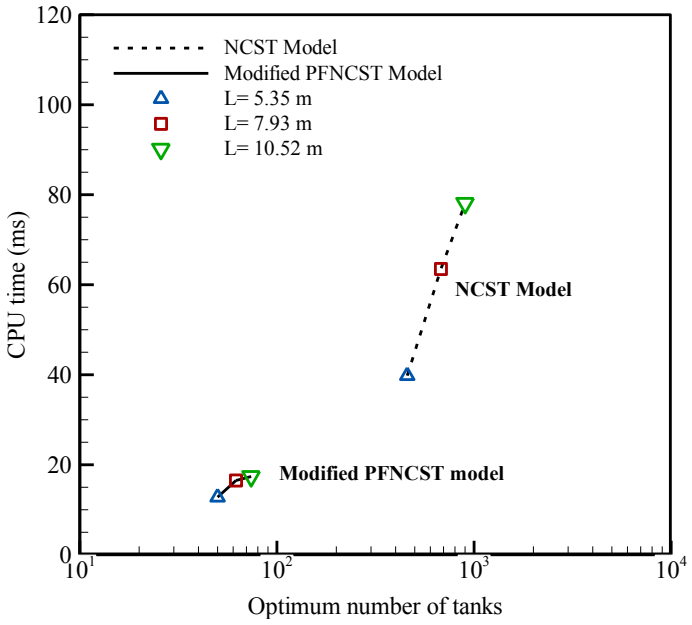

Figure 6.14: Comparison between the CPU time required and the optimum number of tanks for the modified PFNCST model and the NCST model ($L = 10.52\,\mathrm{m}$, $v = 1.244\,\mathrm{m/s}$).

Table 6.1: Root mean square error (RMSE) in relation to the dimensionless outlet temperature calculated by the PFNCST model with optimum number of tanks, the PFNCST model with 40 tanks and the NCST model with the optimum number of tanks for different mass flow rate.

Water velocity (m/s)	Reynolds number	RMSE (PFNCST model)	RMSE (NCST model)
0.4	5890	0.0261	0.0386 (448 tanks)
0.5	7370	0.0043	0.0366 (548 tanks)
0.75	11020	0.0153	0.0319 (708 tanks)
1.0	14730	0.0193	0.0245 (799 tanks)
1.25	18420	0.0216	0.0218 (857 tanks)
1.5	22100	0.0214	0.0199 (898 tanks)

expressed as:

$$N_{\mathrm{M-PFNCST}} = 0.04Pe - 5.34 \tag{6.2}$$

Eq. 6.2 can be used for calculation of the number of tanks for any case with different geometry and Reynolds number. The correlation is equally valid for both insulated cases and those with heat transfer.

Due to the dependency of the optimal number of tanks on Pe number and in turn, Reynolds number, the fluctuations of the mass flow rate directly affect the optimum number of tanks according to Eq. 6.2. This raises the question as to the best procedure for choosing the number of tanks when the model is implemented in a simulation environment, and the flow rate may vary with time, for example, in a circuit with a variable speed pump. In such a situation, the flow rate could be expected to fall to approximately 20% of the full speed value [Frederiksen & Werner (2013)]. An intermediate amount of flow rate, and hence Pe number, may be sufficient to fix the required number of tanks in the model.

To evaluate that suitability of this approach, an intermediate flow rate in the experimental study has been used, leading to a choice of 40 tanks. To investigate the significance of this assumption, the case of a 10 m copper pipe with 0.015 mm diameter with heat interaction with surroundings is modelled while 60 K step change is applied at the pipe inlet at an initial temperate of 20 °C. Six different water velocities are used to compare the prediction of temperature at the pipe outlet.

Fig.6.13 is plotted to display the discrepancies between the dimensionless outlet temperature calculated by the modified PFNCST model with 40 tanks and the optimum number of tanks calculated by Eq.6.2. It can be seen that there are small deviations between the outlet temperature prediction of the model with the optimum number of tanks and 40 tanks for a wide range of Reynolds numbers.

Table 6.1 presents the root mean square error of the outlet temperature calculated by the PFNCST model with the optimum number of tanks and 40 tanks as well as the NCST model with the optimum number of tanks. It is noted that the RMSE of the proposed model with fixed 40 tanks is less than or almost equal to the NCST model with the optimum number of tanks. It is concluded that the sensitivity to the number of tanks is not very significant and that using an intermediate flow rate within the expected range results in a suitable choice of tanks. It does not seem necessary to introduce a procedure to vary the number of tanks during a simulation and that simulating time-varying flow with heat transfer can be achieved in a robust manner.

To evaluate the computational time required to modelling the dynamic thermal response of the pipeline, the proposed modified PFNCST model and NCST model have been compared in terms of the required processor time (Intel(R) CPU E5-2699 @ 2.30GHz) for the case of the insulated copper pipe with a water velocity of 1.244 m/s at three distances, illustrated in Fig.6.14. It is observed the required CPU time is considerably lower for the proposed model than the NCST model. This is due to the much lower number of tanks used in the modified PFNCST model. It can also be seen that as the length of the pipe increases from 5.35 m to 10.52 m, the CPU time required for modelling dynamic thermal responses by the NCST model dramatically rises, while it slightly increases by the proposed modified PFNCST model. This offers a considerable advantage of computational time reduction in modelling the dynamic thermal response of pipelines, particularly, in thermal energy networks where many instances are coupled together and used in annual simulation.

6.3 Conclusions

One of the main aims of this work has been to develop a practical and accurate model with the ability to capture the short timescale dynamic effects of the pipelines such as the impact of longitudinal dispersion of turbulent fluid flow and dynamic radial heat transfer to surroundings. To this end, firstly, four numerical models are

developed and studied in this research, including the three-dimensional model, and three forms of discretised one-dimensional models. They have been implemented to modelling dynamic thermal behaviour of the pipeline under the different operating conditions over the short timescales.

A new numerical model has been proposed that is a modification of the PFNCST model, and extended to include a representation of the pipe material and radial heat transfer to model the short timescale dynamic thermal response of pipelines. This facilitates modelling of the thermal responses of pipe systems considering heat losses from pipe surfaces and the thermal capacity of the pipe. In cases with radial heat transfer, the diffusion of heat is effectively increased compared to a perfectly insulated case. This model is able to simulate the heat propagation through the pipe due to a step change at the inlet of the pipe, and capture short timescale dynamic effects in a good agreement with experimental data. A procedure has been proposed to allow the appropriate number of tanks to be defined, and the model implemented in variable flow simulation applications. The model has been shown to be robust over a wide range of conditions and to offer efficient computational calculation compared to other models. Due to the robustness and the accuracy of the model, the PFNCST model has been proposed to be combined with the DTN method to properly include transient ground heat transfer and interaction with adjacent pipes to allow the representation of district heating buried pipeline network. In the following Chapter, the numeral results of the combination of the DTN model with the PFNCST model are presented and discussed.

Chapter 7

Long Timescale Model Results

The results of the numerical models' calculations of the dynamic thermal responses of buried pipeline over long timescales are presented in this chapter. The numerical models developed in this research to deal with the transient conduction heat transfer of the buried pipeline are discussed in Chapter 3. These numerical models including the three-dimensional model, DTN model and combined DTN-PFST model are used to represent the dynamic thermal behaviour of the buried pipeline in different thermal conditions. The results from the models are later compared with measurement data to assess the ability of the models in predictions of the dynamic heat losses from the buried pipeline and ground surfaces as well as the pipeline outlet temperature.

Firstly, the three-dimensional finite volume model described in Section 3.1 was evaluated in terms of modelling conduction heat transfer process in the ground with convective boundary conditions. The 3D numeral results are compared with the analytical solution of a semi-infinite solid. The details of ground surface heat loss process are also presented and discussed in Section 7.1 of this Chapter. Having validated the finite volume model in modelling the transient conduction heat transfer with convective boundary conditions, the numerical model is combined with the three-dimensional pipeline model presented and validated in Section 6.1. This three-dimensional buried pipeline is regarded as a reference model for tests of the DTN models developed in this research.

Secondly, the results of the simulation of the dynamic thermal behaviour of the buried pipeline over long timescales using the dynamic thermal network models are presented. In the DTN approach, weighting factors are required to be calculated

and initialized in the model prior to simulating the conduction heat transfer process in the system. The weighting factors were calculated both numerically, i.e. using the 3D model and experimentally are shown in this chapter. Comparisons are made between the results of the DTN model using weighting factors based on these two methods, the experimental data, and the results of the 3D model in predicting the dynamic response of the buried pipeline in long term. Moreover, the DTN-PFST model proposed in this research is assessed by comparing the calculated results with the experimental data and the results of the 3D model in this Chapter.

One of the features of the combined DTN-PFST approach is its ability in the calculation of the thermal energy storage in the ground in the buried pipeline system. This can be particularly of interest in the seasonal thermal analysis of the DH systems and where the system is integrated with the underground thermal energy storage. To assess the thermal energy stored in the system, both the cumulative and hourly energy stored in the system over one of the long timescale experiment is calculated using the combined DTN-PFST model. The results are presented and discussed in Section 7.2.3.3

Moreover, the ability of the combined DTN-PFST approach in the prediction of the fluid temperature along the buried pipelines is investigated at different times after applying the step change at the pipeline inlet temperature. This distinct feature of the proposed model over the DTN model allows it to effectively deal with energy stored in the pipeline influencing the thermal response of the pipeline. Due to the low temperature drop in the buried pipeline in the test rig, a longer buried pipeline with higher heat losses was modelled using the finite volume model. The comparison between results from the proposed model and detailed 3D model for the prediction of the variation of fluid temperature and energy stored along the buried pipeline are shown and discussed in Section 7.2.4.

7.1 The Three-dimensional Reference Model Validation

The validation of the three-dimensional model has been carried out by comparing the simulation results with analytical results in terms of prediction of transient conduction heat transfer in the ground with convective boundary condition. The transient heat conduction in the ground exposed to air is simulated using the FVM

considering the thermal properties and conditions of the experiments, as described in Section 7.1.1. The objective is to model the dynamic heat losses from the ground surface due to the boundary temperature step change, i.e. similar to the experiment, and its effects on the variation of ground temperatures in the different depths of ground. The finite volume model validation is made against the analytical solution of the transient ground surface heat losses problem, discussed in Section 2.3.7. Having validated the transient conduction heat transfer of the finite volume model, the model is combined with the detailed three-dimensional pipeline model developed and validated in Section 6.1. This allows developing a detailed 3D buried pipeline model with the high level of accuracy with the reasonable computational cost suitable for the simulation of the experiments conducted in this research.

7.1.1 Conduction Heat Transfer in the Ground Exposed to Air

In general, the ground geometry can be considered as a semi-infinite solid, as it extends to infinity in all but one direction, in which the ground surface is exposed to air. Therefore, by imposing a sudden change at the boundary of this surface, one-dimensional transient conduction heat transfer occurs within the ground, as illustrated in Fig 7.1. This analysis is particularly beneficial to determine transient heat transfer near the surface of the earth. The solution for semi-infinite transient conduction heat transfer problem is presented in Section 2.3.7. The obtained analytical solution (Eq. 2.28) is used to validate the 3D model developed using the FVM and study the mesh independency of the model.

To validate the numerical model against the analytical solution, a three-dimensional rectangle representing a semi-infinite soil domain (depth: $10\,cm$, area: $10\,cm \times 10\,cm$) is modelled with specific thermal properties and initial conditions shown in Fig 7.1. Once the step change of $20\,\mathrm{K}$ is applied to the ground surface, the soil temperature of five points with the depth of one to five centimetre from the ground surface is recorded over 120 min.

The simulated temperature obtained from the 3D model and the temperature calculated from the analytical solution (based on Eq. 2.28) for the specific depths of soil over the simulation time is displayed in Fig 7.2. A very good level of agreement can be observed between the simulation and analytical results for the diffident depth of soil at various times. Moreover, it can be seen, at the beginning of applying

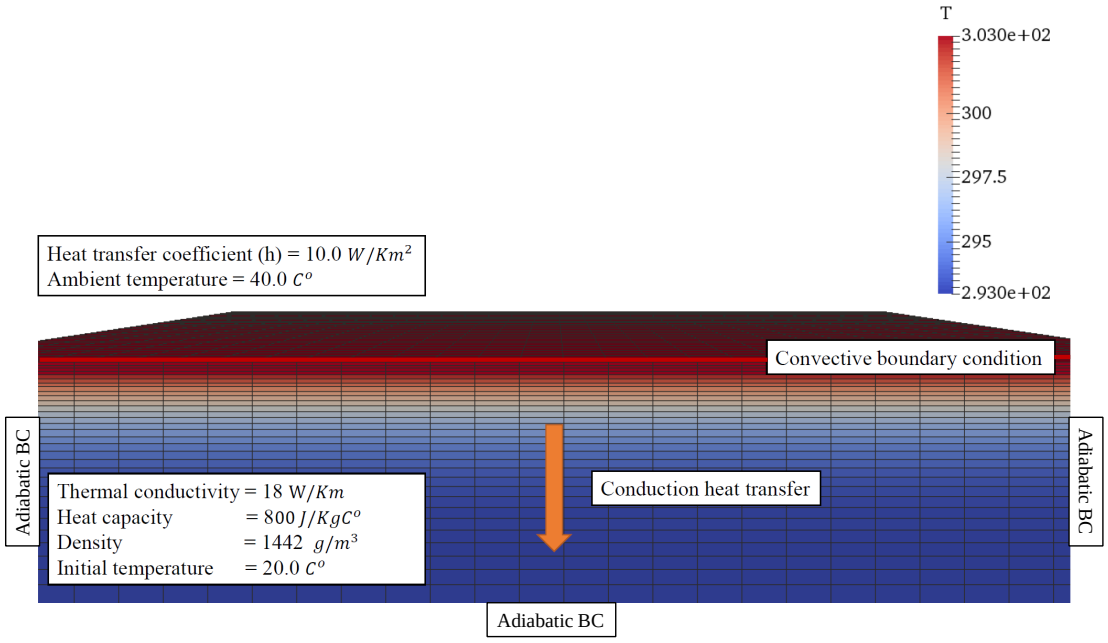

Figure 7.1: A structured mesh representing the ground conduction heat transfer with the convective ground surface exposed to air with the shown thermal properties and boundary conductions (larger soil domain is displayed to better show the soil mesh in this figure).

the step change, the temperature of different depth of soils increases in a non-linear manner with regard to time. As time proceeds and reaching the steady-state condition, the temperature variation becomes more linear.

To attain a reliable solution independent of the mesh size with a reasonable computational cost, five various cell numbers for the mesh independence check are chosen as summarized in Table 7.1. It should be noted that due to the high temperature gradient near the surface, the mesh density is increased near the ground surface to accurately capture such gradients, as shown in Fig 7.1. The RMSE calculation was made between the simulation and analytical results for all cases as presented in Table 7.1. It was found that choosing the mesh size higher than 1920 cells resulted in RMSE values less than 0.05 K. It was concluded that sufficient precision could be achieved by selecting 1920 cells or finer for the mesh representing the conduction heat transfer within the ground exposed to air. It should be noted that as the ground conduction heat transfer is assumed to occur in one direction, i.e. depth of soil, only the number of cells representing the depth of ground is changed for checking the mesh independence.

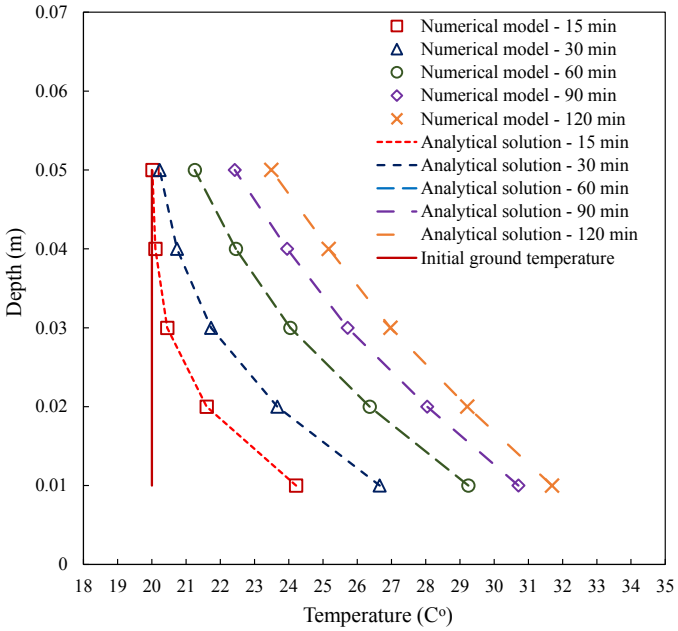

Figure 7.2: Comparisons between the temperature variations of the different depths of soil in transient condition calculated by the numeral model and analytical solution.

7.2 Long timescale Dynamic Thermal Response Models

In this section, the numerical results obtained from the DTN model, combined DTN-PFST model and the three-dimensional models are presented and compared with the measurement data for evaluating the long term dynamic thermal response of buried pipelines. The concept of the DTN method along with the details of the numerical implementation of the method to model heat transfer of the buried pipeline are described in Section 3.3. In addition, the detailed description of the so-called

Table 7.1: RMSE between the results of the numerical model and analytical solution of modelling of the ground conduction heat transfer for five mesh sizes.

Mesh size (D×W×L)	RMSE (K)
$10 \times 8 \times 8$ (640)	0.5527
$20 \times 8 \times 8$ (1280)	0.1673
$30 \times 8 \times 8$ (1920)	0.0468
$40 \times 8 \times 8$ (2560)	0.0249
$50 \times 8 \times 8$ (3200)	0.0466

combined DTN-PFST model is described in Section 3.4. In the DTN approach, the transient fluxes resulting from applying a step change at the boundary temperature conditions should be initially determined so that the weighting factors can be calculated.

One of the main objectives of this research was to experimentally investigate the validity of the DTN approach. To this end, the step response heat flux data determined from the pipeline and ground surfaces from both long timescale experiments are used for calculation of the weighting factor series. These weighting factor series are compared with that calculated from the finite volume model as a convenient way of numerically deriving of weight factor series. For this purpose, a two-dimensional model with convective boundary conditions was developed using the finite volume method (described as case 4 in Section 3.1). This model is used to determine the step response heat flux series from the convective boundary conditions to calculate the weighting factor series numerically. The details of calculation of weighting factor series from the step response heat fluxes are explained in Section 3.3. The weighting factor series obtained experimentally and numerically are presented and discussed in the following Sections.

Moreover, it has been aimed to implement the weighting factors obtained both numerically (from the 2D model) and experimentally (from the measurement) into the combined DTN-PFST model to evaluate the suitability of the proposed model in representing dynamic behaviour of the buried pipeline. The simulation results from both the DTN model and combined DTN-PFST model are compared with the experimental data in terms of the prediction of the dynamic thermal response of the buried pipeline and heat losses from the ground and pipeline surfaces. In all the comparisons made in this Chapter with experimental data, the detailed three-dimensional buried pipeline with turbulent fluid flow is also used in order to compare the proposed numerical model with the finite volume model in terms of the accuracy and computational expense.

7.2.1 Weighting Factors Derivation using the FVM

To implement the DTN approach to representing thermal behaviour of the DH pipelines, the first step is to derive the weighting factor series. A convenient way to derive the weighting factor series is to use the finite volume model to simulate the fluxes resulting from step changes in boundary temperatures. In this way, the

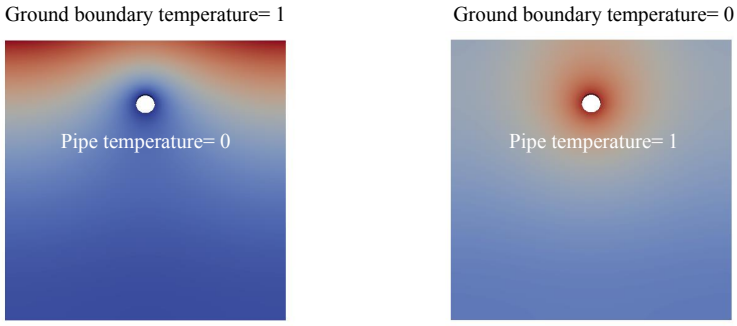

Figure 7.3: Temperature profiles of the sand box after 1000 s from imposing the unit step change to the ground surface (left-hand image), and the pipeline surface (right-hand image).

weighting factor series can be derived based on the procedure described in Section 3.3. Therefore, the main intention is to use the finite volume model for implementations of pipelines defined by users of the model. This allows the users to use the model to represent the thermal behaviour of various configuration of the pipelines, i.e. supply, return and circulation pipelines.

Since the cross-section of the buried pipeline does not change along the pipeline, a 2D model was developed based on the geometries of the buried pipeline described in Section 3.1.6. In this 2D model, the conduction heat transfer is modelled through the sandbox with two convective boundary conditions for the inner surface of the pipeline, and the ground surface representing the convection heat transfer from the fluid flow through the pipeline to the pipeline wall, and the ground surface to the air, respectively.

For derivation of the weighting factor series, the boundary conditions are required to be convective with constant heat transfer coefficients in order to have consistent DTN model calculation. However, once the weighting factors are determined, the heat transfer coefficient of the surfaces can be adjusted in the DTN model for different fluid flow rates and boundary conditions. Therefore, it is necessary to define suitable heat transfer coefficients for each surface for the calculation of the weighting factor series. To this end, the heat transfer coefficients at the inner surface of the pipeline are calculated based on the Reynolds number of fluid flow through the pipeline in the experiments using the well-known Gnielinski's correlation (Eq. 2.9) and calculated to 1454 W/m^2K. The ground surface heat transfer coefficient is estimated to 8.2 W/m^2K based on the measurement data presented in Section 5.2.1. These values along with the thermal properties of the pipeline and

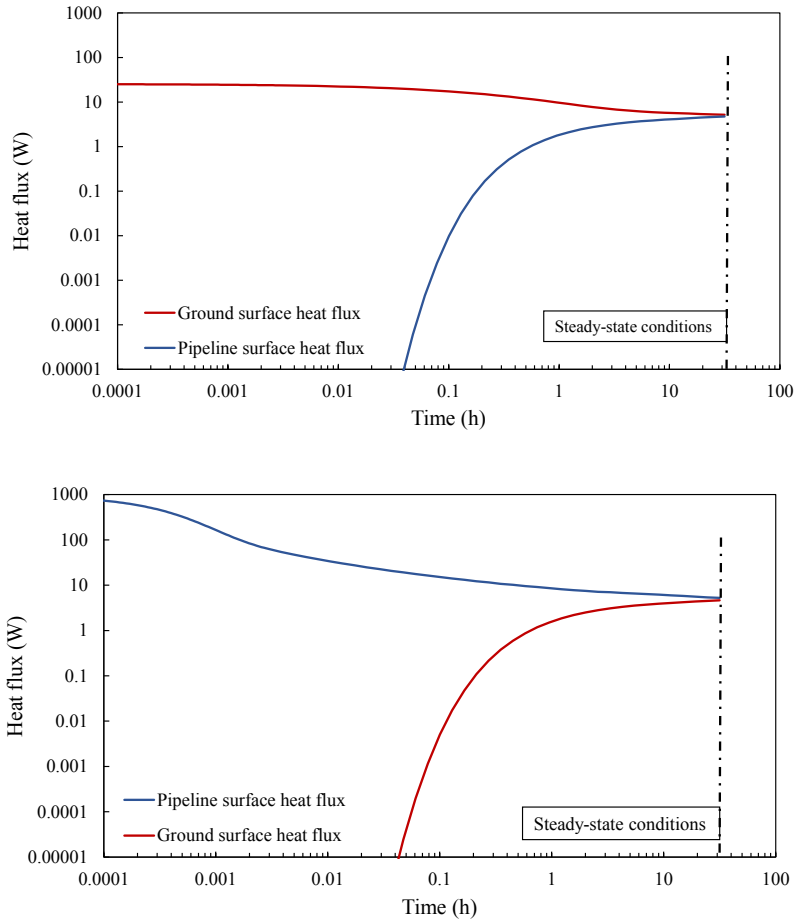

Figure 7.4: The calculated response heat fluxes due to a unit step change (1 K) applied to the pipeline surface (top-image) and the ground surfaces (bottom-image) using the 2D model with the convective BCs.

the sand measured in this work are prescribed at the finite volume models to simulate the transient heat transfer of the buried pipeline system. Fig 7.3 shows the temperature distribution of the sandbox having undergone the unit step change to the pipeline and ground surface.

The dynamic step response fluxes resulting from imposing the unit step change to the boundary temperature at the pipeline and ground surfaces are illustrated in Fig 7.4. It can be seen that at the beginning due to the inrush of heat at the surface due to the step change, one surface has the maximum amount of heat flux, i.e. equal to the surface conductance multiplied by area, and the other surface has no heat flux, as the boundary temperature is held zero. For these cases, the maximum amount of heat fluxes (admittive heat fluxes) for the pipeline and ground surfaces

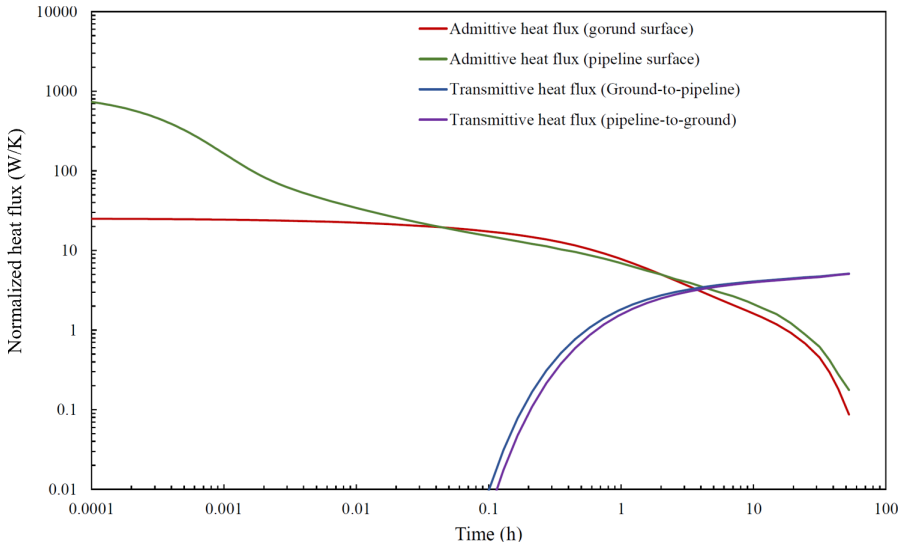

Figure 7.5: The buried pipeline admittives and transmittive response fluxes in logarithmic scales.

are 932.1 and 24.6 W/K, respectively. As time proceeds, the heat moves from one surface to another resulting in decreasing the heat flux from the surface imposed to the step change, and increasing heat flux from another surface. This continues until the system is approached to the steady-state conditions where the amount of heat fluxes from both surfaces getting close to the same value, equal to the steady-state heat transfer coefficient between the surfaces (the reverse of the thermal resistance). For these cases, the steady-state heat transfer coefficient between the pipeline and ground surfaces is approximately 5.42 W/m^2K.

Fig 7.5 shows the admittive and transmittive heat fluxes calculated based on the step response heat fluxes as described in Section 3.3. It can be seen as time passes, the admittive heat flux diminishes and transmitted heat flux between two surfaces increases until the steady-state condition is approached where the admittive heat fluxes approach zero and transmittive fluxes reach the steady-state value (5.42 W/m^2K). Moreover, it can be observed that the pipeline surface experiences noticeably more drop at the first seconds of applying the step change compared with the ground surface. This is because the heat transfer coefficient of the inner surface of the pipeline is much higher (approximately 180 times higher) than that of the ground surface. This causes the heat disperses much more quickly through the pipeline wall than the ground resulting in faster drop at the first minutes of applying the step change.

7.2.2 Weighting Factors Derivation using Experimental Data

The experimental results from two long timescale step response experiments conducted in this research are used to experientially evaluate the validity of the DTN approach. In these two experiments, the step response transient heat fluxes from the surfaces are determined and used for the derivation of the weighting factors experimentally. The details of the experiments and measurement data have been presented and discussed in Chapter 5.

Moreover, a 3D model has been developed based on the experimental conditions of these two tests to simulating the turbulent fluid flow with conjugate forced convection heat transfer (described as case 3 in Section 3.1). The main objective of developing this detailed 3D model is to compare the simulation results with the outcomes of the DTN model, and combined DTN-PFST model in terms of the accuracy and computational cost.

As explained in Chapter 3, to derive the weighting factors, unit step response fluxes need to be applied in the calculation. The step response fluxes are required to be normalized based on the experimental conditions, such that the fluxes are linearly scaled equivalent to a unit step change (0-1) according to the the experimental temperature differences. The normalized step response fluxes resulting from imposing the step change on the boundary temperature from both the experimental data and the 3D model at the pipeline (top-image) and at the ground surface (bottom image) are displayed in Fig 7.6. A good level of agreement can be seen between the 3D model results and experimental data.

Observing the dynamic step response fluxes at Fig 7.6 and Fig 7.4, it can be noted that the initial pipeline admittive fluxes from the 2D model is higher than that of from experimental data. This is due to the fact that in the 2D model, the step change is applied to the entire pipeline, while in the experiments, the step change applied to the inlet temperature. This results in introducing an differences between the values at the first seconds of applying the step change. However, since the difference between the inlet and outlet temperature of the buried pipeline is very low (less than 2.5% of the step change temperature) the fluid temperature along the pipe does not vary noticeable as assumed in the calculation of weighting factors from the 2D finite volume model.

It should be noted that in the case of applying the step change to the boundary temperature of ground surface, the ambient air temperature is kept constant, but

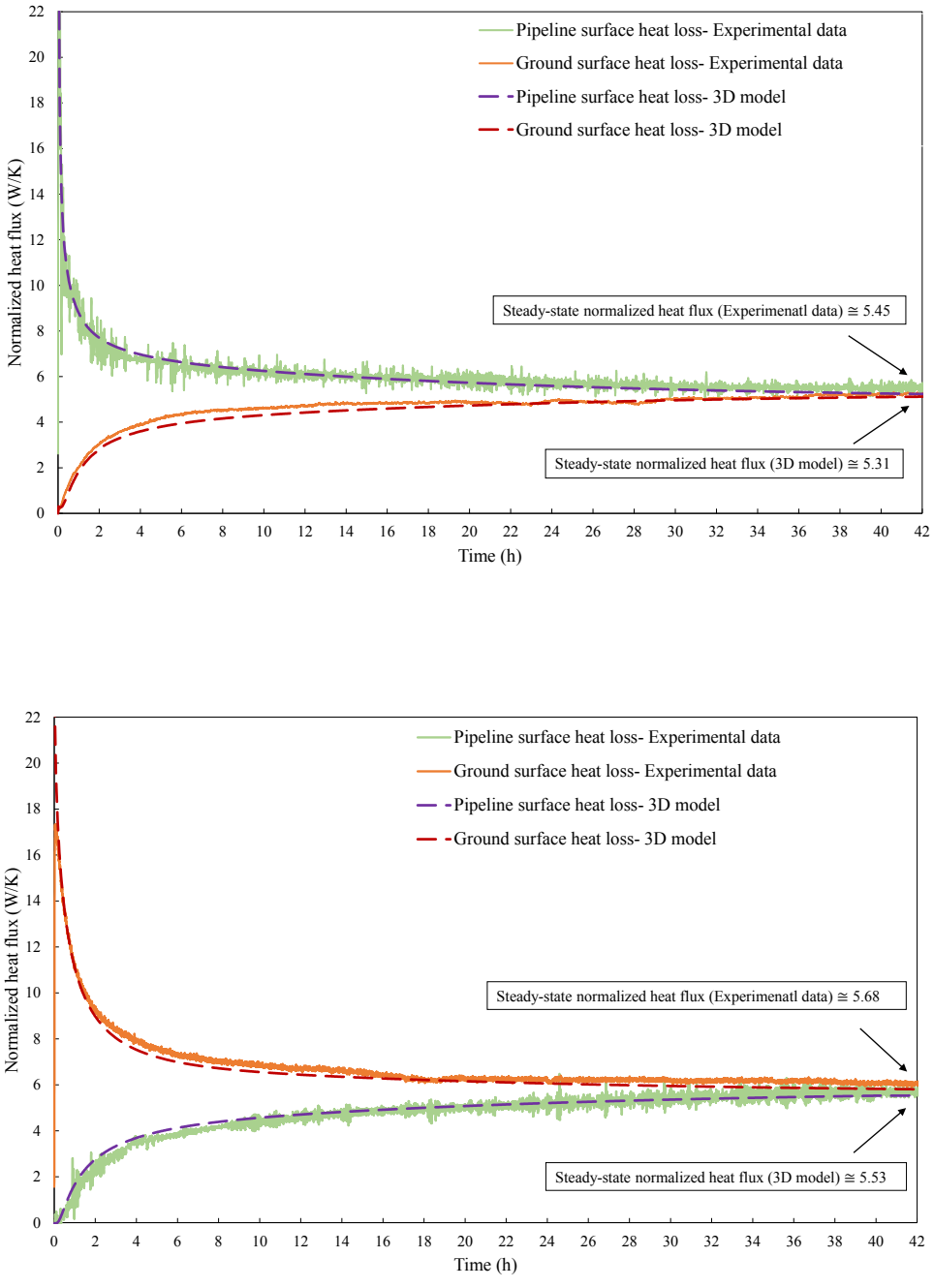

Figure 7.6: The step response fluxes for the pipeline surface (top-image) and the ground surfaces (bottom-image) obtained from the experimental data and the 3D model with the conjugate heat transfer.

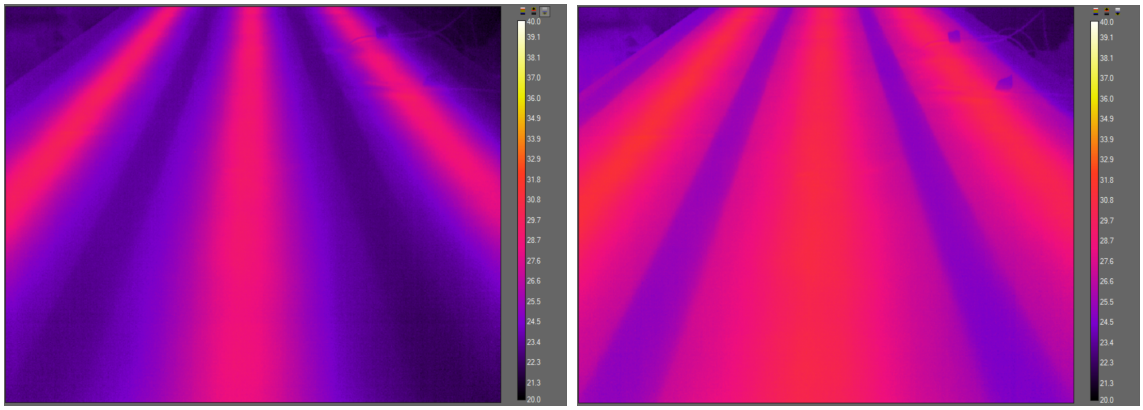

Figure 7.7: The infrared photographs taken by a *flir a300* high resolution thermal camera showing the ground surface temperature variations after 3 h (left-image) and 25 h (right-image) of applying temperature step change to the pipeline inlet temperature.

the surface temperature varies based on the heat losses from the ground surface to the air over the experiments. In this research, a *flir a300* high resolution thermal camera is used to monitor the ground surface temperature variations to make sure the ground surface temperature does not vary along the length of the pipeline over the experiments. The variations of ground surface temperature were observed in all the experiments, and no noticeable difference was found between the ground surface temperatures along the length of the pipeline. The variations of the ground surface temperature after 3 and 25 hours that step change applied to the pipeline inlet temperature are shown in Fig. 7.7.

The comparison between the unit step response dynamic fluxes obtained from the 3D model and the experiments over the entire duration of the tests are illustrated in Fig 7.8. The admittive (Q_{1a}, Q_{2a}) and the transmitive fluxes (Q_{12}) are shown normalized by the corresponding thermal conductances (K_1, K_2, K_{12}). The thermal conductances (K_1, K_2) are calculated based on maximum admittive fluxes (equal to surface area multiplied by the surface heat transfer coefficient), and the thermal conductance (K_{12}) is obtained from the steady-state trasmittive flux to the unit step change. It should be noted that while the required data measured and logged every 4 seconds, the rolling average of the collected data is calculated in every 200 seconds to smooth the experimental heat fluxes.

It can be also observed that the pipeline admittive flux (Q_{1a}) and the ground surface admittive flux (Q_{2a}) diminish at the beginning and approach zero at the

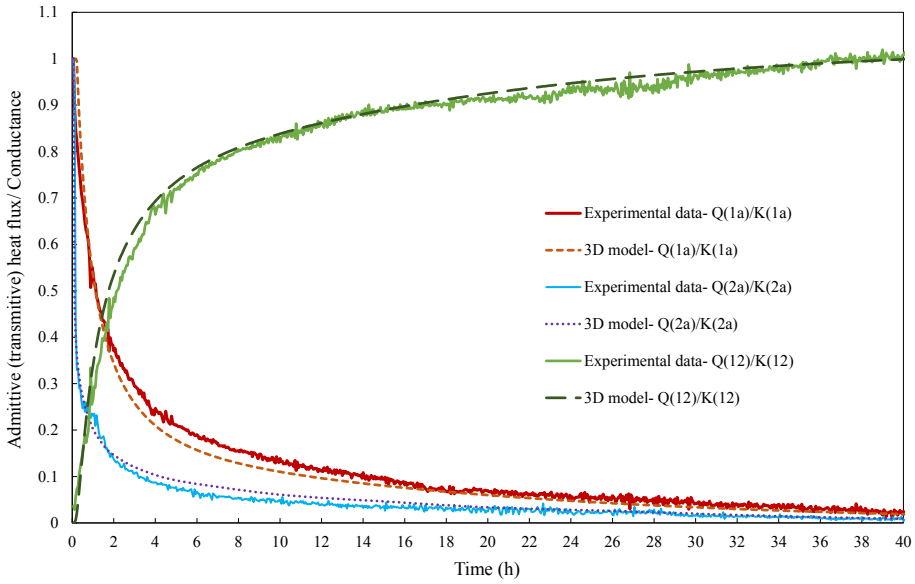

Figure 7.8: The buried pipeline admittives and transmittive response fluxes obtained from the 3D model and the experiments normalized by the corresponding conductances.

steady-state condition. However, the rate of the decrease of the pipeline admittive flux is higher than the ground admittive flux, as the pipeline admittive flux drops 10% of the maximum value after 4.2 h compared with 13.5 h for the ground admittive flux. Also, the admittive fluxes (Q_{1a}, Q_{2a}) have fallen 2% of their maximum after 29.8, 38.1 h, respectively. In addition, it can be observed that the admittive flux increases to 80% of the steady-state value after 7.5 h and then increases more slowly before reaching its final value. This flux reaches 99% of its steady-state values after 36.1 h.

These heat flux data are used to derive the weighting factors numerically and experimentally, based on Eq. 3.48 and 3.49, given in Section 3.3. The weighting factor series derived from the numerical model and experimental data are later used as input parameters in the DTN model calculation to predict the pipeline outlet temperature and the pipeline and ground heat fluxes and compared with the measurement data.

The weighting factor curves are shaped based on the gradients of the step response fluxes over the corresponding thermal conductances as shown in Fig 7.8. Fig 7.9 displays the corresponding weighting factors for the buried pipeline admittive and transmittive fluxes determined both numerically and experimentally over the first seven hours of the tests according to Eq. 3.48 and 3.49. It can be seen that

after 7 hours, the weighting factors corresponding to the pipeline admittive and transmittive flux diminish to below 0.0004 and 0.0271 (3% of the maximum value), respectively.

A good match between the weighting factor series derived from experimental data and numerical model shows the verification of the DTN approach, as for the first time the weighting factor series derived purely from the experimental data. After the process of weighting factors reduction (explained in 3.3.6) the weighting factor series are used in the DTN model, and combined DTN-PFST model for further investigation of ability of the models in prediction of dynamic thermal behaviour of the buried pipeline.

The weighting factor series derived experimentally can be observed more scattered than that of calculated numerically. This is can be due to the experimental noises and uncertainty of the measurement. The uncertainty of calculated fluid heat balance and ground surface heat flux are estimated 2.18%, and 0.63%, respectively (See Appendix A). The effects of the scattered weighting factors obtained from the experimental measurement on the output of the DTN models are discussed in the following Sections.

7.2.3 Combined DTN-PFST Model Validation

The combined DTN-PFST model along with the DTN model developed in this research have been evaluated in prediction of buried pipeline thermal behaviour in long timescales using weighting factor series derived both experimentally and numerically. This has been carried out by making a series of comparisons with experimental data in terms of prediction of the pipeline outlet temperatures and the heat losses from both the pipeline and ground surfaces. Moreover, the 3D conjugated heat transfer model developed in this research was used along with the DTN models to compare the computational cost and prediction differences of both the proposed models and 3D model.

In the following sections, the output results of the DTN models and combined DTN-PFST model where weighting factors are determined numerically and experimentally along with the 3D model are compared with the experimental data obtained from the conducted tests. The main advantages of the combined DTN-PFST model is the ability of the model in prediction of fluid temperature along the pipeline at different distances, and dividing the system into the number of sections with the

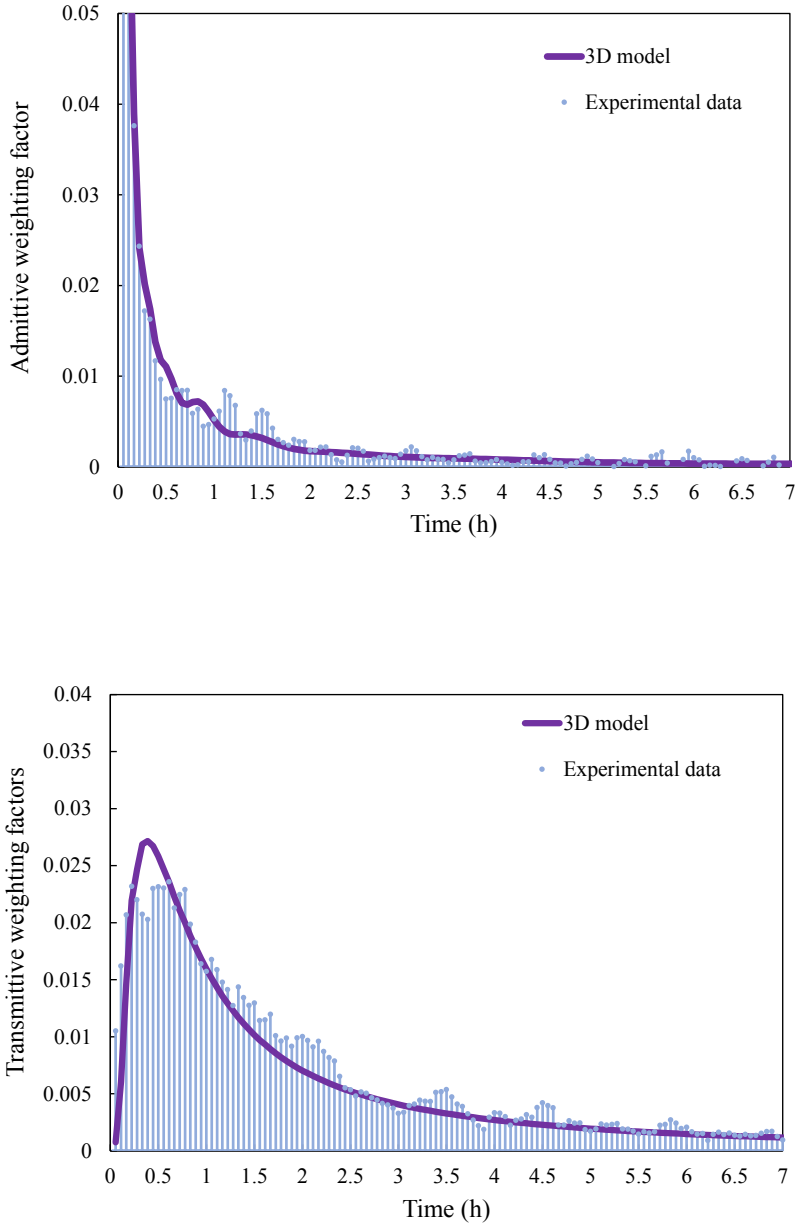

Figure 7.9: The buried pipeline admittives (top-image) and transmittive (bottom-image) weighting factors calculated based on the corresponding the step response fluxes from both the experimental measurement and the 3D model.

desired initial thermal conditions and thermal properties. Given the flow rate of fluid flow and the geometry of the pipeline, the pipeline systems is divided into 41 and 46 sections depending the water velocity in each experiment. However, since the length of the pipeline is relatively short and the experiments have been performed over long timescales, the fluid temperature variation along the pipe is very small, i.e. mostly less than 2.5% of the temperature step change. This results in the benefits of the proposed model over the conventional DTN model cannot be properly seen. Therefore, a 100 m buried pipeline is modelled using the FVM to enable the proposed model to be compared with the conventional model in terms of the predicted outlet temperatures while the variation of fluid temperature is higher along the buried pipeline. The simulation results of 100 m buried pipeline are presented and discussed in Secion 7.2.4.

The comparisons made between the numerical models in this section are carried out for the following main purposes: (i) to evaluate the implementation of the DTN calculation procedure without using any analytical and numerical models, and purely using experimental data. (ii) to assess the proposed model combining the DTN model with the PFST model. (iii) to examine the accuracy and computational cost of the combined DTN-PFST model and DTN models with the 3D model using the finite volume method (FVM).

7.2.3.1 Outlet Temperature Prediction

The predicted outlet temperatures are compared with measured values during the first experiment, i.e. imposing the step change on the pipeline, in Fig 7.10. The general trend of the pipeline temperature predictions by the numerical models can be seen in a good agreement with the measurement data. Since the experimental data measured at the long timescales, the advantages of the proposed combined DTN-PFST model over the DTN model cannot be observed for this length of the buried pipeline. As a results, a longer buried pipeline is modelled for further comparisons presented in Secion **??**.

Moreover, Fig 7.10 shows in the both DTN models that weighting factors (kappa (κ)) are calculated based on the experimental data more fluctuations occur. This is related to the fluctuations of the step response fluxes occurred in the experiment that reflects in the derivation of the weighting factors. The magnitude of the discrepancies between measured and predicted outlet temperatures by the numerical models

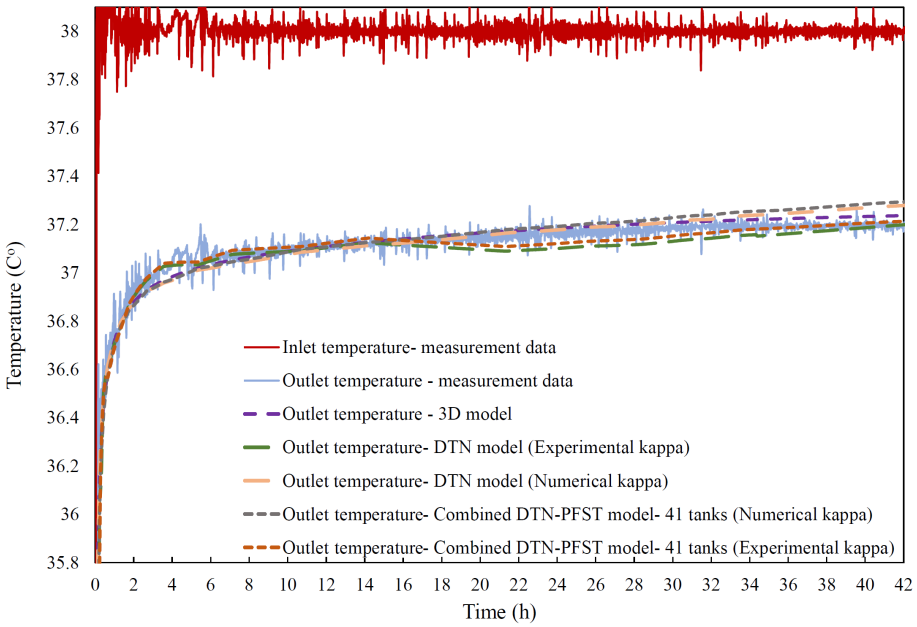

Figure 7.10: Measured and predicted outlet temperatures by the numerical models for the experiment imposing the step change to the pipeline.

are shown Fig 7.11. The difference between the outlet temperatures predicted by the models mostly falls to within the range of experimental temperature measurement error, i.e. approximately 0.07 K (See Appendix A), except for the initial hours of the experiment, as the measured inlet and outlet temperatures experience high fluctuation after applying the step change until the PID controller completely stabilizes the temperatures. To better understand the effects of the dynamic behaviour of the experimental system after applying the step change on the collected data, the fluctuations of the measured inlet and outlet temperatures of the pipeline at the first four hours of the tests are shown in Fig. 5.7 and Fig. 5.11 given in Chapter 5.

Fig 7.12 displays the comparisons between the predicted outlet temperature and measured values during the second experiment, i.e. imposing the step change to the ground surface. The figure shows a very good agreement between the numerical outcomes and measurement data in the prediction of the outlet temperature. The difference between the measured and simulated outlet temperature of the pipeline is illustrated in Fig 7.13. Since the difference between the inlet and outlet temperature is noticeably low in this experiment, around 0.7 K, the discrepancies between the numerical results and measurement data is very low, i.e. mostly lower than 0.1 K. Similar to the first experiment, the reason that the magnitude of the difference

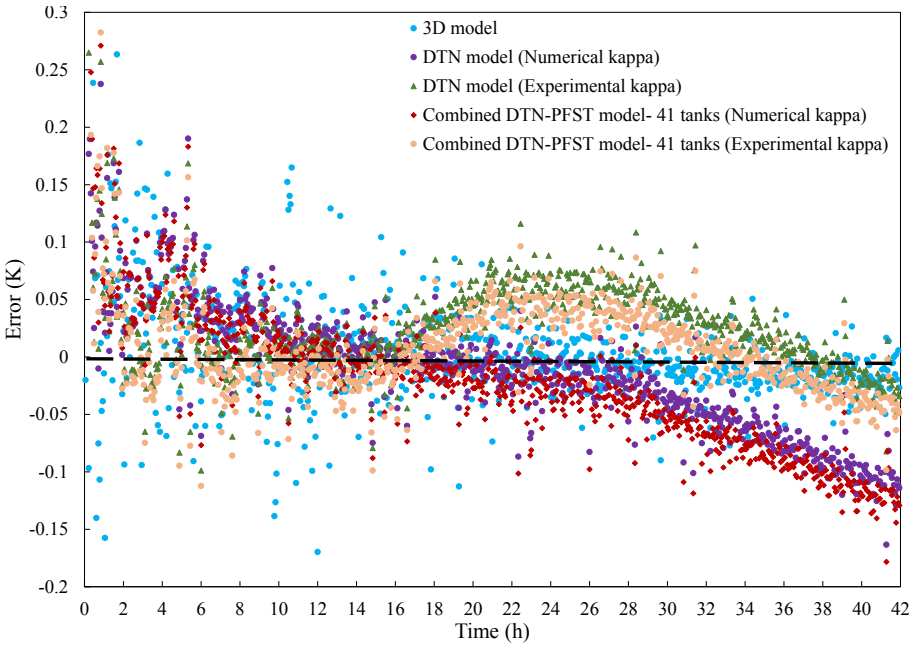

Figure 7.11: Differences between the measured outlet temperature and the predicted values by the numerical models for the experiment imposing the step change to the pipeline.

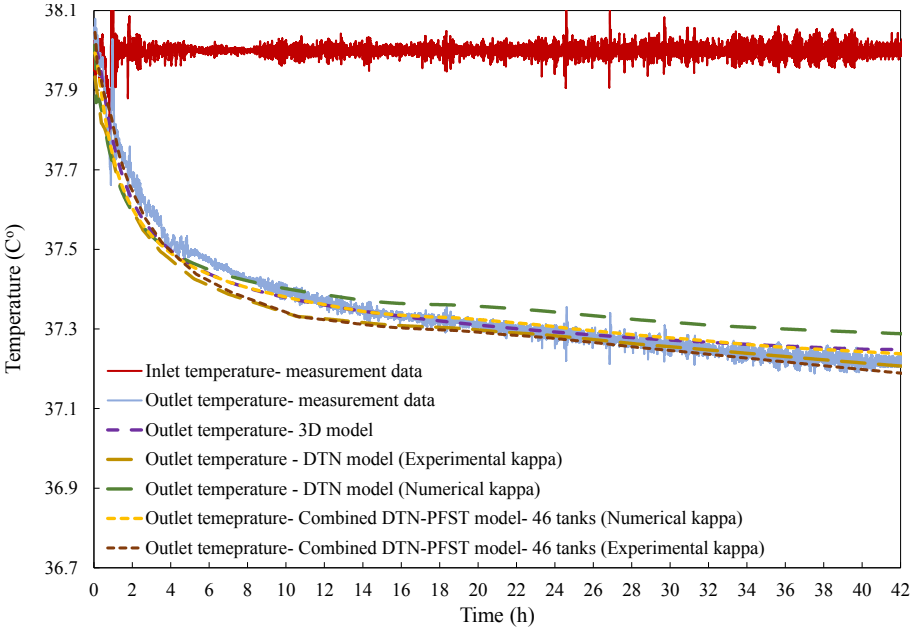

Figure 7.12: Measured and predicted outlet temperatures by the numerical models for the experiment imposing the step change to the ground surface.

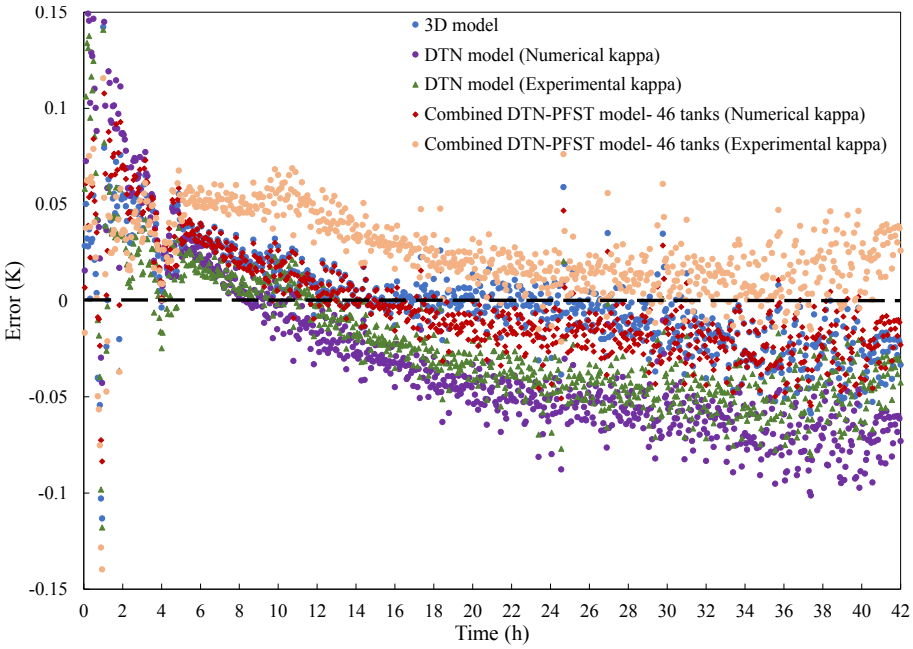

Figure 7.13: Differences between the measured outlet temperature and the predicted values by the numerical models for the experiment imposing the step change to the ground surface.

between the measured and simulated outlet temperature is relatively high at the initial hours is due to the fluctuation of experimental data as a result of the high dynamic behaviour of the system after applying the step change.

Fig 7.14 demonstrates the comparisons between the RMSE between the measured and predicted outlet temperature using the numerical models during the entire test time, i.e 42 hours. Considering the very slight fluctuations of the measured outlet temperatures and the accuracy of the temperature sensors, the results elucidate that combined DTN-PFST model is acceptably able to predict the outlet temperature of the long pipeline as accurate as a detailed 3D model while they are more than almost five orders of magnitudes more computationally efficient. The RMSE calculated for both combined DTN-PFST model and DTN model during the first and second experiments is less than 0.11 and 0.6 K. It can be seen that for the second test, i.e. imposing the step change to the ground surface, the RMSE of all the numerical models is lower than of the other experiment. This is because of the lower variations of the outlet temperature of the pipeline during the second experiment that results in introducing smaller errors between the models and measurement data. Moreover, it can be observed that there is a very small difference between the accuracy of prediction of the outlet temperature by both combined DTN-PFST model

and DTN model using weighting factors obtained both numerically and experimentally. This indicates the flexibility and capacity of the DTN method in modelling the thermal performance of thermal systems dealing with transient conduction. Due to low RMSE between the combined DTN-PFST model, DTN model and experimental results, and considering the uncertainty of the measurement system and the slight fluctuations of the measured outlet temperatures, making further distinctions between the accuracy of the DTN models is not meaningful. To do a more accurate assessment between the combined DTN-PFST model and DTN model, measurement from a much longer buried pipeline with more variation in temperature along the length is needed. Further discussions and suggestions are given in this regard in Chapter 8.

7.2.3.2 Pipeline and Ground Surface Heat Loss Prediction

The predicted ground surface heat losses are compared with the measured values during the first experiment, i.e. imposing the step change to the pipeline, in Fig 7.15. Good agreement between the results of all numerical models and measurement data can be seen in the figure. It is observed that the combined DTN-PFST model and DTN model models are able to predict even the minor fluctuations of the ground surface heat flux occurring related to the small fluctuations of the lab temperature. This is because the lab temperature is read at each time step in the model, along with the other parameters such as inlet temperature, flow rate, etc. This notable feature of the DTN method that the data is read at each time step and updated to the subsequent time step, especially offers a significant computational cost advantage for the cases with very long time-series data concerning the time. In these cases, the inlet temperature was fixed, but the proposed model can deal with a variable temperature boundary condition, as the model updates the temperatures at each time step based on the current boundary temperatures.

The magnitude of the discrepancies between measured and predicted ground surface heat losses by the numerical models are shown Fig 7.16. It can be seen that the difference between the heat fluxes predicted by the models mostly lies below 6% of the steady-state value.

The main sources of the error between the models and experimental data can be related to the uncertainty of thermal properties of sand values and the ground surface convective coefficient. These values set into the models can directly affect

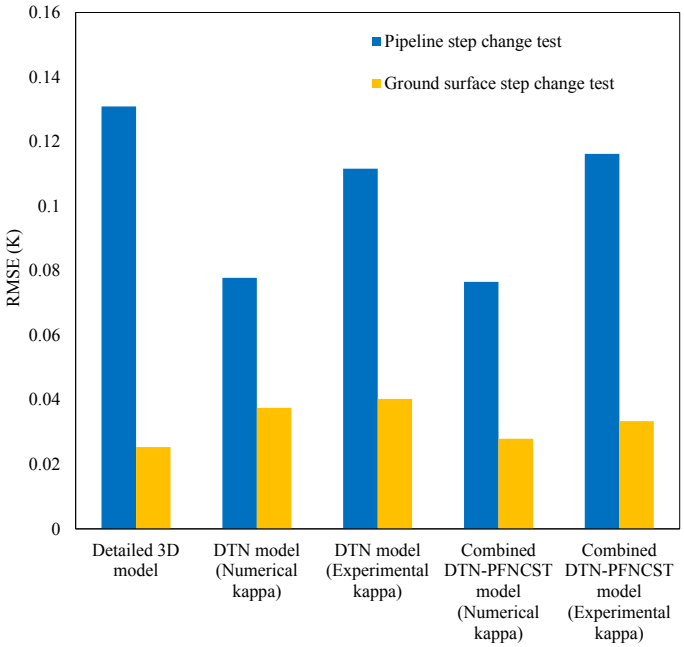

Figure 7.14: RMSE between the pipeline outlet temperature calculated by the numeral models and measured value for both the step change tests.

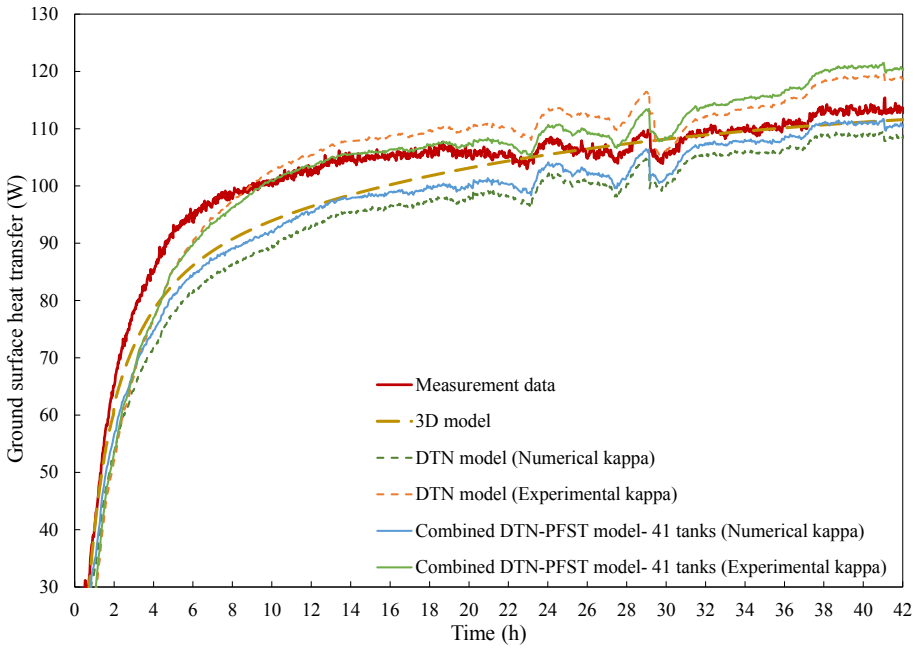

Figure 7.15: Measured and calculated ground surface heat losses using the numerical models.

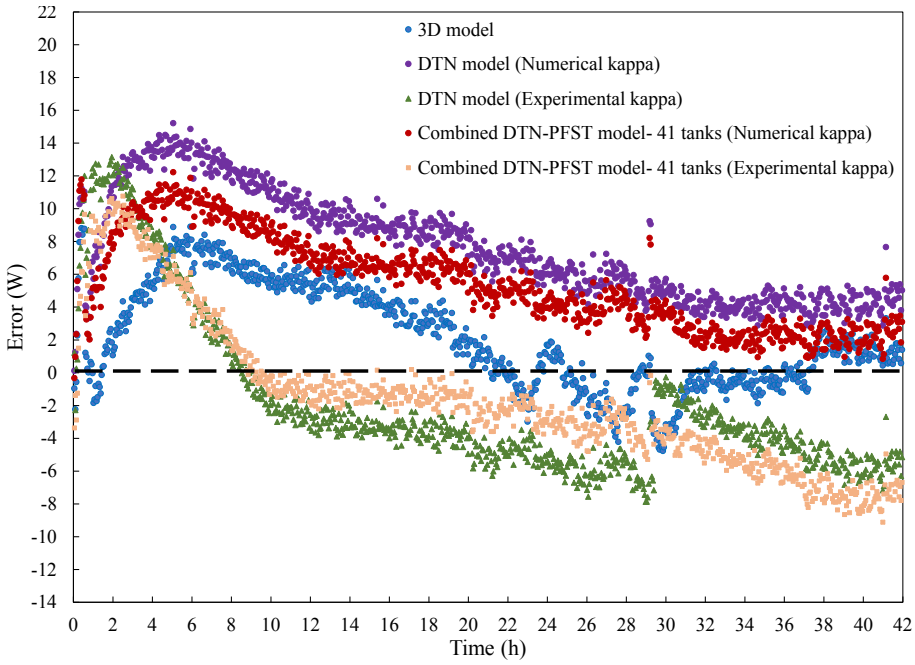

Figure 7.16: Differences between the measured and calculated ground surface heat losses using the numerical models.

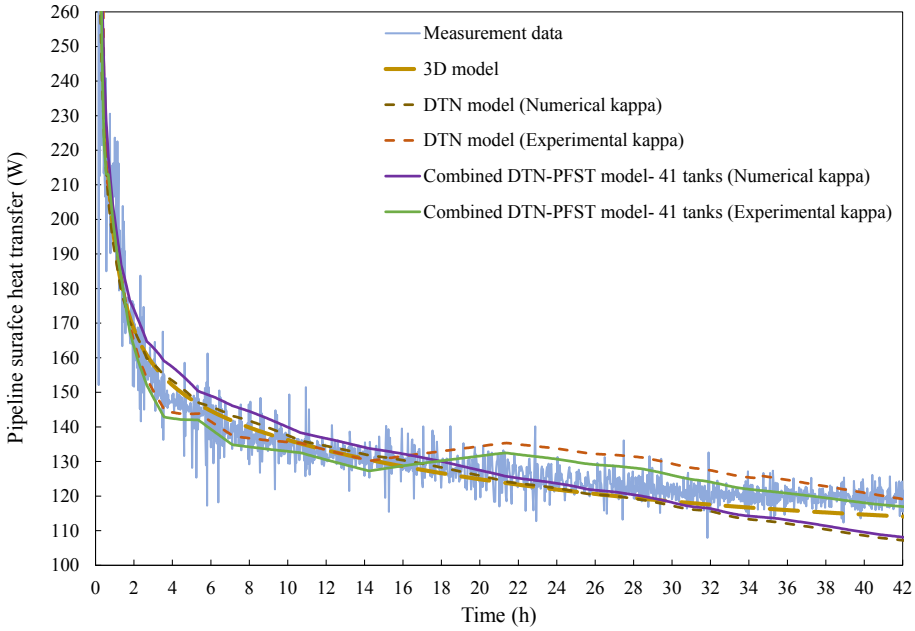

Figure 7.17: Measured and calculated pipeline surface heat losses using the numerical models.

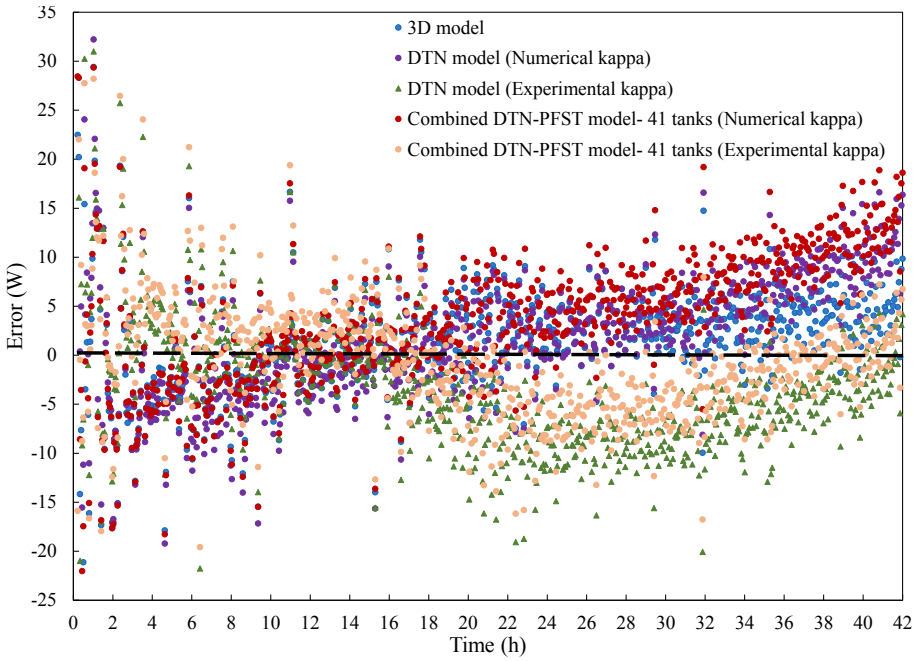

Figure 7.18: Differences between the measured and calculated pipeline surface heat losses using the numerical models.

the numerical simulation of heat transfer process. Therefore, small variations of these values affects the outcome of the models. It is also observed that it seems as the time approaches steady-state condition, the differences decrease. This can be because in the steady-state condition, the heat flux in the sand only depends on the thermal conductivity of sand, and the error associated with uncertainty of the thermal diffusivity of sand vanishes. Since at the first few hours, the measured heat flux is higher than predicted values by all numerical models, this implies that the specific heat capacity of sand is a bit higher than what measured.

Fig 7.17 illustrates the comparisons between the predicted pipeline heat losses and measured values during the first test, i.e. imposing the step change on the pipeline. Some fluctuations are observed in the heat loss prediction by the combined DTN-PFST model and DTN model that the weighting factors are determined experimentally. As mentioned, this is related to the derivation of the weighting factors, as they are calculated using the step response fluxes data consisting of small fluctuations. The differences between the measured and simulated heat losses of the pipeline is illustrated in Fig 7.18. It can be seen that the differences between the measured and simulated values are relatively more scattered reflecting the small fluctuations of measured pipeline heat losses during the experiments shown in Fig 7.17.

Similar to the errors between the models in prediction of outlet temperature, the reason that the magnitude of the differences between the measured and simulated pipeline heat losses are relatively high at the beginning is because of the fluctuations of experimental data as a result of the responsiveness of the system after applying the step change.

Fig 7.19 displays the comparison between the RMSE between the measured and predicted heat losses from the pipeline and ground surfaces during the entire test time, i.e 42 hours. The results show the acceptable ability of the combined DTN-PFST model and DTN model in prediction of heat fluxes from the pipeline and ground surfaces compared with a detailed 3D model. The RMSE of the heat losses calculated for the combined DTN-PFST model and DTN model are approximately less than 6% of the steady state heat transfer. It can be seen that the due to the lower fluctuations of the measured heat losses from the ground surface, the RMSE of all the models is lower than that of for predictions of the pipeline heat losses. Considering the slight fluctuations of the measured heat fluxes from the surfaces and the uncertainty of the sensors, it can be concluded the combined DTN-PFST model and DTN model are acceptably able to predict the heat losses from the long pipeline and the ground surface as close as to the detailed 3D model while they are more than almost five orders of magnitudes more computationally efficient. The maximum RMSE calculated among both the DTN models is for the DTN model that weighting factors are obtained numerically, i.e. about 10.5 W which is around 5 W higher than the detailed 3D model.

The computational time required to modelling the buried pipeline system has been compared between the numerical models for the pipeline step change test, shown in Fig.7.20. It can be seen that both the DTN models are more than five orders of magnitude more computationally efficient than the 3D conjugate heat transfer model using 20 parallel processors (Intel(R) CPU E5-2699 @ 2.30GHz). It should be noted that the solver used for modelling the 3D models was adapted to use increasing time steps, i.e. from 0.001 to around 20 s, to make the calculation more efficient. However, even with applying this approach, the DTN models are considerably more computationally efficient. As in the combined DTN-PFST model, the DTN method is applied several times, i.e. to the number of elements, the required calculation time is slightly higher than the conventional DTN model, i.e. a couple of seconds. Moreover, the both DTN models using experimental data for weighting factors derivation have a bit higher calculation time as the models require

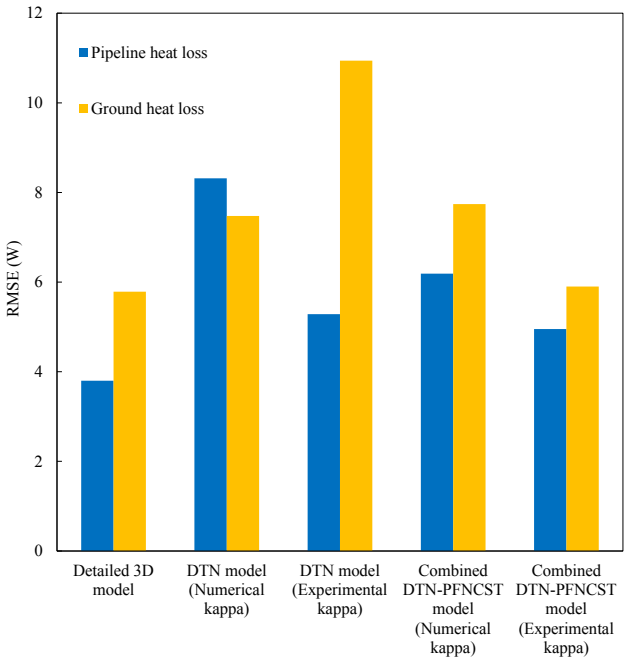

Figure 7.19: RMSE between the calculated heat losses from the pipeline and ground surfaces and experimental data for the pipeline step change test.

to deal with a much higher number of input data for calculating the weighting factors compared with that obtained from the 3D model.

7.2.3.3 Ground Thermal Energy Storage of Buried Pipelines

One of the significant features of the combined DTN-PFST model is the ability of simulation of heat flux from the surfaces involved in the systems at each time step. These surface heat flux data can be used for obtaining the energy stored in the ground over the simulation time at a given time step. For this purpose, it is only needed to deduce the net heat losses from the ground (or other surfaces) from the net energy input to the ground by the pipelines at each time step over the simulation time. This calculation can be particularly used to estimate the seasonal ground energy storage in district heating pipelines.

For calculation of ground energy storage in the buried pipeline system in this research, the heat flux data from first long timescale experiment has been used. Due to the involvement of only two surfaces in this case, the calculations are relatively straightforward. The ground energy stored can be calculated by subtracting the pipeline heat losses (energy input to the ground) from the heat losses from the

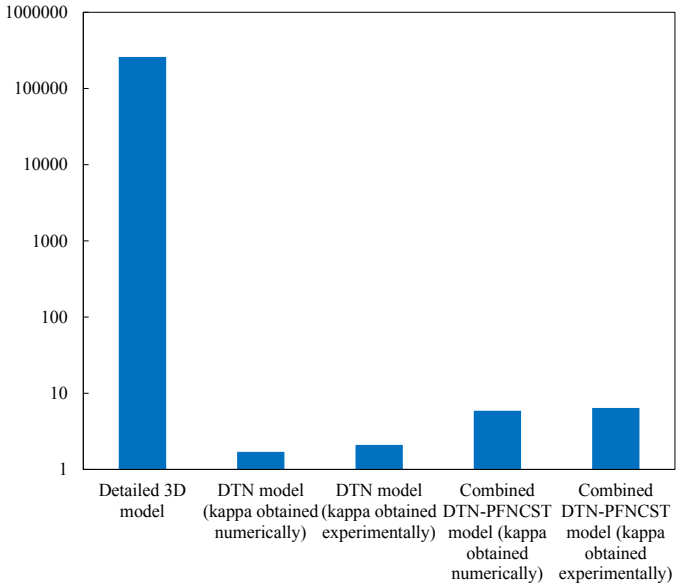

Figure 7.20: Comparison between the calculation time required for the numerical models to modelling the buried pipeline system showing in logarithmic timescale.

ground surface. This calculation provides a reasonable estimation of how much energy is stored in the ground.

Fig. 7.21 illustrates the hourly and cumulative energy stored in the sand from the moment of applying the step change to the pipeline inlet temperature until the system approaches the steady-state conditions. It can be observed the amount of energy enters into the sand at the initial hours is much higher (0.27 KWh for the first hour) than the rest of the experiments time. It is because the amount of heat losses from the sand surface at the first hours is close to zero, and approximately all the pipeline energy losses are stored in the ground. As time proceeds, the energy enters into the sand decrease until it reaches zero in the steady-state condition. In the steady-state conditions, the energy stored in the ground does not change, since the input and output energy to the sand is approximately equal. The amount of energy stored in the sandboxes can be estimated to 1.42 kWh over 42 hours of the experiment. This calculation of the energy storage can be considerably beneficial where the thermal energy storage is integrated into the district heating system.

7.2.4 Variation of Fluid Temperature Along Pipelines

One of the main advantages of the combined DTN-PFST model over the conventional DTN model is that the proposed model is able to calculate the variation of

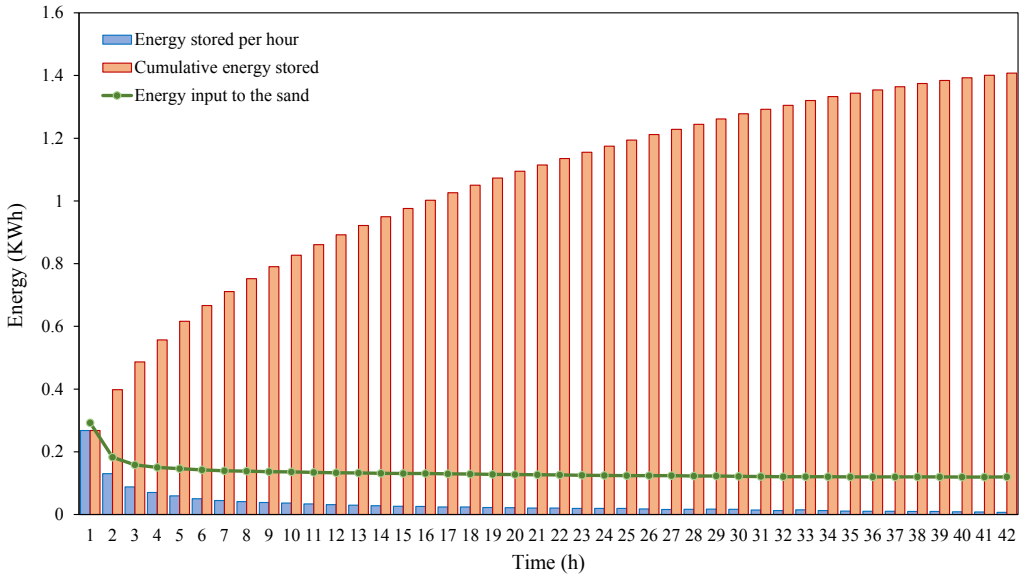

Figure 7.21: Variations of the ground energy storage in the buried pipeline system over the long timescale experiment (case 1).

the fluid temperature and the ground surface along the buried pipeline. This is carried out by dividing the buried pipeline into the numerous sections along the pipeline, and applying the DTN calculation for each section at a given time step. Due to the experimental conditions and relatively short buried pipeline in the test rig, the variation of the fluid temperature along the pipeline was not considerable (less than $1K$), as it was required for the validation of the DTN approach. However, for longer pipelines, e.g. district heating pipeline, these temperature variations along the pipeline will be significant.

To evaluate the proposed model in prediction of the fluid temperature along the buried pipeline, a relatively long buried pipeline has been modelled using the similar geometry of the test rig but $100\,m$ long (the cross-section of the pipeline is shown in Fig. 3.4). The model is developed using the Finite Volume Method in the same way as the development of the detailed 3D model described in Section 3.1. In this case, the turbulent fluid flow with a velocity of 0.5 m/s (Re=10377) has been modelled with the initial thermal conditions of 20 °C. A step change of $30\,K$ is applied to the pipeline inlet temperature to investigate the fluid temperature along the buried pipeline. The simulation results from the 3D model are later used to compare with the output of the combined DTN-PFST model.

To model the buried pipeline using the combined DTN-PFST model, the pipeline

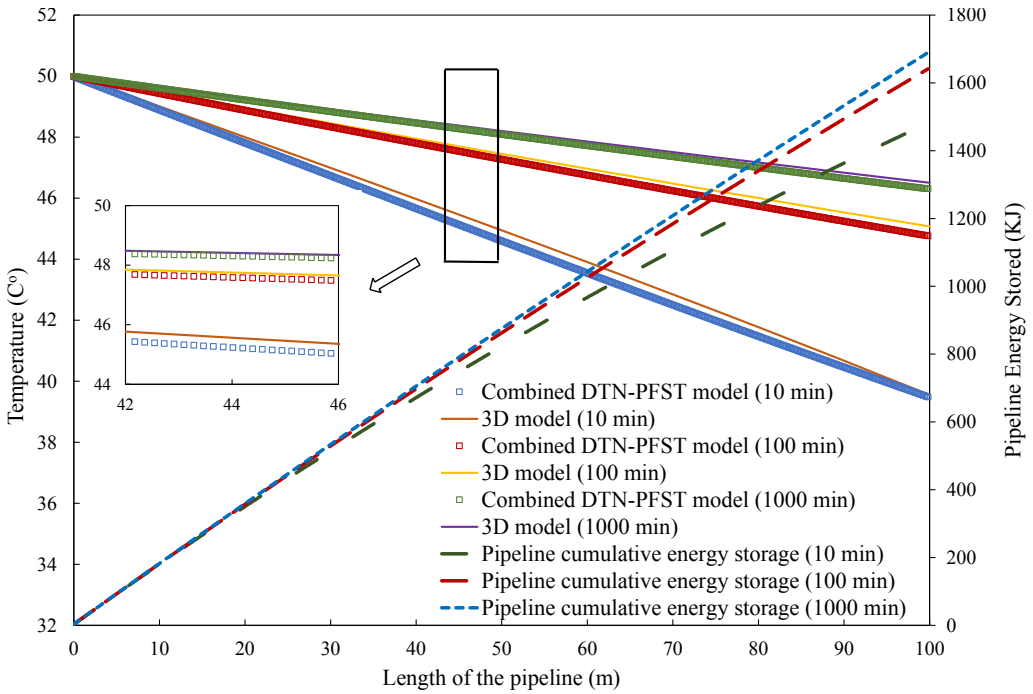

Figure 7.22: Comparison between the variations of fluid temperature and energy stored along 100 m buried pipeline calculated by the 3D model and combined DTN-PFST model at three different time ($Re = 10377$).

system requires to be divided into the number of sections calculated based on the PFNCST model (Eq. 6.2). In this case, the number of pipeline sections can be calculated to 528. Therefore, the 100 m buried pipeline is divided into the sections with the length of approximately 18 cm with specific fluid temperature updated at each time step. The variations of the fluid temperature along the buried pipeline obtained from the 3D model and proposed model at three times after applying the step change to the pipeline inlet temperature are displayed in Fig 7.22.

It can be seen the temperature difference between the inlet temperature and the fluid temperatures increases with the distance from the pipeline inlet. These differences are the highest after applying the step change, but as the system approaches the steady-state conditions, the differences decrease. This indicates the importance of considering the fluid temperature variations along the pipeline in modelling dynamic thermal behaviour of pipelines with fluctuating inlet temperature, e.g. district heating systems. It can also be observed the combined DTN-PFST model is able to predict the variation of the fluid temperature along the buried pipeline in a very good agreement with the detailed 3D model but with of five orders of magnitude

faster.

Due to the mass and thermal capacity of water in pipelines, some amount of the energy input to the pipeline is stored into the water ($Mc_p\Delta T$). This results in thermal resistance for the heat transfer fluid flow leading to both damping and time lags for the thermal response of pipeline. This phenomenon can not be evaluated in the conventional DTN model, since the variation of the fluid temperature is not considered in this model. However, combining the one-dimensional short timescale model (PFSCT model) with the DTN model allows the proposed model to take this issue into account.

Fig 7.22 shows the variations of the cumulative energy stored in the fluid in the pipeline with respect to the initial temperature over the length of the pipeline. The relative energy stored in the water is calculated by the combined DTN-PFST model based on the fluid temperature variations at each specific section along the buried pipeline. With the summation of the relative energy stored ($Mc_p\Delta T$) at each section, the cumulative energy stored along the pipeline can be obtained, as shown in Fig 7.22. It can be seen with the increase of the distance from the pipeline inlet, the pipeline energy storage rises. This implies higher energy requires to overcome the thermal inertia of the fluid through longer pipelines.

It can be observed the variation of fluid temperature and energy stored through the pipeline seems linear in Fig 7.22. This is due to the fact that transient heat losses from the fluid flow through the pipeline to the ground does did not considerably influence the thermal response of the pipeline. However, for longer pipelines with much higher transit time, e.g. of the order of a hundred minutes, the conduction heat loss is expected to distinctly affect the fluid temperature along the pipe. Further work concerting investigation of this issue is suggested in Chapter 8.

7.3 Conclusions

The overall aim of this work has been to develop thermal models suitable to use in district heating pipeline networks over a wide range of timescales. To this end, a novel model has been proposed combining the one-dimensional fluid flow model and the Dynamic Thermal Network model called the combined DTN-PFST model. The proposed model, along with the DTN model and detailed finite volume model have been implemented to modelling dynamic thermal behaviour of the buried pipeline system under the different operating conditions.

Due to the number of beneficial features of the DTN method such as the ability to represent complex geometries and heterogeneous thermal properties and efficiently deal with a very long time series input data, this approach has been taken to represent the transient heat transfer in buried pipeline systems. In this research, the derivation of the weighting factors required for the DTN model calculation has been done both numerically and experimentally. To derive the weighting factors numerically, the finite volume model has been developed with the convective boundary conditions, and the unit step change is applied to the boundary temperatures, in turn. The weighting factors have also been calculated experientially based on the measurement data from the designed tests were presented and compared in Chapter 4.

Although the way of obtaining the step response surface fluxes required for the derivation of the weighting factors was slightly different in the numerical model and the experiments, the results reveal that the weighting factors derived from both approaches are very close. This suggests that the DTN method can be implemented without using any analytical and numeral models, and only based on the measurement data. This finding is significant, as the DTN method has never been implemented purely based on the experimental data in the previous research, and it demonstrates the suitability of the approach independent to any numerical or analytical models.

Validation of proposed DTN-PFST model along with the DTN model using the numerically and experimentally determined weighting factors, has been conducted using the experiential data. The simulation results from the 3D conjugate heat transfer model are also used to compare with the DTN models outcomes in terms of the computational cost and accuracy. The conclusions concerning the performance of the numerical models in the prediction of heat losses and the outlet temperature of the buried pipeline can be summarized as follows:

- The implementation of the DTN calculation procedure without using any analytical and numerical models has been presented in modelling the thermal response of the buried pipeline systems. It is found that the DTN model using the weighting factors obtained experimentally is in a good agreement with the experimental data for both predicting the pipeline outlet temperature and heat fluxes. This indicates the validity of the DTN approach for implementation of buried pipelines.

- The proposed numerical model which is the combination of the DTN model and PFST model has been validated with the experimental data. This novel model with ability to effectively deal with the transient heat transfer of fluid flow along the buried pipeline system demonstrates a very good agreements with the experimental data, and relatively similar to the detailed 3D model. Due to relatively low heat losses and temperature drop in 15.5 m long pipeline, a longer pipeline has been modelled for better evaluation of the model in prediction of fluid temperature along the buried pipeline. It was observed that combined model is able to predict the fluid temperature along the buried pipeline at the same level accuracy of the detailed 3D model with of more than five order of magnitude lower computational cost. However, further investigation is suggested to make on the noticeable advantages of the implementation of the proposed model for realistic district heating pipeline networks, where much higher temperature drop is expected to take place in along the pipeline.

- The output results of the combined DTN-PFST model have been illustrated that the model is not only able to accurately simulate the dynamic behaviour of the buried pipe system in the very good agreement against the experimental data, but also noticeably more computationally efficient than the finite volume method, i.e. more than five orders of magnitudes. The ability of the model to represent the temperature propagation through the pipeline along with transient conditions heat transfer with complex and time-varying boundary conditions in a high level of computational efficiency makes the model widely applicable for efficient routine dynamic thermal analysis and design tasks of current and future thermal energy networks.

Chapter 8

Conclusions and future work

The overall aim of this research was to develop a dynamic thermal model of buried pipelines suitable for use in the simulation of next generation district heating systems. To this end, experimental facilities that represent a scaled-down of district heating system were designed and built to obtain reliable temperature and heat flux data for a various range of operating conditions expected to occur at thermal energy networks. These data have been used to study the dynamic thermal behaviour of the pipeline under different operating conditions both in short and long timescales and accordingly, develop and validate the numerical models proposed in this research.

Based on the aims and objectives of this research, two main numerical models have been proposed to model pipelines for short and long term simulation purposes. Firstly, a novel discretised model is proposed for short timescale simulation with the ability to take into account the effects of the longitudinal dispersion and thermal capacity of fluid flow along with the radial heat transfer to surroundings. Secondly, a novel dynamic thermal numerical model is proposed and developed based on the Dynamic Thermal Network (DTN) method to deal with the dynamic thermal behaviour of the three-dimensional buried pipeline system with the complex time-varying boundary conditions for both short and long timescale simulation. In addition to the proposed numerical models, a three-dimensional conjugate heat transfer model has been developed using finite volume method (FVM) to be used as a reference model to make the comparison between the numerical models in terms of computational cost and the degree of accuracy.

8.1 Conclusions

The significant findings and principal conclusions of this research can be summarised in three parts concerning the experimental work, modelling short timescale dynamic response of pipelines, and modelling the thermal response of the buried pipelines considering transient heat conduction. The main findings of the experimental work can be summarised as follows.

1. The dynamic thermal response of the pipelines with and without insulation was investigated at the short timescales over a wide range of operating conditions to understand the effects of physical phenomena involved in shaping the thermal response of pipelines. It was found that the longitudinal thermal diffusion processes significantly affects the thermal response of pipelines depending on the dynamic transport of the fluid flow through the pipeline. It was observed that the time between pipeline outlet temperature rising and reaching steady-state conditions after applying a step change at the inlet temperature is approximately the transit time and that there is the diffusion of the thermal transport that can be correlated with Reynolds Number. This indicates the importance of considering the longitudinal thermal diffusion processes of pipelines in modelling DHS pipelines, where the transit time is in order of more than tens of minutes.

2. Comparing the normalised outlet temperature responses of the pipeline in the short timescale showed that there is no noticeable difference between the experimental data for the cases with and without insulation. The best explanation of this is that the time duration of the experiments is too short to allow the heat to be transferred from the fluid flow to the outer surface of the pipeline. Variations in RTD are mostly correlated with Reynolds number rather than insulation properties under step change driven conditions. This suggests that the thermal inertia of the pipeline plays a much more dominant role in shaping the outlet temperature profile compared with the heat losses to the surroundings in the short timescales.

3. The dynamic thermal response of the buried pipeline considering the transient conduction heat transfer in the ground has been experimentally investigated over long timescales by applying a step change to the pipeline and ground

boundary temperatures. It was found that using the proposed experimental procedure for calculation of the admittive and transmittive heat flux data from the imposition of the step changes can be implemented for the derivation of weighting factors series as required parameters for the DTN calculations.

4. Evaluation of the dynamic heat losses of the buried pipeline and the ground surfaces over long timescales showed the significant effects of ground surface heat losses at long timescales on the buried pipeline responses. It was found considering the geometry and thermal conditions of the long timescale experiments, over 6 percent of the total pipeline energy was lost to the ambient. This amount of energy can be more considerable, given the long buried pipelines in thermal energy networks. This indicates the necessity of considering the dynamic heat transfer of the pipelines and ground surfaces in modelling the thermal energy networks where the heat interactions between the surfaces are more complex.

To model the short timescale dynamic thermal effects through the pipeline, discretised one-dimensional models along with the 3D FVM model have been developed. In this research, a novel numerical model that is a modification of the PFNCST model and extended to include a representation of the pipe material, longitudinal dispersion of fluid flow and radial heat transfer, has been proposed. The capabilities of this model in capturing the dynamic short timescale effects in the pipelines was compared with other numerical models and measurement data from the experimental work. The main conclusions of modelling the short timescale dynamic thermal response of pipelines using the developed models can be summarised as follows:

5. The comparison between the numerical results with the analytical solution of the ADPF model for ideally insulated conditions has showed that the NCST model even with optimum tank number tends to overpredict the diffusion of heat transfer fluid flow, whereas the PFNCST model predicts the changes of the outlet temperature with a better agreement with the ADPF model. The PFNCST model is able to get better results with fewer tanks in the calculation.

6. Good agreement between the measurement data and both the NCST model and modified PFNCST model was found in the prediction of short timescale dynamic thermal response of the pipeline. However, the number of tanks in the

modified PFNCST is less than one-twentieth that of the NCST model. This feature can be considered a significant advantage in terms of computational resources, particularly for the long and complex thermal networks.

7. The modified PFNCST model showed good ability to capture short timescale dynamic thermal effects in a similar manner of the detailed 3D numerical model, while the proposed model is much more computationally efficient i.e. more than of three orders of magnitude. The good ability of the modified PFNCST model was found in the prediction of both the time of initial temperature rise and the following temperature rise profile that is consistent across the range of conditions studied.

8. In a similar way to the NCST model, it was found that there is the optimal number of tanks in the modified PFNCST model that can be well correlated with Peclet Number. The linear correlation that has been derived can be used for calculation of the number of tanks for any case with different geometry and Reynolds number. It was also shown that the sensitivity to the number of tanks is not very significant and that using an intermediate flow rate within the expected range results in a suitable choice of tanks.

The evaluation of the dynamic thermal behaviour of buried pipelines has been made using Dynamic thermal Network (DTN) approach. In this research, the weighting factors were derived firstly from the data from the experimental work. Simulation of the pipeline using the DTN approach and the experimental weighting factor data have been compared with that of the numerically derived weighting factors. Moreover, to equip the model with the ability to capture the dynamic thermal effects of the fluid flow through pipelines, a novel numerical model has been proposed that is the combination of the DTN model with the PFNCST model, i.e. so-called the combined DTN-PFST model. The significant conclusions concerning modelling the dynamic heat transfer of the buried DHS pipelines using the developed models can be summarised as follows:

9. The DTN approach has been experimentally validated using the weighting factor series derived from the measurement data collected from the experimental setup. In other work, the weighting factors were calculated using the numerical models, e.g. the FVM model, or the analytical solution. The experimental validation of the approach reveals the significant capability of the DTN method to

be implemented in modelling the dynamic thermal behaviour of DH pipelines along with a variety of other thermal applications. It also demonstrates the validity of representing the system based on conduction heat transfer with convective boundary conditions.

10. The novel approach proposed in this research combines DTN representation of the buried pipeline and ground with the PFNCST model to capture fluid transport effects. The model showed very good agreement against the experimental data and is able to capture the dynamic behaviour of buried pipeline in the same manner of the detailed 3D model, while it is more than five orders of magnitude more computationally efficient.

11. The significant feature of combined DTN-PFST model is that it allows the pipeline to be divided into the finite sections, depending on PFCNST model calculation, and allocate specific geometry, material and surface thermal properties for each section. This is noticeably advantageous especially for simulation of long DH pipelines where the diameter, type of soil, and ground surface are likely to be varied along the pipeline.

12. The combined DTN-PFST model offers significant advantages in terms of the computational cost and level of the accuracy in modelling the dynamic behavior of buried pipelines. This makes it well-suited for the simulation thermal response of not only the buried DH pipeline but other networks of buried pipelines, e.g. ground heat exchangers, over a wide range of timescales.

8.2 Recommendations for Future Work

According to the main experimental and numerical findings and outcomes of this research, a number of recommendations can be made for further experimental work and numerical model development. In the following, the recommendations are discussed into two main sections: further experimental work, and future development and application of the proposed models.

8.2.1 Experimental work

Considering the high precision and flexibility of the experimental facilities designed and built in this research, they can be used for further research concerning the

dynamic thermal behaviour of the buried pipelines. In the following, a number of further experimental work are described.

1. The experiments conducted in this research used only one type of soil, i.e. dry sand. It would be useful to investigate the effects of different type of soil along with the moisture content on the dynamic behaviour of the pipeline and ground heat losses. Since the pipeline passes through three separated boxes, it is also possible to fill each box with one type of soil with a specific moisture content. In this way, the effects of the mixture of different type of soil and moisture on the overall dynamic heat transfer of the pipeline system can be usefully investigated.

2. The control system designed and programmed in this research, i.e. using LabVIEW, has been used to apply a step change to the pipeline inlet temperature. It would be beneficial to reprogram the control system and adjust the system to impose different forms of the changes to the inlet temperature of the pipeline, e.g. square or sinusoidal changes, and study the dynamic thermal response of pipeline in these cases. The data can also be used for further assessment of both proposed models in the prediction of thermal behaviour of the system.

3. The experimental setup has been used for one pipeline buried in the sand. This was sufficient to demonstrated the validity and advantages of the DTN approach and extension to three surfaces (supply and return pipes with the ground) is straight forward. Thus, the test rig has been designed and built in a way that makes it possible to add more pipelines parallel to the main pipeline. It would be of interest to study the thermal interaction of the new pipelines with the main pipeline and the ground surface. Moreover, the effects of the dynamic behaviour of each pipeline on the other, and the heat losses from the pipelines and ground surfaces can be evaluated for a wide range of operating conditions.

4. Due to the objectives of this research, a copper pipeline with a thickness of 7 mm has been used in both short and long timescale experiments. It was found the variation of both thickness and the thermal properties of pipelines material can affect the thermal response of pipelines over both short and long timescales. Therefore, it would be of interest to experimentally investigate the

effects of these parameters on the thermal behaviour of pipelines for a range of operating conditions.

5. The development of the combined DTN-PFST model has reached a stage where it can be readily implemented for simulation of the pipeline network in DHSs from minutely to annual timescales. However, experimental data from an operating DHS system would be useful for further assessment of the ability of the model in modelling the dynamic thermal response of pipelines, along with the overall heat losses in the distribution network in a full-scale DHSs . Moreover, gathering further experimental data under a wider range of operating conditions including more complex variations in inlet temperature would be useful to find more general applicable correlations for some parameters, e.i. optimum number of sections.

8.2.2 Future Development and Applications of the Models

In this research, two novel numeral models, i.e. the modified PFNCT model and combined DTN-PFST model proposed to deal with the dynamic thermal response of DH pipelines. These models have been validated with the experimental data and showed very good ability in modelling the DH pipeline system. however, more work can be recommended to be done for future development and applications of the proposed models, as discussed in the following:

1. In this research, the modified PFNCST model was presented and demonstrated that it is well able to represent the dynamic short timescale effects considering longitudinal dispersion and thermal capacity of the fluid flow and pipelines. Due to the simplicity of the concept of the model, it can be simply combined with other numerical models, e.g. the FEM, and implemented in the modelling of a variety of thermal applications, e.g. flat plate solar collectors. Considering the high computational efficiency and accuracy of the model, it would be of interest to evaluate the short timescale dynamic behaviour of other thermal applications, e.g. modelling the wastewater networks using the proposed model.

2. Due to the temperature update process in the DTN calculation, that the data is calculated and updated at each time step and then shifted to the next, the

long time series can be processed very efficiently. This also offers significant advantages of the calculation of heat flux and temperature at each time step, simultaneously. Moreover, since the input data is read at each time step, even small variation of input data (e.g. flow rate, inlet temperature and ambient temperature) are simply taken into account in the DTN-PFST calculation. This allows the model to predict the dynamic thermal behaviour of pipeline networks with relatively low computational cost at the high level of accuracy. making the model well-suited to assess the feasibility of implementation of next generation DHSs where the network dynamic heat losses is much more important and need to be calculated accurately.

3. Considering the advantages of the implementation of the combined DTN-PFST model for modelling thermal energy networks, it would be of interest to compare the simulation results from the model with other simulation tools used in industry such as TRNSYS, Modelica-based tools and EnergyPlus.

4. Although the theory of the combined DTN-PFST model is not complicated, it may not be straightforward for an ordinary user to calculate the step response fluxes, derive the weighting factors and run the combined DTN-PFST model. Developing an automatic routine would be much useful for making the combined DTN-PFST model more practically applicable as a design and simulation tool for modelling the pipeline network. It is recommended to create a library of weighting factor data based on depth and diameter of the pipeline, the thermal properties of the soils and type of the ground surface, e.g. pavement or bare ground. The library can be built-up beside the main program in a way that enables a user to call the specific weighting factors data for each section and run the program for energy analysis or design purposes.

5. The significant advantages of the combined DTN-PFST model in terms of the computational cost and accuracy, make the model well-suited for the simulation of dynamic heat transfer for a variety of thermal applications with any arbitrary three-dimensional geometries. For instance, the dynamic thermal response of pipes and the heat interactions of different types of ground heat exchangers or floor heating systems can be evaluated using the proposed model over a wide range of timescales.

Appendix A

Instrumental Calibration

Due to the importance of the accuracy of measurements for the experiments, the detailed process of calibrating the thermocouples and heat flux sensors used in the experiments has been elaborated in this appendix. Firstly, the instruments and their accuracies used for calibration are introduced. Then, the different types of errors causing uncertainty in measurements during the experiments are explained.

A.1 Calibration of temperature sensors

The thermocouples and RTDs calibration was performed by placing sensors in a Fluke Micro-Bath Thermometer Calibrators (7102) and recording measurements using a compact data acquisition unit (NI-cDAQ-9135). This unit coupled with a high-density thermocouple module (NI-9214) with a front-mount terminal block (TB-9214) including several cold-junction compensation (CJC) sensors to increases the overall accuracy of measurements. This module was used for measuring the input signal from the type T thermocouples. The RTD temperature module (NI-9216) also was also plugged into the cDAQ to measuring the input signal from the 4-wires RTD (pt-100). A precision Thermometer RTD Temperature Probe (5627A) is used to precisely measure the temperature of the micro-bath and connected to the Fluke Chub-E4 Standards Thermometer readout (1529). The calibration setup is shown in Fig. A.1.

Based on the range of temperatures measured by the thermocouples and RTDs for all experiments conducted in this project, six temperatures were chosen for thermocouple calibration. These temperatures i.e. from 10 C° to 60 C° are set to the

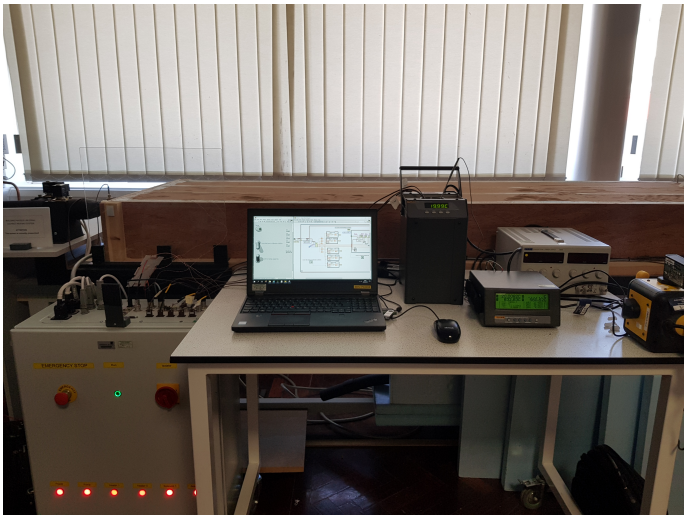

Figure A.1: Thermocouple calibration setup

micro-bath by increments of 10 C° from the highest one to lowest one to achieve better results [Fluke Corporation (2013)]. These temperatures are accurately controlled by the analogue/digital controller which uses a precision platinum RTD as a sensor and a solid-state relay (triac) driven heater. In addition to the micro-bath display shows the bath temperature, the temperature of the bath is measured with the immersed high-accuracy RTD Temperature Probe with accuracy of better than ±0.03 C°. This probe is connected to the readout with an accuracy of ±0.004 C°for this specific type of probe and resolution of 0.0001 C°. Note that the calibration factors provided by the probe manufacturer for each specific RTD probe should be entered to the thermometer readout to reach the maximum accuracy of the RTD probe. These factors came with the calibration certificate of the probe by the manufacturer.

The thermocouples and RTDs used for temperature measurement are placed into the bath basket with the RTD probe and properly immersed into the bath. The sensors are connected to the modules coupled with the cDAQ controller and the controller is connected to the computer to monitor and record the temperature measurements. The software used to control and record the data is LabVIEW software. This software allows the user to program so-called a virtual instrument (VI) for each specific application. For thermocouple calibration, a specific VI was programmed to read the temperatures from each thermocouple in less than every second and write them into the output file. It is recommended to write data into

the TDMS file as a LabVIEW output, since in some cases the number of data is too high for Microsoft excel to deal with that, although this file can be simply converted to the excel file or any other preferable files. This process has been done for RTDs calibration as well.

It is worth to note that according to the manual [Fluke Corporation (2013)] the well requires 30 min to stabilize the bath temperature within $\pm$ 0.03 C°, so that some features were added to the program to write data only after the stabilization time, then the collected temperatures in each sample time were averaged over recording time i.e. 50 sec. The block diagram of the temperature acquisition program is shown in Figure A.2.

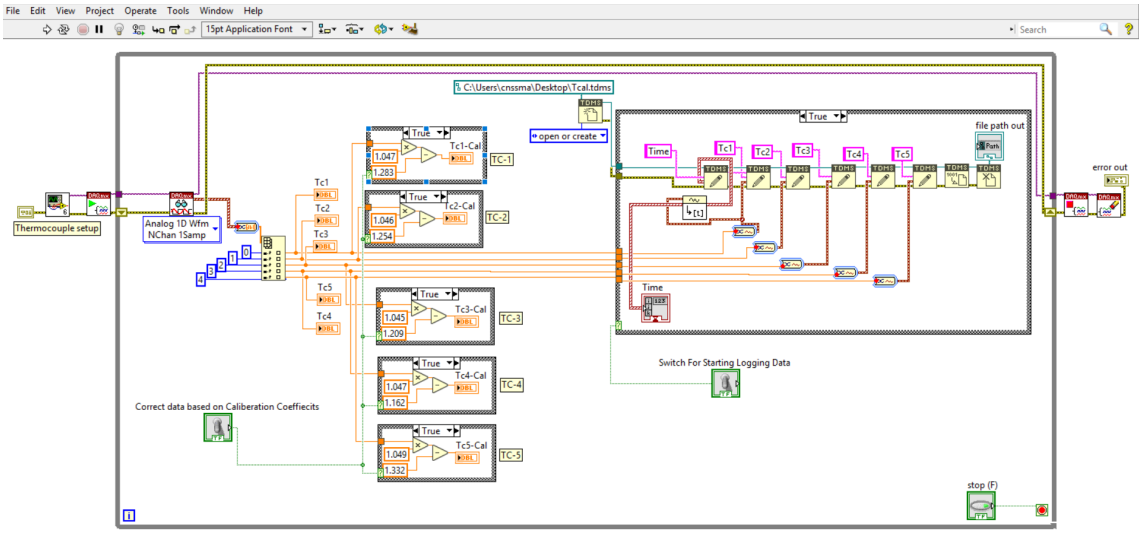

Figure A.2: The block diagram of the temperature acquisition VI.

Thermocouple and RTD calibration was carried out by correcting the raw measurement data using a linear correlation between the raw temperatures recorded by the sensors and actual temperatures recorded by the reference RTD temperature probe. It is known the temperature-voltage characteristic of temperature sensors can be considered linear where the range of temperatures is less than 100 C°. Since the full range of temperatures used in all experiments is less than 50 C°, the results can be considered accurate.

In this process, the temperature sensors and the reference thermometer (RTD thermometer) are immersed in the bath operating at six temperatures. According

to the actual temperature of the bath shown by the RTD reference thermometer (after stabilization of bath temperature), the constants of the linear correlation are calculated for each thermocouple. To increase the certainty of the calibration, this procedure which took around 4 hours repeated six times. These calibration coefficients obtained from this process are applied to correct the raw temperatures in the next set of experiments. Figure A.3 displays the temperature sensors calibration data and the corresponding fitted straight lines for two thermocouples. Calibration coefficients of data for each thermocouple were derived by applying a least-squares fit of a straight line.

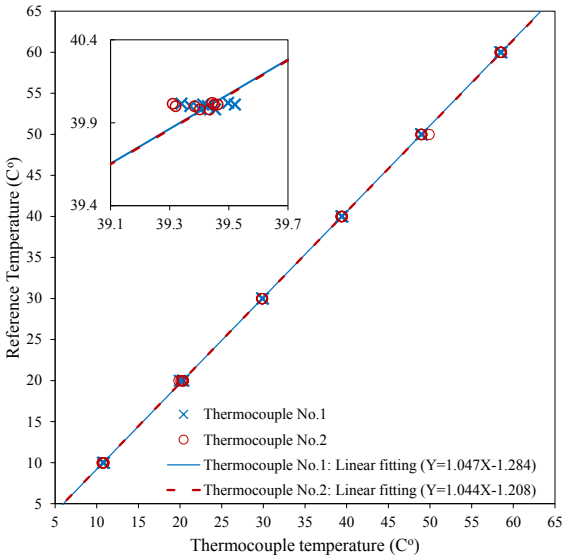

Figure A.3: The calibration data and the fitted straight lines for two temperature thermocouples

It was found that the raw temperatures varied by up to ±0.7 C°compared with the actual temperatures over the 10-60 C°range. This shows the necessity of the calibration of thermocouples. It was also noted that the gain coefficients are close to one with just a few percent difference while the offset coefficient varied between 1 and 2 degrees for all the thermocouples. This shows that offset errors play a more significant role in the thermocouple calibration than gain errors.

A.1.1 Uncertainty in temperature measurements

Measurements of every physical quantity have a degree of error, which is defined as the difference between the measured value and the true value of the variable being measured [Moffat (1988)]. The term "uncertainty" is used to refer to "a possible

value that an error may have in the measurements“ [Kline & Mcclintock (1953)]. In other words, uncertainty is referred to as the interval around the measured value within which the true value lies. These values also provide a way to evaluate the importance of the scatter on repeated experiments and should be reported in all experimental works.

There are two main types of errors in the measurements, and the total error is expressed in terms of these two components: a precision or random error, and a bias or fixed or systematic error [Beach *et al.* (1985)].

The precision error is a random error which varies on repeated observations of the measurement data at the same conditions. Sources of precision error can be from measurement methods, measuring instruments as well as calibration methods. For N repeated measurements from the parameter population(X_i), the sample population standard deviation(S_{X_i}) can be expressed as follows,

$$S_{X_i} = \sqrt{\frac{\sum_{i=1}^{N}(X_i - \bar{X}_i)^2}{N-1}} \tag{A.1}$$

While the sample mean X is represented the mean population of measurement data ($\bar{X}_i = \frac{\sum_{i=1}^{N} X_i}{N}$). The precision error of the average of a set of measurements is always less than that of individual measurement and obtained from [Moffat (1988)]:

$$S_{\bar{X}_i} = \frac{S_{X_i}}{\sqrt{N}} \tag{A.2}$$

To calculate the precision error of a given parameter, the root sum square (RSS) method can be used to combine the precision indices from the K sources of error [Moffat (1988)]:

$$S = \sqrt{{S_1}^2 + {S_2}^2 + ... + {S_K}^2} \tag{A.3}$$

The true value of the parameter is expected to lie within the interval ($X \pm tS$). The student t value is a function of confidence level and the degrees of freedom i.e. associated with the precision of a simple experiment (one set of N observations) is $N-1$ [Moffat (1988)]. For a large number of samples $N > 30$ and 95 percent confidence levels, student t value can be assumed equal to 2, otherwise, it can be obtained from the Welch-Satterthwaite formula [Beach *et al.* (1985)].

Another type of error is the bias error (systematic error) which considered to remain fixed during the experiments and affects all repeated measurements the same. There is no statistical equation to find the bias limit [Beach *et al.* (1985)], and it should be estimated based on the true value. However, with using the proper calibration method to correct the measurement data, it can be assumed that these kinds of errors have been dealt with and measured data and should not be part of the quoted uncertainty [Engel (2005)].

For calculation of precision error of temperature sensor calibration and to check the repeatability of the temperature measurement system, the calibration process was carried on 8 times for the 6 temperatures. The data were collected for each thermocouple and RTD submerged into the bath with the specific temperature and compared with the actual bath temperature measured with the reference RTD thermometer, after applying the calibration procedure described in this section. This data was used to estimate the mean error and standard error according to Eq. A.1. The histogram forms of the data for three thermocouples are shown in Fig.A.4.

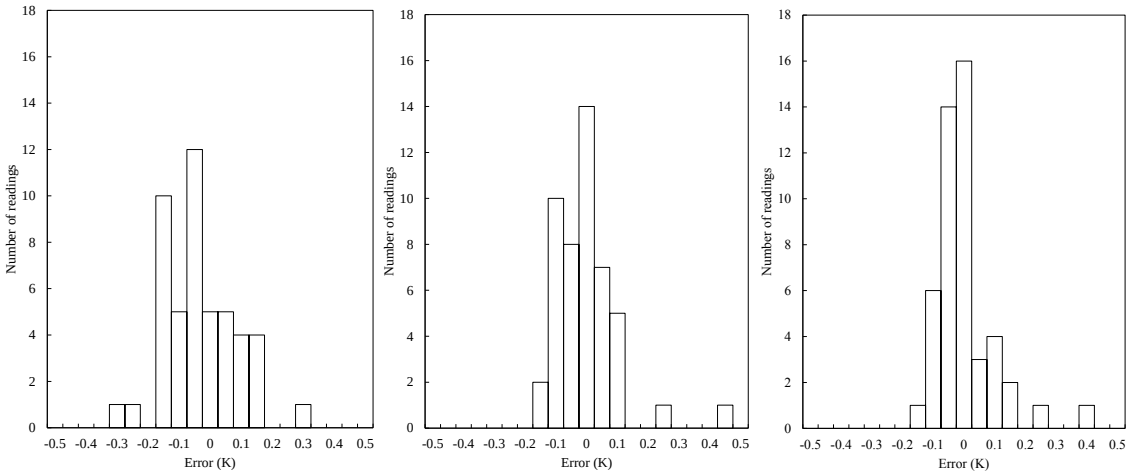

Figure A.4: Thermocouple repeatability test results in histogram form.

The maximum mean error recorded for the thermocouples were -0.027 K with a standard error of 0.135 K. According to Eq.A.2 the precision error of the average of a set of thermocouple data is 0.067 K. However, to estimate the precision error of the temperature measurement, all precision errors from other sources should be considered including the uniformity of the bath i.e. $\pm$0.02 K and thermometer readout accuracy $\pm$0.005 K. By taking into account theses precision errors and 95 confidence level which is recommended confidence level for uncertainty evaluation [Kim *et al.*

(2008); Moffat (1988)] the uncertainty of the thermocouples is calculated to 0.167 K. Similarly, The maximum mean error recorded for the pt-100 sensors were -0.017 K with a standard error of 0.055 K, and the precision error of the average of the pt-100 sensors data is 0.016 K. Accordingly, by considering the 95 confidence level, the uncertainty of the pt-100 sensors can be calculated to 0.062 K.

A.2 Heat flux sensors calibration

In this project, three self-calibrating heat flux sensors (HFP01SC) has been used for the mearsurement of heat fluxes from the sand. HFP01SC is a combination of a heat flux sensor and a film heater. The sensor output is a voltage signal which is proportional to the heat flux through the sensor. This high sensitive heat flux sensor incorporates the film heater to self-test and self-calibrate the sensor to compensate the measurement errors caused by the thermal conductivity of the surrounding soil and sensor contact to the soil.

To perform the heat flux calibration, it is necessary to switch on HFP01SC's heater and record the sensor output signal and the heater power, and after specific time switch the heater off. During the heating interval, a current passes through the heater generates a known heat flux. This value is further used for calculation of new sensitivity of the heat flux sensor. For calculation of this heat flux, the heater current I_{heater} must accurately be measured [Hukseflux (2016)].

In these experiments, the Laboratory DC Bench power supply (EX345RD) was used to turn on the film heater in the HFP01SC and measure the power supply of the heater accurately. According to the manual[Hukseflux (2016)], the heater should be powered 12 VDC (at 0.12 A as the nominal value), although depending on the surrunding soil, the power can be slightly different, consequetly the voltage and current should be presicely measured. The power supply displaying the input voltage and current to the film heater of HFP01SC is shown in fig.1.

Based on the manual, the recommended duration of the test is 360 s. It is divided into a heating interval of 180 s and a settling interval of 180 s, and the sensor voltage output should be recorded at the speific times. Accordingly, The new sensitivity of the HFP01SC can be calculated as follows [Hukseflux (2016)]:

$$\Phi_{selfcalibration} = \frac{R^2_{heater} I_{heater}}{A_{heater}} \tag{A.4}$$

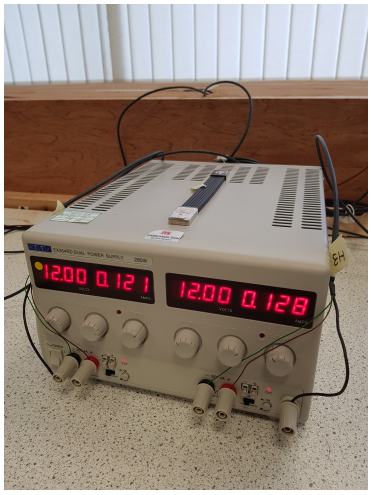

Figure A.5: Power supply unit

$$U_{selfcalibration} = |U_{t=180} - 0.5(U_{t=0} + U_{t=360})| \tag{A.5}$$

$$S_{selfcalibration} = 2U_{selfcalibration}/\Phi_{selfcalibration} \tag{A.6}$$

$U_{selfcalibration}$ of the sensor is multiplied by two as only half of the flux passes the sensor. The values A_{heater} and R_{heater} provided by manufacturer were entered individually for each sensor. The manual [Hukseflux (2016)] recommends defining acceptance intervals to make sure that the heat flux sensor works properly. It is suggested that $S_{selfcalibration}$ should be between +5 and –20 perecnt of the original $S_{reference}$ provided by the manufacturer. Moreover, for making sure that response time is acceptable and not long, two conditions below should be fulfilled.

$$|U_{t=360} – U_{t=0}| < 0.1U_{selfcalibration} \tag{A.7}$$

$$|U_{t=170} – U_{t=180}| < 0.1U_{selfcalibration} \tag{A.8}$$

In the similar way with the thermocouple caliberation, another specific VI was programmed to read the voltage output from the heat flux sensors in less than every second and write them into the TDMS file. The voltage outputs at the specific times were then used to calculate the new sensitivity of the sensors based on Eq.A.4 to Eq.A.6 together with the voltage and current input to the film heater.

For calculation of precision error of heat flux sensors calibration and checking the repeatability of the measurement system, the calibration process was carried out 6 times for all three heat flux sensors.

After conducting calibration for the heat flux sensors, it was found that the sensitivity of heat flux sensors are 63.35, 60.07 and 56.48 $\mu V/(W/m^2)$. The maximum mean error recorded for the heat flux sensors was -0.95$\mu V/(W/m^2)$ with a standard error of 0.58$\mu V/(W/m^2)$. According to Eq.A.2 the precision error of the average of a set of heat flux sensor data is 0.136$\mu V/(W/m^2)$ equal to 0.22 percent of the average sensitivity of the heat flux sensors. However, to estimate the precision error of the heat flux sensor measurement, all precision errors from other sources should be considered including precision errors in reading the current and voltage of power supply which are 0.5 and 0.3 percent of reading, and the accuracy of the voltage input module which is 0.1 percent [National-Instruments (2015)]. Considering these precision errors and 95 confidence level, the uncertainty of the heat flux sensors is calculated to 0.63 percent of the heat flux measurement.

Appendix B

PID controller

The process of controlling the heating system in this research was carried out using a PID controller. Proportional-Integral-Derivative (PID) or three-term controllers are the most widely used controllers in the industries and engineering research works. The general empirical observation shows that PID controllers have been successful in desirably controlling the performance of the systems in most processes [Kaya (1999)].

Principally, a PID controller reads a sensor value from a closed control loop, then calculate the desired output to the process based on calculating proportional, integral, and derivative responses and summing them to compute the output response. Therefore, the PID controller output is obtained based on the current control error (the P-term), the time history of the error (the I-term), and a prediction of the future value of the error (the D-term), as shown in Fig. B.1. The mathematical form of the overall control function can be expressed as below:

$$u(t) = K_c\left(e(t) + \frac{1}{T_i}\int_0^t e(\tau)d\tau + T_d\frac{de(t)}{dt}\right) \tag{B.1}$$

The proportional parameter depends on the difference between the setpoint and the process variable. This determines the ratio of output response to the error signal. The integral parameter sums the error term over time. Hence, even a small error term will cause the integral component to increase slowly to drive the steady-state error to zero. The derivative parameter causes the response to decreasing if the process variable rapidly increases. This parameter is highly sensitive to the noise of the process variable signal; hence if the sensor feedback is noisy, this should be chosen very small in order to keep the system stable.

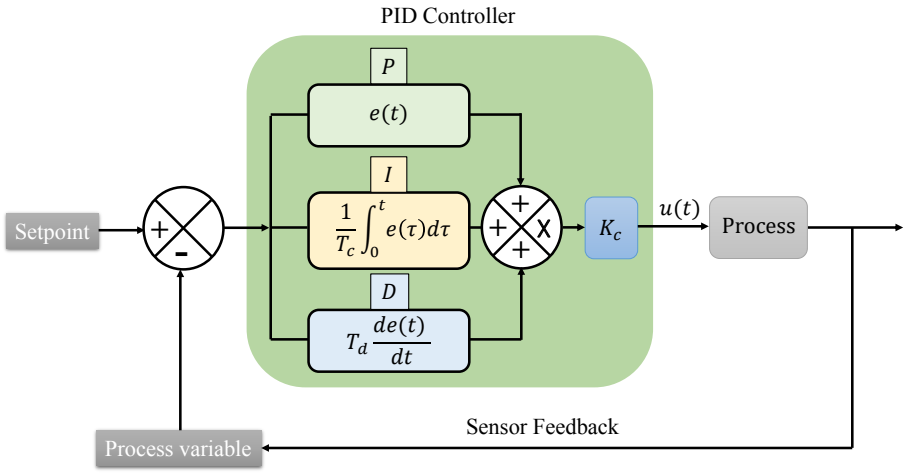

Figure B.1: A block diagram of a basic PID control algorithm

In a PID controller, it is essential to find proper values of the controller parameters. The process of obtaining the parameters is called tuning. There are two approaches for finding the parameters. First one is to mathematically model the process, which is generally quite difficult specifically in the system with the presence of the disturbance sources, i.e. unpredictable sources that have undesirable effects on the system. The second approach is to choose the parameters, based on the behaviour of the feedback loop and modify the controller parameters until the desired behaviour is achieved, then fix them in the controller for further use in the application. The Ziegler-Nichols method is the most popular method of tuning a PID controller based on the behaviour of the feedback loop [Goodwin (2015)]. In this work, this method has been applied with some modification for tuning the control system.

Initially, the I and D terms were set to zero and the proportional gain was increased gradually until the output of the loop started to oscillate. It should be noted that increasing the proportional gain (K_c) results in a faster response of the system which is desirable for the most applications. However, rising proportional gain (K_c) may make the system unstable (overshoot response). Therefore, this parameter needed to increase carefully in ramp manner to make sure that the system stayed stable and fast enough. Once output response started to oscillate in the certain proportional gain (K_c), based on the period of the oscillations (P_c), T_i and T_d could be adjusted and set in the LabVIEW program as presented in table B.1:

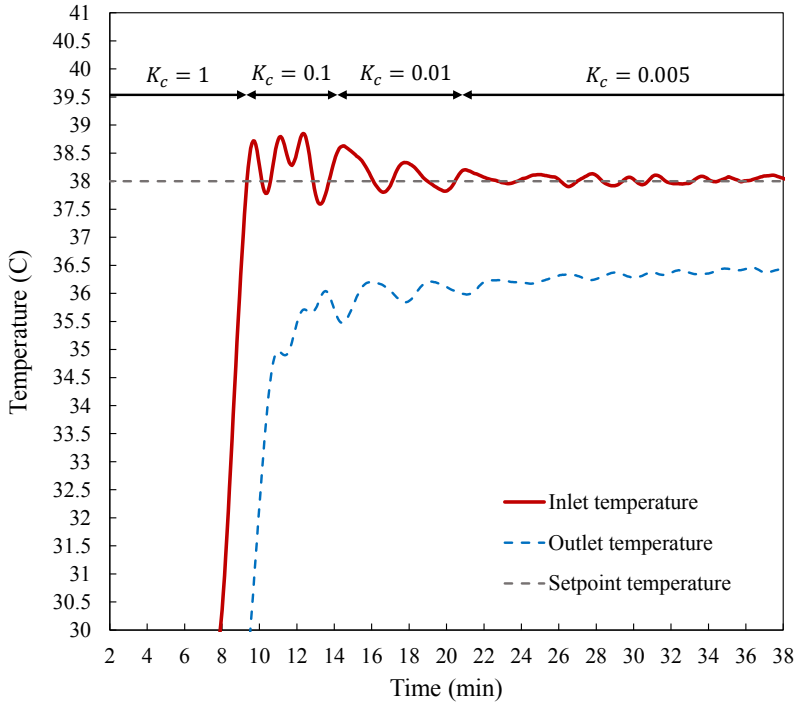

Figure B.2: The pipeline inlet temperature in the experimental setup controlled via the PID controller by decreasing the proportional gain (K_c) output to the heaters.

As explained in section 4.3.3, in this research the heaters in the experimental setup needed to be precisely controlled such that the inlet temperature of the pipeline is constant. Therefore, at any given moment, the difference between the inlet temperature as the process variable and the setpoint temperature was used by the control system algorithm to drive the power of heaters. Based on the setpoint temperature and the PID parameters obtained according to the Ziegler-Nichols tuning method, the PID controller determined the desired actuator output in a given loop rate to the heaters between the output rage of the heaters, i.e. between 0 and 10 V. The voltage output was proportional to the input power of the heater between, i.e. 0 to 6 kW.

Due to the highly dynamic behaviour of the system at the beginning of the experiments, i.e. increasing the inlet temperature by almost 20 °C and then keeping it

Table B.1: Ziegler-Nichols tuning method

Control	T_i	T_d
PID	$0.50P_c$	$0.125P_c$

constant while the output temperature rapidly increases, the PID controller tuned by the Ziegler-Nichols method failed to sufficiently control the system without overshoot or overtime rising temperature. Therefore, the Ziegler-Nichols method was applied for different stages of the controlling system. Firstly, the proportional gain (K_c) was set to the maximum possible value to have the fastest output response, but not overshoot. Then, the proportional gain was decreased in every stage to reduce transient errors. Due to the high sensitivity of the controller to the proportional gain, this process required mindful attention; otherwise, the system failed to keep the inlet temperature constant. It is worth noting that depending on the fluid velocity, the process of obtaining the suitable proportional gains for each step needed to be repeated and revised. The inlet temperature of the pipe controlled by the PID controller for one experiment is displayed in Fig. B.2.

In controlling the heaters for in this set of the experiments conducted in this research, the proportional gain decreased in each step and the period of the oscillations measured in the stable condition in order to determine the T_i and T_d required to be set into the controller. It was found that at the first hour of the experiment, the system does not depend on the integral, and derivative responses, due to the highly dynamic behaviour of the system. However, after the system almost reached the stable condition, setting the suitable values for these parameter based on the Ziegler-Nichols method could help the system to reduce and eliminate the slight discrepancies between the inlet and setpoint temperature.

Appendix C

Thermal Properties Measurement of Sand

Soil thermal properties are necessary parameters in modelling heat transfer process in a variety of thermal engineering applications with buried pipeline. The thermal conductivity (λ) and the thermal diffusivity (α) often constitute the input data for modelling heat flow in soils. The values of the soil thermal properties reported in the literature are within a relatively broad range due to the sensitivity of the values to the porosity and water content. Therefore, it is desirable to determine values on site when possible [Yavuzturk *et al.* (2000)].

The standard approach for measuring thermal properties is called the steady-state method. In the steady-state method, heat applied to the soil until there are no more temperature changes with time. Using the temperature gradient and heat flux density, the thermal properties of soil can be obtained. This process takes a long time, e.g. days, to reach steady-state conditions resulting in moisture migration in soil. As a result, it is practically impossible to use this method for measuring the thermal properties of moist and porous soils.

Another approach to measuring the thermal properties of soils is the transient line heat source method. This approach has been used for measuring thermal properties of porous materials for over 60 years. In this approach, a probe consists of a needle with a heater and temperature sensor inside is typically used. A current passes through the heater and the system collect the temperature of the sensor over time. By analysis of the time dependence of sensor temperature, the thermal properties of sand can be determined.

In this research, the *TEMPOS* Thermal Properties Analyser is used for measurement of soil thermal properties. Firstly, the thermal diffusivity of sand has been measured using the dual-needle sensor (SH-3) (30-mm long, 1.3-mm diameter). Prior to the thermal diffusivity measurement process, the TEMPOS collects data for at least 30 s to determine the temperature drift. If the drift is below a threshold, a current is applied to the heater needle for 30 s, during which time the temperature of the sensing needle is monitored and logged every second. TEMPOS keeps heating times as short as possible to minimise thermally induced moisture movement. Use of relatively short heating times and low heating rates require high-resolution temperature measurements provide by TEMPOS resolving temperature to ±0.001 °C [Meter-Group (2018)]. After 30 s of heating, the current is shut off, and the temperature is monitored for another 90 s. The starting temperature and drift are then subtracted from the temperatures giving the temperature difference values required to solve the infinite line heat source equations (Eq. C.1 and Eq. C.2 for the heater is on and off, respectively) [Low *et al.* (2014)].

$$\Delta T = \left(\frac{q}{4\pi\lambda}\right) E_i \left(\frac{-r^2}{4\alpha t_{heat}}\right) \tag{C.1}$$

$$\Delta T = \left(\frac{q}{4\pi\lambda}\right) \left[E_i \left(\frac{-r^2}{4\alpha(t-t_h)}\right) - E_i \left(\frac{-r^2}{4\alpha t}\right)\right] \tag{C.2}$$

While E_i, q, r, t and t_h are the exponential integral, input power, radial distance, test time and heating time, respectively. These values are known after tests; thus, the thermal conductivity (λ) and thermal diffusivity (α) can be calculated from the equation using the traditional non-linear least squares method. More details of the method and calculation procedure can be found in [Meter-Group (2018)].

For measurement of the thermal diffusivity of the sand, a number of tests have been conducted to estimate the value and check the repeatability of the measurement. Initially, the thermal diffusivity of the sand has been measured at one location for 9 times, according to the procedure described above. Afterwards, the measurements have been done for different locations of the sand to assess the variations of the value to the locations, and calculate the uncertainty of the thermal diffusivity measurement. The histogram forms of the data for one location and different locations are shown in the left and right side of Fig C.1, respectively. Based on Eq. A.1

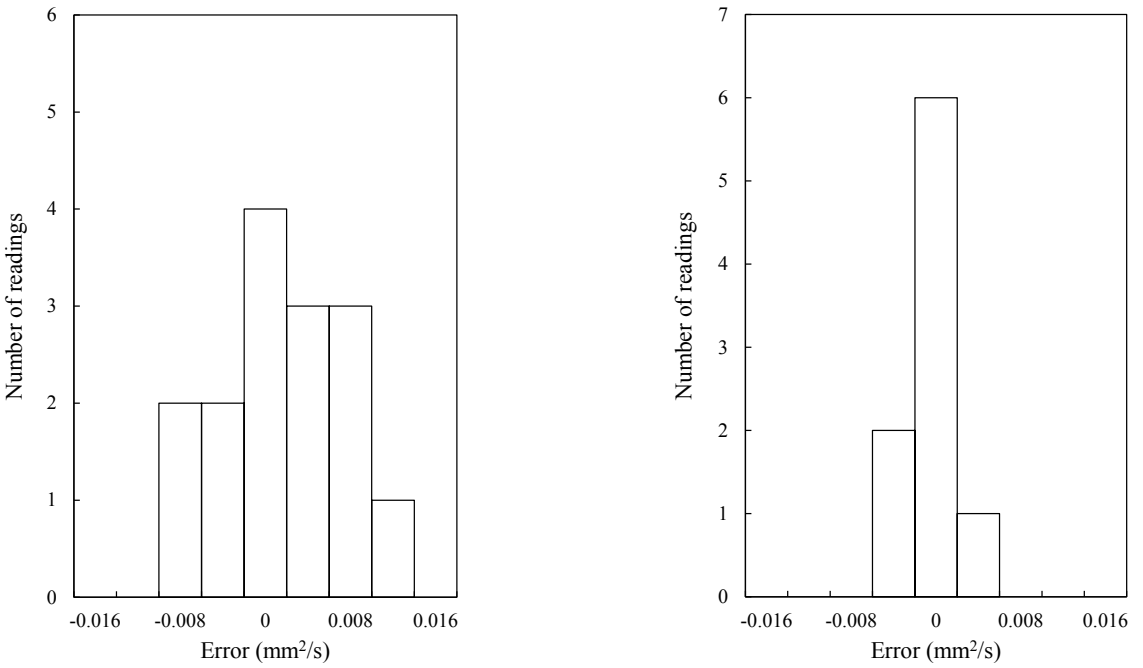

Figure C.1: The sand thermal diffusivity repeatability test results in histogram form.

and Eq. A.3, the thermal diffusivity of sand is estimated to 0.1802 mm^2/s with the uncertainty of 0.0089 mm^2/s (95 percent confidence level).

For measuring the thermal conductivity of the sand, the large (100-mm long, 2.4-mm diameter), single-needle TR-3 sensor has been used. The TR-3 is primarily designed for soil and other porous materials. In the process of thermal conductivity measurement, similar to the thermal diffusivity measurement, The TEMPOS collects data for at least 30 s to determine the temperature drift to make sure that the drift is below a threshold. Afterwards, the current is applied to the heater needle for 30 s, and the temperature of the sensing needle is monitored and logged every second. After the time of heating, the heater is switched off, and the temperature is monitored for another 60 s. Eq. C.1 can be used for single-needle analysis; however, since the only thermal conductivity is desired in this equation, the exponential integral can be expanded in an infinite series, and only the first term in the expansion is retained, as expressed in Eq. C.3. [Meter-Group (2018)].

$$\Delta T = \left(\frac{q}{4\pi\lambda}\right) \ln t + C \tag{C.3}$$

Eq. C.3 indicates that conductivity is proportional to the inverse of the slope when the temperature is plotted with respect to ln t. This expansion is assumed

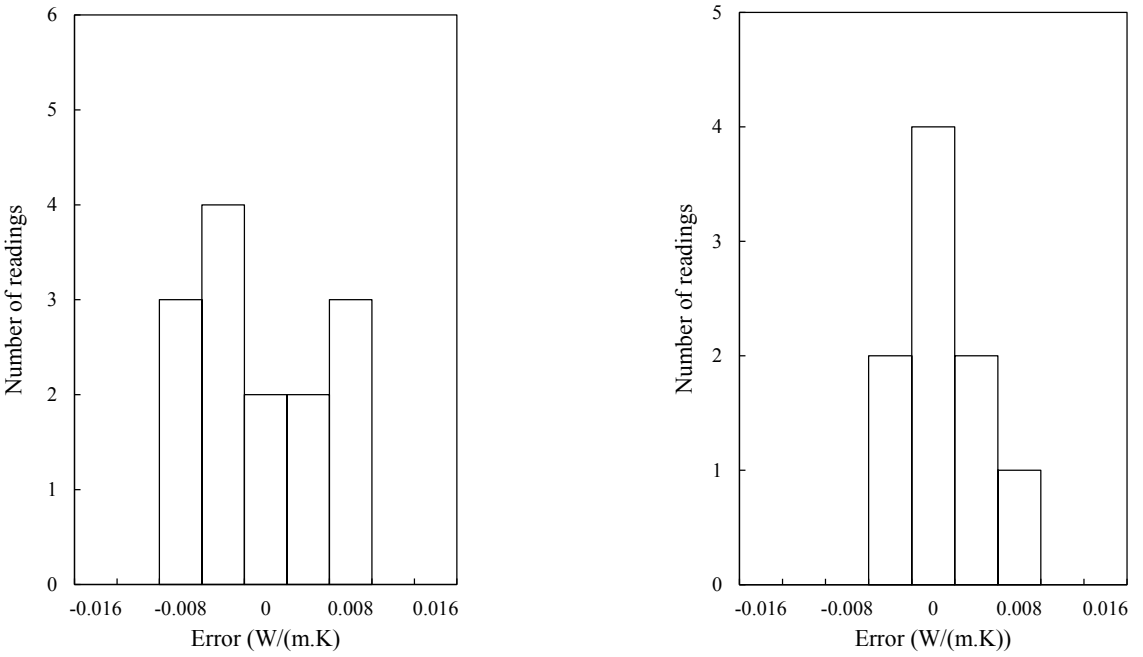

Figure C.2: The sand thermal conductivity repeatability test results in histogram form.

to apply only at long heating times, so early time data are left out of the analysis. At long times the temperature hardly changes, so noise in the measurements can strongly affect the measurement. Additionally, in the line heat source equation, there is no heat capacity, but the real probe has significant heat capacity. It has been found out by changing the time to $(t - t_o)$ while $t_o$is a time offset, all of the data fit well with heating times of 60 s. Consequently, Effects of contact resistance and diffusivity are eliminated or significantly reduced. More details of the method are described in [Meter-Group (2018)].

Similar to the measurement of the sand thermal diffusivity, a number of tests have been carried out for estimation of thermal conductivity of sand at one location and later different locations of the sand. The histogram forms of the thermal conductivity of sand for one location and different locations are shown in the left and right side of Fig C.1, respectively. Based on Eq. A.1 and Eq. A.3, the thermal conductivity of sand is estimated to 0.1729 $W/K.m$ with the uncertainty of 0.0105 $W/K.m$ (95 percent confidence level).

.

Appendix D

List of publications and presentations

The following publications and presentations have been prepared and produced based on the research done in this thesis.

D.1 Publications

- **S. S. Meibodi**, S. J. Rees, "Dynamic thermal response modelling of turbulent fluid flow through pipelines with heat losses" (International Journal of Heat and Mass Transfer 151 (2020) 119440)
- **S. S. Meibodi**, S. J. Rees, D. Yang "Modelling the dynamic thermal response of turbulent fluid flow through pipelines" (Proceedings of the 16^{th} International Building Performance Simulation Association (IBPSA) Conference, Rome, Italy, 1357- 1364)
- **S. S. Meibodi**, S. J. Rees, "Experimental validation of the dynamic thermal network approach in modelling buried pipes" (in progress to submit to the journal of Applied Thermal Engineering)

D.2 Presentations

- **S. S. Meibodi**, S. J. Rees (2019), "Dynamic thermal response modelling of turbulent fluid flow through pipelines with heat losses", oral presentation at

the 16^{th} IBPSA Conference, Rome, Italy.

- **S. S. Meibodi**, S. J. Rees (2019) "Experimental validation of dynamic thermal response modelling for turbulent fluid flow through 4GDH pipelines", oral presentation at the 7^{th} Annual Civil Engineering PGR conference, the University of Leeds, UK.
- **S. S. Meibodi**, S. J. Rees (2018) "Modelling the dynamic thermal response of pipelines in 4GDH", oral presentation at the 6^{th} Annual Civil Engineering PGR conference, the University of Leeds, UK.
- **S. S. Meibodi**, S. J. Rees (2017) "Next generation district heating systems", poster presentation at the 5^{th} Annual Civil Engineering PGR conference, the University of Leeds, UK.

.

References

Adeosun, J.T. & Lawal, A. (2010). Residence-time distribution as a measure of mixing in T-junction and multilaminated/elongational flow micromixers. *Chemical Engineering Science*, **65**, 1865–1874. 19

Arpaci, V. (1966). *Conduction heat transfer*. Addison-Wesley series in mechanics and thermodynamics, Addison-Wesley Pub. Co. 32

Ashrae Standard (2001). ASHRAE Handbook 2001 Fundamentals. *Ashrae Standard*, **53**, 1689–1699. 27

Beach, W.P., Benedict, R.P. & Dowdell, R.B. (1985). ASME measurement uncertainty. *Journal of Fluids Engineering*, **107**, 161–164. 188, 189

Benonysson, A. (1991). *Dynamic Modelling and Operational Optimization of District Heating Systems.*. Ph.D. thesis, Technical University of Denmark. 32

Benonysson, A., Bøhm, B. & Ravin, H.F. (1995). Operational optimization in a district heating system. *Energy Conversion and Management*, 297–314. 32

Bergman, T., Lavine, A. & Incropera, F. (2011). *Fundamentals of Heat and Mass Transfer, 7th Edition*. John Wiley & Sons, Incorporated. ix, 17, 20, 21, 25, 29, 56

Boesten, S., Ivens, W., Dekker, S.C. & Eijdems, H. (2019). 5Th Generation District Heating and Cooling Systems As a Solution for Renewable Urban Thermal Energy Supply. *Advances in Geosciences*, **49**, 129–136. 7

Bosworth, R. (1949). XXIX. Distribution of reaction times for turbulent flow in cylindrical reactors. *The London, Edinburgh, and Dublin Philosophical Magazine and Journal of Science*, **40**, 314–324. 32

Breeze, P. (2019). Chapter 6 - Combined Heat and Power. *Power Generation Technologies, Third Edition*, 121–143. 12

Buffa, S., Cozzini, M., D'Antoni, M., Baratieri, M. & Fedrizzi, R. (2019). 5th generation district heating and cooling systems: A review of existing cases in Europe. *Renewable and Sustainable Energy Reviews*, **104**, 504–522. 13

Chauvaud de Rochefort, H. (2018). Market Report: Heat Networks in the UK. Tech. rep., The Association for Decentralised Energy. 8

Chung, B., Kim, S., Johnson, P.C. & Popel, A.S. (2009). Computational fluid dynamics. *Computer methods in biomechanics and biomedical engineering*, **12**, 385–97. 39, 45, 47

Claesson, J. (2002). Dynamic Thermal Networks. Outlines of a General Theory. In *Proceedings of the 6th Symposium on Building Physics in the Nordic Countries Trondheim, Norway*, 47–54, Trondheim, Norway. 59, 62, 63, 64

Claesson, J. (2003). Dynamic thermal networks: a methodology to account for timedependent heat conduction. In *Proceedings of the Second International Conference on Research in Building Physics*, 407–415, Leuven, Belgium. 59, 64

Comstock, C., Zargary, A. & Brock, J.E. (1974). On the Delayed Hot Water Problem. *Journal of Heat Transfer*, **96**, 166. 32

Connolly, D., Lund, H., Mathiesen, B.V., Werner, S., Möller, B., Persson, U., Boermans, T., Trier, D., Østergaard, P.A. & Nielsen, S. (2014). Heat roadmap Europe: Combining district heating with heat savings to decarbonise the EU energy system. *Energy Policy*, **65**, 475–489. 1, 10

Dalla Rosa, A., Li, H. & Svendsen, S. (2011). Method for optimal design of pipes for low-energy district heating, with focus on heat losses. *Energy*, **36**, 2407–2418. 33

Dalla Rosa, A., Li, H. & Svendsen, S. (2013). Modeling transient heat transfer in small-size twin pipes for end-user connections to low-energy district heating networks. *Heat Transfer Engineering*, **34**, 372–384. 33, 81

del Hoyo Arce, I., López, S.H., Perez, S.L., Rämä, M., Klobut, K. & Febres, J.A. (2018). Models for fast modelling of district heating and cooling networks. *Renewable and Sustainable Energy Reviews*, **82**, 1863 – 1873. 32, 81

Dénarié, A., Aprile, M. & Motta, M. (2019). Heat transmission over long pipes: New model for fast and accurate district heating simulations. *Energy*, **166**, 267–276. 32

Eames, P., Loveday, D., Haines, V. & Romanos, P. (2014). The Future Role of Thermal Energy Storage in the UK Energy System : An Assessment of the Technical Feasibility and Factors Influencing Adoption. *Ukerc*. 1

Eggels, J.G.M., Unger, F., Weiss, M.H., Westerweel, J., Adrian, R.J., Friedrich, R. & Nieuwstadt, F.T.M. (2006). Fully developed turbulent pipe flow: a comparison between direct numerical simulation and experiment. *Journal of Fluid Mechanics*, **268**, 175. xii, 129, 131

Engel, J. (2005). Uncertainty Analysis. *Eindhoven University of Technology*. 189

Escudie, J.C. & Laret, L. (1994). a Simulation Tool for Building and Heating System Analysis Within TRNSYS. In *System simulation in buildings*, no. December 1994 in Proceedings of the fourth international conference, 642. 33

Fan, D., Rees, S. & Spitler, J. (2013). A dynamic thermal network approach to the modelling of Foundation Heat Exchangers. *Journal of Building Performance Simulation*, **6**, 81–97. ix, 26, 28, 29, 59, 64, 69, 71, 72

Farouki, O.T. (1986). *Thermal Properties of Soils*. Trans Tech Publications, Germany. 21, 22

Ferziger, J.H. & Peric, M. (2002). *Computational Methods for Fluid Dynamics*. Springer, 3rd edn. 42, 43, 44, 45, 47

Fluke Corporation (2013). User's Guide for Micro-Bath (7102). 185, 186

Frederiksen, S. & Werner, S. (2013). *District Heating and Cooling*. Studentlitteratur AB. 142

Gabrielaitiene, I., Bøhm, B. & Sunden, B. (2007). Modelling temperature dynamics of a district heating system in Naestved, Denmark-A case study. *Energy Conversion and Management*, **48**, 78–86. 32

Gabrielaitiene, I., Bøhm, B. & Sunden, B. (2008). Evaluation of approaches for modeling temperature wave propagation in district heating pipelines. *Heat Transfer Engineering*, **29**, 45–56. 16, 32, 33, 83

Gao, Y., Muzzio, F.J. & Ierapetritou, M.G. (2012). A review of the residence time distribution (rtd) applications in solid unit operations. *Powder Technology*, **228**, 416 – 423. 18

Gebremedhin, A. (2014). Optimal utilisation of heat demand in district heating system - A case study. *Renewable and Sustainable Energy Reviews*, **30**, 230–236. 10

Gida, M.I. (2019). District Energy in Iceland. Tech. rep., Icelandic Energy & Utilities. 8

Giraud, L., Baviere, R., Vallée, M. & Paulus, C. (2015). Presentation, Validation and Application of the DistrictHeating Modelica Library. *Proceedings of the 11th International Modelica Conference*, 79–88. 32

Goodwin (2015). *Control System Design*. Pearson Education. 194

Greenshields, C.J. (2019). OpenFOAM User Guide. 46, 47

Greiciunas, E. (2019). *Modelling Novel Heat Exchangers for Aircraft Thermal Management*. Ph.D. thesis, University of Leeds. 42, 45

Ham, J.H. & Platzer, B. (2004). Semi-Empirical Equations for the Residence Time Distributions in Disperse Systems - Part 1: Continuous Phase. *Chemical Engineering & Technology*, **27**, 1172–1178. 18, 19, 129, 130, 131

Hanby, V., Wright, J., Fletcher, D. & Jones, D. (2002). Modeling the dynamic response of conduits. *HVAC & R Research*, **8**, 1–12. ix, 19, 33, 54, 133

He, M. (2012). *Numerical modelling of geothermal borehole heat exchanger systems*. Ph.D. thesis, De Montfort University. 33

Holman, J.P. (2010). *Heat transfer*. McGraw-Hill, tenth edition edn. 15, 24, 30

Holzmann, T. (2017). *Mathematics, Numerics, Derivations and OpenFOAM*. Leoben. 40, 46

Hukseflux (2016). *Hukseflux Thermal Sensors User Manual HFP01*. Hukseflux Thermal Sensors B.V. 190, 191

Jassen, H. (2004). *The Influece of Soil Moisture Transfer on Building Heat Loss Via the Ground*. Ph.D. thesis, Katholieke Universiteit Leuven. 23

Karl, T.R. & Trenberth, K.E. (2003). Modern Global Climate Change. *Science*, **302**, 1719–1723. 1

Kauko, H., Kvalsvik, K.H., Rohde, D., Nord, N. & Utne, A. (2018). Dynamic modeling of local district heating grids with prosumers: A case study for Norway. *Energy*, **151**, 261–271. 13

Kaya, I. (1999). *Relay Feedback Identification and Model Based Controller Design*. Ph.D. thesis, University of Sussex. 193

Kim, J.H., Simon, T.W. & Viskanta, R. (2008). Reporting Uncertainties in Experimental Measurements and Results. *Journal of Heat Transfer*, **115**, 5. 189

Klein, S.A., Beckman, W.A. & Mitchell, J.W. (1997). TRNSYS – A transient system simulation program. 33

Kline, S. & Mcclintock, F. (1953). Describing Uncertainties in Single-Sample Experiments. *Mechanical Engineering*, **1**, 3–8. 188

Lake, A., Rezaie, B. & Beyerlein, S. (2017). Review of district heating and cooling systems for a sustainable future. *Renewable and Sustainable Energy Reviews*, **67**, 417–425. 10, 31

Launder, B.E. & Spalding, D.B. (1983). The numerical computation of turbulent flows. *Numerical Prediction of Flow, Heat Transfer, Turbulence and Combustion,*, **40**, 96—-116. 42

Levenspiel, O. & Smith, W.K. (1957). Notes on the diffusion-type model for the longitudinal mixing of fluids in flow. *Chemical Engineering Science*, **6**, 227–235. 52

Loveridge, F. (2012). *The Thermal Performance of Foundation Piles used as Heat Exchangers in Ground Energy Systems*. Ph.D. thesis, University of Southampton. 17, 18, 22

Low, J.E., Loveridge, F.A. & Powrie, W. (2014). Thermal conductivity of soils by the needle probe method, for energy foundation applications. In *International Thermal Conductivity Conference*. 198

Lund, H., Möller, B., Mathiesen, B.V. & Dyrelund, A. (2010). The role of district heating in future renewable energy systems. *Energy*, **35**, 1381–1390. 12

Lund, H., Werner, S., Wiltshire, R., Svendsen, S., Thorsen, J.E., Hvelplund, F. & Mathiesen, B.V. (2014). 4th Generation District Heating (4GDH). Integrating smart thermal grids into future sustainable energy systems. *Energy*, **68**, 1–11. 2, 10, 12, 15

Lund, H., Ostergaard, P.A., Chang, M., Werner, S., Svendsen, S., Sorknæs, P., Thorsen, J.E., Hvelplund, F., Mortensen, B.O.G., Mathiesen, B.V., Bojesen, C., Duic, N., Zhang, X. & Moller, B. (2018). The status of 4th generation district heating: Research and results. *Energy*, **164**, 147–159. 13

Lund, J.W. & Lienau, P.J. (2009). Geothermal district heating. *International Geothermal Days*, p.18. 8

Lund, R. & Mohammadi, S. (2016). Choice of insulation standard for pipe networks in 4th generation district heating systems. *Applied Thermal Engineering*, **98**, 256–264. 12, 13

Markvart, T. & Castalzer, L. (2012). 26

Meibodi, S.S. & Rees, S. (2020). Dynamic thermal response modelling of turbulent fluid flow through pipelines with heat losses. *International Journal of Heat and Mass Transfer*, **151**, 119440. 73, 74

Menter, F.R. (1994). Two-equation eddy-viscosity turbulence models for engineering applications. *AIAA journal*, **41**, 1598—-1605. 42

Menter, F.R., Kuntz, M. & Langtry, R. (2003). Ten years of industrial experience with the sst turbulence model. *Turbulence, heat and mass transfer*, **41**, 625—-632. 42

Meter-Group (2018). TEMPOS Manual. Tech. rep. 198, 199, 200

Millar, M.A., Burnside, N.M. & Yu, Z. (2019). District heating challenges for the UK. *Energies*, **12**. 8

Moffat, R.J. (1988). Describing the uncertainties in experimental results. *Experimental Thermal and Fluid Science*, **1**, 3–17. 187, 188, 190

Moukalled, F., Mangani, L. & Darwish, M. (2016). *The Finite Volume Method in Computational Fluid Dynamics*, vol. 113. 39, 40, 42

National Instrument (2003). LabVIEW TM User Manual LabVIEW User Manual. Tech. rep. 94

National-Instruments (2015). *NI cDAQ™-9135 datasheet*. national instruments corporation (uk) ltd. 192

Nguyen, N.T. & Wereley, S.T. (2006). *Fundamentals and Applications of Microfluidics Second Edition*. Artech house, second edition edn. 40

Patil, A., Ajah, A. & Herder, P. (2009). Recycling industrial waste heat for sustainable district heating: a multi-actor perspective. *International Journal of Environmental Technology and Management*, **10**, 412–426. 9

Peng, C., Geneva, N., Guo, Z. & Wang, L.P. (2018). Direct numerical simulation of turbulent pipe flow using the lattice Boltzmann method. *Journal of Computational Physics*, **357**, 16–42. 129

Rees, S. & Van Lysebetten, G. (2020). A response factor approach to modelling long-term thermal behaviour of energy piles. *Computers and Geotechnics*, **120**. 38, 66, 67, 68

Rees, S.J. (2015). An extended two-dimensional borehole heat exchanger model for simulation of short and medium timescale thermal response. *Renewable Energy*, **83**, 518–526. 33, 54, 57, 67, 73, 75, 133

Rees, S.J. (2016). *Advances in Ground-Source Heat Pump Systems*, vol. 53. Elsevier Ltd. 21, 23, 29

Rees, S.J. & Fan, D. (2013). A numerical implementation of the Dynamic Thermal Network method for long time series simulation of conduction in multi-dimensional non-homogeneous solids. *International Journal of Heat and Mass Transfer*, **61**, 475–489. x, 59, 72, 73

Rees, S.W., Adjali, M.H., Zhou, Z., Davies, M. & Thomas, H.R. (2000). Ground heat transfer effects on the thermal performance of earth-contact structures. *Renewable and Sustainable Energy Reviews*, **4**, 213–265. 21

Revesz, A., Jones, P., Dunham, C., Davies, G., Marques, C., Matabuena, R., Scott, J. & Maidment, G. (2020). Developing novel 5th generation district energy networks. *Energy*, **201**, 117389. ix, 8, 11, 14

Rezaie, B. & Rosen, M.A. (2012). District heating and cooling: Review of technology and potential enhancements. *Applied Energy*, **93**, 2–10. 9, 10

Sartor, K. & Dewalef, P. (2017). Experimental validation of heat transport modelling in district heating networks. *Energy*, **137**, 961–968. 83

Seliktar, M. & Rorres, C. (1994). The Flow of Hot Water from a Distant Hot-Water Tank. *SIAM Review*, **36**, 474–479. 32

Shafagh, I., Rees, S., Mardaras, I.U., Janó, M.C. & Carbayo, M.P. (2020). A model of a diaphragm wall ground heat exchanger. *Energies*, **13**, 1–23. 38, 66, 67, 72

Skoglund, T. & Dejmek, P. (2007). A dynamic object-oriented model for efficient simulation of fluid dispersion in turbulent flow with varying fluid properties. *Chemical Engineering Science*, **62**, 2168–2178. 33, 54, 55, 57

Skoglund, T. & Dejmek, P. (2008). A dynamic object-oriented model for efficient simulation of microbial reduction in dispersed turbulent flow. *Journal of Food Engineering*, **86**, 358–369. 53, 55, 75

Strand, R. (1995). *Heat Source Transfer Functions and Their Application to Low Temperature Radiant Heating Systems*. University of Illinois at Urbana-Champaign. 57

Talebi, B., Mirzaei, P.A., Bastani, A. & Haghighat, F. (2016). A Review of District Heating Systems: Modeling and Optimization. *Frontiers in Built Environment*, **2**, 1–14. 9, 10

Taylor, G. (1954a). The Dispersion of Matter in Turbulent Flow through a Pipe. *Proceedings of the Royal Society A: Mathematical, Physical and Engineering Sciences*, **223**, 446–468. 32

Taylor, G.I. (1954b). Diffusion and mass transport in tubes. *Proceedings of the Physical Society. Section B*, **67**, 857–869. 52

Tunzi, M., Østergaard, D.S., Svendsen, S., Boukhanouf, R. & Cooper, E. (2016). Method to investigate and plan the application of low temperature district heating to existing hydraulic radiator systems in existing buildings. *Energy*, **113**, 413–421. 8

van der Heijde, B., Fuchs, M., Ribas Tugores, C., Schweiger, G., Sartor, K., Basciotti, D., Müller, D., Nytsch-Geusen, C., Wetter, M. & Helsen, L. (2017). Dynamic equation-based thermo-hydraulic pipe model for district heating and cooling systems. *Energy Conversion and Management*, **151**, 158–169. 32, 81

Versteeg, H.K. & Malalasekera, W. (2007). *An Introduction to Computational Fluid Dynamics Second Edition*. Pearson Publication. 41

Walter, I. (2005). Task Committee on Standardization of Reference Evapotranspiration. *Environmental and Water Resources Institute of the American Society of Civil Engineers*. 26, 27, 29

Wang (2014). *Sensor Technologies for Civil Infrastructures, Volume 1: Sensing Hardware and Data Collection Methods for Performance Assessment*. Elsevier Science. 92

Wang, H. & Meng, H. (2018). Improved thermal transient modeling with new 3-order numerical solution for a district heating network with consideration of the pipe wall's thermal inertia. *Energy*, **160**, 171 – 183. 32

Weber, C., Maréchal, F. & Favrat, D. (2007). Design and optimization of district energy systems. In *European Symposium on Computer Aided Process Engineering*, 1127 – 1132, Elsevier Science, Bucharest, Romania. 9

Weller, H.G., Tabor, G., Jasak, H. & Fureby, C. (1998). A tensorial approach to computational continuum mechanics using object-oriented techniques. *COMPUTERS IN PHYSICS*, **12**, 620–631. 69

Wen, C. & Fan, L. (1975). *Models for flow systems and chemical reactors*. Chemical processing and engineering, Dekker. 33, 53, 54

Wentzel, E. (2005). *Thermal Modeling of Walls, Foundations and Whole Buildings Using Dynamic Thermal Networks*. Ph.D. thesis, Chalmers University of Technology. x, 70, 71, 73

Wetter, M., Zuo, W., Nouidui, T.S. & Pang, X. (2014). Modelica Buildings library. *Journal of Building Performance Simulation*, **7**, 253–270. 32

Wilcox, D.C. (1988). Reassessment of the scale-determining equation for advanced turbulence models. *AIAA journal*, **26**, 1299–1310. 42

Wirtz, M., Kivilip, L., Remmen, P. & Müller, D. (2020). 5th Generation District Heating: A novel design approach based on mathematical optimization. *Applied Energy*, **260**, 114158. 10, 13, 14

Wood, R. (2015). *Experimental and Theoretical Studies of Contaminant Transport Due to Human Movement in a Hospital Corridor*. Ph.D. thesis, University of Leeds. 42

Xing, L. (2008). *Analytical and Numerical Modeling of Foundation Heat Exchanger*. Ph.D. thesis, Oklahoma State University. 27, 28, 29

Yavuzturk, C., In, S.J.R., Measurement, S., Properties, T., Terrastock, P., Spitler, J.D. & Rees, S.J. (2000). citation is : In Situ Measurement of Ground Thermal Properties. *Proceedings of Terrastock 2000*, **1**, 165–170. 197

Zhang, H., Baeyens, J., Cáceres, G., Degrève, J. & Lv, Y. (2016). Thermal energy storage: Recent developments and practical aspects. *Progress in Energy and Combustion Science*, **53**, 1–40. 14